Journal of Ophthalmology

Personalized Optical Designs and Manipulating Optics: Applications on the Anterior Segment of the Eye

Lead Guest Editor: Pablo Pérez-Merino
Guest Editors: Damian Siedlecki, Laura Remon, Maria Vinas, Jorge Aliò, and Jos J. Rozema

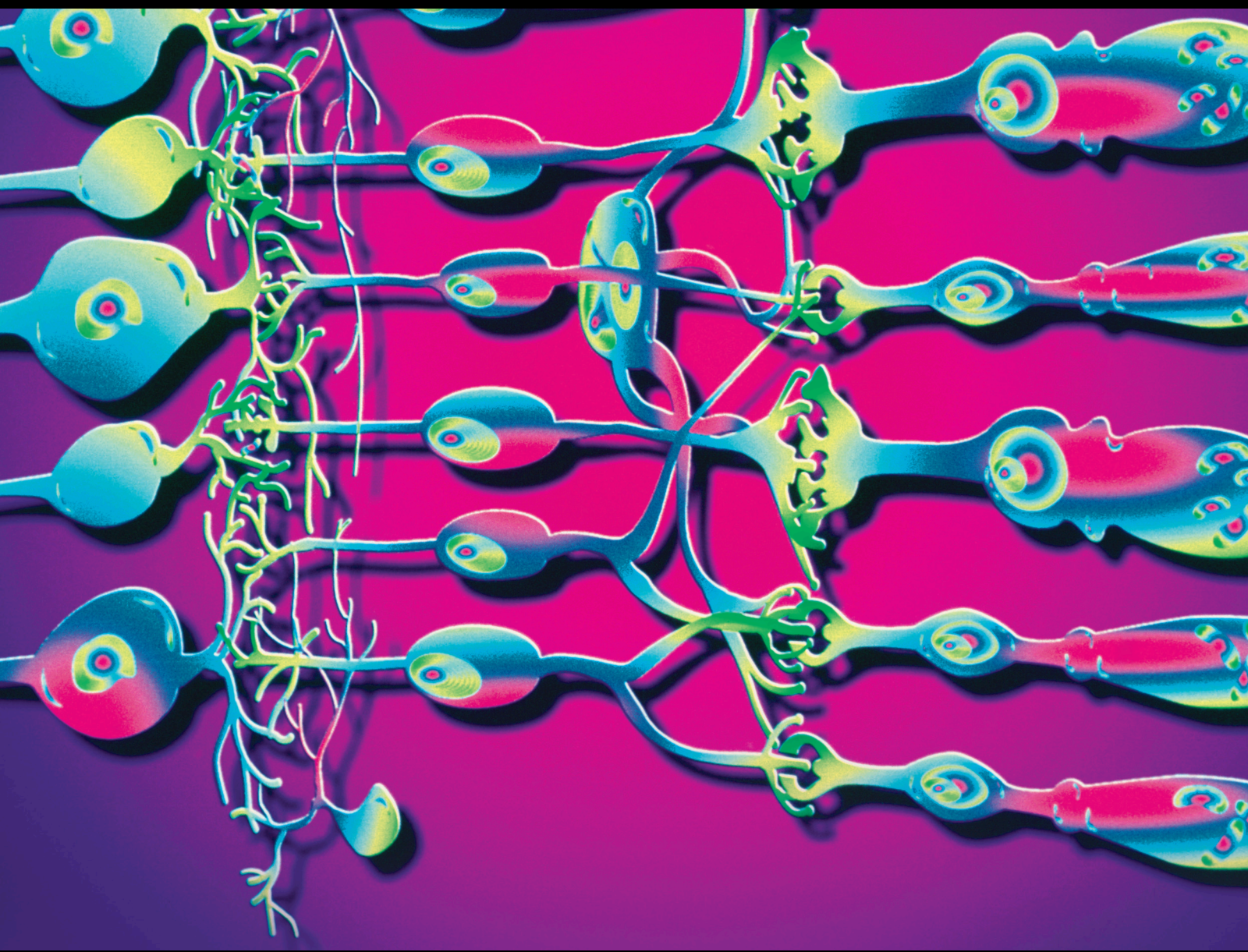

Personalized Optical Designs and Manipulating Optics: Applications on the Anterior Segment of the Eye

Journal of Ophthalmology

Personalized Optical Designs and Manipulating Optics: Applications on the Anterior Segment of the Eye

Lead Guest Editor: Pablo Pérez-Merino
Guest Editors: Damian Siedlecki, Laura Remon, Maria Vinas, Jorge Aliò, and Jos J. Rozema

Contents

Personalized Optical Designs and Manipulating Optics: Applications on the Anterior Segment of the Eye
Pablo Pérez-Merino, Damian Siedlecki, Laura Remón, Maria Vinas, Jorge L. Alió, and Jos J. Rozema
Editorial (3 pages), Article ID 9586062, Volume 2020 (2020)

Bifocal and Multifocal Contact Lenses for Presbyopia and Myopia Control
Laura Remón, Pablo Pérez-Merino, Rute J. Macedo-de-Araújo, Ana I. Amorim-de-Sousa, and José M. González-Méijome
Review Article (18 pages), Article ID 8067657, Volume 2020 (2020)

Comparison of Two Wavefront Autorefractors: Binocular Open-Field versus Monocular Closed-Field
Gonzalo Carracedo, Carlos Carpena-Torres, Laura Batres, Maria Serramito, and Anahí Gonzalez-Bergaz
Research Article (10 pages), Article ID 8580471, Volume 2020 (2020)

Novel Technique of Pneumatic Posterior Capsulorhexis for Treatment and Prevention of Posterior Capsular Opacification
Ahmed M. Eid, Shaaban Abd-Elhamid Mehany Elwan, Ahmed M. Sabry, Hossam M. Moharram, and Ashraf M. Bakhsh
Clinical Study (6 pages), Article ID 3174709, Volume 2019 (2019)

Influence of Angle κ and Higher-Order Aberrations on Visual Quality Employing Two Diffractive Trifocal IOLs
Cecilio Velasco-Barona, Claudia Corredor-Ortega, Alejandra Mendez-Leon, Nadia L. Casillas-Chavarín, Daniel Valdepeña-López Velarde, Guadalupe Cervantes-Coste, Daniel Malacara-Hernández, and Roberto Gonzalez-Salinas
Research Article (8 pages), Article ID 7018937, Volume 2019 (2019)

Influence of Overnight Orthokeratology Lens Treatment Zone Decentration on Myopia Progression
Anken Wang and Chenhao Yang
Research Article (7 pages), Article ID 2596953, Volume 2019 (2019)

Optical Evaluation of New Designs of Multifocal Diffractive Corneal Inlays
Diego Montagud-Martínez, Vicente Ferrando, Juan A. Monsoriu, and Walter D. Furlan
Research Article (6 pages), Article ID 9382467, Volume 2019 (2019)

Comparison of the Clinical Outcomes between Echelette Extended Range of Vision and Diffractive Bifocal Intraocular Lenses
Xin Liu, Xiaohui Song, Wei Wang, Yanan Zhu, Danni Lyu, Xingchao Shentu, Peiqing Chen, Yibo Yu, and Ke Yao
Clinical Study (9 pages), Article ID 5815040, Volume 2019 (2019)

Assessment of the Association between In Vivo Corneal Morphogeometrical Changes and Keratoconus Eyes with Severe Visual Limitation
J. S. Velázquez, F. Cavas, J. Alió del Barrio, D. G. Fernández-Pacheco, and J. Alió
Research Article (7 pages), Article ID 8731626, Volume 2019 (2019)

Correlations of Corneal Spherical Aberration with Astigmatism and Axial Length in Cataract Patients
Min Zhang, Dongjin Qian, Qinghe Jing, Jiahui Chen, Michael Deng, and Yongxiang Jiang
Research Article (7 pages), Article ID 4101256, Volume 2019 (2019)

Quantitative Multiparameter Evaluation of Vacuoles in Intraocular Lenses Employing a High-Magnification Digital Microscopy Method
Vincent Spiezio, Bennett N. Walker, Don Calogero, and Ilko K. Ilev
Research Article (13 pages), Article ID 7929014, Volume 2019 (2019)

Diagnostic Sensitivity of Different Reference Bodies When Using Scheimpflug Tomography in a Myopic Population with Keratoconus
Daniel Garcerant, Ignacio Jiménez-Alfaro, and Nicolás Alejandre
Research Article (7 pages), Article ID 2593404, Volume 2019 (2019)

New Approach for the Calculation of the Intraocular Lens Power Based on the Fictitious Corneal Refractive Index Estimation
Joaquín Fernández, Manuel Rodríguez-Vallejo, Javier Martínez, Ana Tauste, and David P. Piñero
Research Article (9 pages), Article ID 2796126, Volume 2019 (2019)

Hindawi
Journal of Ophthalmology
Volume 2020, Article ID 9586062, 3 pages
https://doi.org/10.1155/2020/9586062

Editorial

Personalized Optical Designs and Manipulating Optics: Applications on the Anterior Segment of the Eye

Pablo Pérez-Merino,[1] **Damian Siedlecki**,[2] **Laura Remón**,[3] **Maria Vinas**,[4] **Jorge L. Alió**,[5] **and Jos J. Rozema**[6,7]

[1]*Department of Ophthalmology, Instituto de Investigación Sanitaria Fundación Jiménez Díaz, Madrid, Spain*
[2]*Wroclaw University of Science and Technology, Wroclaw, Poland*
[3]*Departamento de Física Aplicada, Universidad de Zaragoza, Zaragoza, Spain*
[4]*Instituto de Óptica, Consejo Superior de Investigaciones Científicas (CSIC), Madrid, Spain*
[5]*Vissum Corporacion Oftalmologica, Alicante, Spain*
[6]*Department of Ophthalmology, Antwerp University Hospital, Edegem, Belgium*
[7]*University of Antwerp, Antwerp, Belgium*

Correspondence should be addressed to Pablo Pérez-Merino; pablo.perezm@quironsalud.es

Received 28 December 2019; Accepted 30 December 2019; Published 1 April 2020

The image-forming properties of the eye can be described in terms of wave aberration. Understanding the link between aberrations and the anterior segment geometry is therefore of crucial importance for (i) comprehending how the eye works, (ii) modelling the optics of individual eyes, (iii) optimizing optical solutions, or (iv) designing surgical strategies. The eye has many innate adaptations that minimize optical aberrations. In most normal young eyes, the magnitude of aberrations of the cornea is significantly larger than for the whole eye, indicating a significant role of the crystalline lens in compensating corneal aberrations. However, due to geometrical and structural changes, this ocular compensation gets disturbed in different anterior segment conditions, such as keratoconus, presbyopia, or cataract. Keratoconus progressively degrades the corneal shape and, consequently, vision in the adolescence, with a prevalence of 0.05% in the general population. Meanwhile, presbyopia and cataract are conditions related to aging that affect the structure of the crystalline lens, one referring to a loss in accommodative amplitude (presbyopia) and the other to a progressive loss of transparency (cataract). Presbyopia affects 100% of the population older than 45 years of age, impairing reading and near work activities as a result of the loss of the eye's crystalline lens ability to focus at near objects, whereas cataracts affect more than 50% of the population over 75. Furthermore, the prevalence of myopia has alarmingly increased in recent years, especially in the developing economies of the East Asian area, making the identification of the optical changes in the eye associated with myopia particularly important.

Given the large numbers of potential patients for optical correction of presbyopia and cataract, managing keratoconus, or slowing down the progression of myopia, the potential impact of new solutions based on personalized optical designs is undoubtedly tremendous and will offer both remarkable opportunities and challenges in a wide range of anterior segment applications. Combining the technological advances in aberrometry and three-dimensional anterior segment imaging techniques with dedicated ray-tracing and processing tools will allow building patient-specific eye models for the selection of the contact and/or intraocular lens design that provides the best optical quality [1–3].

Furthermore, a better understanding of the optical corrections and how they interact with the patient's optics will help clinicians with selecting the correction that optimizes the visual performance in their patients, for example,

using visual simulators that allow the patient to experience the difference in visual performance between monofocal or different multifocal solutions [4]. With the recent expansion of presbyopia-correcting contact/intraocular lenses by the many variations in design (diffractive and refractive, or new class of extended depth-of-focus lenses), multiple zones, and add power, the ability to satisfy the patient's visual demands has never been greater, possibly leading to unprecedented customized eye treatments. In this special issue, eleven scientific articles and one review article discuss the implications and possible future directions of personalized optical designs and manipulating optics through different applications on the anterior segment of the eye.

It is well established that favourable interactions between low- and high-order aberrations can improve the visual performance [5]. In particular, adding a certain amount of spherical aberration to defocus can improve visual quality over defocus alone. Besides defocus, specific combinations of astigmatism and coma also increase optical quality. Zhang et al. investigated the correlations between spherical aberration, astigmatism, and axial length in a large cohort (6747 eyes) and found that in eyes with low astigmatism axial length was correlated with spherical aberration (e.g., a gradual decrease as axial length increases). In the presence of larger astigmatism (>2D), however, the authors found different tendencies between axial length and spherical aberration that would clearly affect the selection of a toric IOL. Velasco-Barona et al. evaluated the effect of angle kappa and aberrations on the visual performance of two different presbyopia-correcting IOLs (diffractive trifocal: Acrysof IQ PanOptix and AT LISA tri 839MP). The authors did not notice association between angle kappa and the postoperative visual quality. In a different study, Liu et al. provided clinical advice in choosing presbyopia-correcting IOLs by comparing the visual performance between the Echelette Extended Range of Vision (Tecnis Symfony ZXR00) and the diffractive bifocal (Tecnis ZMB00). Regarding IOL power calculation, Fernández et al. described that the postoperative residual refractive error with current IOL power calculation formulas could be associated with an under- or overestimation of the real estimated lens position (ELP). But even if ELP was perfectly predicted, there may still be some postoperative refractive error depending on the axial length. Hence, the authors proposed a fictitious corneal refractive index estimation as an additional method to optimize the IOL power calculation.

The replacement of the crystalline lens by an intraocular lens modifies the chromatic dispersion properties of the eye, depending on the dispersion properties of the IOL material. Moreover, different IOL materials have different tendencies to form small fluid-filled vacuoles (glistenings) within the bulk of the IOL with different effects on light scattering. Spiezio et al. proposed a new methodology based on high-magnification digital microscopy to quantitatively evaluate and characterize such IOL vacuoles using their critical optical characteristics, such as vacuole size, density, shape, and orientation within the IOL material. Elwan et al. showed a new technique for the treatment of primary posterior capsule opacification (PCO) or prevention of postoperative PCO based on a pneumatic technique to perform a posterior capsulorhexis.

Progressive distortion of the cornea in keratoconus leads to abnormal corneal topography, resulting in irregular astigmatism, progressive myopia, and increased high-order aberrations. Although the anterior corneal surface supposes the dominant factor to corneal aberrations, the posterior corneal surface also has a remarkable implication in ocular aberrations. Therefore, an accurate three-dimensional quantification of both anterior and posterior corneal surfaces is critical for managing keratoconus. Velázquez-Blázquez et al. proposed a three-dimensional virtual model of the cornea by means of computational geometry as a novel tool for keratoconic classification. Corneal surface analysis in corneal topographers is usually based on fitting the elevation data to parametric models to obtain the relevant information. Regarding keratoconus classification based on Scheimpflug-imaging surface fitting, Garcerant et al. defined a toric ellipsoid with fixed eccentricity at the thinnest point as the best-performing parameter to discriminate between normal and keratoconus within a myopic population.

In the contact lens field, Wang and Yang described the effect of decentration of the orthokeratology lens on myopia progression. Meanwhile, the review article by Remón et al. proposed novel experimental paradigms for presbyopia correction and myopia control, such as material platforms, optical designs, and computational simulations of bifocal and multifocal contact lenses. In a different study, Carracedo et al. compared the agreement and repeatability of binocular open-field and monocular closed-field wavefront autorefractor systems. The binocular open-field provided better results in terms of spherical equivalent and J_0 and could be an excellent tool to evaluate refractive errors in the clinical practice.

Interestingly, Montagud-Martínez et al. showed a novel concept of using diffractive corneal inlays for presbyopia correction. This design not only surpasses the multifocal performance of the commercial small aperture corneal inlays but also compensates their limitations in terms of degraded contrast sensitivity and stereoscopic acuity.

Conflicts of Interest

P.P.M. and M.V. have personal interest in 2EyesVision SL. D. S., L. R., J. L. A., and J. J. R. declare that they have no conflicts of interest.

Acknowledgments

We would like to extend our gratitude to all the authors who have submitted their studies for consideration in our special issue, to the reviewers for their essential feedback, and to the editorial board members for their fundamental support and help in the process. We hope that this collection of works provides motivation for all the readers and help to stimulate

further exchanges between ophthalmologists and visual scientists.

Pablo Pérez-Merino
Damian Siedlecki
Laura Remón
Maria Vinas
Jorge L. Alió
Jos J. Rozema

References

[1] C. Canovas and P. Artal, "Customized eye models for determining optimized intraocular lenses power," *Biomedical Optics Express*, vol. 2, no. 6, pp. 1649–1662, 2011.

[2] J. J. Rozema, P. Rodriguez, I. Ruiz Hidalgo et al., "SyntEyes KTC: higher order statistical eye model for developing keratoconus," *Ophthalmic and Physiological Optics*, vol. 37, no. 3, pp. 358–365, 2017.

[3] E. Martinez-Enriquez, P. Pérez-Merino, S. Durán-Poveda, I. Jiménez-Alfaro, and S. Marcos, "Estimation of intraocular lens position from full crystalline lens geometry: towards a new generation of intraocular lens power calculation formulas," *Scientific Reports*, vol. 8, no. 1, 2018.

[4] C. Dorronsoro, A. Radhakrishnan, J. R. Alonso-Sanz et al., "Portable simultaneous vision device to simulate multifocal corrections," *Optica*, vol. 3, no. 8, pp. 918–921, 2016.

[5] R. A. Applegate, J. D. Marsack, R. Ramos, and E. J. Sarver, "Interaction between aberrations to improve or reduce visual performance," *Journal of Cataract & Refractive Surgery*, vol. 29, no. 8, pp. 1487–1495, 2003.

Hindawi
Journal of Ophthalmology
Volume 2020, Article ID 8067657, 18 pages
https://doi.org/10.1155/2020/8067657

Review Article

Bifocal and Multifocal Contact Lenses for Presbyopia and Myopia Control

Laura Remón,[1] **Pablo Pérez-Merino**,[2] **Rute J. Macedo-de-Araújo**,[3] **Ana I. Amorim-de-Sousa**,[3] **and José M. González-Méijome**[3]

[1]*Department of Applied Physics, University of Zaragoza, 50009 Zaragoza, Spain*
[2]*Department of Ophthalmology, Biomedical Research Institute Fundación Jiménez Díaz, 28040 Madrid, Spain*
[3]*Clinical and Experimental Optometry Research Lab (CEORLab), Center of Physics, University of Minho, 4710-057 Braga, Portugal*

Correspondence should be addressed to Laura Remón; lauremar@unizar.es

Received 30 August 2019; Revised 10 February 2020; Accepted 24 February 2020; Published 1 April 2020

Academic Editor: Michele Figus

Bifocal and multifocal optical devices are intended to get images into focus from objects placed at different distances from the observer. Spectacles, contact lenses, and intraocular lenses can meet the requirements to provide such a solution. Contact lenses provide unique characteristics as a platform for implementing bifocality and multifocality. Compared to spectacles, they are closer to the eye, providing a wider field of view, less distortion, and their use is more consistent as they are not so easily removed along the day. In addition, contact lenses are also minimally invasive, can be easily exchangeable, and, therefore, suitable for conditions in which surgical procedures are not indicated. Contact lenses can remain centered with the eye despite eye movements, providing the possibility for simultaneous imaging from different object distances. The main current indications for bifocal and multifocal contact lenses include presbyopia correction in adult population and myopia control in children. Considering the large numbers of potential candidates for optical correction of presbyopia and the demographic trends in myopia, the potential impact of contact lenses for presbyopia and myopia applications is undoubtedly tremendous. However, the ocular characteristics and expectations vary significantly between young and older candidates and impose different challenges in fitting bifocal and multifocal contact lenses for the correction of presbyopia and myopia control. This review presents the recent developments in material platforms, optical designs, simulated visual performance, and the clinical performance assessment of bifocal and multifocal contact lenses for presbyopia correction and/or myopia progression control.

1. Introduction

Bifocal and multifocal contact lenses (CLs) for presbyopia correction and/or myopia control can be made available in a wide variety of platforms, including rigid gas permeable (RGP) lenses of different sizes from corneal to scleral supported, soft contact lenses, and hybrid lenses [1]. In addition to the lens optical structure, bifocality and multifocality can also be achieved by reshaping the cornea with the application of CLs in the technique called orthokeratology and has been used widely for myopia correction and myopia control [2, 3] although its application for presbyopia correction is still limited [4]. While presbyopia correction with contact lenses accounts for up to 25–35% of the contact lens fittings in several countries [5], myopia control contact lens fittings are still limited to 2–5% of the contact lenses fitted [6].

The pupil size of the eye and the power distribution across the lens are related to providing the desired effect for presbyopia and myopia applications [1, 2, 7]. In presbyopia correction, the main goal is to provide images focused at different distances along the optical axis and is, therefore, a matter of central (foveal) viewing. For older patients senile miosis imposes a limitation of the area of the device that is useful to form images in the retinal proximity. However, in the case of myopia control, in addition to foveal imaging, off-

axis imaging should also be taken into account as it could be relevant to achieve the therapeutic effect and slow eye growth (yet to be confirmed) [8].

In this review article, we present an overview of the recent developments of bifocal and multifocal contact lens designs for the correction of presbyopia and myopia control, including the optical design of different platforms for bifocality and multifocality, computational simulations and performance assessment, and their connection with the visual performance, patient acceptance, and efficacy. For further information on the performance of earlier designs for presbyopia correction [1, 9] and myopia control, including orthokeratology [10, 11], the reader must consult the abundant existing literature including several systematic reviews and meta-analyses on the former topic [12–16].

2. Platforms for Bifocality and Multifocality in Contact Lenses

Contact lenses that allow the lens to change the relative position with the pupil depending on the viewing distance are mostly built in RGP platforms. Although segmented bifocal spectacles have been used for myopia control, alternating bifocal contact lenses have not been used for such purpose. Contact lenses whose optical zone remains stable regarding the pupil on different eyesight directions can be built in any platform from corneal to scleral RGP, soft and hybrid materials.

Most of the more effective bifocal and multifocal contact lens designs are currently manufactured in soft platforms. Due to its larger diameter and flexibility, it enables better control of centration and lens movement compared to corneal RGP contact lenses. Recently, these multifocal designs that have been introduced on hybrid (in which the central area of the contact lens is manufactured with rigid gas permeable materials) and scleral lenses also offer an excellent solution for presbyopia compensation and myopia progression control.

While soft, corneal RPG, and hybrid contact lens platforms have been the object of previous reviews [1], multifocal scleral supported contact lenses have been recently used for presbyopia correction. Modern RGP scleral lenses have a large diameter, without any mechanical interactions between the lens, the cornea, and the sclerocorneal limbus. Scleral contact lenses (SL) are considered as one of the best visual correction options for eyes that were unsuccessful with conventional contact lens modalities, which led to an exponential increase in the number of publications in the last years [17]. Progress in the manufacturing process, lens materials, and improved knowledge on the scleral anatomy boosted the indications for SL fitting. SL are mostly fitted to improve vision in cases of irregular astigmatism (from primary corneal ectasias to keratoplasty) and for providing a therapeutic environment for managing severe anterior eye diseases (severe dry eye due to Sjögren's or Stevens–Johnson syndrome) and also for normal/healthy corneas with high refractive errors [18–21].

The optical principles for scleral lenses are identical to corneal RGP and hybrid contact lenses, as corneal astigmatism (regular or irregular) and high-order aberrations are partially or completely compensated by the tear film reservoir between the lens and the cornea. However, SL wearers and manufacturers could also take advantage of the unique stability on-eye during lens wear: these lenses are rotationally stable and have lack of movement with blinking [22, 23].

Although SL are very stable on-eye, they tend to decenter. The geometric characteristics of the ocular surface beyond the corneal borders (flatter sclera in the nasal side), gravity, and eyelids effect usually make the SL to decenter inferotemporally [24–29]. However, some manufacturers are able to overcome this issue by decentering the optic zone to compensate for this misalignment with the visual axis, which could be very beneficial for presbyopic and myopia control designs. Nowadays, multifocal SL account for approximately 2% of all contact lenses prescribed [30]. Several SL designs have been introduced to the market in the last few years, with parameters varying considerably between manufacturers (center distance or near designs, different central optic zone diameter, addition powers, and power profiles), which enhance the importance to follow the fitting guides and recommendations [31].

3. Optical Designs

3.1. Bifocal and Multifocal Contact Lenses. There are different bifocal and multifocal contact lens designs commercially available [32–34]. The International Organization for Standardization (ISO) [35] Ophthalmic Optics-Contact Lenses, Part 1: Vocabulary, Classification System and Recommendations for Labelling Specifications. ISO 18369-1: 2006 (Geneva, Switzerland: ISO; 2006) defined the following concepts related to the matter of this review article as (i) *bifocal contact lenses*: contact lens designed with two optic zones, usually for distance- and near-vision correction, (ii) *multifocal contact lens*: contact lens designed to provide two or more zones of different refractive power, and (iii) *progressive power contact lens/varifocal power contact lens*: contact lens designed to provide correction for more than one viewing range in which the refractive power changes continuously, rather than discretely. Most of these contact lens designs can also be designed with toric geometry for the correction of astigmatism, particularly for rigid gas permeable lenses and also for some hydrophilic soft contact lenses. Figure 1 shows different examples of multifocal contact lens designs.

These design concepts work under two different principles [9, 32, 36]: (i) *alternating image*, in which a translating movement of the lens when looking downwards results in viewing through an area with a different refractive power; and (ii) *simultaneous image,* where the simultaneous projection of the images coming from multiple target distances are presented to the eye at the same time at different focal planes. Then, in the simultaneous image, there must be a neural adaptation to select the sharp image depending on the visual target.

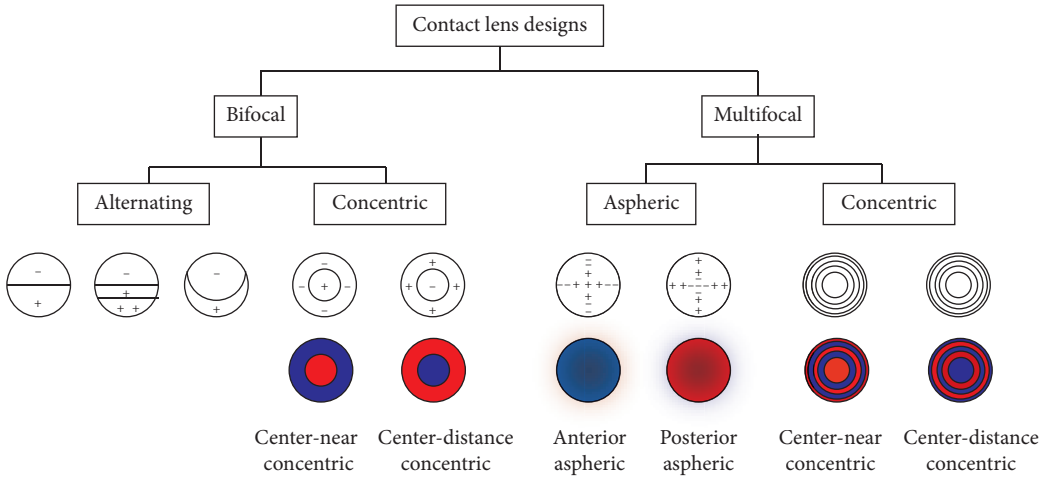

Figure 1: Illustration of different contact lens designs. In red: areas for near vision; in blue: areas for distance vision.

3.2. Simultaneous Image Contact Lens Designs. In simultaneous image designs, specific regions of the contact lens are designed for far and near vision correction, refracting simultaneously light from far and near targets through the pupil for all gaze positions. In this situation, the retina receives several images: in-focus and out-of-focus. Thus, lens centration, pupil size, ocular optics, and neural adaptation are essential for efficient visual performance with these contact lenses [37]. Further details on the power profiles of the most current multifocal contact lenses for presbyopia correction can be found in previous publications: Plainis et al. [37], Montés-Micó et al. [38], Wagner et al. [39], and Kim et al. [40].

There are two main types of simultaneous image contact lens designs *concentric multifocal contact lenses* and *aspheric multifocal contact lenses.*

(i) Concentric multifocal contact lenses: these contact lens designs have a primary viewing zone in the center of the lens, which provides either distance or near power, surrounded by concentric rings of near or distance power, respectively (see Figure 1). These lenses are designed as near-center or distance-center and are classified as biconcentric or multiconcentric [41–43].

(ii) Aspheric multifocal contact lenses: these contact lenses designs are based on aspheric designs fitted by conics, allowing the manipulation of the spherical aberration to modify the depth of focus. These designs comprise a power gradient that changes radially across the lens, most frequently in a radially symmetric fashion [44].

Unlike the discrete segmented rings of distance and near refractive power surrounding the center of the lens in the concentric designs, the aspheric designs show gradual changes in power from the center (center-distance or center-near) to the periphery of the lens (see Figure 1).

3.3. Characterization of the Simultaneous Image Contact Lens Design. Recent studies have published the designed phase patterns of different multifocal contact lens models (e.g., Charman described in its review article the power profile of the Purevision and Acuvue Oasys along a radius of 3.0 and 3.5 mm, respectively, of nominally 0.00 D distance power [32]). This information is essential to develop realistic individual simulations on model eyes, understand the multifocal performance of different distributions of near/far zones across the pupil, and interpret the visual outcomes [37, 38, 43, 45].

To date, there are different commercial devices that measure objectively the contact lens power profile and power maps following the specifications of ISO 18369-2: 2013 (Ophthalmic optics—Contact lenses—Part 2: tolerances) [46] and ISO 18369-3:2017 (Ophthalmic optics—Contact lenses—Part 3: measurement methods) [47]: *ConTest II* (Rotlex, Israel), which uses a Moiré fringe method; *Visionix 2001* (Visionix Ltd, Jerusalem, Israel) [43] and *SHSOphthalmic* (Optocraft GmbH, Erlangen, Germany) [39], which are based on Hartmann-Shack technology; and *NIMO TR1504* (Lambda-X, Nivelles, Belgium), based on a deflectometry technique and the combination of the Schlieren principle with a phase-shifting method [38, 45]. In Figure 2, we illustrate the power maps (left), the proportion of the total pupil area covered by the distance and near correction as a function of the pupil diameter (center), and the through-focus Visual Strehl (right) for four different soft multifocal contact lenses (A: Acuvue Oasys for presbyopia, medium addition; B: Dual Focus for myopia progression control; C: Purevision Multifocal, high addition; D: Airoptix, as they exemplify different design concepts, are widely used in the clinical practice and information exist about their visual performance in the literature [37]). Two of these lenses (A and B) have a multizone design with central-far design, while C and D are center-near designs. Acuvue Oasys (A) differs from Dual Focus (B) in the size of the zones, especially in the central annular. The consequence is an

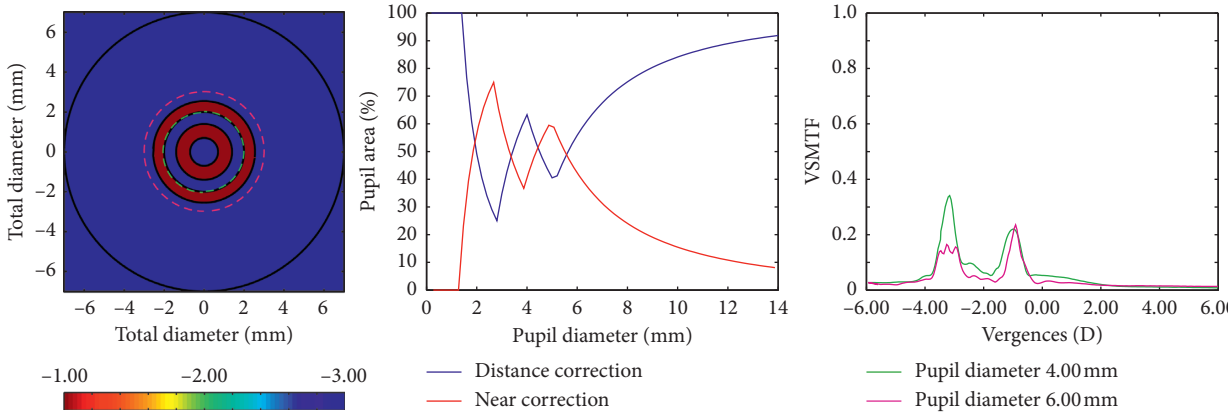

(a)

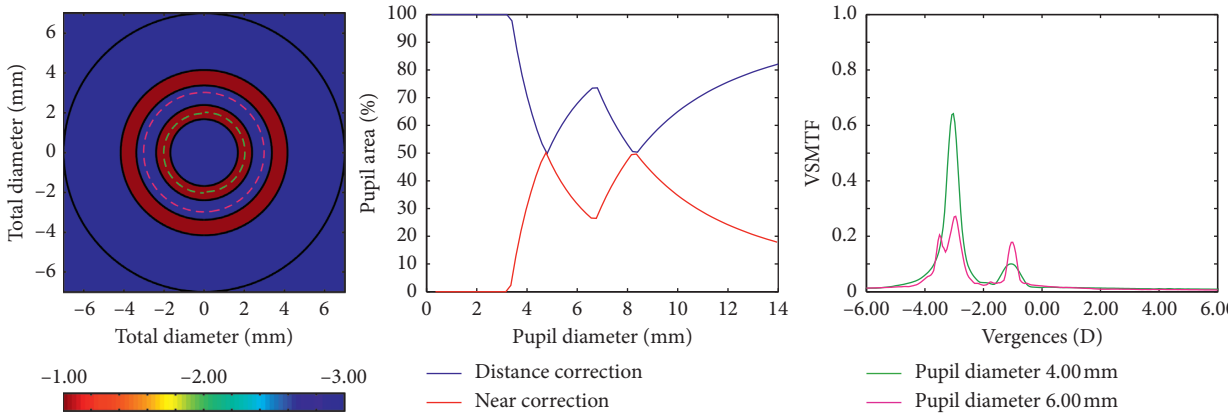

(b)

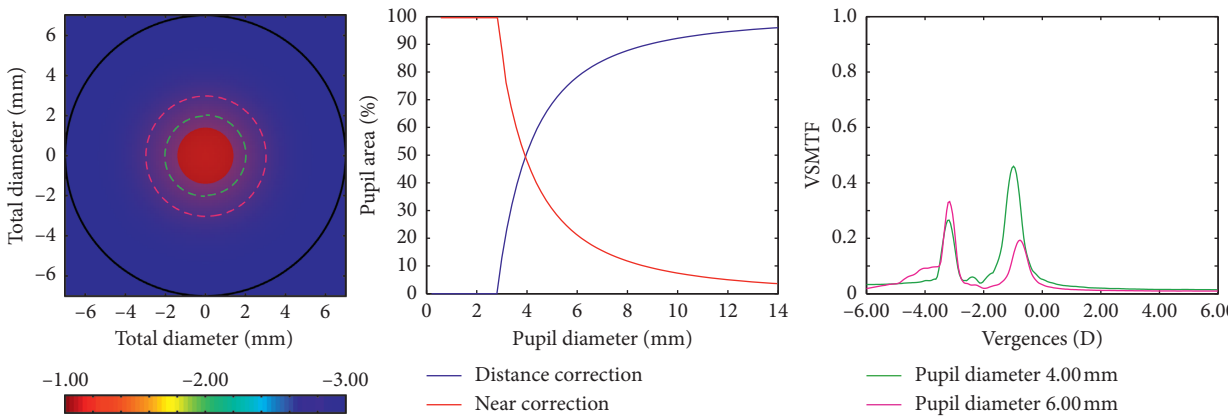

(c)

Figure 2: Continued.

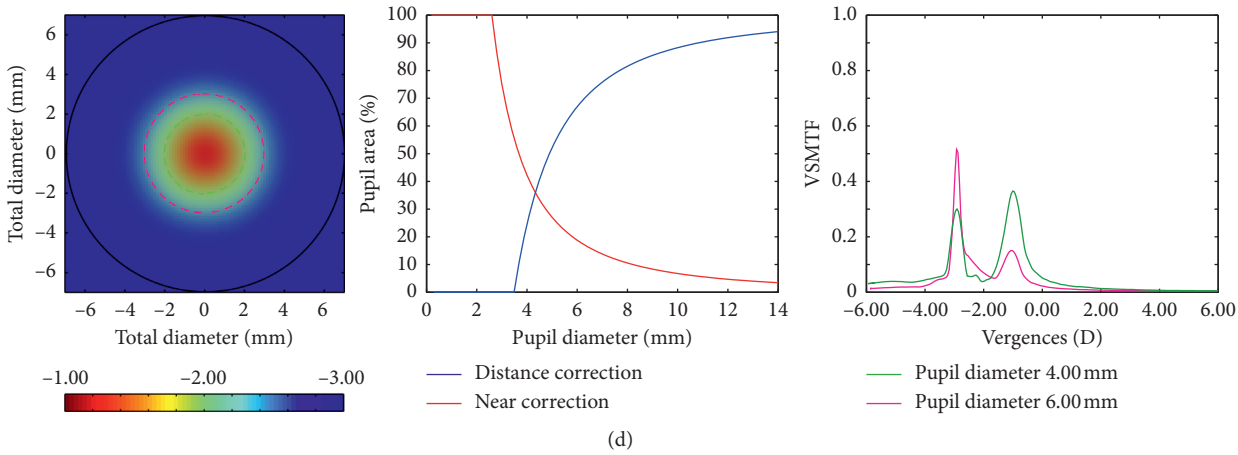

Figure 2: Illustration of the power maps (left), the proportion of the total pupil area covered by the distance and near correction as a function of the pupil diameter (center), and the through-focus Visual Strehl for pupil diameters of 4 mm and 6 mm (right) of different simultaneous image multifocal and bifocal contact lenses: (a) Acuvue Oasys for presbyopia, (b) Dual Focus, (c) PV: Purevision and (d) Airoptix (redrawn from Plainis et al. [37]). Profiles are designed to provide a distance correction power of −3.00 and an addition power of +2.00 diopters resulting in −1.00 of near correction power.

improvement for distance vision, especially with small pupil sizes (around 2 mm). For higher pupil diameters, the area of the pupil is covered equally by far and near vision corrections, ensuring reasonable contrast for both far and near images. Dual Focus (B) provides a clear dominance for far focus with different pupil diameters. Purevision Multifocal (C) and Airoptix (D) become strongly biased towards distance correction as the pupil diameter increase. The design of these multifocal contact lenses (C and D) differs in the transition zone between near and distance vision.

4. Simultaneous Image

In simultaneous image contact lenses, the resultant image is a sharp image (in-focus) superimposed on a blurred background from the out-of-focus images, and it is expected that patients are able to progressively adapt to this simultaneous image situation [48]. However, this blurred background is sometimes described as ghost images or halo by patients. Figure 3 illustrates the Snellen E-letter for a theoretical diffraction-limited eye (top) and an aspheric-based design with +0.25 spherical aberration (bottom) from −1.75 to +1.75 diopters (D). This figure exemplifies the challenges potentially faced by subjects when viewing through multifocal simultaneous vision contact lenses (Figure 3 bottom). Beyond the function for which the lens is designed, either enhancing the depth of focus or halting myopia progression, the device has to provide functional visual acuity at different target distances either without accommodation or with minimal residual accommodation in the older presbyopic eye or couple with the subjects accommodation in the case of the younger eye in myopia control devices.

Multifocal contact lenses relay strongly on centration in the pupil and pupil size variations with luminance and/or aging (note that only rays of light of the multifocal pattern transmitted through the pupil are relevant to the visual performance). Figure 4 illustrates the through-focus Visual Strehl of the theoretical diffraction-limited eye and the aspheric-based design for different environmental light levels (from high-photopic 1000 cd/m^2 to mesopic 1 cd/m^2). The theoretical performance of the aspheric-based design shows a depth of focus of 2.5 D under high-photopic conditions (for 4 mm pupil diameter) but is limited to 1.0 D for low-photopic conditions and under the threshold in mesopic environmental light levels.

In addition to these limitations, multifocality and blur tolerance vary substantially across individuals due to ocular aberrations and neural adaptation. Therefore, understanding the coupling effect between the contact lens design, ocular optics, and visual adaptation is essential to explain the mechanism of action of a specific multifocal design for presbyopia and myopia applications.

4.1. Evaluation of the Visual Performance in Simultaneous Image Designs. Most clinical studies with multifocal contact lenses are limited to reports of through-focus visual acuity and contrast sensitivity, generally aiming at a depth of focus analysis and the improvement in near vision without compromising distance visual acuity. Aberrometry is an important clinical tool for objective evaluation of the image quality and visual performance prediction; however, due to the coupling of the phase of concentric multifocal designs there are some technical difficulties in the wavefront reconstruction of current sensors (true ocular aberrations and the power distribution in the pupil area), requiring an accurate reconstruction method for a proper combination of the wavefront slopes estimated at far and near distances [49]. Recently, theoretical visual simulations in eye models with multifocal designs and experimental visual simulators have shown the theoretical and real visual performance of different lens designs.

Computational models revealed that the multifocal benefit varied with the number of multifocal zones, showing

Figure 3: Illustration of the phase pattern and through-focus theoretical simulations of the Snellen E-letter of 30 arc-min for 4 mm pupil diameter (from −1.5 to +1.5). Top: diffraction-limited eye; bottom: aspheric-based design (spherical aberration: +0.25 μm).

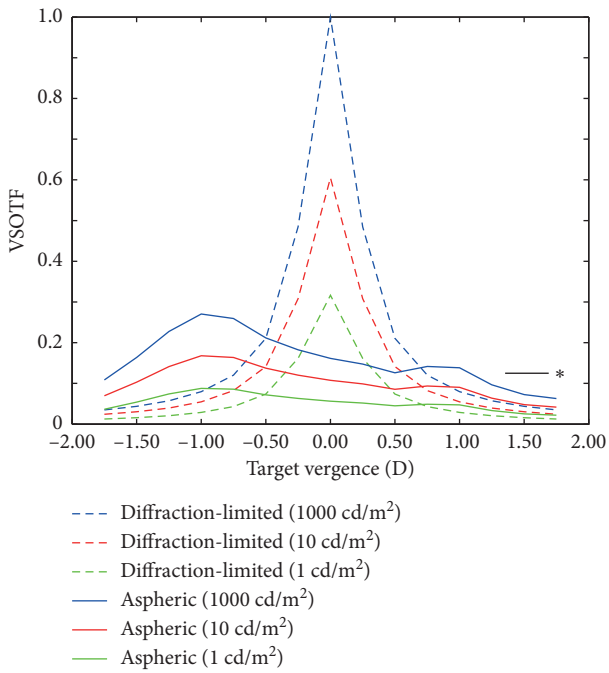

Figure 4: Through-focus Visual Strehl for the theoretical diffraction-limited eye (dashed) and the aspheric design (solid) for 4 mm pupil diameter and different light level conditions: 1000 cd/m^2, 10 cd/m^2, and 1 cd/m^2. * Threshold for acceptable vision.

that multiple refractive zone concentric rings (up to 3-4) were more robust in expanding the depth of focus for different pupil sizes than two-zone designs [50]. However, unlike theoretical models, experimental visual simulators incorporate both ocular optics and neural factors, showing visual testing of different multifocal patterns and offering patients a direct visual experience before fitting a specific multifocal contact lens design. These simulators are based on adaptive optics elements (deformable mirrors or spatial light modulators [51–53]) or temporal multiplexing (e.g., SimVis technology [54–56]) and work by projecting the theoretical multifocal pattern design onto the patient´s pupil plane, allowing us to evaluate the effect of different distance-near pupillary distribution and to test directly the visual performance. Recent studies have demonstrated that the through-focus visual performance with the same multifocal pattern varied across individuals, indicating that the specific performance of the design is highly patient-specific since not all patients tolerate well the out-of-focus image components in simultaneous vision [55]. de Gracia et al. [50] showed that the amount of near addition affected visual acuity differently, with the largest decrease for intermediate additions (around 2D). In addition, Radhakrishnan et al. [57] demonstrated that the perceived visual quality under simultaneous vision is affected by both the near addition magnitude and the distance-near energy ratio, showing maximal perceptual degradation at around 0.5D additions. Dorronsoro et al. [48, 55] found that bifocal rotationally asymmetric designs outperform other designs in real subjects. Different studies have also shown that there is an adaptation to the amount and orientation of blur caused by high-order aberrations [58, 59]. Interestingly, different patients preferred different orientations of the multifocal pattern (specifically, for angular designs [60, 61]) and this subjective orientation preference was predicted by ocular aberrations [48].

5. Patient Selection Criteria

This section intends to discuss the ocular factors that affect the performance of multifocal devices. The frequency of selecting a multifocal correction for presbyopia correction or in myopia progression control, as well as the number of designs commercially available, is rapidly increasing. However, the adaptation of multifocal contact lenses is still challenging for patients and practitioners. The problem is more complicated than coupling the multifocal design of the lens and an average value of spherical aberration for the eye (e.g., +0.25 μm), as one needs to consider other critical factors for considering the optimum optical design for presbyopia or myopia application: *pupil diameter* (especially, variations with accommodation, aging, and lighting levels); *ocular changes with accommodation and aging* (in particular, the magnitude and sign of astigmatism and/or spherical aberration); the *on-eye performance* (since depending on the ocular aberrations the lens design could add other ocular aberrations or subtract them); and the *tear film dynamics* (with aging there is a generalized decrease of tear production and stability).

5.1. Pupil Diameter. Winn et al. [62] investigated the variation in pupil size over a large range of age and luminance levels, showing that the pupil size becomes smaller in an almost linear manner with increasing age (see Figure 16 at ref. [32]). The typical pupil diameter for a luminance level of approximately 220 cd/m^2 in subjects between 20 and 29 years is around 5.5 mm, in subjects between 50 and 59 years

old is around 4.5 mm, and in subjects between 70 and 79 years is around 3.5 mm. The average presbyopic pupil size for distance vision is below 5.00 mm in diameter under any light conditions, and a pupil diameter higher than 6.00 mm would be expected with younger presbyopes and under low lighting conditions. As mentioned above, the pupil diameter changes with the accommodation, so that the near pupil is smaller than the distance pupil. This fact is more relevant in younger subjects than in presbyopic subjects where the ability to accommodate is reduced. The reduced pupil diameter has the potential disadvantage of leading to lower retinal illuminance that affects the visual performance under low levels of illumination. However, smaller pupils have the advantage of producing an increasing depth of focus and better visual performance at distance because the peripheral less-focused light is excluded. Furthermore, although the high-order aberrations increase with age, its impact is attenuated when the pupil size decreases. In addition to the effect of pupil size on light transmission, the pupil size also may influence the effectiveness of the photoreceptor function due to the directional sensitivity of the photoreceptors (Stiles-Crawford effect). Despite its retinal origin, it may be regarded as effectively because of apodization at the pupil plane; so the rays passing through the pupil periphery have lower transmission in comparison to the central pupil. The potential benefits of the Stiles-Crawford effect are greatest with large pupils, while pupils smaller than 4 mm tend to minimize this effect affecting the retinal image quality significantly. So, the reintroduction of pupil transmission apodization is considered as an option to improve the through-focus retinal image quality [63–66]. Zheleznyak et al. [67] demonstrated that the pupil's periphery contains near addition power for positive spherical aberration, similar to center-distance designs. As a result, presbyopic eyes with negative spherical aberration improved with pupil transmission apodization.

5.2. Ocular Aberrations. Because of structural changes in the crystalline lens (shape, position, and refractive index) that occur during accommodation, wave aberrations are expected to change. Spherical aberration has been reported to shift towards negative values, and different studies also showed changes in coma, trefoil, and astigmatism, but the direction of the change was variable [68–73]. With aging, the optical performance of the eye also changes. Due to the disruption of the compensatory effect between the anterior cornea and the internal aberrations, there is an increase in high-order aberrations. In particular, the spherical aberration and horizontal coma tend to increase in older eyes [74]. Tabernero et al. [75] showed that the RMS of the higher-order ocular and corneal aberrations increased with age at a rate of 0.0032 μm/year and 0.0015 μm/year, respectively. In this study, the authors did not observe changes in the optical alignment with age (i.e., the angle kappa remains stable), assuming, therefore, that variations in the crystalline lens shape with age might explain most of the increment of ocular aberrations. Interestingly, it has been also demonstrated that the optical quality could be improved by adding certain amounts of spherical aberration to a given level of defocus, as well as specific amounts of astigmatism and coma can interact favorably to increase the depth of focus while minimizing the decrease of visual acuity [76, 77]. Therefore, the aberrations of individual eyes will determine the effectiveness of a multifocal correction and the achieved depth of focus.

5.3. Off-Axis Ocular Aberrations. A comparison between refractive groups shows that myopic eyes have more relative peripheral defocus as well as a prolate retinal shape than emmetropic and hypermetropic eyes. However, substantial differences in relative peripheral refraction for different degrees of myopia appear at high eccentricities of the visual field. The horizontal meridian is more myopic than the vertical meridian. The largest off-axis optical aberrations are represented by oblique astigmatism, which is induced by the oblique angle, and coma, showing little difference between refractive groups. The spherical aberration is more positive for hyperopes than for myopes and emmetropes [78–80].

5.4. On-Eye Contact Lens Performance. When a contact lens is placed on the eye, there is an interaction between the lens design and the patients' native aberrations. One of the most common options used to expand the depth of focus is by modulating the magnitude of the spherical aberration. Multifocal center-near designs commonly have a negative spherical aberration; however, there is wide individual variability in the spherical aberration coefficient across the population. Therefore, it is possible to find similar values of ocular spherical aberrations but opposite in sign in comparison to the lens design, reducing or cancelling the expected depth of focus [81–85]. Also, the on-eye performance of the contact lens may induce aberrations due to decentration [86]. As multifocal contact lens designs become more complex, centration is more critical. Decentration is due to lens flexure or fitting results in an induction of astigmatism and coma, with this induction being proportional to the amount of decentration. Likewise, decentration of a multifocal design with a higher magnitude of spherical aberration will produce higher magnitude of inducing astigmatism and coma; this could be of practical significance since many contact lenses wearers have their astigmatism uncorrected. The connection between spherical aberration and coma and the possibility of balancing coma by modulation of aspheric designs are recognized in the classic Seidel aberration theory; so, luckily to date, there are some strategies that modulate the optical surfaces to decrease the impact of decentration (e.g., aspheric balance curve) [87]. Furthermore, with binocular viewing multifocal concentric designs showed temporal decentration, supporting the strategy of asymmetrical concentric multifocal design to coincide with the line of sight [88–90].

5.5. Tear Film. Changes in the tear fluid dynamics can induce changes in high-order aberrations [91–94]. Koh et al. [91, 95] demonstrated that during dynamic aberrometry (10

seconds after blinking), most of the clinically normal subjects showed fluctuations in the high-order aberration pattern, with these fluctuations being higher in patients with tear film instability and ocular surface damage.

5.6. Accommodation. The interactions between the multifocal designs and the subject´s accommodative response should be considered to evaluate the visual performance in the myopia control application.

6. Performance of Contact Lenses for Presbyopia Correction

Evaluating the performance of contact lenses for presbyopia correction requires different levels of analysis, including the assessment of visual acuity at different distances/vergences, contrast sensitivity function under different lighting levels, stereoacuity, and the occurrence of subjective complains related to dysphotopsia [96]. For clarity, the binocular visual performance is presented in this section. The monocular performance is usually worse and, in some cases, asymmetric between dominant and nondominant eye, with possible implications in stereoacuity [97].

6.1. Visual Acuity. High and low contrast LogMAR visual acuity has become the standard for clinical visual performance assessment during the last ten years (see Table 1). The results from Fernandes et al. [97] showed better high contrast visual acuity (HCDVA) compared to previous studies with Proclear multifocal [99] while high contrast near visual acuity (HCNVA) was comparable to previous results reported by Ferrer-Blasco and Madrid-Costa [106] and slightly better than monovision fitting with the single vision Proclear lens. Gupta et al. [99] compared a multifocal contact lens (Purevision multifocal) against monovision and showed a slightly poorer performance for monovision in terms of distance visual acuity as in our study. The present sample is very similar to that study in terms of sample size and procedures. Similar results to those reported by Gupta et al. [99] and from Fernandes et al. [97] have been reported by Richdale et al. [98] for Monovision compared to multifocal soft contact lenses (SofLens Multifocal, B&L). Those authors also measured high and low contrast distance and near LogMAR visual acuity also presenting the values for spectacle correction (Baseline). Results from Fernandes et al. [97] were within ±1 line of their reported VA for all the experimental conditions except for Monovision under near low contrast visual acuity (LCNVA), which performed better than Multifocal lens in their study. Recently, several clinical studies also evaluated visual performance with different contact lenses [103–105, 107]. Bakaraju et al. [103] measured the high contrast visual acuity (HCVA) and the low contrast visual acuity (LCVA) for the Airoptix Aqua, the Acuvue Oasys and extended depth of focus (EDOF) contact lens. They found that the EDOF provided better intermediate and near visual performance, with no difference for distance vision in comparison with the other multifocal contact lens designs. In a different study, Diec et al. [107] investigated if the initial multifocal contact lens performance predicts short-term dispensing performance, but their results were not able to predict the short-term performance of a multifocal contact lens.

6.2. Contrast Sensitivity Function. Contrast sensitivity function has been recorded in different studies with different instruments, being a remarkable limitation due to the lack of comparability among them [108]. More recently, the Functional Acuity Contrast Test (F.A.C.T) housed on a Functional Visual Analyzer machine (StereoOptical Co. Inc., Chicago, IL) for spatial frequencies of 1.5, 3, 6, 12, and 18 cycles/degree has been increasingly used. This device allows a systematic control of distance of examination and luminance conditions and has proved to report comparable values to Vision Contrast Test System VCTS 6500 (Vistech Consultants, Dayton, OH) in the same study. A summary of different studies reporting binocular distance contrast sensitivity is presented in Table 2.

In a study conducted by Fernandes et al. [97], it was remarkable that in spite of the good vision that Monovision patients have at distance in the dominant eye, they do not perform better than Biofinity MF after 15 days of lens wear. Similar results have been reported for distance vision with Distance contrast sensitivity function (CSF) at 3 m using the VCTS 6500 by Gupta et al. [99] comparing a multifocal contact lens and Monovision.

Llorente-Guillemot et al. [101] and Madrid-Costa et al. [102] measured the contrast sensitivity under photopic as well as mesopic conditions and found an overall decay. The loss of sensitivity was in the range of 0.25 LogCS units for lower frequencies of 1.5 and 3 cpd and 0.05 to 0.10 for medium frequencies of 6 and 12 cpd. Interestingly, it was under the mesopic conditions where the lenses under comparison presented statistically significant differences. For example, Madrid-Costa et al. [102] did not find significant differences between Acuvue Oasys and Purevision under photopic conditions but did for mesopic conditions at 6, 12, and 18 cpd where the Purevision lens performed significantly better. Llorente-Guillemot et al. [101] showed that the presence of glare could decrease further the performance of Purevision multifocal compared to spectacle correction.

Different authors have also measured the CSF at near for presbyopic patients wearing contact lens correction for presbyopia, and these results are presented in Table 3. When compared with distance values of CS, some authors found similar values between distance and near as in the case of Llorente-Guillemot et al. [101] while others found systematically higher values for low and medium frequencies at distance while found higher CS values at the higher frequency (18 cpd) at near [99]. Madrid-Costa et al. [102] using the same measuring device, obtained much lower values of CS for the low and medium frequencies at near and similar values for the highest frequencies of 12 and 18 cpd. Differences in the control of the near distance, ambient illumination, age of the patients, and the impact of different lens designs used, might explain such a diversity of trends when

Table 1: Summary of results of recent studies evaluating the photopic binocular high and/or low contrast visual acuity at distance (4 to 6 m) and near (33 to 40 cm) in presbyopic patients fitted with simultaneous image contact lenses. Visual acuity is expressed in LogMAR units.

Author (year)	Lens type/ fitting	n (Rx) (age)	Distance high contrast (LogMAR)	Distance low contrast (LogMAR)	Near high contrast (LogMAR)	Near low contrast (LogMAR)
Richdale et al. (2006) [98]	Monovision SofLens 59 MF	38 (−0.81 ± 0.10) (50.11 ± 4.70)	−0.10 ± 0.10 −0.12 ± 0.09	0.08 ± 0.15 0.08 ± 0.15	−0.03 ± 0.09 0.01 ± 0.12	0.14 ± 0.10 0.21 ± 0.14
Gupta et al. (2009) [99]	Monovision Purevision MF	20 (−1.42 ± 2.87) (55.0 ± 5.1)	−0.01 ± 0.07 0.05 ± 0.08		0.11 ± 0.11 0.21 ± 0.13	
García-Lázaro et al. (2012) [100]	Monovision Pinhole	22 (0.11 ± 0.12) (57.3 ± 5.8)	0.00 ± 0.09 0.02 ± 0.04	0.13 ± 0.12 0.16 ± 0.06	0.08 ± 0.16 0.40 ± 0.19	
Llorente-Guillemot et al. (2012) [101]	Spectacles Purevision MF	20 (−1.42 ± 2.87) (53.2 ± 5.3)	−0.05 ± 0.07 −0.01 ± 0.03	0.10 ± 0.06 0.18 ± 0.05	−0.08 ± 0.06 −0.02 ± 0.05	
Madrid-Costa et al. (2013) [102]	Purevision MF Oasys MF	20 (+0.35 ± 1.78) (45.1 ± 2.3)	0.00 ± 0.08 0.01 ± 0.08	0.11 ± 0.09 0.20 ± 0.58	0.15 ± 0.08 0.20 ± 0.05	
Fernandes et al. (2013) [97]	Monovision Biofinity MF	20 (−0.91 ± 2.25) 48.7 ± 3.3	−0.08 ± 0.09 −0.09 ± 0.08	0.11 ± 0.08 0.11 ± 0.06	0.05 ± 0.10 0.04 ± 0.07	0.23 ± 0.12 0.21 ± 0.09
Bakaraju et al. (2018) [103]	Airoptix Oasys MF EDOF	43 (−0.65 ± 0.88) (53 ± 5)	−0.07 ± 0.08 −0.06 ± 0.08 −0.07 ± 0.06	0.22 ± 0.10 0.27 ± 0.09 0.27 ± 0.10	0.13 ± 0.13 0.12 ± 0.11 0.10 ± 0.11	
Sha et al. (2016) [104]	Airoptix Oasys MF	42 (−0.35 ± 0.80) (58 ± 6)	−0.04 ± 0.06 −0.02 ± 0.09	0.28 ± 0.08 0.31 ± 0.12	0.48 ± 0.20 0.52 ± 0.22	
Tilia et al. (2017) [105]	Airoptix EDOF	41 (−0.6 ± 0.70) (53 ± 6)	−0.06 ± 0.05 −0.06 ± 0.05	0.25 ± 0.10 0.24 ± 0.04	0.48 ± 0.22 0.42 ± 0.18	

Table 2: Summary of results of recent studies evaluating the photopic binocular distance CSF in presbyopic patients wearing contact lenses for presbyopia correction. Units are LogCS.

Author (year)	Lens type/ fitting	*n* (Rx) (age)	LogCS (1.5 cpd)	Log CS (3 cpd)	Log CS (6 cpd)	Log CS (12 cpd)	Log CS (18 cpd)
Gupta et al. (2009) [99]	Monovision Purevision MF	20 (−1.42 ± 2.87) (55.0 ± 5.1)	1.75 1.75	1.89 1.93	1.77 1.74	1.33 1.12	0.68 0.65
García-Lázaro et al. (2012) [100]	Monovision Pinhole	22 (0.11 ± 0.12) (57.3 ± 5.8)	1.49 1.40	1.69 1.64	1.46 1.41	0.94 0.90	0.63 0.60
Llorente-Guillemot et al. (2012) [101]	Spectacles Purevision MF	20 (−1.42 ± 2.87) (53.2 ± 5.3)	1.51	1.76	1.69	1.28	0.67
Madrid-Costa et al. (2013) [102]	Purevision MF Oasys MF	20 (+0.35 ± 1.78) (45.1 ± 2.3)	1.63 1.54	1.73 1.73	1.35 1.33	1.09 1.07	0.7 0.67
Bakaraju et al. (2018) [103]	Airoptix Oasys MF EDOF	43 (−0.65 ± 0.88) (53 ± 5)			1.47 1.44 1.44	1.26 1.21 1.21	1.01 0.92 0.95

trying to compare distance and near values of CS among studies.

6.3. Steroacuity. Stereoacuity is relevant in presbyopia correction with contact lenses because some modalities, as monovision, affect the ability of both eyes to work together in an effective way to the highest level of binocularity and stereoscopic perception. In a study conducted by Fernandes et al. [97] in 20 presbyopes wearing Biofinity single vision lenses for monovision and Biofinity Multifocal, stereoacuity was obtained with the Stereo Fly SO-001 (StereoOptical Co, Inc., Chicago, IL). There were statistically significant differences in stereopsis between both modalities being worse for Monovision, as expected ($p = 0.002$). Furthermore, values for this parameter in the Monovision group were quite scattered with patients showing much worse outcomes than others. Such differences between groups remained even after 15 days of adaptation. Values for multifocal lenses after 15 days were very similar to those obtained by previous authors with other multifocal lenses using other tests [106] and with Proclear Multifocal using the same test [109]. The

Table 3: Photopic binocular near contrast sensitivity function for different studies. See also Table 2 for comparison with distance outcomes for the same studies. Units are LogCS.

Author (year)	Lens type/ fitting	n (Rx) (age)	Log CS (1.5 cpd)	Log CS (3 cpd)	Log CS (6 cpd)	Log CS (12 cpd)	Log CS (18 cpd)
Gupta et al. (2009) [99]	Monovision Purevision MF	20 (−1.42 ± 2.87) (55.0 ± 5.1)	1.62 1.58	1.73 1.73	1.60 1.53	1.19 1.10	0.80 0.70
García-Lázaro et al. (2012) [100]	Monovision Pinhole	22 (0.11 ± 0.12) (57.3 ± 5.8)	1.52 1.48	1.60 1.43	1.49 1.21	1.09 0.79	0.85 0.60
Llorente-Guillemot et al. (2012) [101]	Spectacles Purevision MF	20 (−1.42 ± 2.87) (53.2 ± 5.3)	1.54	1.62	1.63	1.21	0.60
Madrid-Costa et al. (2013) [102]	Purevision MF Oasys MF	20 (+0.35 ± 1.78) (45.1 ± 2.3)	1.37 1.30	1.59 1.54	1.24 1.12	1.05 0.96	0.67 0.60

Table 4: Summary of results of recent studies evaluating stereoacuity with different methods in presbyopic patients wearing simultaneous image multifocal and bifocal soft contact lenses. The unit of stereoacuity is seconds of arc (arcsec).

Author (year)	Lens type/fitting	n (Rx) (age)	Method (s)	Stereoacuity (arcsec)
Richdale et al. (2006) [98]	Monovision SofLens 59 MF	38 (−0.81 ± 0.10) (50.11 ± 4.70)	Randot Preschool stereoacuity test	205 ± 214 126 ± 137
Gupta et al. (2009) [99]	Monovision Purevision MF	20 (−1.42 ± 2.87) (55.0 ± 5.1)	TNO random dot stereogram test	273 ± 102 174 ± 95.2
García-Lázaro et al. (2012) [100]	Monovision Pinhole	22 (0.11 ± 0.12) (57.3 ± 5.8)	Howard-Dolman system	210 ± 49 221 ± 32
Fernandes et al. (2013) [97]	Monovision Biofinity MF	20 (−0.91 ± 2.25) 48.7 ± 3.3	Stereo Fly SO-001	105 ± 95 51 ± 67
Bakaraju et al. 2018 [103]	Airoptix Oasys MF EDOF	43 (−0.65 ± 0.88) (53 ± 5)	Stereo Fly test Circles	97 ± 129 74 ± 63 61 ± 37
Sha et al. (2016) [104]	Airoptix Oasys MF	42 (−0.35 ± 0.80) (58 ± 6)	Stereo Fly test Circles	148 ± 131 100 ± 84
Tilia et al. (2017) [105]	Airoptix EDOF	41 (−0.6 ± 0.70) (53 ± 6)	Stereo Fly test Circles	141 ± 114 98 ± 88

main results of several recent studies are summarized in Table 4.

Overall, it can be observed that all simultaneous image multifocal and bifocal soft contact lenses provide a good level of stereoacuity while monovision significantly impairs this function. Moreover, the effect of monovision in stereoacuity seems to remain unchanged after 15 days wearing the modality, which suggests that if stereoacuity improves over time with monovision, this is not likely to happen in the short term.

6.4. Through-Focus Performance. Through-focus performance is reported in the so-called defocus curves, which provide information on the visual performance of the presbyopic patient at different vergence distances. While used extensively in clinical research related to surgical solutions for presbyopia [110], it has not been until recently that these metrics have been more intensively applied to the assessment of multifocal contact lenses.

We have to differentiate the through-focus performance of through-focus curves from the depth of focus (DoF), which is the ability of the eye to see objects in a relatively wide range of vergences or distances without changing the accommodation. This phenomenon has been extensively reviewed by Wang and Ciuffreda [111] and their work provides relevant information that might also apply in the context of multifocal contact lens performance because, if the DoF changes with age, pupil size, or other factors associated with the ageing process of the human eye, this might also affect the performance of the patients and this might limit our ability to discriminate which part of the improvement effect with a certain contact lens is associated with the optics of the lens itself or to the DoF of the patient. According to the summary, they provide in Table 5 the average DoF of the eye ranges from 0.13 to 0.5 D approximately. Their summary of information also shows that for the majority of studies dealing with different variables, DoF increases with ageing and is better for smaller pupil sizes. Both factors will certainly play a role in the performance of presbyopes with multifocal contact lenses and highlight the importance of the pupil size in multifocal contact lens performance.

Table 5: Results from the defocus curves obtained with different contact lenses in different studies. The approximate values have been extracted from the graphs presented by the authors for 0.0 D of vergence (distance), 1.0 D (1 meter), 1.5 D (67 cm), 2.5 D (40 cm), and 3.0 D (33 cm). Units are presented in LogMAR values. Above the shaded row are presented baseline data for no lens situation. Note that Plainis et al.'s [90] study has been performed on young people under cycloplegia.

Author (year)	Lens type/ fitting	n (Rx) (age)	VA 0.0 D (distance)	VA −1.0 D (1 meter)	VA −1.5 D (67 cm)	VA −2.5 D (40 cm)	VA −3.0 D (33 cm)
Kingston and Cox (2013) [112]	Baseline (no lens)	64 eyes presbyopes	0.00	0.05	0.20	0.45	0.60
Plainis et al. (2013) [90]	Naked eye Monocular 3 mm pupil 6 mm pupil	12 (−2.24 ± 2.12) (27 ± 5) cyclopleged	 −0.10 −0.10	 0.0 0.5	 0.10 0.20	 0.32 0.36	 0.42 0.52
Plainis et al. (2013) [90]	Naked eye Binocular 3 mm pupil 6 mm pupil	12 (−2.24 ± 2.12) (27 ± 5) cyclopleged	 −0.15 −0.15	 0.0 0.0	 0.18 0.22	 0.30 0.32	 0.48 0.52
Gupta et al. (2009) [99]	Monovision Purevision MF	20 (−1.42 ± 2.87) (55.0 ± 5.1)	0.0 0.05	0.02 0.04	0.05 0.05	0.18 0.24	0.32 0.40
Madrid-Costa et al. (2012) [113]	Proclear MF toric	20 (−0.51 ± 2.01) (50.4 ± 7.8)	0.0	0.02	0.05	0.18	0.35
García-Lázaro et al. (2012) [114]	Monovision Pinhole	22 (0.11 ± 0.12) (57.3 ± 5.8)	0.0 0.0	0.18 0.07	0.18 0.20	0.08 0.4	0.3 0.52
Plainis et al. (2013) [90]	Airoptix MF Binoc 3 mm LOW Binoc 3 mm MED Binoc 3 mm HIGH	12 (−2.24 ± 2.12) (27 ± 5) cyclopleged	 −0.15 −0.05 −0.04	 −0.05 −0.05 −0.05	 0.04 −0.06 −0.06	 0.24 0.10 0.02	 0.32 0.22 0.12
Plainis et al. (2013) [90]	Airoptix MF Binoc 6 mm LOW Binoc 6 mm MED Binoc 6 mm HIGH	12 (−2.24 ± 2.12) (27 ± 5) cyclopleged	 −0.10 −0.02 −0.02	 −0.02 −0.04 −0.02	 0.08 −0.02 −0.06	 0.30 0.10 0.05	 0.40 0.24 0.16
Madrid-Costa et al. (2013) [102]	Purevision MF Oasys MF	20 (+0.35 ± 1.78) (45.1 ± 2.3)	0.0 0.0	0.04 0.04	0.06 0.08	0.16 0.20	0.24 0.34
Bakaraju et al. 2018 [103]	Airoptix Oasys MF EDOF	43 (−0.65 ± 0.88) (53 ± 5)	−0.07 −0.06 −0.07		−0.03 0.00 −0.07		0.13 0.12 0.10
Tilia et al. (2017) [105]	Airoptix EDOF	41 (−0.6 ± 0.70) (53 ± 6)	−0.06 −0.06		0.13 0.12		0.48 0.42

The first references to the analysis of defocus curves in contact lenses are found in Bradley and coauthor's work, back in the 1990s [115]. They evaluated the through-focus performance in two subjects wearing a single vision, a 2-zone bifocal, and a diffractive bifocal contact lens by assessing the contrast sensitivity for a 6/9 (20/30) visual acuity letter over a range of +2 to −4 D of vergence, in 0.5 D steps. Their results showed an extension of the depth of focus with the bifocal refractive and diffractive contact lenses at the expense of an overall drop in contrast sensitivity at distance compared with the single vision lens. In one subject, the depth of focus was expanded from distance to a vergence of 2.5 D if a cut-off point is set at 0.6 log CS values [115].

Gupta et al. [99] showed that the defocus focus performance in early presbyopes between 45 and 55 years of age was similar between monovision and multifocal aspheric center-near lenses. Their results showed an average LogMAR visual acuity for monovision and multifocal lenses of 0.00 and 0.05 at distance, 0.05 and 0.05 at intermediate vision at 66.67 cm, and an average 0.32 and 0.40 at 33 cm (−3 diopters of vergence), respectively. Madrid-Costa et al. [102] evaluated the performance of two different refractive multifocal soft contact lenses with an aspheric center-near design (Purevision Multifocal) and a zonal concentric design (Acuvue Oasys for Presbyopia). Both lenses performed similarly for distance and intermediate distances, but the Purevision lens performed slightly better by half a line of visual acuity for near distance. Table 5 shows the results of different studies evaluating the defocus curves with different multifocal contact lenses.

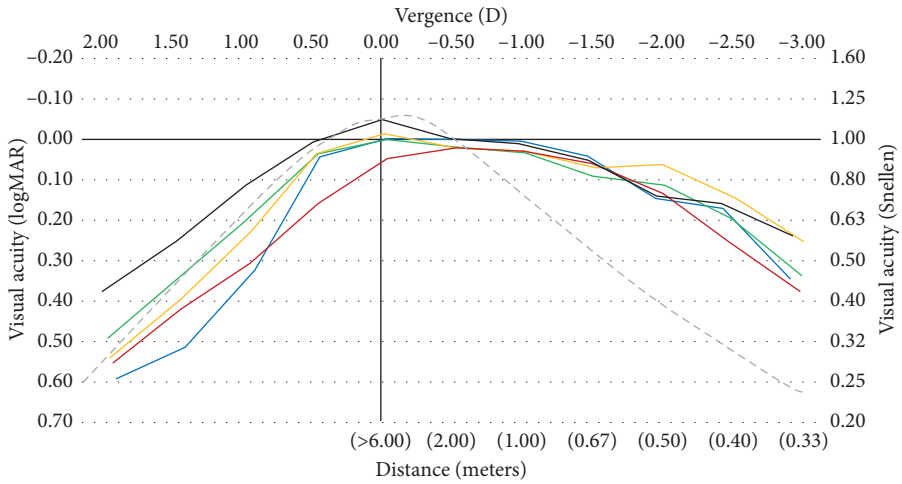

Figure 5: Reconstruction of the binocular defocus curves drawn at the same scale from different studies: red line: 20 subjects (49–67 years of age) fitted with Softlens multifocal (Gupta et al. [99]). Blue line: 20 subjects (age: 45–63 yrs) Proclear Toric Multifocal (Madrid-Costa et al. [113]). Orange line: 20 subjects (age: 42–48 yrs) Acuvue Oasys (Madrid-Costa et al. [102]). Green line: 20 subjects (age: 42–48 yrs) Acuvue Oasys presbyopia (Madrid-Costa et al. [102]). Black line: 38 subjects (age: 48–62 yrs) Proclear Multifocal (Garcia-Lázaro et al. [116]). Dashed grey line: expected performance for fully presbyopic eyes (unpublished data from CEORLab-UMinho).

According to the power distribution in multifocal contact lenses [37, 38] along with the computational predictions (see Figures 2 and 3), different multifocal contact lenses in the market should render significantly different performance. However, as seen in different studies, the clinically recorded through-focus curves are very similar (Figure 5). Interestingly while all the lenses give the same result for negative vergences, positive vergences render different results between different lenses. This might be related to the spherical aberration of the contact lenses and the ability to couple constructively with the positive spherical defocus to sustain or degrade vision as defocus increases. The common behavior for negative vergences might be the result of statistical regression to the mean for each vergence such that despite the different performances of different patients, the average behavior is very similar when compared between samples of different studies. Thought with some differences due to the ability to control several variables such as pupil size and aberration structure of synthetic eyes, similar results were found by Faria-Ribeiro et al. [117] when evaluating the through-focus performance of different contact lens designs. The same study confirms the variability of performance with varying pupil sizes and over and less than average spherical aberration. Altogether this confounding results point to the need to better match the lens design to the pupil size and remaining characteristics of the patient as described in the previous section regarding patient selection criteria. In the near future it should be possible to develop more sophisticated fitting algorithms that take into account all these variables.

7. Performance of Contact Lenses for Myopia Control

Considering the intended treatment, myopia control contact lenses have to prove efficacy in the reduction of axial elongation besides providing appropriate visual performance and safety. Till recently, the use of soft contact lenses for myopia control has been done off-label, and few have been subject to clinical trials to evaluate the longer-term efficacy of these devices. Those include two multifocal soft contact lenses for presbyopia correction used successfully to reduce myopia progression. Aller et al. [118] obtained a reduction of 72% in axial elongation in pediatric eyes wearing Acuvue Bifocal contact lens. Walline et al. [2] obtained a 29% reduction in axial elongation with Proclear Multifocal center-distance design in a pediatric population. Over the last 10 years, at least 5 different contact lenses specifically designed for myopia control in children have been subject to clinical trials. Those include peripheral gradient contact lenses that emulate the peripheral convergent power induced by orthokeratology [119], soft contact lenses that induce negative spherical aberration with the intended effect of improving accommodative response in myopic children [120], bifocal/dual-focus contact lenses with larger central zone devoted to distance vision [42, 121–123], and extended depth of focus contact lenses with alternating areas of positive and negative power modulated by inducing primary and secondary spherical aberration on the front surface of the contact lens ([119]; see also medium-add power design in Bakaraju et al. [103, 124] for further information about lens design). Table 6 presents a summary of some relevant aspects to be considered when evaluating the performance of bifocal and multifocal contact lenses for myopia control in children.

7.1. Visual Acuity and Dysphotopsia. Since a pediatric patient has generally full accommodation capability, near vision is not usually a concern in visual evaluation. However, the ghosting induced by some contact lens designs used for myopia control requires that near vision needs to be assessed. Other more sophisticated modes to evaluate vision

Table 6: Outcomes from clinical trials involving the use of bifocal/dual-focus and multifocal (including peripheral gradient and extended depth of focus) contact lenses for myopia control.

Author (year)	Lens design (trial duration, moths)	*N*	Axial growth (%)*	Binocular distance visual acuity	Binocular near visual acuity HC	Accomm.	Wearing time hours/day	Discont.	Adverse events
Anstice and Phillips (2011) [42]	DF (10 months)	T: 52 C: 56	0.10 mm 0.22 mm (−55%)	99.9 ± 3.5** 100 ± 2.9		No change	13.2 ± 2.8 11.9 ± 2.0	N.R	N.R
Allen et al. (2013) [120]	−SA (24)	T: 29 C: 30	0.15 0.16 (−6%)	N.R	N.R	Improves Acc flexibility	N.R	12/41 15/45	N.R
Walline et al. (2013) [2]	CDMF (24)	T: 27 C: 27	0.29 0.41 (−29%)	N.R	N.R	N.R	N.R	5/32 5/32	N.R
Lam et al. (2014) [125]	DISC (24)	T: 65 C: 63	0.25 0.36 (−31%)	N.R	N.R	N.R	6.5 ± 2.2 6.3 ± 1.7	46/111 47/110	N.R
Cheng et al. (2016) [126]	+SA (12)	T: 53 C: 59		0.06 ± 0.06 0.00 ± 0.08	N.R	N.R	N.R	53/64 50/63	N.R
Aller et al. (2016) [118]	CDBF (12)	T: 39 C: 40	0.05 0.24 (−79%)	N.R	N.R	N.R	N.R		N.R
Pauné et al. (2016) [11]	PG (24)	T: 19 C: 21	0.38 0.52 (−27%)	N.R	N.R	N.R	N.R	11/30 20/41	N.R
Ruiz-Pomeda et al. (2018) [127]	DF (24)	T: 41 C: 43	0.28 0.45 (−38%)	N.R	N.R	N.R	12.2 ± 1.8 11.8 ± 2.1	5/41 0/33	N.R
Sankaridurg et al. (2019) [119]	EDOF (24)	T: 43 C: 39	0.44 0.58 (−24%)	0.07	Visual clarity subjectively reported better than distance	N.R	N.R	28/73 28/78	N.R
Chamberlain et al. (2019) [123]	DF (36)	T: 52 C: 56	0.30 0.62 (−52%)	0.00 ± 0.10 N.R	−0.10 ± 0.08	N.R	13.7 ± 1.5 13.3 ± 1.5	12/65 14/70	No serious adverse events

*Axial length growth: defined as the % of growth in the test group compared to the control group $[(\Delta T - \Delta C)/\Delta C]$; negative value implies a benefit of the treatment. ** Visual Acuity Rating Scale (100 = 6/6). DISC: defocus incorporated contact lens, concentric refractive; EDoF: extended depth of focus, only Design III is considered–currently manufactured by mark'ennovy; PG: peripheral gradient; DF: bifocal concentric design with large central zone for distance vision; CDMF: center-distance multifocal for presbyopia; CDBF: center-distance bifocal for presbyopia; +SA: soft contact lens with the induction of positive spherical aberration; −SA: soft contact lens with the induction of negative spherical aberration; T: test device: C: control device; $\Delta T|\Delta C$: increment in treatment|control groups; HC: high contrast; LC: low contrast N.R: not reported; Accomm.: accommodation; Discont.: discontinuation.

should be used in the future as myopia control devices can induce some degree of dysphotopsia, particularly under dim lighting conditions [85, 127]. These complaints could worsen as the children evolve into young-adults, and they are exposed to situations where these complaints might be more noticeable with bifocal and multifocal contact lenses or even orthokeratology [128] such as night driving. Those results in the context of clinical trials as well as experimental studies conducted recently with different lens prototypes [129] reveal that for the pupil size of younger subjects, distance visual performance could not be compromised as measured with visual acuity charts as long as the lens preserves a significant proportion of the optic zone devoted to distance vision focus. These findings are compatible with the simulations presented in Figure 2(b) such that better distance performance is warranted for larger pupil sizes with the lens specifically designed for myopia control in children (dual-focus, MiSight, Coopervision).

7.2. Accommodation Function. Few studies have evaluated the accommodation and binocular vision balance in children undergoing myopia control treatments. In the context of the Cambridge Antimyopia Study, though improvements in accommodative efficiency were observed with soft contact lenses inducing negative spherical aberration, these devices were not successful in retarding axial elongation in teenagers [120]. Other studies reporting such results generally agreed that no significant changes are observed with peripheral gradient contact lenses [11], concentric dual-focus [42, 122], and defocus incorporated soft contact lens [125]. This is consistent with the computational calculations of Faria-

Ribeiro and González-Méijome [130], who found no visual advantage in using the near focus to see closer to the add power of the lens with the current designs of dual-focus lens. This is consistent with the wider area of distance vision in the contact lens with proximal miosis. Instead, some benefit in using the near focus of the lens if the central zone of the lens dedicated to distance vision was narrower. However, such undesirable effect, as underaccommodation at near vision, would result in hyperopic defocus for light refracting through the distance zone under such accommodation inhibition at near.

7.3. Ocular Length Retardation. Retardation of eye growth has been the main outcome in most clinical trials related to the use of contact lenses for myopia control. The effect varies from nearly 30% in some studies to over 70% in others [2, 118]. In some instances, the same device renders quite different efficacy results. However, we have to bear in mind that the current approach to myopia control with bifocal and multifocal lenses uses unique "treatment" parameters for the same device, and therefore the same "dose" is applied to all patients. As discussed for multifocal contact lenses for presbyopia and their similar performance for defocus curves, better patient-to-device selection algorithms could provide better results in the future. However, this will require a better understanding of the mechanisms governing the myopization process in young children and the mechanisms of action of optical devices that are able to control the ocular growth.

7.4. Adverse Events. Adverse events have been rarely found in the context of clinical trials involving pediatric populations wearing contact lenses for the purpose of myopia control for periods from 1 to 3 years. The attrition of patients to the study varies from over 80% in some studies to less than 60% in others [131]. However, this seems not to be related to the performance or safety of the contact lenses and most studies show that those discontinuing their participation do so for other aspects not related to adverse events.

8. Conclusions

Current bifocal and multifocal contact lens designs for presbyopia correction and myopia progression control are focused on providing a robust distance and near visual performance over a wide range of pupil sizes. However, considering the different purposes (presbyopia vs. myopia), ocular characteristics (young vs. adults), and neural adaptation, the bifocal and multifocal design of the contact lenses should evolve in different directions considering the significant difference in pupil sizes and the aberrometric profile of the potential candidates for presbyopia correction or myopia control. Presbyopia correction is now available over a diverse range of material platforms including soft, hybrid, corneal, and scleral rigid gas permeable contact lenses. Besides orthokeratology, performance with corneal rigid gas permeable contact lenses, myopia control evolves mainly in the soft contact lens materials with several lenses undergoing long-term clinical trials (2 or more years). While presbyopia correction with contact lenses accounts for up to 25 to 35% of the contact lens fittings in several countries [5], myopia control contact lens fittings are still limited to 2 to 5% of the contact lenses fitted [6]. Considering the positive results with the contact lenses evaluated in the studies summarized in this review, the demographic trends and the increase in myopia among the younger, it is expected that both fields of contact lens application experience an expansion in number and diversity of devices being produced, subjected to clinical trials and launched to the market over the next decade. This trend might be more significant in the myopia control field considering the yet low penetration and the fact that contact lenses offer a nonpharmacological, minimally invasive, and well-accepted form of treatment. On the other side, the presbyopic correction might increase more moderately as it shares a significant market with the surgical interventions, and spectacle correction will probably continue being the dominant option for the next years. It will be interesting to follow these trends to understand where the next years take the contact lens field, with these two applications being at the forefront of the evolution requiring more effective designs.

Conflicts of Interest

The authors declare that they do not have any proprietary or financial interest in any of the materials mentioned in this article.

Acknowledgments

LR gratefully acknowledges the financial support of the Ministerio de Economía y Competitividad, Project: (DPI2017-84047-R (MINICO-FEDER)). This research has received funding from the Spanish Government (DTS18/00107) to PPM; PPM also declares Personal Financial Interest (2EyesVision). This project was also supported by the Portuguese Foundation for Science and Technology (FCT) in the framework of projects PTDC/SAU-BEB/098392/2008 and PTDC/FIS-OPT/0677/2014 granted to JMG-M, the FCT Strategic Funding UID/FIS/04650/2013 granted to the Center of Physics, UMinho, and predoctoral grant SFRH/BD/136684/2018 to AA-S.

References

[1] E. S. Bennett, "Contact lens correction of presbyopia," *Clinical and Experimental Optometry*, vol. 91, no. 3, pp. 265–278, 2008.

[2] J. J. Walline, K. L. Greiner, M. E. McVey, and L. A. Jones-Jordan, "Multifocal contact lens myopia control," *Optometry and Vision Science*, vol. 90, no. 11, pp. 1207–1214, 2013.

[3] T. Hiraoka, T. Kakita, F. Okamoto, H. Takahashi, and T. Oshika, "Long-term effect of overnight orthokeratology on axial length elongation in childhood myopia: a 5-year follow-up study," *Investigative Opthalmology & Visual Science*, vol. 53, no. 7, pp. 3913–3919, 2012.

[4] P. Gifford and H. A. Swarbrick, "Refractive changes from hyperopic orthokeratology monovision in presbyopes," *Optometry and Vision Science*, vol. 90, no. 4, pp. 306–313, 2013.

[5] P. B. Morgan, N. Efron, C. A. Woods, and J. Santodomingo-Rubido, "International survey of orthokeratology contact lens fitting," *Contact Lens and Anterior Eye*, vol. 42, no. 4, pp. 450–454, 2019.

[6] N. Efron, P. B. Morgan, C. A. Woods, J. Santodomingo-Rubido, and J. J. Nichols, "International survey of contact lens fitting for myopia control in children," *Cont Lens Anterior Eye*, vol. 43, no. 1, pp. 4–8, 2020.

[7] E. Papadatou, A. J. Del Águila-Carrasco, J. J. Esteve-Taboada, D. Madrid-Costa, and A. Cerviño-Expósito, "Objective assessment of the effect of pupil size upon the power distribution of multifocal contact lenses," *International Journal of Ophthalmology*, vol. 10, no. 1, pp. 103–108, 2017.

[8] R. Rosén, B. Jaeken, A. Lindskoog Petterson, P. Artal, P. Unsbo, and L. Lundström, "Evaluating the peripheral optical effect of multifocal contact lenses," *Ophthalmic and Physiological Optics*, vol. 32, no. 6, pp. 527–534, 2012.

[9] R. Pérez-Prados, D. P. Piñero, R. J. Pérez-Cambrodí, and D. Madrid-Costa, "Soft multifocal simultaneous image contact lenses: a review," *Clinical and Experimental Optometry*, vol. 100, no. 2, pp. 107–127, 2017.

[10] J. Pauné, H. Morales, J. Armengol, L. Quevedo, M. Faria-Ribeiro, and J. M. González-Méijome, "Myopia control with a novel peripheral gradient soft lens and orthokeratology: a 2-year clinical trial," *BioMed Research International*, vol. 2015, Article ID 507572, 10 pages, 2015.

[11] J. Pauné, S. Thivent, J. Armengol, L. Quevedo, M. Faria-Ribeiro, and J. M. González-Méijome, "Changes in peripheral refraction, higher-order aberrations, and accommodative lag with a radial refractive gradient contact lens in young myopes," *Eye & Contact Lens: Science & Clinical Practice*, vol. 42, no. 6, pp. 380–387, 2016.

[12] Y. Sun, F. Xu, T. Zhang et al., "Orthokeratology to control myopia progression: a meta-analysis," *PLoS One*, vol. 10, no. 4, Article ID e0124535, 2015.

[13] J. Huang, D. Wen, Q. Wang et al., "Efficacy comparison of 16 interventions for myopia control in children: a network meta-analysis," *Ophthalmology*, vol. 123, no. 4, pp. 697–708, 2016.

[14] S.-M. Li, M.-T. Kang, S.-S. Wu et al., "Efficacy, safety and acceptability of orthokeratology on slowing axial elongation in myopic children by meta-analysis," *Current Eye Research*, vol. 41, no. 5, pp. 600–608, 2016.

[15] S.-M. Li, M.-T. Kang, S.-S. Wu et al., "Studies using concentric ring bifocal and peripheral add multifocal contact lenses to slow myopia progression in school-aged children: a meta-analysis," *Ophthalmic and Physiological Optics*, vol. 37, no. 1, pp. 51–59, 2017.

[16] E. Prousali, A. B. Haidich, A. Fontalis, N. Ziakas, P. Brazitikos, and A. Mataftsi, "Efficacy and safety of interventions to control myopia progression in children: an overview of systematic reviews and meta-analyses," *BMC Ophthalmology*, vol. 19, no. 1, p. 106, 2019.

[17] E. van der Worp, L. Johns, and M. Barnett, "Scleral schism," *Contact Lens and Anterior Eye*, vol. 42, no. 1, pp. 1-2, 2019.

[18] P. Rosenthal and A. Croteau, "Fluid-ventilated, gas-permeable scleral contact lens is an effective option for managing severe ocular surface disease and many corneal disorders that would otherwise require penetrating keratoplasty," *Eye & Contact Lens: Science & Clinical Practice*, vol. 31, no. 3, pp. 130–134, 2005.

[19] F. Alipour, A. Kheirkhah, and M. J. Behrouz, "Use of mini scleral contact lenses in moderate to severe dry eye," *Contact Lens and Anterior Eye*, vol. 35, no. 6, pp. 272–276, 2012.

[20] E. van der Worp, D. Bornman, D. L. Ferreira, M. Faria-Ribeiro, N. Garcia-Porta, and J. M. González-Meijome, "Modern scleral contact lenses: a review," *Contact Lens and Anterior Eye*, vol. 37, no. 4, pp. 240–250, 2014.

[21] M. M. Schornack, "Scleral lenses: a literature review," *Eye & Contact Lens: Science & Clinical Practice*, vol. 41, no. 1, pp. 3–11, 2015.

[22] E.-S. Visser, B. J. J. J. Van der Linden, H. M. Otten, A. Van der Lelij, and R. Visser, "Medical applications and outcomes of bitangential scleral lenses," *Optometry and Vision Science*, vol. 90, no. 10, pp. 1078–1085, 2013.

[23] E.-S. Visser, R. Visser, and H. J. J. Van Lier, "Advantages of toric scleral lenses," *Optometry and Vision Science*, vol. 83, no. 4, pp. 233–236, 2006.

[24] L. Sorbara, J. Maram, D. Fonn, C. Woods, and T. Simpson, "Metrics of the normal cornea: anterior segment imaging with the Visante OCT," *Clinical and Experimental Optometry*, vol. 93, no. 3, pp. 150–156, 2010.

[25] L. Sorbara, J. Maram, and K. Mueller, "Use of the Visante OCT to measure the sagittal depth and scleral shape of keratoconus compared to normal corneae: pilot study," *Journal of Optometry*, vol. 6, no. 3, pp. 141–146, 2013.

[26] M. Ritzmann, P. J. Caroline, R. Börret, and E. Korszen, "An analysis of anterior scleral shape and its role in the design and fitting of scleral contact lenses," *Contact Lens and Anterior Eye*, vol. 41, pp. 205–213, 2017.

[27] R. J. Macedo-de-Araújo, E. van der Worp, and J. M. González-Méijome, "In vivo assessment of the anterior scleral contour assisted by automatic profilometry and changes in conjunctival shape after miniscleral contact lens fitting," *Journal of Optometry*, vol. 12, no. 2, pp. 131–140, 2019.

[28] D. P. Piñero, A. Martínez-Abad, R. Soto-Negro et al., "Differences in corneo-scleral topographic profile between healthy and keratoconus corneas," *Contact Lens and Anterior Eye*, vol. 42, no. 1, pp. 75–84, 2019.

[29] J. C. Lee, G. B. Chiu, D. Bach, S. R. Bababeygy, J. Irvine, and M. Heur, "Functional and visual improvement with prosthetic replacement of the ocular surface ecosystem scleral lenses for irregular corneas," *Cornea*, vol. 32, no. 12, pp. 1540–1543, 2013.

[30] J. J. Nichols and D. Fisher, "Contact lenses 2018," *Contact Lens Spectrum*, vol. 34, pp. 18–23, 2019.

[31] M. Barnett, "Multifocal scleral lenses 2015," *Contact Lens Spectrum*, vol. 30, pp. 26–31, 2015.

[32] W. N. Charman, "Developments in the correction of presbyopia I: spectacle and contact lenses," *Ophthalmic and Physiological Optics*, vol. 34, no. 1, pp. 8–29, 2014.

[33] P. B. Morgan and N. Efron, "Contact lens correction of presbyopia," *Contact Lens and Anterior Eye*, vol. 32, no. 4, pp. 191-192, 2009.

[34] E. Bennett, "Innovations in gas permeable multifocal contact lenses," *Clinical Optometry*, vol. 2, pp. 85–90, 2010.

[35] International Organization for Standardization (ISO), *Ophtalmic Optics-Contact Lenses, Part 1: Vocabulary, Classification System and Recommendations for Labelling Specifications*, ISO, Geneva, Switzerland, 2006.

[36] H. Toshida, K. Takahashi, K. Sado, A. Kanai, and A. Murakami, "Bifocal contact lenses: history, types, characteristics, and actual state and problems," *Clinical Ophthalmology*, vol. 2, no. 4, pp. 869–877, 2008.

[37] S. Plainis, D. A. Atchison, and W. N. Charman, "Power profiles of multifocal contact lenses and their interpretation," *Optometry and Vision Science*, vol. 90, no. 10, pp. 1066–1077, 2013.

[38] R. Montés-Micó, D. Madrid-Costa, A. Domínguez-Vicent, L. Belda-Salmerón, and T. Ferrer-Blasco, "In vitro power profiles of multifocal simultaneous vision contact lenses," *Contact Lens and Anterior Eye*, vol. 37, no. 3, pp. 162–167, 2014.

[39] S. Wagner, F. Conrad, R. C. Bakaraju, C. Fedtke, K. Ehrmann, and B. A. Holden, "Power profiles of single vision and multifocal soft contact lenses," *Contact Lens and Anterior Eye*, vol. 38, no. 1, pp. 2–14, 2015.

[40] E. Kim, R. C. Bakaraju, and K. Ehrmann, "Reliability of power profiles measured on NIMO TR1504 (Lambda-X) and effects of lens decentration for single vision, bifocal and multifocal contact lenses," *Journal of Optometry*, vol. 9, no. 2, pp. 126–136, 2016.

[41] J. Guispets, M. Arjona, J. Pujol, M. Vilaseca, and G. Cardona, "Task oriented visual satisfaction and wearing success with two different simultaneous vision multifocal soft contact lenses," *Journal of Optometry*, vol. 4, no. 3, pp. 76–84, 2011.

[42] N. S. Anstice and J. R. Phillips, "Effect of dual-focus soft contact lens wear on axial myopia progression in children," *Ophthalmology*, vol. 118, no. 6, pp. 1152–1161, 2011.

[43] J. Ruiz-Alcocer, "Analysis of the power profile of a new soft contact lens for myopia progression," *Journal of Optometry*, vol. 10, no. 4, pp. 266–268, 2017.

[44] A. Pérez-Escudero, C. Dorronsoro, and S. Marcos, "Correlation between radius and asphericity in surfaces fitted by conics," *Journal of the Optical Society of America A*, vol. 27, no. 7, pp. 1541–1548, 2010.

[45] D. Madrid-Costa, J. Ruiz-Alcocer, S. García-Lázaro, T. Ferrer-Blasco, and R. Montés-Micó, "Optical power distribution of refractive and aspheric multifocal contact lenses: effect of pupil size," *Contact Lens and Anterior Eye*, vol. 38, no. 5, pp. 317–321, 2015.

[46] International Organization for Standardization (ISO), *Ophtalmic Optics-Contact Lenses, Part 2: Tolerances*, ISO, Geneva, Switzerland, 2017.

[47] International Organization for Standardization (ISO), *Ophtalmic Optics-Contact Lenses, Part 3: Measurement Methods*, ISO, Geneva, Switzerland, 2017.

[48] C. Dorronsoro, A. Radhakrishnan, P. de Gracia, L. Sawides, and S. Marcos, "Perceived image quality with simulated segmented bifocal corrections," *Biomedical Optics Express*, vol. 7, no. 11, pp. 4388–4399, 2016.

[49] V. Akondi, P. Pérez-Merino, E. Martinez-Enriquez et al., "Evaluation of the true wavefront aberrations in eyes implanted with a rotationally asymmetric multifocal intraocular lens," *Journal of Refractive Surgery*, vol. 33, no. 4, pp. 257–265, 2017.

[50] P. de Gracia, C. Dorronsoro, and S. Marcos, "Multiple zone multifocal phase designs," *Optics Letters*, vol. 38, no. 18, pp. 3526–3529, 2013.

[51] E. J. Fernández, P. M. Prieto, and P. Artal, "Binocular adaptive optics visual simulator," *Optics Letters*, vol. 34, no. 17, pp. 2628–2630, 2009.

[52] C. Canovas, S. Manzanera, C. Schwarz et al., "Binocular performance of IOL combinations studied with a visual simulator," *Investigative Ophthalmology & Visual Science*, vol. 55, p. 4024, 2014.

[53] L. Hervella, E. A. Villegas, P. M. Prieto, and P. Artal, "Assessment of subjective refraction with a clinical adaptive optics visual simulator," *Journal of Cataract & Refractive Surgery*, vol. 45, no. 1, pp. 87–93, 2019.

[54] P. de Gracia, C. Dorronsoro, Á. Sánchez-González, L. Sawides, and S. Marcos, "Experimental simulation of simultaneous vision," *Investigative Opthalmology & Visual Science*, vol. 54, no. 1, pp. 415–422, 2013.

[55] C. Dorronsoro, A. Radhakrishnan, J. R. Alonso-Sanz et al., "Portable simultaneous vision device to simulate multifocal corrections," *Optica*, vol. 3, no. 8, pp. 918–924, 2016.

[56] M. Vinas, C. Benedi-Garcia, S. Aissati et al., "Visual simulators replicate vision with multifocal lenses," *Scientific Reports*, vol. 9, no. 1, p. 1539, 2019.

[57] A. Radhakrishnan, C. Dorronsoro, L. Sawides, and S. Marcos, "Short-term neural adaptation to simultaneous bifocal images," *PLoS One*, vol. 9, no. 3, Article ID e93089, 2014.

[58] P. Artal, L. Chen, E. J. Fernández, B. Singer, S. Manzanera, and D. R. Williams, "Neural compensation for the eye's optical aberrations," *Journal of Vision*, vol. 4, no. 4, pp. 281–287, 2004.

[59] L. Sawides, C. Dorronsoro, A. M. Haun, E. Peli, and S. Marcos, "Using pattern classification to measure adaptation to the orientation of high order aberrations," *PLoS One*, vol. 8, no. 8, Article ID e70856, 2013.

[60] M. Vinas, C. Dorronsoro, V. Gonzalez, D. Cortes, A. Radhakrishnan, and S. Marcos, "Testing vision with angular and radial multifocal designs using adaptive optics," *Vision Research*, vol. 132, pp. 85–96, 2017.

[61] P. de Gracia and A. Hartwig, "Optimal orientation for angularly segmented multifocal corrections," *Ophthalmic and Physiological Optics*, vol. 37, no. 5, pp. 610–623, 2017.

[62] B. Winn, D. Whitaker, D. B. Elliott, and N. J. Phillips, "Factors affecting light-adapted pupil size in normal human subjects," *Investigative Opthalmology & Visual Science*, vol. 35, pp. 1132–1137, 1994.

[63] W. Stiles and B. Crawford, "The luminous efficiency of rays entering the eye pupil at different points," *Proceedings of the Royal Society of London Series B*, vol. 112, no. 778, pp. 428–450, 1933.

[64] R. A. Applegate and V. Lakshminarayanan, "Parametric representation of Stiles-Crawford functions: normal variation of peak location and directionality," *Journal of the Optical Society of America A*, vol. 10, no. 7, pp. 1611–1623, 1993.

[65] X. Zhang, M. Ye, A. Bradley, and L. Thibos, "Apodization by the Stiles-Crawford effect moderates the visual impact of retinal image defocus," *Journal of the Optical Society of America A*, vol. 16, no. 4, pp. 812–820, 1999.

[66] D. A. Atchison, D. H. Scott, N. C. Strang, and P. Artal, "Influence of Stiles-Crawford apodization on visual acuity," *Journal of the Optical Society of America A*, vol. 19, no. 6, pp. 1073–1083, 2002.

[67] L. Zheleznyak, H. Jung, and G. Yoon, "Impact of pupil transmission apodization on presbyopic through-focus visual performance with spherical aberration," *Investigative Opthalmology & Visual Science*, vol. 55, no. 1, pp. 70–77, 2014.

[68] P. Artal and A. Guirao, "Contributions of the cornea and the lens to the aberrations of the human eye," *Optics Letters*, vol. 23, no. 21, pp. 1713–1715, 1998.

[69] L. Chen, P. B. Kruger, H. Hofer, B. Singer, and D. R. Williams, "Accommodation with higher-order monochromatic aberrations corrected with adaptive optics," *Journal of the Optical Society of America A*, vol. 23, no. 1, pp. 1–8, 2006.

[70] N. López-Gil, I. Iglesias, and P. Artal, "Retinal image quality in the human eye as a function of the accommodation," *Vision Research*, vol. 38, no. 19, pp. 2897–2907, 1998.

[71] N. López-Gil, F. J. Rucker, L. R. Stark et al., "Effect of third-order aberrations on dynamic accommodation," *Vision Research*, vol. 47, no. 6, pp. 755–765, 2007.
[72] E. Gambra, L. Sawides, C. Dorronsoro, and S. Marcos, "Accommodative lag and fluctuations when optical aberrations are manipulated," *Journal of Vision*, vol. 9, no. 6, p. 4, 2009.
[73] P. Pérez-Merino, M. Velasco-Ocana, E. Martinez-Enriquez, and S. Marcos, "OCT-based crystalline lens topography in accommodating eyes," *Biomedical Optics Express*, vol. 6, no. 12, pp. 5039–5054, 2015.
[74] P. Artal, E. Berrio, A. Guirao, and P. Piers, "Contribution of the cornea and internal surfaces to the change of ocular aberrations with age," *Journal of the Optical Society of America A*, vol. 19, no. 1, pp. 137–143, 2002.
[75] J. Tabernero, A. Benito, E. Alcón, and P. Artal, "Mechanism of compensation of aberrations in the human eye," *Journal of the Optical Society of America A*, vol. 24, no. 10, pp. 3274–3283, 2007.
[76] R. A. Applegate, C. Ballentine, H. Gross, E. J. Sarver, and C. A. Sarver, "Visual acuity as a function of Zernike mode and level of root mean square error," *Optometry and Vision Science*, vol. 80, no. 2, pp. 97–105, 2003.
[77] P. de Gracia, C. Dorronsoro, E. Gambra, G. Marin, M. Hernández, and S. Marcos, "Combining coma with astigmatism can improve retinal image over astigmatism alone," *Vision Research*, vol. 50, no. 19, pp. 2008–2014, 2010.
[78] D. A. Atchison, N. Pritchard, and K. L. Schmid, "Peripheral refraction along the horizontal and vertical visual fields in myopia," *Vision Research*, vol. 46, no. 8-9, pp. 1450–1458, 2006.
[79] L. Lundström, J. Gustafsson, and P. Unsbo, "Population distribution of wavefront aberrations in the peripheral human eye," *Journal of the Optical Society of America A*, vol. 26, no. 10, pp. 2192–2198, 2009.
[80] U. L. Osuagwu, M. Suheimat, and D. A. Atchison, "Peripheral aberrations in adult hyperopes, emmetropes and myopes," *Ophthalmic and Physiological Optics*, vol. 37, no. 2, pp. 151–159, 2017.
[81] C. Dorronsoro, S. Barbero, L. Llorente, and S. Marcos, "On-eye measurement of optical performance of rigid gas permeable contact lenses based on ocular and corneal aberrometry," *Optometry and Vision Science*, vol. 80, no. 2, pp. 115–125, 2003.
[82] D. Lopes-Ferreira, P. Fernandes, A. Queirós, and J. M. González-Meijome, "Combined effect of ocular and multifocal contact lens induced aberrations on visual performance: center-distance versus center-near design," *Eye & Contact Lens: Science & Clinical Practice*, vol. 44, no. Suppl 1, pp. S131–S137, 2018.
[83] J. A. Martin and A. Roorda, "Predicting and assessing visual performance with multizone bifocal contact lenses," *Optometry and Vision Science*, vol. 80, no. 12, pp. 812–819, 2003.
[84] C. Fedtke, J. Sha, V. Thomas, K. Ehrmann, and R. C. Bakaraju, "Impact of spherical aberration terms on multifocal contact lens performance," *Optometry and Vision Science*, vol. 94, no. 2, pp. 197–207, 2017.
[85] P. S. Kollbaum, B. M. Dietmeier, M. E. Jansen, and M. E. Rickert, "Quantification of ghosting produced with presbyopic contact lens correction," *Eye & Contact Lens: Science & Clinical Practice*, vol. 38, no. 4, pp. 252–259, 2012.
[86] C. Fedtke, K. Ehrmann, V. Thomas, and R. C. Bakaraju, "Association between multifocal soft contact lens decentration and visual performance," *Clinical Optometry*, vol. Volume 8, pp. 57–69, 2016.
[87] P. Pérez-Merino and S. Marcos, "Effect of intraocular lens decentration on image quality tested in a custom model eye," *Journal of Cataract & Refractive Surgery*, vol. 44, no. 7, pp. 889–896, 2018.
[88] N. W. El-Nimri and J. J. Walline, "Centration and decentration of contact lenses during peripheral gaze," *Optometry and Vision Science*, vol. 94, no. 11, pp. 1029–1035, 2017.
[89] R. L. Davis, "Determining multifocal parameters for a better fit," *Review of Optometry*, vol. 153, pp. 50–55, 2016.
[90] S. Plainis, G. Ntzilepis, D. A. Atchison, and W. N. Charman, "Through-focus performance with multifocal contact lenses: effect of binocularity, pupil diameter and inherent ocular aberrations," *Ophthalmic and Physiological Optics*, vol. 33, no. 1, pp. 42–50, 2013.
[91] S. Koh, "Irregular astigmatism and higher-order aberrations in eyes with dry eye disease," *Investigative Opthalmology & Visual Science*, vol. 59, no. 14, pp. DES36–DES40, 2018.
[92] R. Montesmico, J. L. Alió, G. Muñoz et al., "Postblink changes in total and corneal ocular aberrations," *Ophthalmology*, vol. 111, no. 4, pp. 758–767, 2004.
[93] R. Montés-Micó, J. L. Alió, and W. N. Charman, "Dynamic changes in the tear film in dry eyes," *Investigative Ophthalmology & Visual Science*, vol. 46, pp. 1615–1619, 2005.
[94] K. Y. Li and G. Yoon, "Changes in aberrations and retinal image quality due to tear film dynamics," *Optics Express*, vol. 14, no. 25, pp. 12552–12559, 2006.
[95] S. Koh, N. Maeda, T. Kuroda et al., "Effect of tear film break-up on higher-order aberrations measured with wavefront sensor," *American Journal of Ophthalmology*, vol. 134, no. 1, pp. 115–117, 2002.
[96] J. S. Wolffsohn and L. N. Davies, "Presbyopia: effectiveness of correction strategies," *Progress in Retinal and Eye Research*, vol. 68, pp. 124–143, 2019.
[97] P. R. B. Fernandes, H. I. F. Neves, D. P. Lopes-Ferreira, J. M. M. Jorge, and J. M. González-Meijome, "Adaptation to multifocal and monovision contact lens correction," *Optometry and Vision Science*, vol. 90, no. 3, pp. 228–235, 2013.
[98] K. Richdale, G. L. Mitchell, and K. Zadnik, "Comparison of multifocal and monovision soft contact lens corrections in patients with low-astigmatic presbyopia," *Optometry and Vision Science*, vol. 83, no. 5, pp. 266–273, 2006.
[99] N. Gupta, S. A. Naroo, and J. S. Wolffsohn, "Visual comparison of multifocal contact lens to monovision," *Optometry and Vision Science*, vol. 86, no. 2, pp. E98–E105, 2009.
[100] S. García-Lázaro, T. Ferrer-Blasco, H. Radhakrishnan, A. Cerviño, N. W. Charman, and R. Montés-Micó, "Visual function through 4 contact lens-based pinhole systems for presbyopia," *Journal of Cataract & Refractive Surgery*, vol. 38, no. 5, pp. 858–865, 2012.
[101] A. Llorente-Guillemot, S. García-Lazaro, T. Ferrer-Blasco, R. J. Perez-Cambrodi, and A. Cerviño, "Visual performance with simultaneous vision multifocal contact lenses," *Clinical and Experimental Optometry*, vol. 95, no. 1, pp. 54–59, 2012.
[102] D. Madrid-Costa, S. García-Lázaro, C. Albarrán-Diego, T. Ferrer-Blasco, and R. Montés-Micó, "Visual performance of two simultaneous vision multifocal contact lenses," *Ophthalmic and Physiological Optics*, vol. 33, no. 1, pp. 51–56, 2013.
[103] R. C. Bakaraju, D. Tilia, J. Sha et al., "Extended depth of focus contact lenses vs. two commercial multifocals: part 2. Visual performance after 1 week of lens wear," *Journal of Optometry*, vol. 11, no. 1, pp. 21–32, 2018.
[104] J. Sha, R. C. Bakaraju, D. Tilia et al., "Short-term visual performance of soft multifocal contact lenses for

presbyopia," *Arquivos Brasileiros de Oftalmologia*, vol. 79, no. 2, pp. 73–77, 2016.

[105] D. Tilia, A. Munro, J. Chung et al., "Short-term comparison between extended depth-of-focus prototype contact lenses and a commercially-available center-near multifocal," *Journal of Optometry*, vol. 10, no. 1, pp. 14–25, 2017.

[106] T. Ferrer-Balsco and D. Madrid-Costa, "Stereoacuity with simultaneous vision multifocal contact lenses," *Optometry and Vision Science*, vol. 87, no. 9, pp. E663–E668, 2010.

[107] J. Diec, D. Tilia, T. Naduvilath, and R. C. Bakaraju, "Predicting short-term performance of multifocal contact lenses," *Eye & Contact Lens: Science & Clinical Practice*, vol. 43, no. 6, pp. 340–345, 2017.

[108] K. Pesudovs, C. A. Hazel, R. M. Doran, and D. B. Elliot, "The usefulness of Vistech and FACT contrast sensitivity charts for cataract and refractive surgery outcomes research," *British Journal of Ophthalmology*, vol. 88, no. 1, pp. 11–16, 2004.

[109] T. Ferrer-Blasco and D. Madrid-Costa, "Stereoacuity with balanced presbyopic contact lenses," *Clinical and Experimental Optometry*, vol. 94, no. 1, pp. 76–81, 2011.

[110] P. J. Buckhurst, J. S. Wolffsohn, N. Gupta, S. A. Naroo, L. N. Davies, and S. Shah, "Development of a questionnaire to assess the relative subjective benefits of presbyopia correction," *Journal of Cataract & Refractive Surgery*, vol. 38, no. 1, pp. 74–79, 2012.

[111] B. Wang and K. J. Ciuffreda, "Depth-of-focus of the human eye: theory and clinical implications," *Survey of Ophthalmology*, vol. 51, no. 1, pp. 75–85, 2006.

[112] A. C. Kingston and I. G. Cox, "Predicting through-focus visual acuity with the eye's natural aberrations," *Optometry and Vision Science*, vol. 90, no. 10, pp. 1111–1118, 2013.

[113] D. Madrid-Costa, E. Tomás, T. Ferrer-Blasco, S. García-Lázaro, and R. Montés-Micó, "Visual performance of a multifocal toric soft contact lens," *Optometry and Vision Science*, vol. 89, no. 11, pp. 1627–1635, 2012.

[114] S. García-Lázaro, T. Ferrer-Blasco, H. Radhakrishnan, C. Albarrán-Diego, and R. Montés-Micó, "Visual comparison of an artificial pupil contact lens to monovision," *Optometry and Vision Science*, vol. 89, no. 7, pp. E1022–E1029, 2012.

[115] A. Bradley, H. A. Rahman, P. S. Soni, and X. Zhang, "Effects of target distance and pupil size on letter contrast sensitivity with simultaneous vision bifocal contact lenses," *Optometry and Vision Science*, vol. 70, no. 6, pp. 476–481, 1993.

[116] S. García-Lázaro, T. Ferrer-Blasco, H. Radhakrishnan, C. Albarrán-Diego, and R. Montés-Micó, "Artificial pupil versus contralateral balanced contact lens fit for presbyopia correction," *Arquivos Brasileiros de Oftalmologia*, vol. 77, no. 2, pp. 76–80, 2014.

[117] M. Faria-Ribeiro, A. Amorim-de-Sousa, and J. M. González-Méijome, "Predicted accommodative response from image quality in young eyes fitted with different dual-focus designs," *Ophthalmic and Physiological Optics*, vol. 38, no. 3, pp. 309–316, 2018.

[118] T. A. Aller, M. Liu, and C. F. Wildsoet, "Myopia control with bifocal contact lenses: a randomized clinical trial," *Optometry and Vision Science*, vol. 93, no. 4, pp. 344–352, 2016.

[119] P. Sankaridurg, R. C. Bakaraju, T. Naduvilath et al., "Myopia control with novel central and peripheral plus contact lenses and extended depth of focus contact lenses: 2 year results from a randomised clinical trial," *Ophthalmic and Physiological Optics*, vol. 39, no. 4, pp. 294–307, 2019.

[120] P. M. Allen, H. Radhakrishnan, H. Price et al., "A randomised clinical trial to assess the effect of a dual treatment on myopia progression: the cambridge anti-myopia study," *Ophthalmic and Physiological Optics*, vol. 33, no. 3, pp. 267–276, 2013.

[121] A. R. Pomeda, B. Pérez-Sánchez, M. d. P. Cañadas Suárez, F. L. Prieto Garrido, R. Gutiérrez-Ortega, and C. Villa-Collar, "MiSight assessment study Spain: adverse events, tear film osmolarity, and discontinuations," *Eye & Contact Lens: Science & Clinical Practice*, vol. 44, no. Suppl 2, pp. S99–S104, 2018.

[122] A. Ruiz-Pomeda, B. Pérez-Sánchez, I. Valls, F. L. Prieto-Garrido, R. Gutiérrez-Ortega, and C. Villa-Collar, "MiSight assessment study Spain (MASS). A 2-year randomized clinical trial," *Graefe's Archive for Clinical and Experimental Ophthalmology*, vol. 256, no. 5, pp. 1011–1021, 2018.

[123] P. Chamberlain, S. C. Peixoto-de-Matos, N. S. Logan, C. Ngo, D. Jones, and G. Young, "A 3-year randomized clinical trial of MiSight lenses for myopia control," *Optometry and Vision Science*, vol. 96, no. 8, pp. 556–567, 2019.

[124] R. C. Bakaraju, K. Ehrmann, and A. Ho, "Extended depth of focus contact lenses vs. two commercial multifocals: part 1. Optical performance evaluation via computed through-focus retinal image quality metrics," *Journal of Optometry*, vol. 11, no. 1, pp. 10–20, 2018.

[125] C. S. Y. Lam, W. C. Tang, D. Y.-Y. Tse, Y. Y. Tang, and C. H. To, "Defocus incorporated soft contact (DISC) lens slows myopia progression in Hong Kong Chinese schoolchildren: a 2-year randomised clinical trial," *British Journal of Ophthalmology*, vol. 98, no. 1, pp. 40–45, 2014.

[126] X. Cheng, J. Xu, K. Chehab, J. Exford, and N. Brennan, "Soft contact lenses with positive spherical aberration for myopia control," *Optometry and Vision Science*, vol. 93, no. 4, pp. 353–366, 2016.

[127] A. Ruiz-Pomeda, P. Fernandes, A. Amorim-de-Sousa et al., "Light disturbance analysis in the controlled randomized clinical trial MiSight assessment study Spain (MASS)," *Contact Lens and Anterior Eye*, vol. 42, no. 2, pp. 200–205, 2019.

[128] E. Santolaria-Sanz, A. Cerviño, and J. M. González-Méijome, "Corneal aberrations, contrast sensitivity, and light distortion in orthokeratology patients: 1-year results," *Journal of Ophthalmology*, vol. 2016, Article ID 8453462, 8 pages, 2016.

[129] C. Martins, A. Amorim-De-Sousa, M. Faria-Ribeiro, J. Pauné, J. M. González-Méijome, and A. Queirós, "Visual performance and high-order aberrations with different contact lens prototypes with potential for myopia control," *Current Eye Research*, vol. 45, no. 1, pp. 24–30, 2019.

[130] M. Faria-Ribeiro and J. M. González-Méijome, "Multifocal contact lenses: towards customisation?" *Ophthalmic and Physiological Optics*, vol. 39, no. 1, pp. 37–45, 2019.

[131] J. J. Walline, K. B. Lindsley, S. S. Vedula et al., "Interventions to slow progression of myopia in children," *Cochrane Database Systematic Reviews*, vol. 13, no. 1, Article ID CD004916, 2011.

Hindawi
Journal of Ophthalmology
Volume 2020, Article ID 8580471, 10 pages
https://doi.org/10.1155/2020/8580471

Research Article

Comparison of Two Wavefront Autorefractors: Binocular Open-Field versus Monocular Closed-Field

Gonzalo Carracedo,[1,2] **Carlos Carpena-Torres**,[1] **Laura Batres**,[1] **Maria Serramito**,[1] **and Anahí Gonzalez-Bergaz**[1]

[1]*Department of Optometry and Vision, Faculty of Optics and Optometry, Universidad Complutense de Madrid, Madrid, Spain*
[2]*Ocupharm Diagnostics Research Group, Department of Biochemistry and Molecular Biology, Faculty of Optics and Optometry, Universidad Complutense de Madrid, Madrid, Spain*

Correspondence should be addressed to Gonzalo Carracedo; jgcarrac@ucm.es

Received 28 August 2019; Revised 14 November 2019; Accepted 17 December 2019; Published 3 January 2020

Guest Editor: Laura Remon

Purpose. To evaluate the agreement and repeatability between a new commercially available binocular open-field wavefront autorefractor, as part of the Eye Refract system, and a monocular closed-field wavefront autorefractor (VX110). *Methods*. A cross-sectional, randomized, and single-masked study was performed. Ninety-nine eyes of 99 healthy participants (37.22 ± 18.04 years, range 8 to 69 years) were randomly analyzed. Three measurements with the Eye Refract and the VX110 were taken on three different days, under noncycloplegic conditions. Mean spherical equivalent (MSE), cylindrical vectors (J0 and J45), and binocular corrected distance visual acuity (BCDVA) were compared between both autorefractors. An intersession repeatability analysis was done considering the values of repeatability (S_r) and its 95% limit (r). *Results*. The VX110 showed more negative values ($P < 0.001$) in terms of MSE in comparison with the Eye Refract (0.20 D). Regarding cylindrical vectors, J45 showed statistically significant differences ($P = 0.001$) between both wavefront autorefractors, but they were not clinically relevant (<0.05 D). In BCDVA, there were no statistically significant differences ($P = 0.667$) between both wavefront autorefractors. Additionally, the Eye Refract was more repeatable than the VX110 in terms of both MSE ($S_{r\ \text{EYE REFRACT}} = 0.21$ D, $S_{r\ \text{VX110}} = 0.53$ D) and J0 ($S_{r\ \text{EYE REFRACT}} = 0.12$ D, $S_{r\ \text{VX110}} = 0.35$ D). *Conclusions*. The Eye Refract provided enough accuracy and reliability to estimate refractive errors in different age groups, achieving better results than the VX110. Therefore, the Eye Refract proved to be a useful autorefractor to be incorporated into clinical practice.

1. Introduction

Subjective refraction is the gold standard method to assess the refractive error because it considers both optical and neural factors of visual perception. Nevertheless, autorefractors provide objective refraction as a starting point to facilitate subjective refraction.

Based on the current ways to measure objective refraction, autorefractors can be classified as monocular or binocular, closed- or open-field, and traditional or wavefront-based [1–4]. Binocular or monocular indicates if the binocularity is present or not during the measurement, while closed- or open-field alludes to whether the image of fixation is virtual or real.

Besides autorefractors that use traditional methods to measure objective refraction, wavefront autorefractors have been developed to become a usual device in clinical practice, especially during the last decade [5]. The main limitation of wavefront autorefractors is an overestimation of myopia or underestimation of hyperopia [6–8]. This issue is also important for traditional autorefractors, both monocular closed-field [3, 9–12] and binocular closed-field [9, 13]. Despite this limitation, some models of wavefront autorefractors demonstrated a good agreement with subjective refraction in terms of spherical and cylindrical refractive errors [2, 14–18].

Binocular open-field traditional autorefractors were developed to avoid myopia that a monocular closed-field

environment may be generated without cycloplegia [19]. This idea is supported by different studies that showed similar results between these autorefractors and subjective refraction in terms of spherical refractive error [1, 4, 20–23].

In the case of wavefront autorefractors, all the commercially available models are monocular closed-field, except a new binocular open-field wavefront autorefractor, as part of the Eye Refract system (Luneau Technology; Chartres, France). The clinical implications and limitations of the Eye Refract are still unknown.

For this reason, the purpose of the current study was to evaluate the agreement and repeatability between this new binocular open-field wavefront autorefractor (Eye Refract) and a monocular closed-field wavefront autorefractor (VX110). Both systems are commercially distributed by Luneau Technology (Chartres, France).

2. Methods

2.1. Design of the Study. A cross-sectional, randomized, and single-masked study was performed. The study was conducted in compliance with good clinical practice guidelines and institutional review board regulations and following the tenets of the Declaration of Helsinki, revised and actualized in 2013 [24]. All trials were performed in the University Clinic of Optometry of the Universidad Complutense de Madrid (Madrid, Spain). All participants were voluntarily included in the study after signing a written informed consent, where the procedure of all the trials and the purpose of the study were explained. Participants were free to leave the study at any time.

Three measurements of the objective refraction with two wavefront autorefractors (Eye Refract and VX110) were taken. One of the autorefractors was used randomly in first place and the other in second place. All the measurements were performed on three different days (one measurement with each wavefront autorefractor per day) in the morning by the same optometrist, under noncycloplegic conditions. All visits of each participant were done during a maximum period of two weeks based on their availability. Refractive parameters (MSE, J0, and J45) and binocular corrected distance visual acuity (BCDVA) were compared between both wavefront autorefractors.

2.2. Sample. Ninety-nine eyes of 99 healthy participants (37.22 ± 18.04 years, range 8 to 69 years) were evaluated, considering one eye per participant randomly. The recruitment was made to obtain the most heterogeneous sample as possible concerning the age of participants, trying to involve the same number of participants in each decade of life. The participants were classified into four groups (total, teenagers, adults, and presbyopes), whose demographic characteristics are detailed in Table 1.

Inclusion criteria were as follows: aged between 7 and 69 years and understanding and signing the informed consent (by the legal tutors, in case of participants under 18 years). Exclusion criteria were amblyopia, strabismus, or other ocular dysfunction affecting the binocular autorefraction, the presence of any ocular disease, surgery or traumatism, and the use of systemic or ocular drugs that could affect the results.

2.3. Eye Refract System. The Eye Refract system (Luneau Technology; Chartres, France) is a binocular open-field aberrometer combined with a phoropter. The Eye Refract incorporates two Hartmann–Shack sensors that perform objective refraction in both eyes at the same time. The wavefront metric used for the objective refraction determination is based on the principle of equivalent quadratic, using the method of paraxial curvature matching proposed by Thibos et al. [25] This method considers the high-order aberrations analysis up to 4th order, using the Zernike coefficients C_2^0 and C_4^0 for MSE determination, C_2^2 and C_4^2 for J0 determination, and C^{2-2} and C_4^{-2} for J45 determination The Eye Refract measures the wavefront under physiological pupil conditions, and it recalculates the refractive parameters for 3 mm. If pupil size is equal to or less than 3 mm, the Eye Refract provides the values for its exact size. The Hartmann–Shack sensors use a near-infrared light of 800 nm, and the pitch of the microlens array is 0.1 mm.

Since the Eye Refract is an aberrometer combined with a phoropter, it provides both objective and subjective refraction. The results of its efficacy to perform aberrometry-based subjective refraction in comparison with conventional subjective refraction were already published [26]. In the current manuscript, we only report on the results of objective refraction.

Following the manufacturer instructions, subjects were instructed to put their chin and forehead on the chinrest and to look ahead to a test of fixation on the digital screen set at 4 m distance. Then, binocular wavefront aberrometry was measured.

2.4. VX110 System. The VX110 system (Luneau Technology; Chartres, France) is a multidiagnostic platform that incorporates an aberrometer [2]. The VX110 has a Hartmann–Shack sensor that performs a monocular and closed-field objective refraction. The wavefront metric used for the objective refraction determination is also based on the principle of equivalent quadratic, using the method of paraxial curvature matching proposed by Thibos et al. [25] All the refractive variables were considered for a pupil size of 3 mm. If pupil size is equal to or less than 3 mm, the VX110 provides the values for its exact size. The Hartmann–Shack sensor also uses a near-infrared light of 800 nm, and it measures 1500 points for a pupil diameter of 7 mm.

Following the manufacturer instructions, subjects were instructed to put their chin and forehead on the chinrest and to look ahead to a virtual image of fixation at infinity. Then, monocular wavefront aberrometry was performed in each eye consecutively.

2.5. Refractive Parameters. Refractive parameters were analyzed in terms of mean spherical equivalent (MSE) and vertical and oblique cylindrical vectors (J0 and J45) with the

Table 1: Demographic characteristics of the participants in the study.

Groups	Number of participants	Age (years)	Age range (years)	Gender (male/female)
Teenagers	21	13.05 ± 4.31	8 to 19	9/12
Adults	33	29.89 ± 5.71	22 to 39	8/25
Presbyopes	45	55.00 ± 8.14	40 to 69	18/27
Total	99	37.22 ± 18.04	8 to 69	35/64

method proposed by Thibos et al. [27]. The following expressions were used to calculate MSE, J0, and J45:

$$\text{MSE} = \text{sphere} + \text{cylinder}/2$$
$$\text{J0} = -(\text{cylinder}/2) \times \cos\ (2\ x \text{ axis})$$
$$\text{J45} = -(\text{cylinder}/2) \times \sin\ (2\ x \text{ axis})$$

2.6. Visual Acuity Measurement. Binocular corrected distance visual acuity (BCDVA) was immediately measured after finishing each objective refraction. BCDVA was assessed through the oculars of the Eye Refract, in the case of the objective refraction with this system, and with trial frame, in the case of the objective refraction with the VX110. The high-contrast (100%) ETDRS chart of the digital screen set at 4 meters of distance was used to measure the BCDVA.

2.7. Statistical Analysis. Statistical analysis was performed using the SPSS Statistics 23 software (IBM, Chicago, Illinois, USA). Sample size calculations were performed with statistical software Granmo 6.0 (Institut Municipal d'Investigació Mèdica, Barcelona, Spain). A statistical significance of 95% was established ($P < 0.05$). Results are shown as mean ± standard deviation.

The normality of the variables (MSE, J0, J45, and BCDVA) was assessed using the Shapiro–Wilk test. A statistical comparison between the values of both wavefront autorefractors inside each group (total, teenagers, adults, presbyopes) was done. Once the normal distribution of all the variables was confirmed, Student's t test for paired samples was chosen for this statistical comparison. Additionally, a Bland–Altman plot analysis was done to assess the agreement between both wavefront autorefractors [28].

An intersession repeatability analysis was done considering the following variables: mean difference between sessions (bias), its standard deviation (SD), repeatability (S_r), and its 95% limit (r). S_r is defined as the square root of the mean square within-subject standard deviation. r is mathematically defined as $2.77 \times S_r$, and it represents the limit value within which 95% of measurements should be [29]. The one-way analysis of variance (ANOVA) for paired samples with Bonferroni correction was done to assess the statistical differences between sessions.

3. Results

Table 2 summarizes the mean values of the different variables under study (MSE, J0, J45, and BCDVA) for both wavefront autorefractors and their statistical comparison.

In relation to MSE, the VX110 showed more negative values ($P < 0.05$) in comparison with the Eye Refract for all groups, except teenagers. Figure 1 shows the Bland–Altman plot for both objective refractions in terms of MSE. Mean difference (VX110-Eye Refract) and limits of agreement [upper, lower] were −0.20 [0.59, −0.99] D for total group, −0.30 [1.06, −1.66] D for teenagers, −0.24 [0.22, −0.70] D for adults, and −0.13 [0.50, −0.76] D for presbyopes.

In relation to J0, there were no statistically significant differences ($P \geq 0.05$) between both wavefront autorefractors. Figure 2 shows the Bland–Altman plot for both objective refractions in terms of J0. Mean difference (VX110-Eye Refract) and limits of agreement [upper, lower] were −0.02 [0.22, −0.24] D for total group, 0.00 [0.10, −0.10] D for teenagers, 0.00 [0.18, −0.18] D for adults, and −0.03 [0.27, −0.33] D for presbyopes.

In relation to J45, there were statistically significant differences ($P < 0.05$) between both wavefront autorefractors for total group and adults. Figure 3 shows the Bland–Altman plot for both objective refractions in terms of J45. Mean difference (VX110-Eye Refract) and limits of agreement [upper, lower] were 0.02 [0.13, −0.09] D for total group, 0.01 [0.11, −0.09] D for teenagers, 0.04 [0.14, −0.06] D for adults, and 0.00 [0.12, −0.12] D for presbyopes.

In relation to BCDVA, there were no statistically significant differences ($P \geq 0.05$) between both wavefront autorefractors. Figure 4 shows the Bland–Altman plot for both objective refractions in terms of J45. Mean difference (VX110-Eye Refract) and limits of agreement [upper, lower] were 0.00 [0.12, −0.12] D for total group, 0.02 [0.21, −0.17] D for teenagers, 0.00 [0.08, −0.08] D for adults, and 0.00 [0.10, −0.10] D for presbyopes.

Tables 3–5 summarize the intersession repeatability analyses of the refractive variables (MSE, J0, and J45, respectively) for both wavefront autorefractors and the statistical comparison between sessions.

The intersession repeatability analysis of MSE showed no statistically significant differences ($P \geq 0.05$) between sessions with both wavefront autorefractors. The Eye Refract was more repeatable than the VX110 for all the groups, especially for teenagers ($S_{r\ \text{EYE REFRACT}} = 0.14$ D, $S_{r\ \text{VX110}} = 0.92$ D). In total group, the values of S_r were 0.21 D with the Eye Refract and 0.53 D with the VX110.

The intersession repeatability analysis of J0 only showed statistically significant differences ($P = 0.033$) between session 1 and session 3 for adults with the Eye Refract. The Eye Refract was also more repeatable than the VX110 for all the groups. In total group, the values of S_r were 0.12 D with the Eye Refract and 0.35 D with the VX110.

The intersession repeatability analysis of J45 showed statistically significant differences ($P < 0.05$) between session 1 and session 3 for total group and presbyopes with the VX110. The VX110 was more repeatable than the Eye

Table 2: Mean values of mean spherical equivalent (MSE), cylindrical components (J0 and J45), and binocular corrected distance visual acuity (BCDVA) obtained with both binocular open-field (eye refract) and monocular closed-field (VX110) autorefractors.

Parameter	Wavefront autorefractor	Total group ($n = 99$)	Teenagers ($n = 21$)	Adults ($n = 35$)	Presbyopes ($n = 43$)
MSE (D)	Eye refract	-0.85 ± 2.65	-0.50 ± 1.86	-2.19 ± 3.17	-0.03 ± 2.16
	VX110	-1.05 ± 2.69	-0.80 ± 1.94	-2.43 ± 3.25	-0.16 ± 2.11
	P value	$<0.001^*$	0.065	$<0.001^*$	0.002^*
J0 (D)	Eye refract	0.10 ± 0.41	0.09 ± 0.31	0.19 ± 0.42	0.03 ± 0.43
	VX110	0.08 ± 0.40	0.09 ± 0.32	0.19 ± 0.40	0.00 ± 0.42
	P value	0.241	0.622	0.669	0.161
J45 (D)	Eye refract	-0.01 ± 0.30	-0.01 ± 0.12	-0.01 ± 0.18	0.00 ± 0.41
	VX110	0.01 ± 0.31	0.00 ± 0.14	0.03 ± 0.18	0.00 ± 0.42
	P value	0.001^*	0.168	0.004^*	0.095
BCDVA (logMAR)	Eye refract	-0.10 ± 0.10	-0.07 ± 0.11	-0.14 ± 0.08	-0.09 ± 0.11
	VX110	-0.10 ± 0.11	-0.05 ± 0.13	-0.14 ± 0.08	-0.09 ± 0.11
	P value	0.667	0.419	0.716	0.978

The results are expressed as mean ± SD. The statistical comparison was done between both autorefractors inside each group. $^*P < 0.05$, Student's t test for paired samples.

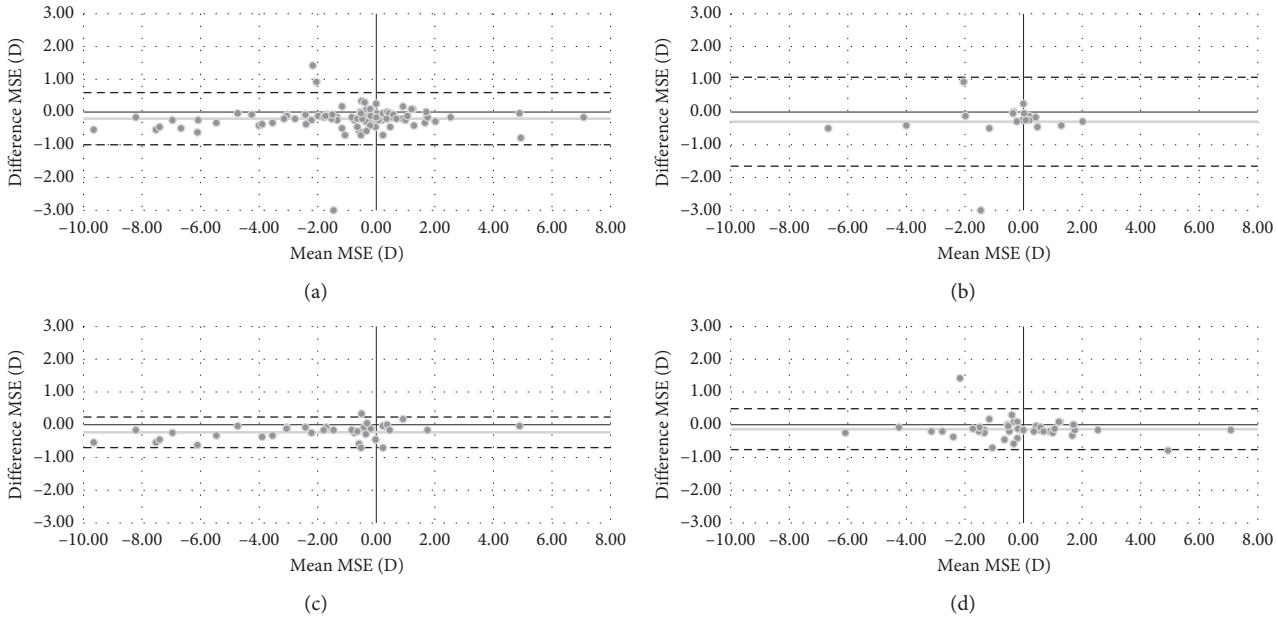

Figure 1: Bland–Altman plot describing the agreement between mean spherical equivalent (MSE) of both wavefront autorefractors for total group (a), teenagers (b), adults (c), and presbyopes (d). The middle line shows the mean difference (VX110-Eye Refract), and the two dashed side lines show the 95% limits of agreement.

Refract for all the groups, especially for presbyopes ($S_{r\ \text{EYE REFRACT}} = 0.15$ D, $S_{r\ \text{VX110}} = 0.08$ D). In the total group, the values of S_r were 0.11 D with the Eye Refract and 0.06 D with the VX110.

4. Discussion

The current study is the first to evaluate the performance of a binocular open-field autorefractor (Eye Refract) based on wavefront analysis. The performance of the Eye Refract was compared with the VX110, a monocular closed-field autorefractor. The results showed that the objective refraction performed by the VX110 was more negative in terms of MSE than the Eye Refract for all groups, except teenagers. Additionally, the Eye refract was more repeatable in terms of both MSE and J0 than the VX110 for all groups, but the VX110 was more repeatable in terms of J45.

Overestimation of myopia or underestimation of hyperopia has been the main limitation of wavefront autorefractors since they appeared on the market until nowadays [6–8], but this issue also affects traditional autorefractors, both monocular closed-field [3, 9–12] and binocular open-field [9, 13]. More negative values in the sphere are associated with the stimulation of the accommodation during the measurement process. For the total group of the current study, the VX110 showed more negative values in terms of MSE in comparison with the Eye Refract (0.20 D) (see Table 2). These differences could

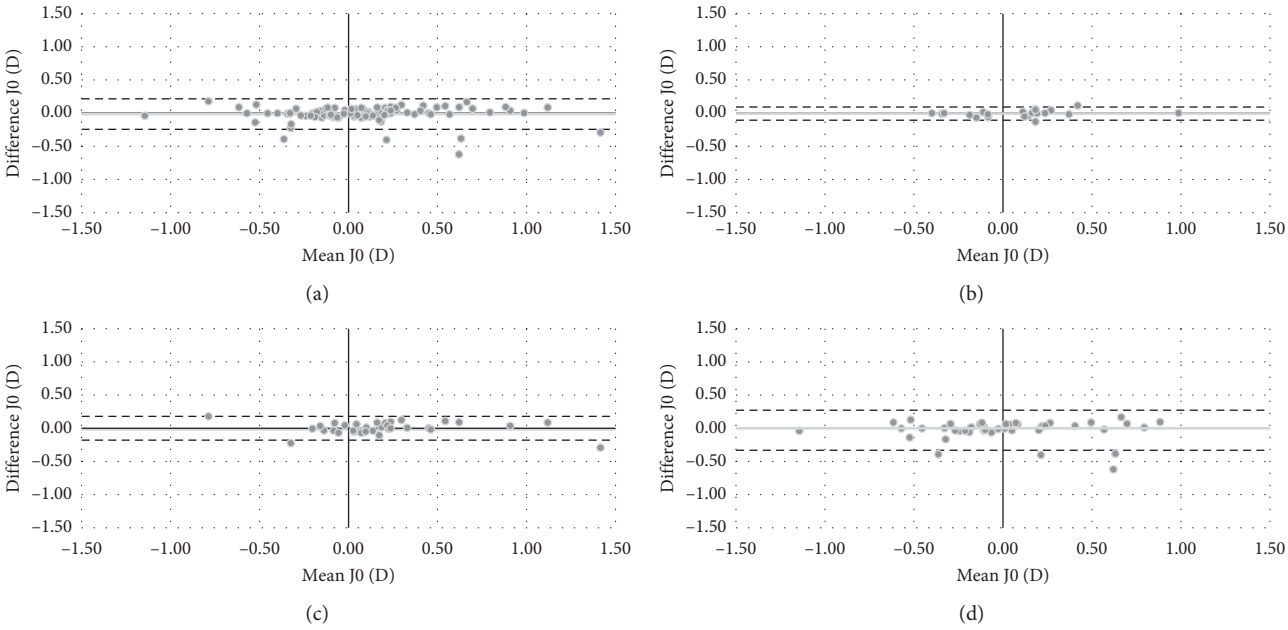

Figure 2: Bland–Altman plot describing the agreement between J0 of both wavefront autorefractors for total group (a), teenagers (b), adults (c), and presbyopes (d). The middle line shows the mean difference (VX110-Eye Refract), and the two dashed side lines show the 95% limits of agreement.

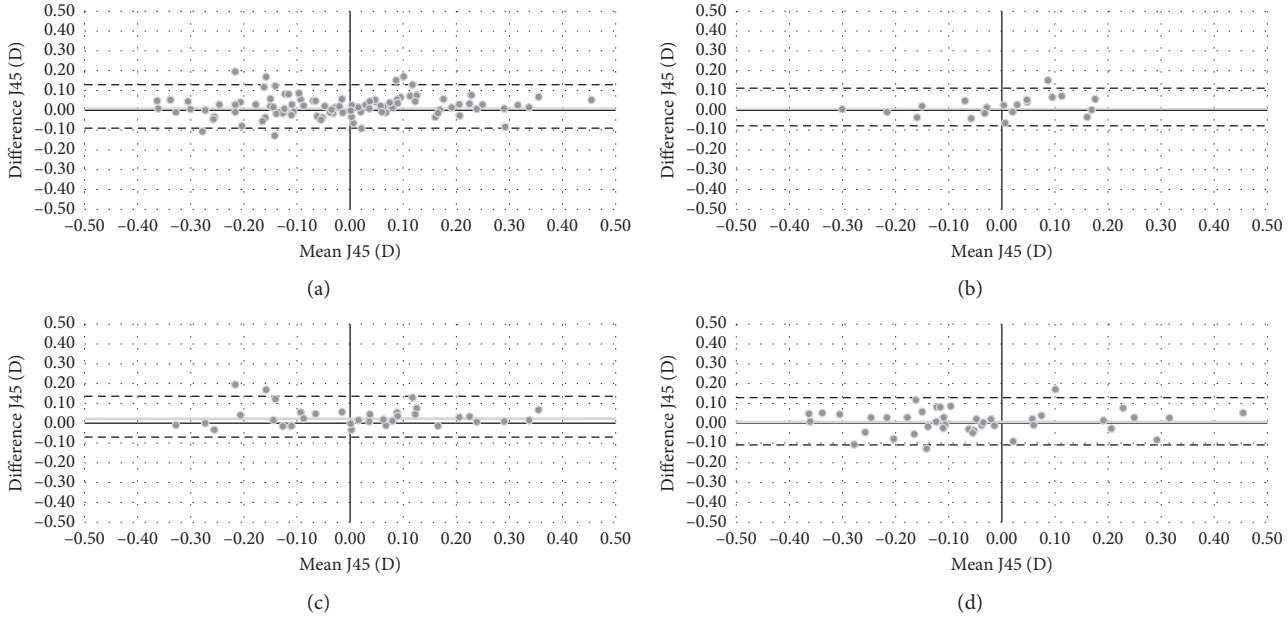

Figure 3: Bland–Altman plot describing the agreement between J45 of both wavefront autorefractors for total group (a), teenagers (b), adults (c), and presbyopes (d). The middle line shows the mean difference (VX110-Eye Refract), and the two dashed side lines show the 95% limits of agreement.

be considered clinically relevant since they were close to 0.25 D, values which could be affecting vision [30]. Additionally, the Bland–Altman plot for both objective refractions (Figure 1) showed more negative values with the VX110 in most of the participants. This trend was continued in all age groups. Also, teenagers were the only group that did not have statistical differences in MSE between both wavefront autorefractors (Table 2). Nevertheless, the difference for teenagers was maximum (0.30 D) in comparison with the rest of the groups. This maximum difference without statistical significance was associated with a single participant who obtained more negative values (around 3.00 D) with the VX110 (Figure 1(b)).

As explained above, the overestimation of myopia with the VX110 could be associated with higher stimulation of

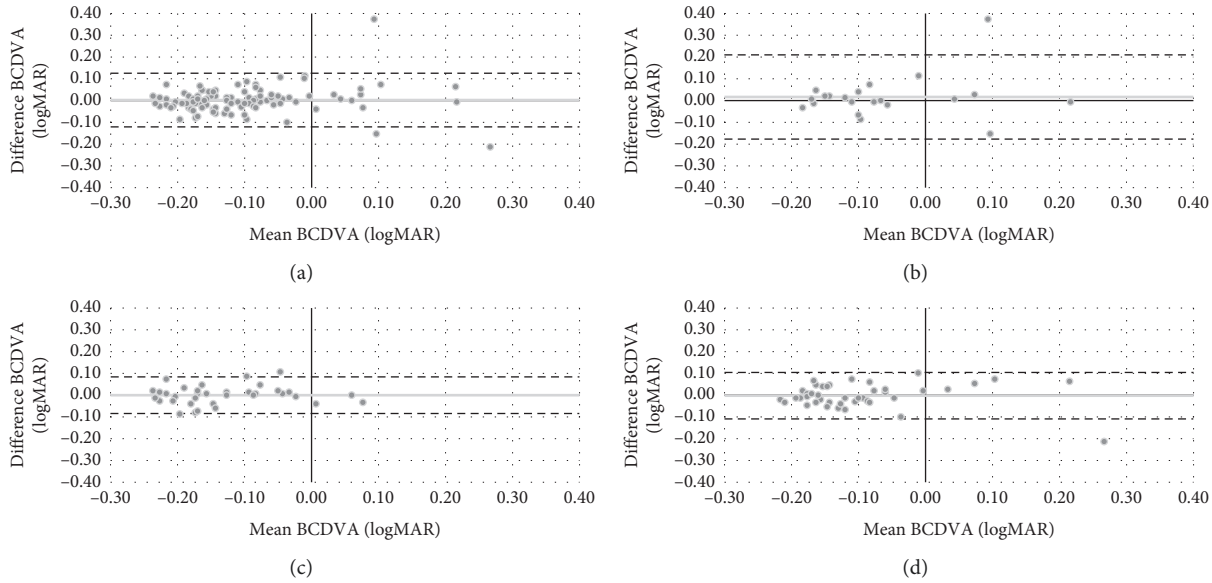

Figure 4: Bland–Altman plot describing the agreement between binocular corrected distance visual acuity (BCDVA) of both wavefront autorefractors for total group (a), teenagers (b), adults (c), and presbyopes (d). The middle line shows the mean difference (VX110-Eye Refract), and the two dashed side lines show the 95% limits of agreement.

Table 3: Intersession repeatability of mean spherical equivalent (MSE) obtained with both binocular open-field (eye refract) and monocular closed-field (VX110) autorefractors in terms of mean difference between sessions (bias), its standard deviation (SD), repeatability (S_r), and its 95% limit (r).

Wavefront autorefractor	Group	MSE	Session 1-session 2	Session 1–session 3	Session 2-session 3	Repeatability [95% limit] (D)
Eye refract	Total	Bias ± SD (D)	−0.02 ± 0.33	0.00 ± 0.28	0.02 ± 0.29	0.21 [0.59]
		P value	1.000	1.000	1.000	
	Teenagers	Bias ± SD (D)	−0.08 ± 0.16	−0.10 ± 0.24	−0.02 ± 0.19	0.14 [0.40]
		P value	0.102	0.188	1.000	
	Adults	Bias ± SD (D)	−0.02 ± 0.21	−0.02 ± 0.23	0.00 ± 0.20	0.15 [0.41]
		P value	1.000	1.000	1.000	
	Presbyopes	Bias ± SD (D)	0.01 ± 0.45	0.06 ± 0.32	0.04 ± 0.37	0.27 [0.75]
		P value	1.000	0.692	1.000	
VX110	Total	Bias ± SD (D)	−0.07 ± 0.40	−0.05 ± 0.87	0.02 ± 0.88	0.53 [1.47]
		P value	0.325	1.000	1.000	
	Teenagers	Bias ± SD (D)	−0.18 ± 0.77	0.18 ± 1.52	0.36 ± 1.49	0.92 [2.55]
		P value	0.906	1.000	0.843	
	Adults	Bias ± SD (D)	−0.06 ± 0.28	−0.09 ± 0.22	−0.04 ± 0.23	0.18 [0.50]
		P value	0.760	0.071	1.000	
	Presbyopes	Bias ± SD (D)	−0.02 ± 0.17	−0.12 ± 0.77	−0.10 ± 0.76	0.44 [1.23]
		P value	1.000	0.933	1.000	

The statistical comparison was done between sessions. $^*P < 0.05$, one-way ANOVA for paired samples with Bonferroni correction.

accommodation [6–8]. However, it seems that this problem could also affect to open-field autorefractors [21], which would not explain the differences between both wavefront autorefractors. Besides, this overestimation with the VX110 only affected adults and presbyopes who are supposed to be the groups of age with lower accommodation.

Considering that accommodative response was not evaluated, it is necessary to explore other theories that could

Table 4: Intersession repeatability of vertical cylindrical vector (J0) obtained with both binocular open-field (eye refract) and monocular closed-field (VX110) autorefractors in terms of mean difference between sessions (bias), its standard deviation (SD), repeatability (S_r), and its 95% limit (r).

Wavefront autorefractor	Group	J0	Session 1-session 2	Session 1–session 3	Session 2-session 3	Repeatability [95% limit] (D)
Eye refract	Total	Bias ± SD (D)	−0.04 ± 0.19	−0.03 ± 0.12	0.02 ± 0.19	0.12 [0.34]
		P value	0.077	0.059	1.000	
	Teenagers	Bias ± SD (D)	−0.04 ± 0.10	−0.03 ± 0.10	0.01 ± 0.09	0.07 [0.20]
		P value	0.276	0.767	1.000	
	Adults	Bias ± SD (D)	−0.03 ± 0.09	−0.04 ± 0.09	−0.01 ± 0.10	0.06 [0.18]
		P-value	0.171	0.033*	1.000	
	Presbyopes	Bias ± SD (D)	−0.06 ± 0.27	−0.02 ± 0.14	0.04 ± 0.26	0.16 [0.46]
		P value	0.478	1.000	0.982	
VX110	Total	Bias ± SD (D)	0.02 ± 0.22	−0.01 ± 0.10	−0.04 ± 0.20	0.35 [0.98]
		P value	0.909	0.355	0.196	
	Teenagers	Bias ± SD (D)	−0.01 ± 0.09	−0.02 ± 0.08	−0.02 ± 0.08	0.26 [0.73]
		P value	1.000	0.588	1.000	
	Adults	Bias ± SD (D)	0.02 ± 0.15	0.00 ± 0.10	−0.02 ± 0.13	0.33 [0.92]
		P value	1.000	1.000	1.000	
	Presbyopes	Bias ± SD (D)	0.04 ± 0.29	−0.02 ± 0.10	−0.06 ± 0.27	0.40 [1.11]
		P value	1.000	0.502	0.458	

Table 5: Intersession repeatability of oblique cylindrical vector (J45) obtained with both binocular open-field (Eye Refract) and monocular closed-field (VX110) autorefractors in terms of mean difference between sessions (bias), its standard deviation (SD), repeatability (S_r), and its 95% limit (r).

Wavefront autorefractor	Group	J45	Session 1-session 2	Session 1–session 3	Session 2-session 3	Repeatability [95% limit] (D)
Eye refract	Total	Bias ± SD (D)	−0.02 ± 0.20	−0.01 ± 0.15	0.01 ± 0.11	0.11 [0.30]
		P value	0.812	1.000	1.000	
	Teenagers	Bias ± SD (D)	0.00 ± 0.06	0.02 ± 0.10	0.02 ± 0.10	0.06 [0.18]
		P value	1.000	1.000	1.000	
	Adults	Bias ± SD (D)	0.00 ± 0.10	0.00 ± 0.09	0.00 ± 0.07	0.06 [0.18]
		P value	1.000	1.000	1.000	
	Presbyopes	Bias ± SD (D)	−0.05 ± 0.28	−0.04 ± 0.20	0.01 ± 0.13	0.15 [0.41]
		P value	0.671	0.565	1.000	
VX110	Total	Bias ± SD (D)	0.02 ± 0.10	0.02 ± 0.07	0.00 ± 0.10	0.06 [0.18]
		P value	0.215	0.031*	1.000	
	Teenagers	Bias ± SD (D)	0.02 ± 0.07	0.01 ± 0.06	0.00 ± 0.07	0.04 [0.12]
		P value	0.831	0.796	1.000	
	Adults	Bias ± SD (D)	−0.01 ± 0.07	0.00 ± 0.06	0.01 ± 0.07	0.04 [0.12]
		P value	1.000	1.000	1.000	
	Presbyopes	Bias ± SD (D)	0.04 ± 0.12	0.03 ± 0.08	−0.01 ± 0.12	0.08 [0.77]
		P value	0.160	0.038*	1.000	

The statistical comparison was done between sessions. *$P < 0.05$, one-way ANOVA for paired samples with Bonferroni correction.

explain the differences found in MSE between both wavefront autorefractors. The results of Elsner et al. [31] and Teel et al. [32] suggested that the differences in the sphere could be associated with the infrared light of the wavefront sensors reflecting off in external retinal layers. However, this theory would not explain the differences in the sphere between both wavefront refractors since they use the same near-infrared light of 800 nm. The fact that the Eye Refract measured the refraction with a test of fixation at 4 m and the VX110 with a virtual image of fixation at infinity would not support the differences in MSE either since the Eye Refract uses a fogging with positive lenses before measuring objective refraction.

On the other hand, it is known that convergence is accompanied by accommodation [33]. By this, it could be thought that the differences in MSE between both wavefront autorefractors were related to the fact that both measurements were performed under binocular and monocular conditions. Despite this, it would be necessary for an additional study about the influence of the vergence and accommodation in both wavefront autorefractors to confirm this theory.

The authors of the current study reported the values of MSE obtained with conventional subjective refraction [26]. The values of MSE were −0.86 D for the total group, −0.63 D for teenagers, −2.08 D for adults, and +0.25 D for presbyopes. Comparing these values with the current study (Table 2), it can be observed that the Eye Refract only showed an overestimation of myopia superior to 0.25 D for presbyopes ($P = 0.021$). However, the VX110 showed an overestimation of myopia superior to 0.25 D for adults and presbyopes ($P < 0.001$) [26]. This overestimation of myopia found with the VX110 contrast with the results of Gordon-Shaag et al. [2]. They found no differences in MSE with the same wavefront autorefractor in comparison with the subjective refraction performed by a single optometrist. These differences between both studies could be explained considering that they only performed one refraction by the same optometrist who could have its prescription criteria. The results of the current study concerning the VX110 also contrast with other authors that did not report differences in the spherical refraction between the newest wavefront autorefractors and subjective refraction [2, 15–18]. Nevertheless, some authors reported more negative sphere values with different wavefront aberrometers in comparison with subjective refraction during the last decade [8, 32, 34–36], coinciding with the results obtained with the VX110 in the current study. No studies assessing the performance of commercial open-field wavefront autorefractors were found in the scientific literature.

In terms of intersession repeatability of MSE, the Eye Refract was more repeatable than the VX110 for all the groups and sessions (Table 3), but both autorefractors were very similar for adults. The major benefit of the Eye Refract was for teenagers since its value of S_r (0.14 D) was 6.5 times lower than the S_r of the VX110 (0.92 D). However, this affirmation should be carefully interpreted because the sample of teenagers was inferior to the rest of the groups (Table 1).

Other studies analyzed the intersession repeatability of MSE with different wavefront autorefractors. In adults, several authors reported values of r between 0.28 D and 0.53 D [2, 16, 23, 37, 38], which agrees with the adults of the current study (Table 3). All these wavefront autorefractors keep their differences within a range of ±0.25 D. No studies assessing the intersession repeatability with wavefront autorefractors in other age groups were found in the scientific literature.

Astigmatism is a parameter that wavefront autorefractors offer properly [7, 8, 14–18]. Only a few studies reported differences when comparing cylinder between wavefront autorefractors and subjective refraction [2, 6], but these differences were approximate of 0.25 D, which is a value well tolerated by the human eye [39]. In the current study, despite there were statistically significant differences in cylindrical component J45 between both wavefront autorefractors for some groups, they could not be considered clinically relevant since the mean differences only reached a maximum value of 0.04 D (Table 2). Therefore, it could be affirmed that both wavefront autorefractors have the accuracy to properly determine astigmatism for all age groups since they did not show higher differences in comparison with conventional subjective refraction ($P \geq 0.05$) [26].

The intersession repeatability of astigmatism showed that the Eye Refract was more repeatable than the VX110 (Table 4) for all age groups, while the VX110 was more repeatable than the Eye Refract in terms of J45 (Table 5). In J45, since the differences between both wavefront autorefractors in terms of r were inferior to 0.25 D (except for presbyopes) and that the magnitude of J45 obtained with both wavefront autorefractors was substantially lower than MSE and J0 (Table 2), the improvement in J45 repeatability with the VX110 was not considered clinically relevant. In adults, other studies reported similar values of r in terms of J0 and J45 with different wavefront autorefractors [2, 16, 23, 37, 38].

In terms of BCDVA, there were no statistical differences between both wavefront autorefractors for all age groups (Table 2). In the case of the VX110, it is logical to think that BCDVA is not affected although it seems to overestimate myopia in comparison with the Eye Refract. This is due to the capacity of the lens to compensate for a negative overcorrection, especially in teenagers and adults. Presbyopes would have more difficulty to accommodate, but their negative overcorrection was not higher to 0.75 D in any participant (Figure 1(d)). In comparison with conventional subjective refraction [26], both wavefront autorefractors showed a statistically significant deterioration ($P < 0.05$) of BCDVA for all the groups, except with the Eye Refract for teenagers ($P = 0.126$). In total group, this deterioration was only 0.02 logMAR (1 letter), which is not considered clinically relevant [40].

The current study had some limitations that could be improved upon in future studies. Visual acuity was measured under unmasked conditions and using trial frame with the VX110 and through the oculars with the Eye Refract. A study of Ohlendorf et al. [41] showed that phoropter could induce more negative spherical values than trial frame. On the other hand, all the objective refractions should have been performed under cycloplegic conditions to prove that the

VX110 measurement is not influencing the accommodation stimulus because it is thought that a closed-field environment could overestimate myopia [19]. Also, it is necessary to check if these autorefractors could replace conventional subjective refraction since the objective refraction of the Eye Refract presented similar efficacy to subjective refraction [26]. Finally, more studies would be necessary for understanding the efficacy, applications, and limitations of open-field binocular wavefront autorefractors.

5. Conclusions

In conclusion, the VX110 showed more negative values in terms of MSE than the Eye Refract. Besides, the Eye Refract was more repeatable in terms of both MSE and J0 than the VX110. Both wavefront autorefractors showed similar results in terms of J45 and BCDVA.

The Eye Refract provided enough accuracy and reliability to estimate refractive errors in different age groups, achieving better results than the VX110. Therefore, the Eye Refract proved to be a useful autorefractor to be incorporated into clinical practice.

Data Availability

The data used to support the findings of this study are available from the corresponding author upon request.

Conflicts of Interest

The authors declare that there are no conflicts of interest regarding the publication of this paper.

Acknowledgments

The authors want to thank Luneau Technology (Chartres, France) for providing the Eye Refract system during the conduct of the study. Gonzalo Carracedo received a personal grant from Luneau Technology for the performance of the study with the Eye Refract system at the Universidad Complutense de Madrid.

References

[1] A. L. Sheppard and L. N. Davies, "Clinical evaluation of the grand seiko auto ref/keratometer WAM-5500," *Ophthalmic and Physiological Optics*, vol. 30, no. 2, pp. 143–151, 2010.

[2] A. Gordon-Shaag, D. P. Pinero, C. Kahloun et al., "Validation of refraction and anterior segment parameters by a new multi-diagnostic platform (VX120)," *Journal of Optometry*, vol. 11, no. 4, pp. 242–251, 2018.

[3] N. Paudel, S. Adhikari, A. Thakur, B. Shrestha, and J. Loughman, "Clinical accuracy of the nidek ARK-1 autorefractor," *Optometry and Vision Science*, vol. 96, no. 6, pp. 407–413, 2019.

[4] J. Wosik, M. Patrzykont, and J. Pniewski, "Comparison of refractive error measurements by three different models of autorefractors and subjective refraction in young adults," *Journal of the Optical Society of America A*, vol. 36, no. 4, pp. B1–b6, 2019.

[5] R. Applegate, D. Atchison, A. Bradley et al., "Wavefront refraction and correction," *Optometry and Vision Science*, vol. 91, no. 10, pp. 1154-1155, 2014.

[6] S. A. Nissman, R. E. Tractenberg, C. M. Saba, J. C. Douglas, and J. M. Lustbader, "Accuracy, repeatability, and clinical application of spherocylindrical automated refraction using time-based wavefront aberrometry measurements," *Ophthalmology*, vol. 113, no. 4, pp. 570.e2–577.e2, 2006.

[7] D. Z. Reinstein, T. J. Archer, and D. Couch, "Accuracy of the WASCA aberrometer refraction compared to manifest refraction in myopia," *Journal of Refractive Surgery*, vol. 22, no. 3, pp. 268–274, 2006.

[8] X. Zhu, J. Dai, R. Chu, Y. Lu, X. Zhou, and L. Wang, "Accuracy of WASCA aberrometer refraction compared to manifest refraction in Chinese adult myopes," *Journal of Refractive Surgery*, vol. 25, no. 11, pp. 1026–1033, 2009.

[9] Y.-F. Choong, A.-H. Chen, and P.-P. Goh, "A comparison of autorefraction and subjective refraction with and without cycloplegia in primary school children," *American Journal of Ophthalmology*, vol. 142, no. 1, pp. 68–74, 2006.

[10] B. Kinge, A. Midelfart, and G. Jacobsen, "Clinical evaluation of the allergan humphrey 500 autorefractor and the nidek AR-1000 autorefractor," *British Journal of Ophthalmology*, vol. 80, no. 1, pp. 35–39, 1996.

[11] J. Gwiazda and C. Weber, "Comparison of spherical equivalent refraction and astigmatism measured with three different models of autorefractors," *Optometry and Vision Science*, vol. 81, no. 1, pp. 56–61, 2004.

[12] K. Pesudovs and H. S. Weisinger, "A comparison of autorefractor performance," *Optometry and Vision Science*, vol. 81, no. 7, pp. 554–558, 2004.

[13] A. Queirós, J. González-Méijome, and J. Jorge, "Influence of fogging lenses and cycloplegia on open-field automatic refraction," *Ophthalmic and Physiological Optics*, vol. 28, no. 4, pp. 387–392, 2008.

[14] T. O. Salmon, R. W. West, W. Gasser, and A. T. Kenmore, "Measurement of refractive errors in young myopes using the COAS Shack-Hartmann aberrometer," *Optometry and Vision Science*, vol. 80, no. 1, pp. 6–14, 2003.

[15] J. Cooper, K. Citek, and J. M. Feldman, "Comparison of refractive error measurements in adults with Z-view aberrometer, Humphrey autorefractor, and subjective refraction," *Optometry-Journal of the American Optometric Association*, vol. 82, no. 4, pp. 231–240, 2011.

[16] E. Shneor, M. Millodot, O. Avraham, S. Amar, and A. Gordon-Shaag, "Clinical evaluation of the L80 autorefractometer," *Clinical and Experimental Optometry*, vol. 95, no. 1, pp. 66–71, 2012.

[17] S. McGinnigle, S. A. Naroo, and F. Eperjesi, "Evaluation of the auto-refraction function of the Nidek OPD-Scan III," *Clinical and Experimental Optometry*, vol. 97, no. 2, pp. 160–163, 2014.

[18] K. A. Lebow and C. E. Campbell, "A comparison of a traditional and wavefront autorefraction," *Optometry and Vision Science*, vol. 91, no. 10, pp. 1191–1198, 2014.

[19] E. A. H. Mallen, B. Gilmartin, J. S. Wolffsohn, and S.-I. Tsujimura, "Clinical evaluation of the Shin-Nippon SRW-5000 autorefractor in adults: an update," *Ophthalmic and Physiological Optics*, vol. 35, no. 6, pp. 622–627, 2015.

[20] E. Mallen, J. S. Wolffsohn, B. Gilmartin, and S. Tsujimura, "Clinical evaluation of the Shin-Nippon SRW-5000 autorefractor in adults," *Ophthalmic and Physiological Optics*, vol. 21, no. 2, pp. 101–107, 2001.

[21] S. Chat and M. H. Edwards, "Clinical evaluation of the Shin-Nippon SRW-5000 autorefractor in children," *Ophthalmic and Physiological Optics*, vol. 21, no. 2, pp. 87–100, 2001.

[22] L. N. Davies, E. A. H. Mallen, J. S. Wolffsohn, and A. B. Gilmartin, "Clinical evaluation of the shin-nippon NVision-K 5001/grand seiko WR-5100K autorefractor," *Optometry and Vision Science*, vol. 80, no. 4, pp. 320–324, 2003.

[23] G. Cleary, D. J. Spalton, P. M. Patel, P.-F. Lin, and J. Marshall, "Diagnostic accuracy and variability of autorefraction by the tracey visual function analyzer and the Shin-Nippon NVision-K 5001 in relation to subjective refraction," *Ophthalmic and Physiological Optics*, vol. 29, no. 2, pp. 173–181, 2009.

[24] World Medical Association Declaration of Helsinki, "Ethical principles for medical research involving human subjects," *JAMA*, vol. 310, no. 20, pp. 2191–2194, 2013.

[25] L. N. Thibos, X. Hong, A. Bradley, and R. A. Applegate, "Accuracy and precision of objective refraction from wavefront aberrations," *Journal of Vision*, vol. 4, no. 4, pp. 329–351, 2004.

[26] G. Carracedo, C. Carpena-Torres, M. Serramito, L. Batres-Valderas, and A. Gonzalez-Bergaz, "Comparison between aberrometry-based binocular refraction and subjective refraction," *Translational Vision Science & Technology*, vol. 7, no. 4, p. 11, 2018.

[27] L. N. Thibos, W. Wheeler, and D. Horner, "Power vectors: an application of fourier analysis to the description and statistical analysis of refractive error," *Optometry and Vision Science*, vol. 74, no. 6, pp. 367–375, 1997.

[28] J. M. Bland and D. G. Altman, "Measuring agreement in method comparison studies," *Statistical Methods in Medical Research*, vol. 8, no. 2, pp. 135–160, 1999.

[29] C. McAlinden, J. Khadka, and K. Pesudovs, "Precision (repeatability and reproducibility) studies and sample-size calculation," *Journal of Cataract & Refractive Surgery*, vol. 41, no. 12, pp. 2598–2604, 2015.

[30] D. A. Atchison, K. L. Schmid, K. P. Edwards, S. M. Muller, and J. Robotham, "The effect of under and over refractive correction on visual performance and spectacle lens acceptance," *Ophthalmic and Physiological Optics*, vol. 21, no. 4, pp. 255–261, 2001.

[31] A. E. Elsner, S. A. Burns, J. J. Weiter, and F. C. Delori, "Infrared imaging of sub-retinal structures in the human ocular fundus," *Vision Research*, vol. 36, no. 1, pp. 191–205, 1996.

[32] D. F. W. Teel, R. J. Jacobs, J. Copland, D. R. Neal, and L. N. Thibos, "Differences between wavefront and subjective refraction for infrared light," *Optometry and Vision Science*, vol. 91, no. 10, pp. 1158–1166, 2014.

[33] S. J. Judge, "How is binocularity maintained during convergence and divergence?," *Eye*, vol. 10, no. 2, pp. 172–176, 1996.

[34] M. Kilintari, A. Pallikaris, N. Tsiklis, and H. S. Ginis, "Evaluation of image quality metrics for the prediction of subjective best focus," *Optometry and Vision Science*, vol. 87, no. 3, pp. 183–189, 2010.

[35] A. Jinabhai, C. O'Donnell, and H. Radhakrishnan, "A comparison between subjective refraction and aberrometry-derived refraction in keratoconus patients and control subjects," *Current Eye Research*, vol. 35, no. 8, pp. 703–714, 2010.

[36] G. D. Hastings, J. D. Marsack, L. C. Nguyen, H. Cheng, and R. A. Applegate, "Is an objective refraction optimised using the visual Strehl ratio better than a subjective refraction?," *Ophthalmic and Physiological Optics*, vol. 37, no. 3, pp. 317–325, 2017.

[37] M. J. Dobos, M. D. Twa, and M. A. Bullimore, "An evaluation of the bausch & lomb zywave aberrometer," *Clinical and Experimental Optometry*, vol. 92, no. 3, pp. 238–245, 2009.

[38] C. Otero, M. Vilaseca, M. Arjona, J. A. Martínez-Roda, and J. Pujol, "Repeatability of aberrometric measurements with a new instrument for vision analysis based on adaptive optics," *Journal of Refractive Surgery*, vol. 31, no. 3, pp. 188–194, 2015.

[39] E. A. Villegas, E. Alcón, and P. Artal, "Minimum amount of astigmatism that should be corrected," *Journal of Cataract & Refractive Surgery*, vol. 40, no. 1, pp. 13–19, 2014.

[40] I. L. Bailey, M. A. Bullimore, T. W. Raasch, and H. R. Taylor, "Clinical grading and the effects of scaling," *Investigative Ophthalmology & Visual Science*, vol. 32, no. 2, pp. 422–432, 1991.

[41] A. Ohlendorf, A. Leube, and S. Wahl, "Steps towards smarter solutions in optometry and ophthalmology-inter-device agreement of subjective methods to assess the refractive errors of the eye," *Healthcare*, vol. 4, no. 3, 2016.

Hindawi
Journal of Ophthalmology
Volume 2019, Article ID 3174709, 6 pages
https://doi.org/10.1155/2019/3174709

Clinical Study

Novel Technique of Pneumatic Posterior Capsulorhexis for Treatment and Prevention of Posterior Capsular Opacification

Ahmed M. Eid,[1] **Shaaban Abd-Elhamid Mehany Elwan**,[1,2] **Ahmed M. Sabry**,[1] **Hossam M. Moharram**,[1] **and Ashraf M. Bakhsh**[2,3]

[1]*Ophthalmology Department, Faculty of Medicine, Minia University, 61519 El-Minia, Egypt*
[2]*Ophthalmology Department, Security Forces Hospital, Riyadh, Saudi Arabia*
[3]*Ophthalmology Department, Faculty of Medicine, Al-Faisal University, Riyadh, Saudi Arabia*

Correspondence should be addressed to Shaaban Abd-Elhamid Mehany Elwan; shaabanhamid29@gmail.com

Received 7 July 2019; Revised 7 October 2019; Accepted 5 December 2019; Published 23 December 2019

Guest Editor: Damian Siedlecki

Purpose. To evaluate a new technique of posterior capsulorhexis using air support to treat primary posterior capsular opacification (PCO) during cataract extraction surgery or to prevent postoperative PCO. *Setting*. (1) Ophthalmology department, Faculty of Medicine, Minia University, 61519, El-Minia, Egypt. (2) Security Forces Hospital, Ophthalmology Department, Riyadh, Kingdom of Saudi Arabia. *Design*. Prospective, randomized, consecutive case comparative non controlled study. *Methods*. One hundred eyes of 100 patients with a mean age of 63.3 years with dense cataract were enrolled in the study. Fifty of them (group (1)) were with primary PCO (discovered during the operations) and fifty (group (2)) with clear posterior capsule. All of the patients underwent phacoemulsification and posterior capsulorhexis using the air to support the posterior capsule. Then, IOL implantations were done between the anterior and posterior capsular rims. Postoperatively, each patient was evaluated for the following: visual acuity (UCVA and BCVA), manifest refractive spherical equivalent (MRSE), intraocular pressure, intraocular lens (IOL) stability, visual axis opacification, and posterior segment complications as retinal breaks, retinal detachment, or cystoid macular edema (CME). *Results*. There were no significant differences in UCVA, BCVA, and MRSE. All cases had a clear visual axis, with stable IOL and normal IOP during the follow-up period without posterior segment complications. The VA improved significantly throughout the follow-up periods in both groups without significant clinical difference. *Conclusion*. Pneumatic posterior capsulorhexis is a new effective technique for the treatment of primary PCO in dense cataract and for prevention of postoperative PCO with the good visual outcomes and minimal complications. This trial is registered with NCT04007965.

1. Introduction

Posterior capsular opacification (PCO) is one of the common late postoperative complications of phacoemulsification and ECCE rather than its presence in a good number of patients of long-standing and hypermature cataract in developing countries. The treatment of PCO by YAG laser capsulotomy usually leads to the famous annoying symptom (Musca) and carries the risk of IOL damage, elevation, decentration, and tilting [1, 2]. Moreover, it may lead to the posterior segment complications (cystoid macular edema, retinal breaks, and retinal detachment). While, there is no reliable treatment for prevention of PCO, this finding arouses our thinking about this novel technique for treatment and prevention of PCO.

The currently available modalities to prevent postoperative PCO are as follows:

(i) Some surgical modifications such as hydrodissection, repeated nucleus rotation, and meticulous polishing of the lens epithelial cells (LECs) from the anterior capsular rim and the equator. In 1989, David Apple and his colleagues [3] had demonstrated the value of hydrodissection. In 1992, they emphasized that hydrodissection acts as a barrier to migration of equatorial cells to the

posterior capsule and this could reduce PCO [4]. Fine described "cortical cleaving hydrodissection" technique, [5] which was designed to break the equatorial adhesions between lens epithelial cells and the capsule, thus clearance of these cells which are the progenitors of PCO. In 2006, they pointed out to the laboratory and clinical evidence that good hydrodissection, coupled with mechanical "scouring" of LECs from the equator may have a beneficial effect on decreasing PCO incidence [6, 7].

(ii) Changes in the IOL design and materials: e.g., the square edge optic heparin coated and acrylic IOL decreasing the incidence of postoperative PCO than with PMMA IOLs of similar design with several studies demonstrated this concept [8–12].

(iii) Pharmacological strategies either to kill the residual epithelial cells or to prevent their proliferation. Moreover, the ideal agent must be toxic to these cells only without being toxic to the corneal endothelium. Experimentally, few agents have been partially successful without clinical application until now [13, 14].

Improvement in lens materials and design are well documented to decrease the incidence of postoperative PCO [15, 16]. Rotation three times of the hydrodissected nucleus prior to phacoemulsification and a second hydrodissection after nucleus removal improve the results [17]. Bimanual irrigation/aspiration may also help to decrease the incidence of postoperative PCO [18].

1.1. Current Treatment Options for PCO. Nd: YAG laser posterior capsulotomy has minor complications such as IOP rise [19, 20], and serious potential complications are reported such as corneal perforation in a patient with systemic scleroderma [21]. Other options for PCO treatment are surgical posterior capsulotomy or capsulectomy, either primary (intraoperative) or secondary.

2. Patients and Methods

The study was approved by the local ethical board committee and before the surgical procedure, each patient was adequately educated about the surgery and signed an informed consent in accordance with the Declaration of Helsinki. The patients were chosen from the outpatient clinic and operated at El-Minia University Hospital and Security Forces Hospital, from Jan. 2017 to Jun. 2018. One hundred eyes of 100 patients with dense cataract were included in the study. *The inclusion criteria* were as follows: patient age ranged from 50–73 years with a clear cornea, dense cataract, and without any local or systemic causes for the cataract. *Exclusion criteria* were patients with intraoperative positive pressure, high myopia, and axial length more than 25 mm, corneal dystrophy, retinal disease, previous ocular surgery, active ocular diseases, and glaucoma. The study consisted of fifty eyes (group 1) with PCO and fifty eyes (group 2) with clear posterior capsule (discovered intraoperative).

2.1. Preoperative Examination. All cases were subjected to complete ophthalmological examinations including UCVA, BCVA, slit lamp biomicroscopy, tonometry, biometery, dilated fundus examination, and medical history, including any systemic diseases, and the data were recorded echographically.

2.2. Surgery. After complete phacoemulsification and irrigation-aspiration of cortical matter, we did posterior capsulorhexis using the air to support the posterior capsule and separate it from the vitreous face using the following unique novel technique.

2.2.1. The Novel Technique

(1) A dispersive viscoelastic material Viscoat (sodium chondroitin sulfate 4%-sodium hyaluronate 3%, Alcon Co) was injected to make the anterior chamber formed without deepening so that the posterior capsule is not forcibly pushed backward and to protect the corneal endothelium.

(2) The posterior capsule punctured centrally using cystotome, as shown in (Figure 1).

(3) Controllable one-shot injection of 0.1 ml of sterile air through the posterior capsule puncture (Figure 2) into the patellar fossa or Berger space (Figure 3). The air elevates, support, and separates the posterior capsule from the vitreous face (insulin syringe and Healon cannula were used) as shown in (Figure 4).

(4) Another viscoelastic injection to the anterior chamber to stretch the posterior capsule and sandwich it between, visco-elastic above and the air below as shown in (Figure 5).

(5) Posterior capsulorhexis 4 mm is now performed easily using capsulorhexis forceps (Figure 6).

(6) A foldable IOL was implanted between the anterior and posterior capsular rims (Figure 7).

(7) Complete the operation with I/A of viscoelastic material (Figure 8) and wound closure followed by eye dressing.

2.3. Postoperative Examinations. Postoperatively, each patient was prescribed Tobradex eye drops 0.3% (tobramycin 0.3%—dexamethasone 0.1%, Alcon Co.) with a tapering dose for 1 month and Vigamox eye drops (moxifloxacin 0.5%, Alcon Co.) for 2 weeks. Patients were evaluated at each postoperative visits at 1 day, 1 week, 1 month, 3 months, 6 months, and one year for the following: visual acuity (UCVA and BCVA), MRSE, intraocular pressure, intraocular lens (IOL) stability, visual axis opacification, and posterior segment complications such as retinal breaks, retinal detachment, or cystoid macular edema, and data were registered (Tables 1 and 2).

2.4. Statistical Analysis. Patients' data were registered in Microsoft Excel, entered, and analyzed using Sigma Plot-Scientific Data Program for the 2 groups, paired Student's *t*-

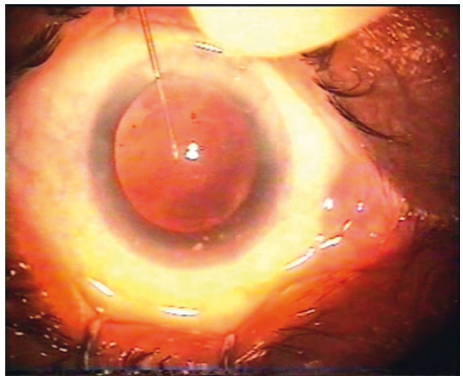

Figure 1: Central puncture of the posterior capsule.

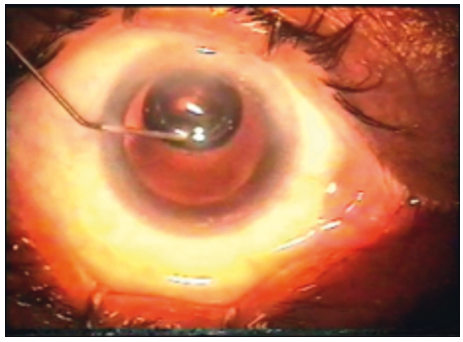

Figure 2: Injection of the air under the posterior capsule.

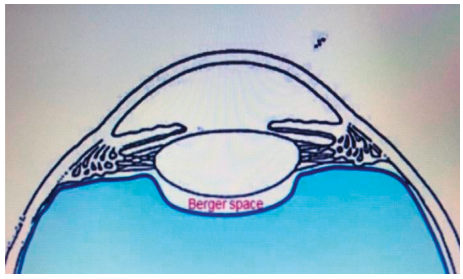

Figure 3: Retrolental Berger space or patellar fossa (animation).

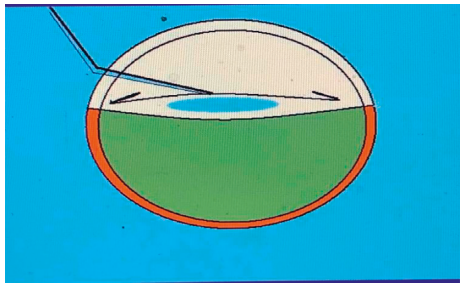

Figure 4: The air elevates, supports, and separates the posterior capsule from the vitreous face (animation).

test was used for the UCVA & BCVA means in decimal values and for MRSE means. For all tests, a P value < 0.05 was considered statistically significant.

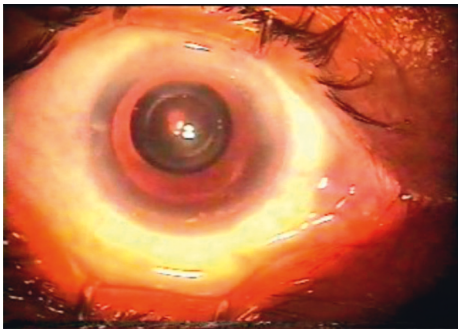

Figure 5: Air under the posterior capsule and viscoat above it.

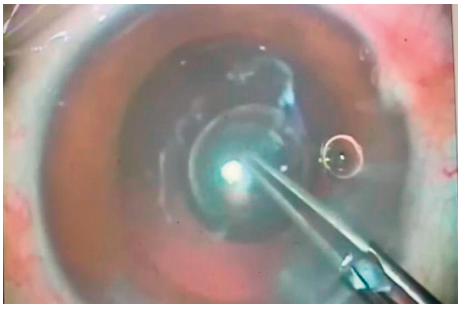

Figure 6: Posterior capsulorhexis using capsulorhexis forceps in a case of primary OPC.

Figure 7: IOL in place between the anterior and posterior capsular rims.

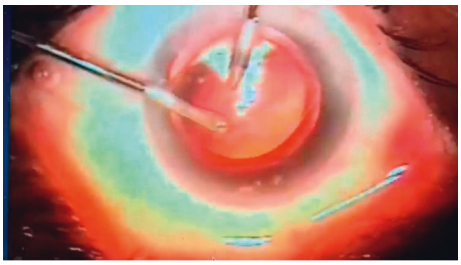

Figure 8: I/A of viscoelastic material.

3. Results

The patient's age ranged from 50–73 years, with a mean age of 62.3 years. Fifty males and fifty female patients with dense white cataract were included in the study. Group 1 included fifty eyes with Primary PCO discovered intraoperatively, and

Table 1: Postoperative visual and refractive outcomes in both of the groups.

Parameters	Group 1	Group 2	P value
UCVA	Mean	Mean	
3 months	0.75 ± 0.08	0.80 ± 0.050	0.82
6 months	1.01 ± 0.112	1.03 ± 0.96	1.0
12 months	1.034 ± 0.85	1.024 ± 0.65	0.95
BCVA	Mean	Mean	
3 months	0.96 ± 0.056	0.993 ± 0.035	0.90
6 months	1.036 ± 0.095	1.037 ± 0.15	1.0
12 months	1.040 ± 0.085	1.044 ± 0.075	1.0
MRSE	Mean	Mean	
1 month	-1.75 ± 2.50 D	-1.65 ± 2.00 D	0.88
3 months	-1.25 ± 1.50 D	-1.35 ± 1.25 D	0.95
6 months	-0.65 ± 1.25 D	-0.50 ± 1.38 D	0.98
12 months	-0.75 ± 1.05	-0.75 ± 1.03 D	1.0

UCVA = uncorrected visual acuity, BCVA = best corrected visual acuity, and MRSE = manifest refractive spherical equivalent. There were no statistically significant differences in the means of both of the groups. $P < 0.05$ was considered statistically significant.

Table 2: Demographics and minimal postoperative complications in both of the groups.

	Group 1	Group 2
Number of patients	50	50
IOL stability	Stable	Stable
Visual axis opacification	None	None
IOP rise	2 cases (4%)	One case (2%)
Iritis	One case (2%)	None
CME	None	None
RD	None	None
Retinal break	None	None

IOP = intraocular pressure, IOL = intraocular lens, CME = cystoid macular edema, and RD = retinal detachment.

group 2 had fifty eyes with clear posterior capsule. There were no intraoperative complications including vitreous prolapse or rupture of the anterior vitreous face. The patients were followed postoperatively for 6 visits one day, one week, one month, three months, six months and one year postoperatively, for MRSE, UCVA, BCVA, IOP, IOL stability, visual axis opacification, and posterior segment complications such as CME, retinal detachment, or retinal break. Tables 1 and 2 show demographic patients' data registration.

The differences were not statistically significant regarding the preoperative mean UCVA and BCVA between the two groups. It was ranging from counting fingers (CF) to hand movement (HM) for UCVA in both groups ($P = 0.99$) and for BCVA ($P = 0.95$). There were no significant differences at 3, 6, and 12 months in the mean postoperative UCVA comparing the two groups with visual stability ($< \pm 1.25$ D difference in two consecutive visits) ($P = 0.82$, 1.0 & 0.95): the values were 0.75 ± 0.08 with range, (0.6–0.9), 1.01 ± 0.112 with range, (0.8–1.2), and 1.034 ± 0.085 with range, (1–1.2), respectively, in group 1, while it was 0.80 ± 0.05 with range, (0.7–0.9), 1.03 ± 0.096 with range, (0.9–1.2), and 1.024 ± 0.065 with range, (1–1.2), respectively, in group 2 as shown in (Table 1). The postoperative mean UCVA values were 0.8 in 90% of patients, 1 in 95%, and ≥1 in 100% at 3, 6, and 12 months in group 1, while the corresponding values were 0.85 in 90%, 1 in 96%, and ≥1 in 100% in group 2, respectively. There were no statistically significant differences in the mean postoperative BCVA in both of the groups at 3, 6, and 12 months where the values were 0.96 ± 0.056, 1.036 ± 0.095, and 1.040 ± 0.085 in group 1, and the corresponding values were, 0.993 ± 0.035, 1.037 ± 0.15, and 1.044 ± 0.075 in group 2, respectively, where P values were 0.9, 1.0, and 1.0. There were no statistically significant differences between the two groups regarding the mean 1, 3, 6, and 12 months' postoperative manifest refractive spherical equivalent (MRSE) as shown in Table 1; the mean postoperative MRSE was -1.75 ± 2.50 D, -1.25 ± 1.50 D, -0.65 ± 1.35 D, and -0.75 ± 1.05 D in the group 1, while it was -1.65 ± 2.00 D, -1.35 ± 1.25 D, -0.50 ± 1.38 D, and -0.75 ± 1.03 D in group 2, in which P values were (0.88, 0.95, 0.98, and 1.0).

During the follow-up period, no opacification occurs in the pupillary zone and no posterior segment complications reported. In the 2 groups, only one case presented by mild iritis and another three cases with increase IOP in the first visit, which were controlled by intensifying the specific medical treatment. All patients improved completely in the second follow-up visit. All cases in both groups had stable IOL during the follow-up period with significant improvement of the UCVA and BCVA and refraction stability from one visit to the other one (Tables 1 and 2).

4. Discussion

Cataract surgery is one of the most common ophthalmic operations worldwide performed. It has been demonstrated to have excellent outcomes, not only in terms of visual acuity and low complications but also in terms of reduced functional impairment and improved quality of life measures [14]. However, posterior capsular opacification (PCO) postoperatively continues to be a challenging problem, and the incidence needs to be reduced to zero [7].

Complete removal of all LECs from the capsular equator by "capsule polishing" techniques is impracticable. Cortical clean-up using "hydrodissection" and "lens fiber stripping" may reduce the incidence of PCO formation by reducing the number of equatorial LECs. Full circumferential capsulorhexis-optic overlap and sharp posterior optic edge did not completely and permanently prevent PCO in all eyes, especially over longer periods. Also, primary posterior capsulorhexis is safe and effective and supplements the efficacy of a sharp-posterior optic edge of IOL forming a "second line of defense"; however, the surgical skill required limits its widespread use.

In Egypt, the incidence of primary PCO is higher because white- and long-standing cataract are more common, and this finding is in agreement with Joshi, [22] in which he reported primary PCO incidence of 38% in longstanding and hypermature cataract. The aim of our study was not only to reduce the postoperative PCO but also to treat the intraoperative primary PCO. While anterior capsulorhexis is easy to perform because of the lens support, posterior capsulorhexis is a little

bit difficult because of absence of such a support in which there is a potential, retrolental space (space of Berger), or patellar fossa. Precisely, what we did is we injected the air (0.1 ml) in the patellar fossa through a minute hole in the posterior capsule to cushion, support the posterior capsule, and separate it from the vitreous face and anterior hyaloid membrane during posterior capsulorhexis in cases with primary PCO which may be encountered during phacoemulsification for long-standing cataract and also for clear posterior capsule to prevent postoperative PCO.

In this work, there is a modification of the primary posterior capsulotomy which can be used for the treatment of primary PCO and to prevent postoperative PCO. This technique had reduced the incidence of PCO to zero with minimal complications as postoperative transient rise of IOP. The rise of IOP occurred in two patients out of 50 (4%) in group 1 and in only one patient out of 50 (2%) in group 2 in our cohort and it was controlled by proper medical treatment, and this finding was in agreement with [23] in which they reported a transient rise of IOP after Nd: YAG laser capsulotomy for PCO. By reviewing the literatures, no data could be found about a similar technique to prevent postoperative PCO and to treat the primary PCO. There was some difficulty to implant the IOL between the anterior and posterior capsular rims as it needs meticulous handling and very gentle and slow IOL injection towards the lower part of the equator with good magnification and zooming; we could overcome this difficulty as well as we did the anterior capsulotomy 5.5 mm and the posterior capsulotomy 4 mm. Patients in the study were divided into 2 groups (with or without PCO). As the aim of this study was to manage the primary PCO intraoperatively and to prevent postoperative PCO occurrence in clear posterior capsule in cases of dense cataract with comparing the safety, effectiveness, and results of the novel technique in two different occasions, the primary PCO and the clear posterior capsule because of the posterior capsule behave differently if it is opacified than if it is clear. There was a lack of control group without PCCC as it might be more appropriate; if we do it, we will consider this point on the future study on a larger group of patients, the incidence of PCO is well known in cataract surgery with many literatures, and our study was to evaluate the safety and effectiveness of this novel technique in lowering the incidence of PCO in different capsular types (opacified and clear). By using this technique, we succeeded to decrease the PCO incidence to zero %, and hence there was no need for YAG posterior capsulotomy and its complications.

There are no statistically significant differences in postoperative UCVA, BCVA, and MRSE mean in both of groups as well as during the follow-up period, no opacification occurs in the pupillary zone, no intraoperative complications including vitreous loss or prolapse of anterior vitreous face, and no posterior segment complications reported. All cases in both groups had stable IOL during the follow-up period with significant improvement of the UCVA and BCVA and refraction stability from one visit to the other one. A larger series of patients is needed and is planned to confirm the efficacy and safety of this technique over a longer period of time and follow-up.

5. Conclusions

Pneumatic posterior capsulorhexis is a new effective, safe maneuver for the treatment of primary PCO in dense cataract cases and to prevent postoperative PCO with good visual outcomes and fewer complications, and it can be performed in patients susceptible for early postoperative PCO like diabetic and young-age patient.

Abbreviations

UCVA: Uncorrected visual acuity
BCVA: Best corrected visual acuity
MRSE: Manifest refractive spherical equivalent
PCO: Posterior capsular opacification
CME: Cystoid macular edema
VA: Visual acuity
IOL: Intraocular lens
ECCE: Extracapsular cataract extraction
LECs: Lens epithelial cells
IOP: Intraocular pressure
RD: Retinal detachment
I/A: Irrigation/aspiration.

Data Availability

The data used to support the findings of this study are available from the corresponding author upon request.

Ethical Approval

The study was approved by the local ethical board committee.

Consent

Before the surgical procedure, each patient adequately learned about the study as well as the risks and benefits of the surgery and signed an informed consent in accordance with the Declaration of Helsinki.

Disclosure

Ahmed M. Eid, Ahmed M. Sabry, Hossam M. Moharram, and Ashraf M. Bakhsh are the coauthors.

Conflicts of Interest

The authors declare that they do not have any conflicts of interest.

Authors' Contributions

E A, E SH, S A, and M H were responsible for conducting the study, preparation, design, and critical revision; supervision was performed by BA; data collection, statistical analysis, writing, drafting of manuscript, and editing the paper were carried out by E SH; and material support, follow-up, and review were carried out by E SH, S A, and M H.

Acknowledgments

The authors would like to acknowledge the overwhelming support from all of their colleagues in Ophthalmology department, Faculty of Medicine, Minia University, El-Minia, Egypt, and Ophthalmology Department, Security Forces Hospital, Riyadh, SA.

Supplementary Materials

VIDEO (1). The Steps of the Novel Technique: 1, irrigation/aspiration of cortical matter after finishing phacoemulsification; 2, injection of viscoelastic material; 3, puncture of the posterior capsule with cystitome; 4, air injection under the posterior capsule; 5, pneumatic posterior capsulorhexis; 6, viscoelastic injection and widening of the main incesion; and 7, implantation of the IOL between the anterior and posterior capsular rim. VIDEO (2). Completion of the Novel Technique: 8, irrigation/aspiration of the viscoelastic; 9, IOL in place between the anterior and posterior capsular rim Supplementary File Figure (1): photo of one case of dense cataract from our operated cases. Figure (2): photo of the same case in Figure (1) with primary intraoperative PCO (posterior capsular opacification). (*Supplementary Materials*)

References

[1] K.-S. Shin, H.-J. Park, Y.-J. Jo, and J. Y. Kim, "Efficacy and safety of primary posterior capsulotomy in combined phacovitrectomy in rhegmatogenous retinal detachment," *PLoS One*, vol. 14, no. 3, pp. 1–13, 2019.

[2] C. Gao and F. Lyu, "Tilt of IOLs and change of axial length in patients of posterior capsular opacification after Nd:YAG laser capsulotomy," *Guoji Yanke Zazhi*, vol. 17, no. 8, 2017.

[3] D. J. Apple, R. Casanova, J. Davison et al., "Technique of posterior chamber intraocular lens implantation using a small smooth circular continuous tear capsulotomy-capsulorhexis: a demonstration using the posterior video technique in human cadaver eyes," in *Proceedings of the Video Presented at the Annual Meeting of the American Academy of Ophthalmology*, New Orleans, LA, USA, October 1989.

[4] D. J. Apple, K. D. Solomon, M. R. Tetz et al., "Posterior capsule opacification," *Survey of Ophthalmology*, vol. 37, no. 2, pp. 73–116, 1992.

[5] I. H. Fine, "Cortical cleaving hydrodissection," *Journal of Cataract & Refractive Surgery*, vol. 18, no. 5, pp. 508–512, 1992.

[6] A. R. Vasavada, S. M. Raj, K. Johar, and M. A. Nanavaty, "Effect of hydrodissection alone and hydrodissection combined with rotation on lens epithelial cells surgical approach for the prevention of posterior capsule opacification," *Journal of Cataract & Refractive Surgery*, vol. 32, no. 1, pp. 145–150, 2006.

[7] A. R. Vasavada, S. A. Dholakia, S. M. Raj, and R. Singh, "Effect of cortical cleaving hydrodissection on posterior capsule opacification in age related nuclear cataracts randomized clinical masked trial," *Journal of Cataract & Refractive Surgery*, vol. 32, no. 7, pp. 1196–1200, 2006.

[8] P. Morgan-Warren, J. M. A. Smith, Intraocular lens-edge design and material factors contributing to posterior-capsulotomy rates: comparing Hoya FY60AD, PY60AD, and AcrySof SN60WF," *Clinical Ophthalmology*, vol. 2013, pp. 1661–1667, 2013.

[9] L. Bai, J. Zhang, L. Chen, T. Ma, and H. C. Liang, "Comparison of posterior capsule opacification at 360-degree square edge hydrophilic and sharp edge hydrophobic acrylic intraocular lens in diabetic patients," *International Journal of Ophthalmology*, vol. 8, no. 4, pp. 725–729, 2015.

[10] R. Mudhol, S. Shetti, and D. Dodamani, "Square-edge intraocular lens versus conventional round-edge intraocular lens in prevention of posterior capsule opacification: a randomized clinical trial," *Journal of the Scientific Society*, vol. 43, no. 1, pp. 6–10, 2016.

[11] Yi Zhu, D. Li, S.-C. Wang, J. Yuan, and X.-J. Cai, "Comparison of posterior capsule opacification after implantation of two different intraocular lenses: a Meta-analysis," *Guoji Yanke Zazhi*, vol. 16, no. 4, pp. 642–646, 2016.

[12] B. Takkar, P. Chandra, S. Temkar, A. K. Singh, and I. Bhatia, "Predictors of successful laser capsulotomy for significant posterior capsule opacification after phacoemulsification," *Journal of Ophthalmic & Vision Research*, vol. 12, no. 2, pp. 170–174, 2017.

[13] T. D. Walker, "Pharmacological attempts to reduce posterior capsule opacification after cataract surgery-a review," *Clinical & Experimental Ophthalmology*, vol. 36, no. 9, pp. 883–890, 2008.

[14] U. C. S. Yadav, F. Ighani-Hosseinabad, F. J. G. M. van Kuijk, S. K. Srivastava, and K. V. Ramana, "Prevention of posterior capsular opacification through aldose reductase inhibition," *Investigative Opthalmology & Visual Science*, vol. 50, no. 2, pp. 752–759, 2009.

[15] S. Ostbaum, "White paper. Utilisation, appropriate care, and quality of life for patients with cataracts," *Journal of Cataract & Refractive Surgery*, vol. 32, no. 10, pp. 1748–1751, 2006.

[16] D. J. Apple, "in Tribute to sir harold ridley (dedication)," *Survey of Ophthalmology*, vol. 45, no. Suppl 1, pp. S7–S12, 2000.

[17] D. J. Apple, Q. Peng, N. Visessook et al., "Eradication of the posterior capsule opacification: documentation of a marked decrease in Nd: YAG laser posterior capsulotomy rates noted in an analysis of 5416 pseudophakic human eyes obtained postmortem," *Ophthalmology*, vol. 108, no. 3, pp. 505–518, 2001.

[18] O. Findl, W. Buehl, P. Bauer, and T. Sycha, "Interventions for preventing posterior capsule opacification (systematic review)," *Cochrane Database of Systematic Reviews*, vol. 3, 2007.

[19] N. Polat, İ. Tuncer, E. Karahan, and M. Ö. Zengin, "The effect of Nd: YAG laser capsulotomy on visual acuity, intraocular pressure, central corneal thickness, and refractive status," *Türk Oftalmoloji Dergisi*, vol. 44, no. 4, pp. 275–279, 2014.

[20] W. Cao, H.-P. Cui, S. Ni, and H.-K. Gu, "Influence of size of Nd: YAG capsulotomy on ocular biological parameters and refraction," *Guoji Yanke Zazhi*, vol. 18, no. 10, pp. 1847–1850, 2018.

[21] M. Khreish, R. Hanna, L. Berkovitz, and B. Tiosano, "Corneal perforation after Nd:YAG capsulotomy: a case report and literature review," *Case Reports in Ophthalmology*, vol. 10, no. 1, pp. 111–115, 2019.

[22] R. Joshi, "Primary posterior capsular opacification in Indian rural population undergoing cataract surgery for hypermaturesenile cataract," *Clinical Ophthalmology*, vol. 2013, pp. 1605–1608, 2013.

[23] A. Patil and V. Naik, "Clinical assessment of visual acuity, refractive changes and IOP following ND:Yag laser capsuotomy for posterior capsular opacification," *Journal of Evidence Based Medicine and Healthcare*, vol. 5, no. 31, pp. 2302–2308, 2018.

Hindawi
Journal of Ophthalmology
Volume 2019, Article ID 7018937, 8 pages
https://doi.org/10.1155/2019/7018937

Research Article

Influence of Angle κ and Higher-Order Aberrations on Visual Quality Employing Two Diffractive Trifocal IOLs

Cecilio Velasco-Barona,[1] Claudia Corredor-Ortega,[1] Alejandra Mendez-Leon,[1] Nadia L. Casillas-Chavarín,[1] Daniel Valdepeña-López Velarde,[1] Guadalupe Cervantes-Coste,[1] Daniel Malacara-Hernández,[2,3] and Roberto Gonzalez-Salinas[3,4]

[1]*Anterior Segment Surgery Department, Asociación para Evitar la Ceguera, Mexico City 04030, Mexico*
[2]*Centro de Investigaciones en Óptica A.C. (CIO), León 37150, Guanajuato, Mexico*
[3]*Laboratorio Nacional de óptica de la Visión, León, Mexico*
[4]*Research Department, Asociación para Evitar la Ceguera, México City 04030, Mexico*

Correspondence should be addressed to Roberto Gonzalez-Salinas; dr.gonzalezsalinas@gmail.com

Received 20 June 2019; Revised 21 September 2019; Accepted 25 October 2019; Published 27 November 2019

Guest Editor: Maria Vinas

Prospective, randomized, comparative, and controlled study to estimate the association between angle κ distance and higher-order aberrations (HOAs) with postoperative visual acuity after presbyopia-correcting IOL implantation. Forty-three eyes from 43 patients were included and randomly assigned in two groups for either AT LISA tri 839MP or Acrysof IQ PanOptix IOL implantation. The OPD-Scan III analyzer was utilized to assess the angle κ distance and higher-order aberration (HOAs). Twenty-three eyes were in the Acrysof IQ PanOptix group and 20 patients in the AT LISA tri 839MP group. The uncorrected distance visual acuity (UDVA) for the PanOptix group was 0.092 ± 0.10, whereas for AT LISA tri was 0.050 ± 0.06 ($P = 0.229$). The uncorrected intermediate visual acuity (UIVA) for the PanOptix group was 0.173 ± 0.18, whereas for AT LISA tri, it was 0.182 ± 0.11 ($P = 0.669$). Uncorrected near visual acuity (UNVA) was 0.068 ± 0.04 and 0.085 ± 0.07, respectively ($P = 0.221$). Also, correlation coefficient between HOAs and the Strehl ratio for each group were −0.768 ($P < 0.0001$) and −0.863 ($P = 0.0001$). Patients implanted with both trifocal IOLs showed excellent postoperative visual performance at all distances at the six-month follow-up visit. No association was found between angle κ distance and postoperative visual acuity regardless of the angle κ magnitude or the two trifocal IOLs inner optical diameter. Also, internal aberrations demonstrated a significant inverse correlation with the Strehl ratio for both trifocal IOLs.

1. Introduction

Trifocal intraocular lens implantation has become an ever more common solution for cataract patients who pursuit a spectacle-free option after IOL surgery [1]. Surgical planning, therefore, poses a significant challenge to achieve spectacle independence and at the same time meet visual expectations [1, 2].

Preoperative assessment should be aware among others of pupil size, preoperative angle κ, and significant astigmatism as key variables that may affect the perceived outcome for patients who have a presbyopia-correcting IOL [3]. In addition, tilt and decentration could inflict a negative impact on the eye's optical performance, inducing asymmetric aberrations that in severe cases can decrease optical quality [4, 5].

Also, a functional deviation between the optical center, the visual axis, and the pupillary axis of the multifocal IOL can lead to higher-order aberrations postoperatively, resulting in decreased visual quality. Therefore, some propose including the measurement of angle kappa (κ) and angle alpha (α) in preoperative examinations of eyes

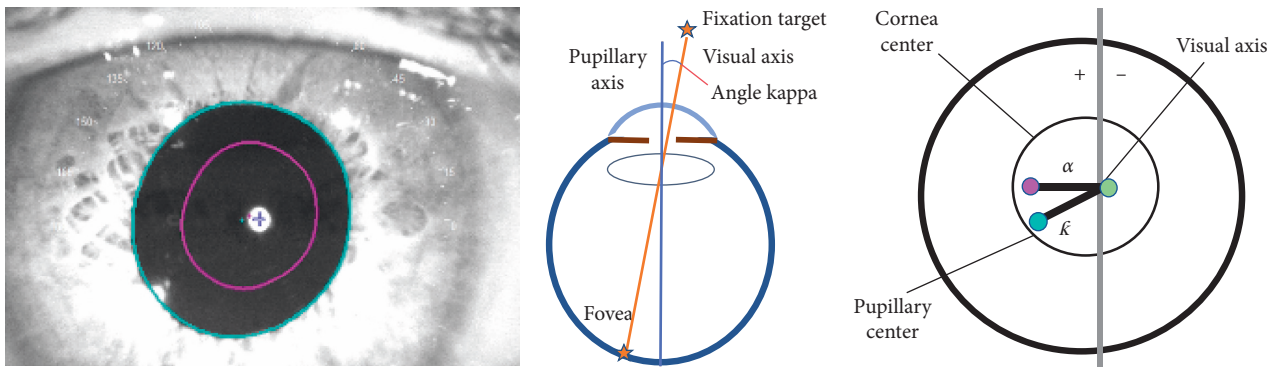

Figure 1: Pupillary diameter display and diagram of κ angle distance. (a) Comparison of pupillary diameter under mesopic and photopic conditions. (b) Diagram of κ angle formed by the visual axis and the pupillary axis. (c) Graphic representation of κ angle, visual axis, and pupillary axis, showing the center of the visual axis (green cross, representing the center of the reflection points), corneal center (violet dot in diagram, similar to the anatomic center), and pupillary center (blue dot, representing the center of the circle). The radial distance between the green cross and the violet dot represents angle alpha (α). The radial distance between the blue dot and the green cross represents angle κ (κ). The + sign represents the positive angle; and the—sign represents the negative angle.

scheduled for multifocal IOL implantation. Although recognition of the importance of angle κ and angle α for successful multifocal IOL implantation is growing, there are little data regarding their impact on objective visual quality.

In cases with a considerable angle κ, there is a greater chance of a decentration due to the increased distance between the pupillary light reflex and corneal light reflex, as depicted in Figure 1, which could lead to functional decentration of the trifocal IOL [6].

Most presbyopia-correcting IOLs have multiple concentric rings in them with varying powers, and therefore a mild IOL decentration could result in decreased vision, inducing high-order aberrations and photic phenomena including decreased contrast sensitivity, glare, and halos [6–8]. Although acknowledgment of the importance of angle κ for successful multifocal IOL implantation is increasing, few data regarding their impact on objective visual quality is widely available.

This study outlines the overall associations between angle κ distance and both the total and the internal HOAs when using two trifocal IOLs. It has been described that the optical axis/center of the capsular bag may not match the patient's visual axis when a considerable angle κ distance (>0.5 mm) is evidenced, leading to potentially poor outcomes when using a trifocal IOL [6].

The purpose of the present study was to estimate the association between angle κ distance and higher-order aberrations (HOAs) with postoperative visual acuity and vision quality after presbyopia-correcting IOL implantation employing either AT LISA tri 839MP or Acrysof IQ PanOptix IOL.

2. Materials and Methods

2.1. Design and Setting. This prospective, randomized, comparative and controlled study included patients undergoing Multifocal IOL surgery at the Anterior Segment Surgery Department at the Asociación para Evitar la Ceguera, Mexico City, Mexico. The Internal Review Board approved this study, which was conducted following the tenets of the Declaration of Helsinki and Good Clinical Practices Guidelines. All participants were briefed extensively and provided written informed consent before measurements were performed.

2.2. Patients. Cataract patients >50 years of age with lens opacities graded from NO1NC1 to NO3NC3 according to the LOCS III classification system undergoing routine phacoemulsification cataract extraction with trifocal IOL implantation were included [9]. Preoperative exclusion criteria for the study included corneal astigmatism over 1.0 D, ocular pathologies such as amblyopia, dry eye disease, evidence for corneal dystrophy, retinal pathology, glaucoma, and previous ocular surgery. The study comprised a total of 43 eyes from 43 patients: twenty-three eyes in the Acrysof IQ PanOptix group and twenty patients in the AT LISA tri 839MP group.

2.3. Experiment Design. Prior to the surgical procedure, partial coherence interferometry- (PCI-) based IOL calculation was obtained for all cases (IOLMaster 500, Carl Zeiss Meditec AG). Forty-six included patients were randomly assigned to two groups for either an AT LISA tri 839MP or an Acrysof IQ PanOptix IOL implantation after routine cataract removal (twenty-three patients per group). An OPD-Scan III analyzer (NIDEK CO., LTD., Tokyo, Japan) was utilized to assess both the angle κ distance, defined by the radial distance between the center of the pupil and the visual axis (see Figure 1), HOAs measurements, and the Strehl ratio for vision quality at the six-month follow-up visit, as depicted in Figure 2.

2.4. Instrumentation

2.4.1. IOL Master 500. A noncontact optical biometer was employed; measuring the distance from the corneal vertex to

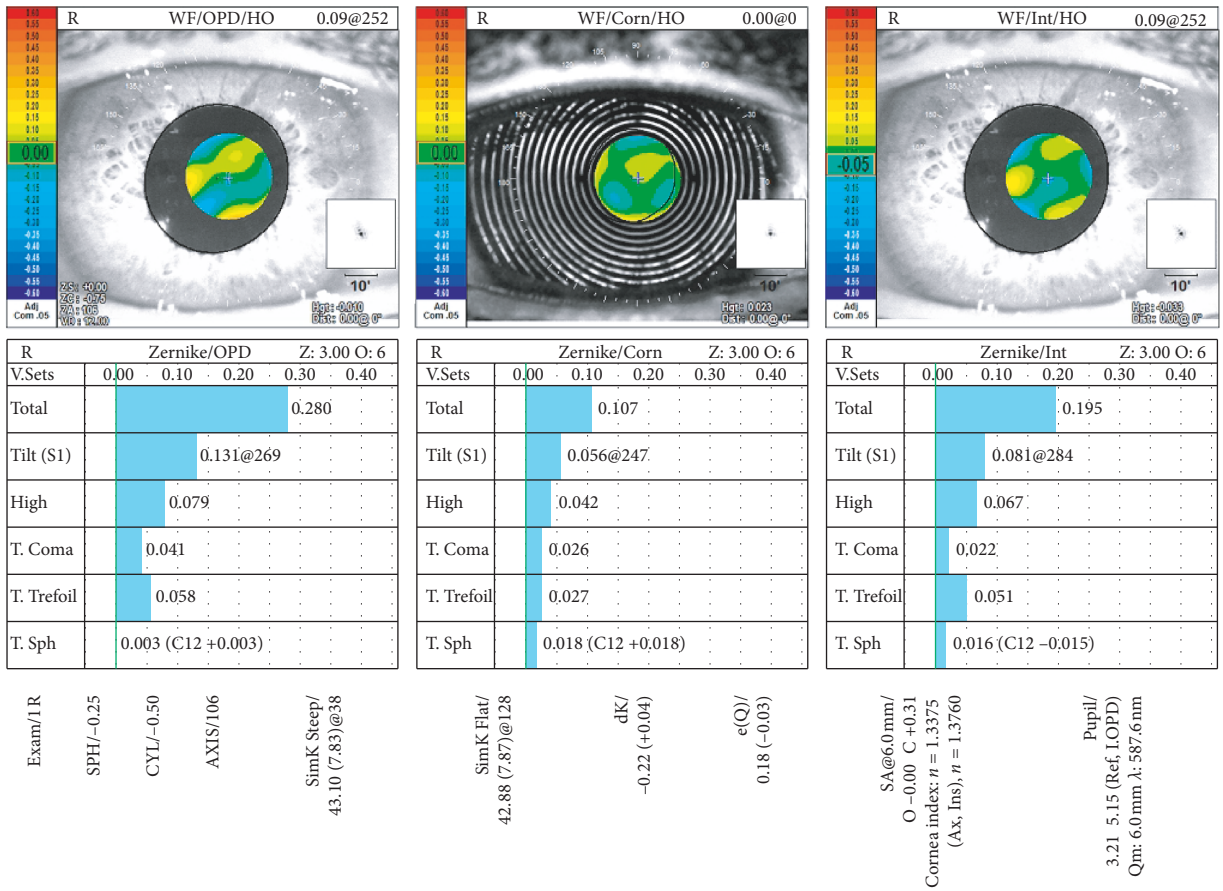

Figure 2: HOAs measurements using an OPD-Scan III analyzer obtained at the six-month follow-up visit.

the retinal pigmented epithelium (RPE): The IOL Master 500 (Carl Zeiss Meditec AG) measures the axial length, using PCI with a 780 nm laser diode infrared light. Also, keratometry, white to white distance, and anterior chamber dept, from the corneal epithelium to the anterior surface of the lens, were measured using image analysis. Each measurement requires the instrument to be aligned with the visual axis [10].

2.4.2. OPD-Scan III Analyzer. An OPD-Scan III aberrometer provided the total and intraocular high-order aberration (HOA) data, including the Strehl ratio, with a mesopic pupil under mesopic (3 cd/m2) lighting conditions [11]. The OPD-Scan III provides a complete set of maps, including four different corneal topography maps, local refractive power of the entire eye due to aberrations at various locations within the pupil, a variety of wavefront aberration maps, and photopic and mesopic pupillometry. By computing the corneal wavefront aberration and comparing it with the total wavefront map, it is possible to estimate optical quality due to the internal aberrations of the eye. The internal aberrations represent all aberrations behind the anterior corneal surface. Wavefront data are gathered from available zones up to a 9.5 mm area including 2,520 data point analyses, in 7 zone measurement, adding the capability to provide for the calculation of mesopic refractions. Placido disc topography measures 33 rings in a vertical position and 39 in the horizontal position, including 11,880 data points [11].

2.5. Main Outcome Measure. Angle κ distance was assessed as the extrapolated distance that overlapped the center of the pupil and the corneal reflex. The total and internal aberrations were evaluated separately to differentiate aberrations originated from the total optic system from the internal aberrations of the eye.

Also, the uncorrected distance visual acuity (UDVA), uncorrected near visual acuity (UNVA), and uncorrected intermediate visual acuity (UIVA) were evaluated. Visual acuities were measured under photopic conditions using Snellen visual charts and then converted into logarithm of the minimum angle of resolution (logMAR) notation.

Key optical and physical features of each IOL are summarized in Table 1. A depiction of both Trifocal IOLs is shown in Figure 3.

2.6. Surgical Technique. The same surgeon (CFVB) performed all surgical procedures employing the standard stop & chop phacoemulsification technique under topical anesthesia. 2.2 mm clear corneal incisions and 5.0 to 5.5 mm manually created capsulorhexes were employed for all surgeries, using the same ophthalmic viscosurgical device

Table 1: Trifocal IOL features [10].

Feature	Acrysof IQ PanOptix®	AT LISA tri 839MP®
Technology	Trifocal	Trifocal
Diffractive zone (mm)	4.5	6.0
Central zone	Diffractive	Diffractive
Optic type	Nonapodized	Nonapodized
Optic diameter (mm)	6.0/4.5 mm diffractive region	6.0/4.3 mm trifocal/4.3 to 6.0 mm bifocal
Near add power (D)	+3.25	+3.33
Intermediate IOL power (D)	+2.17	+1.66
Asphericity (μm)	−0.10	−0.18
IOL color	Yellow	Clear
Inner ring optical diameter	1.164 mm	1.04 mm

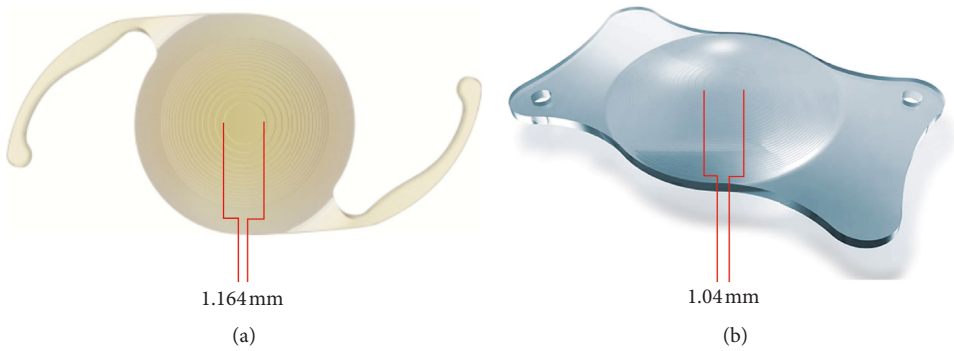

(a) (b)

Figure 3: Inner ring optical diameter of the trifocal IOLs included in the study: (a) Acrysof IQ PanOptix® and (b) the AT LISA tri 839MP®.

(OVD) Duovisc® (3.0% sodium hyaluronate, 4.0% chondroitin sulfate with 1.0% sodium hyaluronate ALCON Laboratories, Forth Worth TX, USA). After cataract removal and cortical material aspiration, all patients had in-the-bag implantation of either an AT LISA tri 839MP or an Acrysof IQ PanOptix in concordance to randomization. Finally, all remaining OVD under the IOL were removed.

2.7. Statistical Analysis. Descriptive data are shown as mean ± SD and range. Significance was assessed using the t-student and Mann–Whitney tests. The Pearson correlation coefficient (r) or the Spearman tests were employed according to data distribution [12]. Also, linear regression analyses were performed between angle κ and HOAs measurements for both presbyopia-correcting IOLs. P values < 0.05 were considered to be statistically significant. Gaussian distribution was determined using the D'Agostino–Pearson omnibus normality test for all variables. Statistical analyses were performed using the Statistical Package for Social Sciences (SPSS) software (version 15, SPSS, Inc., Chicago, IL; USA). Plots and layouts were composed using the Prism GraphPad software (Prism Inc., version 8.0).

3. Results

The study comprised a total of 43 eyes from 43 patients: twenty-three eyes in the Acrysof IQ PanOptix group and twenty patients in AT LISA tri 839MP group. An in-the-bag IOL positioning was achieved in all cases.

3.1. Preoperative Measurements. No statistically significant differences were evidenced for age and gender between groups. Preoperative data of included patients are summarized in Table 2.

3.2. Postoperative Measurements. Six months after the surgical procedure UDVA, UNVA, UIVA, and κ distance measurements were evaluated. Mean postoperative visual acuity for all distances and angle κ distance measurements at the six-month follow-up visit are shown in Table 3.

Total HOAs and internal aberrations were evaluated at the six-month follow-up visit. No statistically significant differences were evidenced between groups, as depicted in Table 4.

The Pearson correlation coefficient (r) and linear regression analyses were obtained between angle κ distance and UDVA, UNVA, and UIVA. A nonsignificant mild inverse correlation was assessed, as shown in Table 5.

Also, the Pearson correlation coefficient (r) was obtained between angle κ distance and total HOAs and internal aberrations. A mild nonsignificant positive correlation was evidenced as depicted in Table 6.

In order to assess visual quality parameters, we obtained the correlation coefficient (r) between total HOAs and the Strehl ratio, finding a statistically significant inverse correlation for both IOLs.

Three patients were withdrawn from the final study analysis due to one surgical complication (zonular dehiscence), and two patients failed to attend to their scheduled appointments after surgery.

Table 2: Preoperative measurements.

Parameter	Value	Acrysof IQ PanOptix	AT LISA tri 839MP	Difference between means	P value*
Age	Mean ± SD	67.52 ± 8.22	65.29 ± 8.12	2.23 ± 2.7	0.423
	Range	57–81	52–80		
UDVA (logMAR)	Mean ± SD	0.324 ± 0.38	0.360 ± 0.42	0.03 ± 0.02	0.251
	Range	0.09–2.00	1.1–2.00		
Spherical equivalent (D)	Mean ± SD	0.24 ± 2.1	0.34 ± 3.2	0.01 ± 0.01	0.224
	Range	−6.25 to +4.50	−7.50 to +3.50		
Corneal astigmatism (D)	Mean ± SD	0.43 ± 031	0.51 ± 0.23	0.04 ± 0.10	0.683
	Range	0–1.00	0.25–0.1.00		
Steep keratometry (D)	Mean ± SD	44.15 ± 1.30	43.80 ± 1.29	0.36 ± 0.70	0.210
	Range	41.7–46.5	42.0–46.3		
Flat keratometry (D)	Mean ± SD	43.50 ± 1.23	43.20 ± 1.47	0.39 ± 0.63	0.152
	Range	40.0–45.3	41.2–45.1		

UDVA = uncorrected distance visual acuity. *Mann–Whitney test.

Table 3: Mean visual acuity and angle κ values per group at the six-month follow-up visit.

Parameter	Value	Acrysof IQ PanOptix	AT LISA tri 839MP	95% CI	P value*
UDVA (logMAR)	Mean ± (SD)	0.092 ± 0.10	0.050 ± 0.06	0.04, 0.13	0.229
	Range	0–0.39	0–0.27		
UIVA (logMAR)	Mean ± (SD)	0.173 ± 0.18	0.182 ± 0.11	0.08, 0.13	0.669
	Range	0–0.91	0–0.39		
UNVA (logMAR)	Mean ± (SD)	0.068 ± 0.04	0.085 ± 0.07	0.08, 0.17	0.221
	Range	0–0.09	0–0.30		
Angle κ distance (mm)	Mean ± (SD)	0.337 ± 0.15	0.278 ± 0.13	−0.24, 0.11	0.093
	Range	0.10–0.62	0.02–0.64		

UDVA = uncorrected distance visual acuity; UIVA = uncorrected intermediate visual acuity; UNVA = uncorrected near visual acuity. *Mann–Whitney test.

Table 4: Comparison of the postoperative total and internal aberrations per group.

	Value	Acrysof IQ PanOptix	AT LISA tri 839MP	Difference between medians	P value*
Total aberrations					
TILT (μm)	Mean ± SD	0.291 ± 0.22	0.467 ± 0.45	0.004	0.387
	Range	0.01–1.05	0.07–1.54		
HOAs (μm)	Mean ± SD	0.381 ± 0.21	0.485 ± 0.26	0.111	0.195
	Range	0.08–0.86	0.10–1.00		
COMA (μm)	Mean ± SD	0.133 ± 0.11	0.247 ± 0.23	0.031	0.164
	Range	0.02–0.58	0.05–0.65		
TREFOIL (μm)	Mean ± SD	0.289 ± 0.18	0.255 ± 0.56	0.081	0.073
	Range	0.02–0.76	0.15–2.17		
SPHERE (μm)	Mean ± SD	0.045 ± 0.04	0.326 ± 0.40	0.098	0.075
	Range	0.00–0.17	0.00–1.00		
Internal aberration					
TILT (μm)	Mean ± SD	0.440 ± 0.39	1.11 ± 2.18	0.015	0.401
	Range	0.05–1.50	0.07–9.30		
HOAs (μm)	Mean ± SD	0.435 ± 0.67	0.831 ± 1.16	0.547	0.065
	Range	0.10–3.46	0.17–4.0		
COMA (μm)	Mean ± SD	0.183 ± 0.20	0.443 ± 0.42	0.086	0.071
	Range	0.01–0.97	0.05–1.2		
TREFOIL (μm)	Mean ± SD	0.289 ± 0.18	0.653 ± 1.15	0.054	0.256
	Range	0.05–2.13	0.15–2.17		
SPHERE (μm)	Mean ± SD	0.140 ± 0.12	0.524 ± 0.65	0.019	0.509
	Range	0.02–0.57	0.00–2.29		

*Mann–Whitney test.

4. Discussion

Implantation of multifocal IOLs has been associated with reduced image quality and undesirable visual phenomena [13–15]. Studies have shown that multifocal IOLs are associated with a higher incidence of optical aberrations, causing more halos and glare, than other types of IOLs [17–20].

There are few studies on the influence of the angle κ on the visual quality of trifocal IOLs [21]. Qi et al. recently

Table 5: Correlation between angle κ distance and UDVA, UNVA, and UIVA.

	r	95% CI	R^2	P value*
Acrysof IQ PanOptix ($n = 23$)				
UDVA (logMAR)	−0.127	−0.52, −0.31	0.016	0.573
UIVA (logMAR)	−0.279	−0.62, 0.16	0.077	0.208
UNVA (logMAR)	−0.095	−0.49, 0.33	−0.009	0.671
AT LISA tri 839MP ($n = 23$)				
UDVA (logMAR)	−0.432	−0.39, 0.87	0.187	0.284
UIVA (logMAR)	−0.360	−0.84, 0.46	0.130	0.380
UNVA (logMAR)	−0.452	−0.87, 0.36	−0.206	0.258

UDVA = uncorrected distance visual acuity; UNVA = uncorrected near visual acuity; UIVA = uncorrected intermediate visual acuity. *Pearson correlation coefficient (r).

Table 6: The correlation coefficient (r) between angle κ distance and internal aberration.

	r	95% CI	R^2	P value*
Acrysof IQ PanOptix				
Total HOAs (D)	0.371	−0.05, 0.68	0.138	0.088
Internal aberration (D)	0.304	−0.13, 0.64	0.092	0.168
AT LISA tri 839MP				
Total HOAs (D)	0.173	−0.27, 0.56	0.030	0.226
Internal aberration (D)	0.240	−0.21, 0.60	0.57	0.146

*Pearson correlation coefficient (r).

reported that the size of angle κ affected the incidence of glare and halo after trifocal IOL implantation, but that there were no significant effects on the postoperative vision. The impact on objective visual quality varied depending on the patient groupings used; these results might have been attributable to the small sample size or short follow-up time [21].

Consequently, among other factors, including the pupil size and the magnitude of preoperative astigmatism, the angle κ is to be considered when analyzing a potential trifocal IOL candidate [3]. Also, several studies have suggested that both the higher-order aberrations and the angle κ play a vital role in predicting the postoperative satisfaction after implanting a multifocal IOL [4–7].

Harrer et al. reported high variability in angle κ measurement in a large number of pseudophakic patients associated with age and axial length. However, in a regression model including all cases, the effect of axial length on the angle κ was weak due to the limited number of hyperopic eyes.

Moreover, HOAs were generally correlated weakly with the amount of angle κ. Nonetheless, a significant correlation was observed for astigmatism of the 4th order [4].

In our study, the mean postoperative visual acuity was optimal for distance, intermediate, and near vision in both groups; which confirms that both trifocal IOLs can provide good postoperative outcomes. However, no significant correlation was evidenced between the postoperative visual acuity and angle κ distance for any trifocal IOL. These findings suggest that the influence of moderate angle κ distance (mean angle κ distance of 0.337 ± 0.15, range 0.10–0.62; and 0.278 ± 0.13 range 0.02–0.64, for each group, respectively) has no significant effect on the visual acuity after trifocal IOL implantation. Similarly, no significant correlation was found between higher-order aberrations, both internal and total aberrations, and the angle κ distance for both trifocal IOLs; which further indicates that there is no significant association between these variables. Previous reports by Basmak et al. have described a significant correlation between positive refractive errors and large positive angle κ values [20]. However, these findings are evident when a considerable number of patients depict large positive angle κ measurements and positive refractive errors.

It is essential to bear in mind that the inner optical diameter of each trifocal intraocular lens is slightly different. The PanOptix inner diameter is 1.164 mm, while the AT LISA tri is 1.04 mm [13]. This particular feature allows the former a larger angle κ of 0.58 mm without associated visual phenomena according to the manufacturer when compared with the latter, with a suggested maximum κ angle of 0.52 mm. Nevertheless, for the included population, this factor seemed to have no influence regardless of the preoperative angle κ measurement on postoperative visual acuity for any distance.

On the other hand, a statistically significant inverse correlation was found between total higher-order aberrations and the Strehl ratio, which indicates the more the decisive decrease on the Strehl ratio, the more HOAs we encounter, with the consequent decrement on vision quality.

The Strehl ratio is the quotient of the peak intensity of an aberrated point spread function (PSF) to the ideal diffraction-limited PSF, with a value of 1.0 signifying perfect optical quality [20]. Moreover, the corneal Strehl ratio indicates the level of image quality in the presence of wavefront aberrations and provides one of the highest correlations with a visual performance. Our findings are in concordance to previously described data on the Strehl ratio and HOAs correlation [16–20].

Previously reported data have described that the size of the angle κ affected the visual quality of patients after trifocal IOL implantations [17]; specifically, when the angle κ distance was greater than 0.5 mm, patients' visual quality decreased, and when the angle κ was more significant than 0.4 mm, the incidence of glare and halo increased. However, in our study, no significant effects were evident in the postoperative vision, regardless of angle κ for both trifocal IOLs.

Another critical aspect of our study is that we yielded the angle κ distance in millimeters using the OPD-Scan III analyzer. The concept of an angle exists primarily in theoretical eye models and ray tracing. Clinically, the concept of displacement or a chord length is more relevant [17]. While some anterior segment imaging devices, like the OPD-Scan III (NIDEK Co., Ltd., Tokyo, Japan) report "angle" kappa, they are in fact reporting a 2-dimensional Cartesian displacement that roughly correlates with the concept of angle κ. The use of the term "chord" instead of "angle" emphasizes

the entity described, as well as its uniqueness in the literature, and the letter "mu" replaces previously used terms with historically conflicting or misused definitions [17]. Since the pupil center can shift with miosis and mydriasis, the description of chord mu should optionally include the state of the pupil [17, 22]. Current optical biometers and topographers report chord length κ (an approximation of angle κ). The Galilei anterior segment analysis system (Ziemer Ophthalmic Systems) displays X-Y Cartesian coordinates between the corneal vertex and pupil center; the distance between the corneal vertex and the pupil center (X and Y Cartesian values) can then be used to estimate the angle κ [17].

Several limitations of this study should be considered. Only objective measurements of visual outcomes were obtained, without taking into consideration the individual subjective patients' perception. Another limitation is that the number of patients with large angle κ distance is limited, and therefore, more cases are needed to support these findings further. Also, the sample size is not sufficient enough to provide information conducive to regulate conduct in this regard. Finally, no preoperative HOAs were measured; which could give a distinctive perspective to the previous state of the patient.

In summary, patients of both groups demonstrated excellent visual performance. No significant correlation was evidenced between the postoperative visual acuity and angle κ distance for both groups. These findings suggest that the influence of angle κ has no significant effect on the visual acuity when using these trifocal IOLs. Further in vivo studies of a population with different preoperative corneal aberrometry profiles would provide insight into the influence of higher-order aberrations on trifocal intraocular lenses.

5. Conclusion

In our study, both trifocal IOLs showed excellent postoperative visual performance at all distances at the six-month follow-up visit. Moreover, no significant association was found between angle κ distance and postoperative visual acuity regardless of the angle κ magnitude and inner optical diameter for the two trifocal IOL included.

Data Availability

The data used to support the findings of this study are available from the corresponding author upon request.

Conflicts of Interest

The authors have no conflicts of interest to disclose.

Acknowledgments

This work was supported by the grant number: INV-18-02 from Asociación Para Evitar la Ceguera, Mexico City, Mexico. This organization had no role in review design, data collection, and analysis, decision to publish, or preparation of the manuscript.

References

[1] M. Karhanová, F. Pluháček, P. Mlčák, O. Vláčil, M. Šín, and K. Marešová, "The importance of angle kappa evaluation for implantation of diffractive multifocal intra-ocular lenses using pseudophakic eye model," *Acta Ophthalmologica*, vol. 93, no. 2, pp. 123–128, 2015.

[2] C. Velasco-Barona, G. Cervantes-Coste, E. Mendoza-Schuster et al., "Comparison of biometric measurements obtained by the verion image-guided system versus the auto-refracto-keratometer," *International Ophthalmology*, vol. 38, no. 3, pp. 951–957, 2018.

[3] R. Braga-Mele, D. Chang, S. Dewey et al., "Multifocal intraocular lenses: relative indications and contraindications for implantation," *Journal of Cataract & Refractive Surgery*, vol. 40, no. 2, pp. 313–322, 2014.

[4] A. Harrer, N. Hirnschall, J. Tabernero et al., "Variability in angle κ and its influence on higher-order aberrations in pseudophakic eyes," *Journal of Cataract & Refractive Surgery*, vol. 43, no. 8, pp. 1015–1019, 2017.

[5] G. Prakash, A. Agarwal, D. R. Prakash, D. A. Kumar, A. Agarwal, and S. Jacob, "Role of angle kappa in patient dissatisfaction with refractive-design multifocal intraocular lenses," *Journal of Cataract & Refractive Surgery*, vol. 37, no. 9, pp. 1739-1740, 2011.

[6] P. Artal, E. Berrio, A. Guirao, and P. Piers, "Contribution of the cornea and internal surfaces to the change of ocular aberrations with age," *Journal of the Optical Society of America A*, vol. 19, no. 1, pp. 137–143, 2002.

[7] H. Hashemi, M. KhabazKhoob, K. Yazdani, S. Mehravaran, E. Jafarzadehpur, and A. Fotouhi, "Distribution of angle kappa measurements with orbscan II in a population-based survey," *Journal of Refractive Surgery*, vol. 26, no. 12, pp. 966–971, 2010.

[8] S. R. Choi and U. S. Kim, "The correlation between angle kappa and ocular biometry in Koreans," *Korean Journal of Ophthalmology*, vol. 27, no. 6, pp. 421–424, 2013.

[9] L. T. Chylack, J. K. Wolfe, D. M. Singer et al., "The lens opacities classification system III," *Archives of Ophthalmology*, vol. 111, no. 6, pp. 831–836, 1993.

[10] R. Saucedo-Urdapilleta, S. González-Godínez, M. Mayorquín-Ruiz, E. Moragrega-Adame, C. Velasco-Barona, and R. González-Salinas, "Comparative analysis and repeatability assessment of IOL Master 500 versus IOL Master 700 biometry in cataract patients," *Revista Mexicana de Oftalmología*, vol. 93, no. 3, pp. 130–136, 2019.

[11] W. He, X. Qiu, S. Zhang et al., "Comparison of long-term decentration and tilt in two types of multifocal intraocular lenses with OPD-Scan III aberrometer," *Eye*, vol. 32, no. 7, pp. 1237–1243, 2018.

[12] J. C. F. de Winter, S. D. Gosling, and J. Potter, "Comparing the Pearson and Spearman correlation coefficients across distributions and sample sizes: a tutorial using simulations and empirical data," *Psychological Methods*, vol. 21, no. 3, pp. 273–290, 2016.

[13] D. Carson, Z. Xu, E. Alexander, M. Choi, Z. Zhao, and X. Hong, "Optical bench performance of 3 trifocal intraocular lenses," *Journal of Cataract & Refractive Surgery*, vol. 42, no. 9, pp. 1361–1367, 2016.

[14] K. Miháltz, M. C. Knorz, J. L. Alió et al., "Internal aberrations and optical quality after femtosecond laser anterior capsulotomy in cataract surgery," *Journal of Refractive Surgery*, vol. 27, no. 10, pp. 711–716, 2011.

[15] T. Yamauchi, H. Tabuchi, K. Takase, H. Ohsugi, Z. Ohara, and Y. Kiuchi, "Comparison of visual performance of multifocal

intraocular lenses with same material monofocal intraocular lenses," *PLoS One*, vol. 8, no. 6, Article ID e68236, 2013.

[16] V. N. Mahajan, "Strehl ratio for primary aberrations in terms of their aberration variance," *Journal of the Optical Society of America*, vol. 73, no. 6, pp. 860-861, 1983.

[17] C. Y. Park, S. Y. Oh, and R. S. Chuck, "Measurement of angle kappa and centration in refractive surgery," *Current Opinion in Ophthalmology*, vol. 23, no. 4, pp. 269–275, 2012.

[18] P. Pérez-Merino and S. Marcos, "Effect of intraocular lens decentration on image quality tested in a custom model eye," *Journal of Cataract & Refractive Surgery*, vol. 44, no. 7, pp. 889–896, 2018.

[19] J. A. Lee, W. K. Song, J. Y. Kim, M. J. Kim, and H. Tchah, "Femtosecond laser-assisted cataract surgery versus conventional phacoemulsification: refractive and aberrometric outcomes with a diffractive multifocal intraocular lens," *Journal of Cataract & Refractive Surgery*, vol. 45, no. 1, pp. 21–27, 2019.

[20] H. Basmak, A. Sahin, N. Yildirim, T. D. Papakostas, and A. John Kanellopoulos, "Measurement of angle kappa with synoptophore and orbscan II in a normal population," *Journal of Refractive Surgery*, vol. 23, no. 5, pp. 456–460, 2007.

[21] Y. Qi, J. Lin, L. Leng et al., "Role of angle κ in visual quality in patients with a trifocal diffractive intraocular lens," *Journal of Cataract & Refractive Surgery*, vol. 44, no. 8, pp. 949–954, 2018.

[22] D. H. Chang and G. O. Waring, "The subject-fixated coaxially sighted corneal light reflex: a clinical marker for centration of refractive treatments and devices," *American Journal of Ophthalmology*, vol. 158, no. 5, pp. 863–874, 2014.

Hindawi
Journal of Ophthalmology
Volume 2019, Article ID 2596953, 7 pages
https://doi.org/10.1155/2019/2596953

Research Article

Influence of Overnight Orthokeratology Lens Treatment Zone Decentration on Myopia Progression

Anken Wang and Chenhao Yang

Department of Ophthalmology, Children's Hospital of Fudan University, Shanghai 201102, China

Correspondence should be addressed to Chenhao Yang; ychben@hotmail.com

Received 21 June 2019; Revised 25 September 2019; Accepted 10 October 2019; Published 15 November 2019

Guest Editor: Maria Vinas

Purpose. To investigate the effect of OK lens treatment zone decentration on myopia control. *Methods*. We retrospectively selected 30 OK lens wearers who met the following conditions in our hospital from more than 1300 cases: wearing lens in both eyes and only one eye was off-center while the other one was centric for more than 12 months. During the period of follow-up, the UCVA of each eye was better than 0.1 of logMAR and there were no obvious tropia, Kappa angle, and complications such as glare and diplopia. *Result*. Among 30 cases, 15 are males and 15 are females, with an average age of $9.3 \pm 1.51Y$. There were no significant differences in equivalent spherical lens, astigmatism, *e* value, flat *K*, steep *K*, astigmatism, lens diameter, and toric between the two groups ($p > 0.05$). The average distance of decentration was 0.73 ± 0.25 mm. Axis growth per year in was 0.20 ± 0.24 mm the OK-lens-decentered group and 0.29 ± 0.20 mm in the OK-lens-centric group, which shows significant difference between them ($p < 0.05$). According to the direction of decentration, 30 decentered eyes were divided into temporal group (20 eyes) and other direction group (10 eyes). The efficiency of myopia control (the growth of AL per year in OK-lens-decentered eye/the growth of AL per year in the contralateral OK-lens-centric eye) was 0.69 ± 0.50 in the temporal decentration group and 0.75 ± 0.52 in the other direction group, showing no significant difference between them ($p > 0.05$). There was no significant correlation between the efficiency of myopia control and the degree of decentration among temporal decentration group ($p > 0.05$). *Conclusion*. This self-control study without much interference factors shows that the decentration of OK lens can delay the development of myopia more effectively than being centric when uncorrected visual acuity was acceptable without obvious corneal complications, glare, or ghosting.

1. Background

Globally, uncorrected refractive errors constitute the second major cause of vision loss of which myopia is the most common and well known [1, 2]. To date, it has been estimated that myopia currently affects approximately 30% of the world's population, and it has been forecasted that the number will rise to 50% by 2050 [3]. The prevalence of myopia in young adolescents is also increasing; for instance, there are about 70% of senior high school students in China who have been diagnosed as myopia nowadays [4]. Therefore, finding effective therapies to slow the progression of myopia could potentially benefit millions of individuals.

Modern orthokeratology (OK) is a clinical nonsurgical method for temporary myopia correction and even controlling myopic progress in adolescents [5–9]. With professional inspection, clinical monitoring, and careful personal hygiene management, the safety of overnight OK treatment has repeatedly been confirmed [10, 11]. Nowadays, orthokeratology is considered to be one of the most promising means of controlling the progress of myopia in children [12, 13]. The mechanism of myopia control is not completely clear, but it is generally believed that wearing OK lenses can reshape the anterior corneal surface, flatten the central cornea, steepen the paracentral cornea, change the image quality of the central and peripheral retina, and finally form the peripheral defocus [14, 15]. However, after orthokeratology, the center of the corneal optical area cannot be consistent with the pupil center in some patients. The decentration of the corneal plastic area may result in the

increase of corneal irregular astigmatism and higher order aberration, which results in glare and other symptoms [16]. Previous reports mostly focused on its prevention and influence; whether the decentration can influence the myopia progression is rarely reported. The purpose of this study was to observe the decentration of optical zone after orthokeratology and its effect on controlling the myopia, so as to provide evidence for the mechanism of controlling myopia after orthokeratology.

2. Methods

2.1. Subjects. In this retrospective study, we reviewed all the patients who started orthokeratology between January 2015 and December 2017 treated at the Children's Hospital of Fudan University.

2.1.1. Clinical Pathway. As the first visit, all the patients underwent comprehensive examination including cycloplegic refraction, uncorrected visual acuity (UCVA), best-corrected visual acuity (BCVA), extraocular movements, corneal light reflection test, intraocular pressure, slit-lamp examination, fluorescein staining, corneal endothelial cell density, axial length, dilated fundoscopy, and corneal topography. Appropriate prescriptions for OK lens were given to them by different experienced doctors, and the patients were asked to wear OK lenses no fewer than 8 h per night and visit subsequently every 3 months. At every follow-up afterwards, they took a detailed list of ocular examinations including corneal light reflection test, slit-lamp evaluation, fluorescein staining, axial length, UCVA, and corneal topography. All subjects were treated according to the tenets of the Declaration of Helsinki.

The inclusion criteria include the following: (1) The spherical refractive error must be less than −5.00 DS with a refractive astigmatism of −1.50 DC or less and BCVA of logMAR (logarithm of the minimum angle of resolution) must be 0.0 or better before treatment. (2) OK lenses must be worn in both eyes, but only one eye should be direction-sustained decentered more than 0.5 mm and less than 1.5 mm only vertically or horizontally while the contralateral eye maintained central location. Both the decentration and central location must maintain for more than 12 months and the amount of decentration must vary within 0.5 mm (determined by corneal topography in four continued visit). (3) The UCVA of each eye must be better than 0.1 (logMar) after removal of lens at each follow-up.

The exclusion criteria include the following: (1) The subjects included should not have obvious corneal complications, glare, duplication, or any other symptoms (during each follow-up, we routinely asked children if they had glare, diplopia, or other symptoms and checked both the condition of corneal and lens care). (2) Subjects with underlying ocular disease such as retinopathy, prematurity, neonatal problems, history of genetic disease, neurodevelopment condition that might affect refractive development, or other system disorders associated myopia were excluded from this study. (3) Enrolled subjects could not have any amount of tropia by cover-uncover test at far (4.0 m) and near (0.33 m) or obvious Kappa angle. Figure 1 is the corneal topography of an included subject as an example.

2.2. Measurements of Optical Parameter. Cycloplegic refraction was measured two times by specialized technicians to make sure of the exactness.

2.2.1. Auto Refract Keratometer. *K* value was measured three times routinely with auto refract keratometer (NIDEK, Co; LTD, Japan. Model: ARK-1) by the same specialized technician, and then, the average value was recorded.

2.2.2. IOL-Master. Axial length was measured three times routinely with IOL-Master 500 (Carl Zeiss Meditec, Ag. jena, Germany) by the same specialized technician, and then, the average value was recorded.

2.2.3. Corneal Topography. Corneal profiles were measured with Carl Zeiss Atlas Corneal Topography System-9000 (Carl Zeiss Meditec, Inc. California, United States of America, Model 9000) by the same specialized technician. And each of the profiles was the best-focus image (the accuracy greater than 95%) from the four frames which were captured automatically. Either the equivalent *e* value, steep *K*, flat *K*, and corneal toricity at baseline or the corneal topography after orthokeratology can be measured precisely by using Placido rings to map the corneal surface and provide topography data.

2.3. Measurement of Treatment Zone Decentration. The amount of decentration of OK lens was measured by finding the distance between the center of the treatment zone and the pupillary center [17, 18].

According to the corneal topography, treatment zones ranged from the corneal apex to where the keratometry values changed within 1 D and less than 2 types of colors in the palette scale. The center of the treatment zone after orthokeratology was determined by marking the farthest 4 edges of the optical zone of the corneal topography map in the vertical and horizontal direction by software (Photoshop 6.0) and then the intersecting point of these 4 points can be the center. The pupillary center was determined by corneal topography with pupil-finding software. The distance between the center of the treatment zone and the pupillary center was measured precisely by the ruler of the software compared with the grid (one grid stands for 1 mm). The way of measurement can be seen in Figure 2.

After the distance between the pupillary center and the center of the treatment zone was measured, the subjects whose decentration is upon 0.5 mm both vertically and horizontally were excluded. Only patients with a decentration larger than 0.5 mm for 12 months were included in the lens-decentration group; in addition, the decentration should be less than 1.5 mm, so that sclera would not interact with the lens.

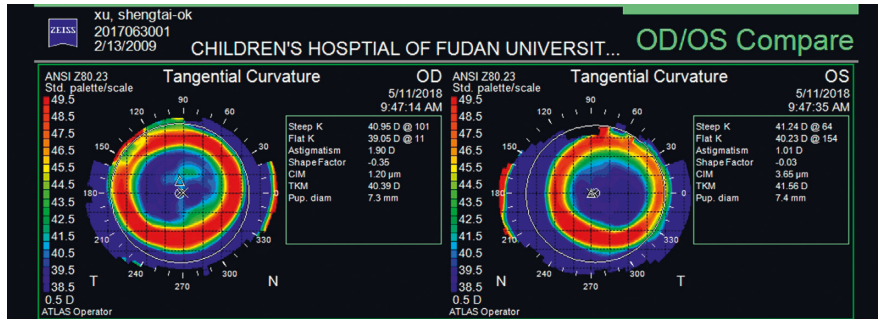

Figure 1: Corneal topography (tangent diagram) of an included subject as an example. x represents the center of corneal topography. Δ represents the corneal apex. ○ represents the pupil center.

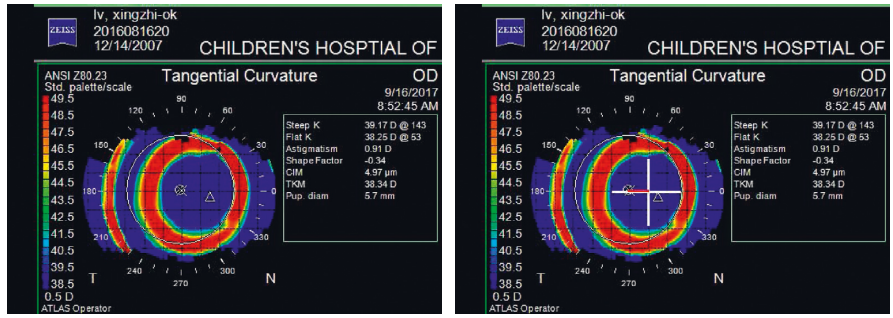

Figure 2: The measurement of treatment zone decentration. The length of the red line in the right part is the amount of decentration.

2.4. Lenses. All OK patients were fitted with five-zone reverse geometry OK lenses (α ORTHO-K®; ALPHA Corp, Nagoya, Japan), with a nominal Dk of 104×10^{-11} (cm^2/s) (mL O_2/mL·mmHg) or (LUCID ORTHO-K®, LUCID Corp, Fenghua County, Korea) with a nominal Dk of 100×10^{-11} (cm^2/s) (mL O_2/mL·mmHg) in accordance with the manufacturer's fitting instructions. After lens dispensing, patients were recommended to wear their OK lenses for at least eight consecutive hours every night. Upon stabilization of refractive error correction, they were instructed to wear their lenses for at least five nights per week. Refraction, visual acuity, corneal topography, and lens fitting were evaluated at every visit. The procedures for fitting, prescription, and replacement of OK lenses were all performed by experienced specialists.

2.5. Statistical Analysis. SPSS Statistics 24.0 (IBM Statistics, Armonk, NY) was used for statistical analysis of the lens fitting decentration and ocular biometric parameters. The Shapiro–Wilk test was used to check the normality. The difference of parameters and axial length growth between every pair of OK-lens-decentered (OLD) eye and OK-lens-centric (OLC) eye was compared using the paired t-test. The rate of axial growth was analyzed concerning lens fitting decentration by the Pearson correlation (r) test. p value less than 0.05 was considered statistically significant.

3. Results

Thirty subjects (15 males and 15 females) were evaluated with their mean age of 9.3 ± 1.51 (mean ± standard deviation, range 8 to 13 years). Before orthokeratology, the spherical equivalent refractive error, spherical refractive error, and regular astigmatism of the OLD eyes were −2.58 ± 1.15 D (range −1.00 to −4.75 D), −2.39 ± 1.05 DS (range −0.75 to −4.75 DS), and −0.44 ± 0.52 DC (range 0.00 to −1.50 DC), respectively, while those in the OLC eyes were −2.53 ± 1.16 D (range −1.00 to −5.00 D), −2.32 ± 1.06 DS (range −0.75 to −4.75 DS), and −0.50 ± 0.50 DC (range 0.00 to −1.50 DC), respectively. The difference between two groups was not statistically significant by paired t test in spherical equivalent refractive error ($p = 0.60$), spherical refractive error ($p = 0.43$), and regular astigmatism ($p = 0.35$). Before orthokeratology, the steep K, flat K, corneal toricity, and equivalent e value of the OLD eye were 43.60 ± 1.42 D (range 39.75 to 46.00 D), 42.78 ± 1.33 D (range 40.00 to 45.00 D), 0.86 ± 0.53 D (range 0.25 to 2.25 D), and 0.61 ± 0.08 (range 0.42 to 0.77), respectively, while those in the OLC eye were 43.61 ± 1.65 D (range 39.25 to 46.25 D), 42.86 ± 1.56 D (range 39.50 to 46.00 D), 0.84 ± 0.54 D (range 0.00 to 2.25 D), and 0.63 ± 0.10 (range 0.42 to 0.85), respectively. The difference between two groups was not statistically different by paired t test in steep K ($p = 0.96$), flat K ($p = 0.40$), corneal toricity ($p = 0.80$), and equivalent e value ($p = 0.15$). The biological parameters of both eyes and data of their lenses can be seen in Table 1.

Among thirty pairs of eyes, there were three subjects who wore different grands OK lens in each eye, but the Wilcoxon signed rank test shows no statistical difference between two groups ($p = 0.102$). The lens diameter and lens toricity were 10.59 ± 0.19 mm (range 10.00 to 11.00 mm) and −0.17 ± 0.38 D (range −1.00 to 0.00 D) in the OLD group, while 10.61 ± 0.17 mm (range 10.20 to 11.00 mm) and

Table 1: Difference of biological parameters and lens between OLD eyes and OLC eyes.

Parameter (mean ± SD)	OLD eye ($n = 30$)	OLC eye ($n = 30$)	p value
Spherical equivalent refractive error (D)	−2.58 ± 1.15	−2.53 ± 1.16	0.60
Spherical refractive error (DS)	−2.39 ± 1.05	−2.32 ± 1.06	0.43
Regular astigmatism (DC)	−0.44 ± 0.52	−0.50 ± 0.50	0.35
Equivalent e value	0.61 ± 0.08	0.63 ± 0.10	0.15
Steep K (D)	43.60 ± 1.42	43.61 ± 1.65	0.96
Flat K (D)	42.78 ± 1.33	42.86 ± 1.56	0.39
Corneal toricity (D)	0.86 ± 0.53	0.84 ± 0.54	0.80
Lens toricity (D)	−0.17 ± 0.38	−0.12 ± 0.36	0.37
Lens diameter (mm)	10.59 ± 0.19	10.61 ± 0.17	0.18

−0.12 ± 0.36 D (range −1.50 to 0.00 D) in the OLC group, showing no statistical difference by the paired t test ($p = 0.184$ and $p = 0.326$).

Distance of lens fitting decentration in the OLD group was 0.73 ± 0.25 mm (range 0.50 to 1.50 mm), including 20 (66.67%) temporal, 4 (13.33%) nasal, 3 (10%) superior, and 3 (10%) inferior (Figure 3). The distance of decentration shows no statistical correlation with its direction by the Spearman rank correlation coefficient test ($p = 0.165$) and no statistical correlation with the spherical equivalent refractive error ($p = 0.65$), corneal toricity ($p = 0.40$), equivalent e value ($p = 0.96$), lens toricity ($p = 0.27$), and lens diameter ($p = 0.99$) by Pearson correlation coefficient test.

Mean axial length growth per year in OLD group is 0.20 ± 0.24 mm and 0.29 ± 0.20 mm in the OLC group. Statistically significant difference was found in mean axial length growth per year between OLD and OLC group by the paired t test ($p = 0.003$) (Figure 4).

Because the major direction is temporal, while the other three directions are too few for statistical analysis, we divided all OLD eyes into temporal group and other direction group. To avoid bring individual differences, it is inappropriate to compare the amount of axial growth directly among different children. Thus, we use the ratio of axial growth rate between paired OLD eye and OLC eye to express the efficiency of myopia control (EMC: growth of AL per year in OLD eye/growth of AL per year in the contralateral OLC eye) instead of value of axial growth. The average EMC is 0.69 ± 0.50 in the temporal decentration group and 0.75 ± 0.52 in the other direction group, which shows no statistical difference by two independent samples t-test ($p = 0.75$). The mean magnitude of decentration is 0.70 ± 0.28 mm in the temporal group and 0.80 ± 0.20 mm in the other direction group, showing no statistical difference by two independent samples t-test ($p = 0.27$), which eliminates the interference caused by the different degrees of decentration between two groups.

20 eyes with temporal decentration were selected for analyzing the relationship between the EMC and the amount of decentration. The average EMC is 0.69 ± 0.50 and the average decentration is 0.70 ± 0.28, and there is no statistical relationship between them by the Pearson correlation analysis ($p = 0.75$) (Figure 5).

4. Discussion

Owing to the effectiveness of controlling myopia in adolescents, there is a gradual increase in application of OK treatment that has been chosen by more than 1.5 million adolescents in China [19]. However, fitting decentration cannot be completely avoided during the whole procedure. In the clinical application of orthokeratology, lens decentration has become a common problem for both physicians and patients, probably nearly to half percent according to some study [16, 20, 21]. Since the off-center of OK lens is so common, whether it can affect the progression of myopia or not aroused the authors' interest and attention.

Whether the decentration of OK lens makes difference on myopia controlling is a fresh and difficult question to solve because it is hard to measure the decentration and to exclude the confounding factors especially individual differences like age, ocular biometric parameters, eye care habits, daily exposure of sunshine outdoor, genetic characteristics, and the frequency of wearing spectacles or lens.

About the measurement of decentration, as far as we are concerned, it can be the distance between the center of the treatment zone and the initial corneal apex, but it will take a lot of efforts to make the difference maps on corneal topography between the new one and initial one for all the patients. It can also be the distance between the center of the treatment zone and the pupillary center which is used by many other reports [17, 18, 22]. In the latter one, just a tangential map at that time is needed and the influence of Kappa angle can be reduced, so we pick the latter one.

About the results, Wu et al. recently found that the decentration of OK lens will slow down the growth of myopia by retrospectively analyzing right eyes of 134 children wearing OK lens decentered in varying degrees [22]. It is an elaborate research but still cannot avoid the individual differences. In our study, we investigated the sole influence of overnight OK lens fitting decentration on myopia progression by self-control study, that is to say, found the subjects who wore OK lens in both eyes while single OK-lens was decentered, excluding most of the individual differences, differing from the previous study. In this research, we found that for the same child, the axial length of the OLD eye grew slower than that in the OLC eye according to the usual definition of decentration [17, 18], which is similar to Wu's result. Of course, this is on the premise that the decentration is less than 1.5 mm and the glare, ghosting, or corneal epithelial staining is not obvious. Therefore, according to the result, since the decentration of OK lens is hard to avoid completely in our clinical practice, we need not worry about the adverse effect of off-center on myopia control too much if the vision of children is acceptable; the amount of

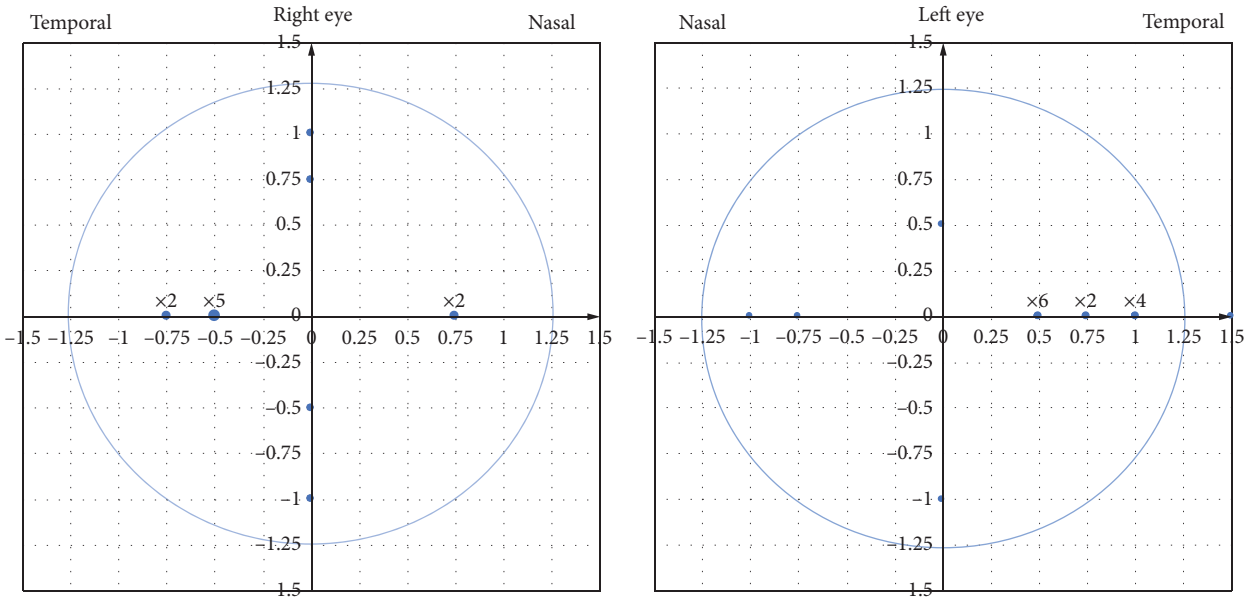

Figure 3: The position of lens fitting among 30 OLD eyes. Each lattice represents 0.25 mm on corneal and the symbol of ×2 means there are two cases of this position, and so on.

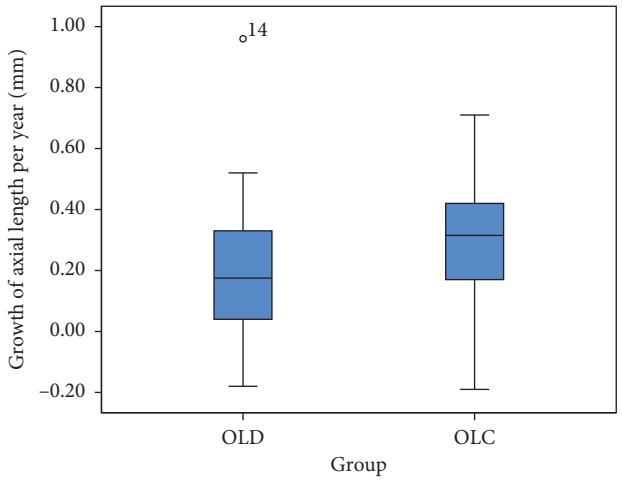

Figure 4: Box plot for comparison about mean axial length growth per year between OLD group and OLC group.

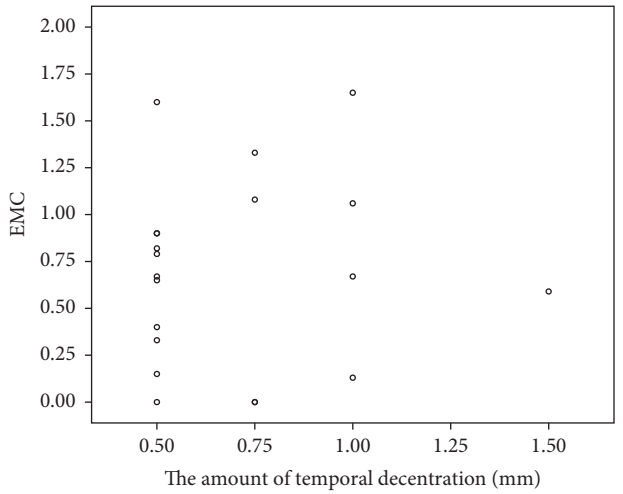

Figure 5: Scatter plot for relationship between EMC and the amount of decentration in 20 eyes with temporal decentration.

decentration is not very serious and there is no obvious complications with the child.

The reason of decentration has always been a hot topic. Chen found that the magnitude of corneal asymmetry vector significantly contributed to the amount of lens decentration, whereas the baseline spherical or astigmatic refractive error, corneal eccentricity, flat *K*, horizontal visible iris diameter, or lens diameter did not affect orthokeratology lens decentration [18]. In our research, there is no significant difference in corneal asymmetry or other ocular parameters between two eyes, so why did the continued condition occur in which one eye is in right position while another is decentered ? According to our conjecture, it may attribute to the different strength of eyelid between two eyes and the doctor's prescription for lens. The strength of eyelid is hard to measure or control, and for that reason, it is rarely reported. The reason why the decentration is monocular is still unknown, promoting us to continue further study.

It is confirmed that temporal is the most frequent direction of decentration (horizontal and vertical); for example, Chen found 84.9% temporal in 106 OK-lens-decentered eye and Yang found 48.5% temporal in 270 OK-lens-decentered eye which is the most common direction [20, 21], and our results are in relatively good agreement with those of previous reports.

It will lead to errors caused by large individual differences if we use the axial length values directly when exploring the relationship between AL growth and direction or degree of decentration among different children, so we introduced the new variable named EMC, which shows how strong the effect of decentration on myopia control is in the same child. In previous comparative

analysis of OLD eyes and OLC eyes, we used paired *t* test because they are from the same child and had the almost same parameters, which can reflect the difference caused by different positions more accurately, but when analyzing EMC, two independent sample *t* tests were used because the subjects in OLD group were from different children. According to the analysis, whether the decentration is temporal or not does not affect the EMC on the premise that the interference from its different degrees has been eliminated. Unfortunately, it is not appropriate to discuss all directions in detail, because the cases with not-temporal-directions decentration are too few for statistical analysis. At the same time, from the analysis of 20 eyes with temporal decentration, we found there was no statistical correlation between EMC and the degree of decentration when the distance is over 0.5 mm, while Wu's study showed the opposite result [22]. Because of the design of this retrospective experiment, the sample size for this problem is relatively small, so we need many large sample studies to confirm this conclusion.

Although orthokeratology has been proved to be effective in controlling myopia, it is mechanism is still not totally clear. The most possible one is considered the peripheral defocus forced by reshaping the anterior corneal surface and then changing the image quality of the central and paracentral retina affecting the axis growth by pathway of choroid, sclera, etc [23]. One possibility is that a dose-response relationship exists where greater amounts of peripheral myopic defocus result in greater reductions in myopia progression. Another possibility is that there is a range-response relationship and that any amount of myopic peripheral defocus above some threshold acts as a "stop" signal to slow myopia progression. If range-response or dose-response relationship exists, the greater reductions in myopia progression in OLD eyes are possible as more peripheral locations may experience the myopic defocus or more total peripheral myopic defocus may be formed when the pupil is closer to the edge of treatment zone [24]. Up to now, there are rare research studies mentioning the measurement of the peripheral defocus accurately when the lens is off-center. In addition, testing the peripheral defocus was limited by the lack of instruments, so it is hard to estimate the difference of the range and degree of peripheral defocus between OLD eyes and OLC eyes. It is worthwhile for us to do further research about peripheral defocus.

In this study, 6 eyes were found to have different degrees of axial shortening. On the one hand, it may be caused by measurement error; on the other hand, the most possible reason is the increase of choroidal thickness after orthokeratology and other scholars have also found some similar cases of shortened axial length [25, 26]. As it is known to all, IOL-Master measures the length between the corneal vertex and retinal pigment epithelium along the visual axis using a red fixation beam, which is the most common way to measure the axial length, so the thicker choroid will lift the retinal pigment epithelium and decrease the axial length measured according to the theory [25, 26]. However, the relationship between formation of thicker choroid and peripheral myopic defocus remains to be studied, so as the question about whether the increase of blood flow in thicker choroid affects the progression of myopia.

One of the limitation of this study is that the sample size is small especially the case with not-temporal-direction decentration. But to be honest, it is very difficult to find 30 cases that meet the inclusion and exclusion criteria from more than 1300 cases. Another limitation is we did not measure the peripheral defocus precisely, which may prompt us to move on to a more complete prospective study.

5. Conclusion

To summarize, lens decentration is a common phenomenon in orthokeratology. By excluding most of the interference factors, we found that OK lens being decentered less than 1.5 mm can delay the development of myopia more effectively than being centric when UCVA was acceptable without obvious corneal complications, glare, or ghosting. And there was no significant correlation between the effect and the degree or direction of decentration. But we still do not recommend the intention to make the lens decentered by modifying original prescription, because the complications still can be intractable problems.

Data Availability

The raw data used to support the findings of this study are included within the supplementary materials.

Conflicts of Interest

The authors report no conflicts of interest.

Acknowledgments

This study was funded by the Project of Shanghai Science and Technology (Grant no. 17411950200 and 17411950202), the Optimization for Prevention and Control of Juvenile Myopia.

Supplementary Materials

The excel sheet can be described as "ocular biometric parameters of 30 children included in this study before orthokeratology and the growth of AL one year after. (*Supplementary Materials*)

References

[1] R. Dandona and L. Dandona, "Refractive error blindness," *Bull World Health Organ*, vol. 79, no. 3, pp. 237–243, 2001.

[2] S.-R. Jacinto, V.-C. César, B. Gilmartin, G.-O. Ramón, and K. Sugimoto, "Long-term efficacy of orthokeratology contact lens wear in controlling the progression of childhood myopia," *Current Eye Research*, vol. 42, no. 5, pp. 713–720, 2017.

[3] B. A. Holden, T. R. Fricke, D. A. Wilson et al., "Global prevalence of myopia and high myopia and temporal trends from 2000 through 2050," *Ophthalmology*, vol. 123, no. 5, pp. 1036–1042, 2016.

[4] Z. Kang, F. Tao, J. Jing, X. Xu, and L. Su, "A meta-analysis for prevalence of myopia among Chinese teenagers journal of

clinical," *Journal of Clinical Ophthalmology*, vol. 24, no. 5, pp. 395–399, 2016.

[5] H. A. Swarbrick, "Orthokeratology review and update," *Clinical and Experimental Optometry*, vol. 89, no. 3, pp. 124–143, 2006.

[6] S. W. Cheung, P. Cho, and D. Fan, "Asymmetrical increase in axial length in the two eyes of a monocular orthokeratology patient," *Optometry and Vision Science*, vol. 81, no. 9, pp. 653–656, 2004.

[7] S. A. Tay, S. Farzavandi, and D. Tan, "Interventions to reduce myopia progression in children," *Strabismus*, vol. 25, no. 1, pp. 23–32, 2017.

[8] P. Cho and Q. Tan, "Myopia and orthokeratology for myopia control," *Clinical and Experimental Optometry*, vol. 102, no. 4, pp. 364–377, 2019.

[9] J. J. Walline, "Myopia control: a review," *Eye & Contact Lens: Science & Clinical Practice*, vol. 42, no. 1, pp. 3–8, 2016.

[10] K.-S. Na, Y.-S. Yoo, H. S. Hwang, J. W. Mok, H. S. Kim, and C.-K. Joo, "The influence of overnight orthokeratology on ocular surface and meibomian glands in children and adolescents," *Eye & Contact Lens: Science & Clinical Practice*, vol. 42, no. 1, pp. 68–73, 2016.

[11] Y. M. Liu and P. Xie, "The safety of orthokeratology—a systematic review," *Eye & Contact Lens: Science & Clinical Practice*, vol. 42, no. 1, pp. 35–42, 2016.

[12] J.-K. Si, K. Tang, H.-S. Bi, D.-D. Guo, J.-G. Guo, and X.-R. Wang, "Orthokeratology for myopia control: a meta-analysis," *Optometry and Vision Science*, vol. 92, no. 3, pp. 252–257, 2015.

[13] D. Wen, J. Huang, H. Chen et al., "Efficacy and acceptability of orthokeratology for slowing myopic progression in children: a systematic review and meta- analysis," *Journal of Ophthalmology*, vol. 2015, Article ID 360806, 12 pages, 2015.

[14] A. Queirós, A. Amorim-de-Sousa, L.-F. Daniela, V.-C. César, Á. R. Gutiérrez, and G.-M. José Manuel, "Relative peripheral refraction across 4 meridians after orthokeratology and LASIK surgery," *Eye and Vision*, vol. 5, no. 1, 2018.

[15] A. Queirós, V.-C. César, Á. R. Gutiérrez et al., "Anterior and posterior corneal elevation after orthokeratology and standard and customized LASIK surgery," *Eye & Contact Lens: Science & Clinical Practice*, vol. 37, no. 6, pp. 354–358, 2011.

[16] T. Hiraoka, T. Mihashi, C. Okamoto, O. Fumiki, H. Yoko, and O. Tetsuro, "Influence of induced decentered orthokeratology lens on ocular higher—order wavefront aberrations and contrast sensitivity function," *Journal of Cataract & Refractive Surgery*, vol. 35, no. 11, pp. 1918–1926, 2009.

[17] V. K. Okamoto, P. Gifford, E. Lum et al., "Treatment zone decentration during orthokeratology on eyes with corneal toricity," *Optometry and Vision Science*, vol. 93, no. 9, pp. 1101–1111, 2016.

[18] Z. Chen, F. Xue, J. Zhou, X. Qu, and X. Zhou, "Prediction of orthokeratology lens decentration with corneal elevation," *Optometry and Vision Science*, vol. 94, no. 9, pp. 903–907, 2017.

[19] P. Xie and X. Guo, "Chinese experiences on orthokeratology," *Eye & Contact Lens: Science & Clinical Practice*, vol. 42, no. 1, pp. 43–47, 2016.

[20] X. Yang, X. M. Gong, Z. Y. Dai, L. Wei, and S. X. Li, "Topographical evaluation on decentration of orthokeratology lenses," *Zhonghua Yan Ke Za Zhi*, vol. 39, no. 6, pp. 335–338, 2003.

[21] J. Chen, W. Huang, Z. Rong, J. Jun, and L. Yiyu, "Influence of overnight orthokeratology lens fitting decentration on corneal topography reshaping," *Eye and Vision*, vol. 5, no. 1, 2018.

[22] G.-Y. Wu, X.-Q. Lai, and X.-D. Dai, "Effect of decentration in controlling the development of myopia after orthokeratology," *International Eye Science*, vol. 18, no. 1, pp. 188–191, 2018.

[23] A. Benavente-Perez, A. Nour, and D. Troilo, "Axial eye growth and refractive error development can be modified by exposing the peripheral retina to relative myopic or hyperopic defocus," *Investigative Ophthalmology & Visual Science*, vol. 55, no. 10, pp. 6765–6773, 2014.

[24] D. A. Berntsen, C. D. Barr, D. O. Mutti, and K. Zadnik, "Peripheral defocus and myopia progression in myopic children randomly assigned to wear single vision and progressive addition lenses," *Investigative Opthalmology & Visual Science*, vol. 54, no. 8, pp. 5761–5770, 2013.

[25] Z. Chen, F. Xue, J. Zhou, X. Qu, and X. Zhou, "Effects of orthokeratology on choroidal thickness and axial length," *Optometry and Vision Science*, vol. 93, no. 9, pp. 1064–1071, 2016.

[26] Z. Li, D. Cui, Y. Hu, S. Ao, J. Zeng, and X. Yang, "Choroidal thickness and axial length changes in myopic children treated with orthokeratology," *Contact Lens and Anterior Eye*, vol. 40, no. 6, pp. 417–423, 2017.

Hindawi
Journal of Ophthalmology
Volume 2019, Article ID 9382467, 6 pages
https://doi.org/10.1155/2019/9382467

Research Article

Optical Evaluation of New Designs of Multifocal Diffractive Corneal Inlays

Diego Montagud-Martínez,[1] Vicente Ferrando,[1] Juan A. Monsoriu,[1] and Walter D. Furlan [2]

[1]*Centro de Tecnologías Físicas, Universitat Politècnica de València, Valencia 46022, Spain*
[2]*Departamento de Óptica y Optometría y Ciencias de la Visión, Universitat de València, Burjassot 46100, Spain*

Correspondence should be addressed to Walter D. Furlan; walter.furlan@uv.es

Received 19 June 2019; Accepted 9 September 2019; Published 11 November 2019

Guest Editor: Pablo Pérez-Merino

Purpose. To assess the imaging properties of two different designs of a new concept of corneal inlays whose working principle is based on diffraction. *Methods*. The quality of the retinal images provided by Diffractive Corneal Inlays (DCIs) was evaluated theoretically in comparison with Small Aperture Corneal Inlay (SACI). ZEMAX OpticStudio software was employed for the simulations in an eye model with different pupil diameters (3.0 mm and 4.5 mm). The employed merit functions in the analysis were the Modulation Transfer Function (MTF), the area under the MTF (MTFa), and the Point Spread Function (PSF). Comparison was made with the SACI at different defocus conditions. *Results*. The bifocal nature of the DCIs was demonstrated in a model eye for the first time. It was shown that the intensity of the near focus depends on the radius of the central zone. Retinal image quality of the DCI was equal to or exceeded the SACI in the majority of visual conditions as was demonstrated with simulated images. *Conclusions*. A new customizable type of corneal inlays has been evaluated using objective numerical simulations. Improvements in imaging of near objects and in light throughput compared with the popular small aperture inlays were demonstrated. These findings open a new technical branch of minimally invasive surgical solutions for the treatment of presbyopia.

1. Introduction

Presbyopia affects almost all adults over 45 years of age, and it has been estimated that globally there are more than 1.8 billion people with presbyopia, 820 million of whom had near visual impairment because they had no, or inadequate, vision correction [1].

At present, the minimum invasive surgical option for presbyopes who do not want glasses or contact lenses is to implant a corneal inlay. By means of a femtosecond laser, the surgeon creates a pocket inside the corneal stroma where the inlay is inserted, rendering the surgical procedure fast, simple, and importantly reversible.

Based on the working principle, different options have been launched in the market in the last years: corneal reshaping device, refractive corneal device, and small aperture corneal inlay (SACI) [2]. The last one, commercially known as Kamra® inlay (AcuFocus, Inc., Irvine, California, USA), is undoubtedly the most popular due to the reported good clinical outcomes [3, 4]. This device is an opaque disk of a biocompatible material (polyvinylidene fluoride) with a central aperture that produces an extended depth of focus. In addition, to facilitate the flow of nutrients to cells of the corneal stroma, the disk has a reduced external diameter and has more than 8,000 micropores, in a size range of 5–11 μm diameter. Unfortunately, although SACI implantation can result in improved intermediate and near vision, it has several important intrinsic drawbacks. Firstly, only about twenty percent of the incident light passes through the disc's central aperture. Secondly, as much as five percent of incident light is diffracted by the disc's microholes. Thirdly, as the SACI is implanted monocularly, the interocular

Table 1: Phakic model eye with corneal inlay (CI).

Surface	Radius (mm)	Asphericity	Thickness (mm)	Refractive index
Anterior cornea	7.80	–0.50	0.20	1.377
Anterior CI	7.80	–0.50	0.005	1.377
Posterior CI	7.80	–0.50	0.315	1.377
Posterior cornea	6.70	–0.30	3.1	1.337
Iris	—	—	0.1	1.337
Anterior lens	10	0	3.7	1.42
Posterior lens	–6	–3.25	16.58	1.336

asymmetry induced by anisocoria combined with monovision deteriorates binocular summation [5] and stereoacuity [6].

In an effort to avoid these drawbacks, our group recently proposed a new concept of corneal inlays that take profit of the diffraction phenomena originated in the micropores of the SACI [7]. The result, DCI, is a device that, by exploiting the photon sieve concept [8], creates a diffractive focus for near vision in the implanted eye, on a personalized basis. In fact, an additional and important benefit of the DCI is that its optical characteristics (addition, intensity ratio between the near and far foci, and so on) can be modified by varying the size of the pinholes and the pattern of their distribution indicating that DCIs could be customized for a variety of specific patient's needs.

2. Materials and Methods

2.1. Model Eye. The assessment of the imaging properties of two different DCIs was investigated by implementing a schematic eye in the Zemax OpticStudio optical design software (http://www.zemax.com/os/opticstudio). The phakic model eye employed in the simulations was the Eye Retinal Image.zmx included in the Zemax software (see Table 1), in which the polychromatic receptor photopic spectral sensitivity is simulated using 470, 510, 555, 610, and 650 nm wavelengths, with relative weights, i.e., of 0.091, 0.503, 1.0, 0.503, and 0.107, respectively.

2.2. Corneal Inlays. Two DCI models with an external diameter of 4.15 mm were evaluated in this study, both designed to provide a near focus corresponding to a typical addition of +2.50 D. Model DCI #1 was designed with a central hole of 1.00 mm diameter surrounded by 8 rings conformed by a total of 6394 holes. DCI #2 was designed with a central hole of 1.6 mm diameter surrounded by 8 rings with a total of 5989 holes. These two models have been considered to show the versatility in the DCI design and to study the influence on the resulting image performance of the central hole diameter. The external diameter corresponds to the original design [7]. A completely opaque SACI with the dimensions of the Kamra® has been evaluated in parallel as a reference. The inlays were located in the model eye at 0.20 mm from the anterior corneal surface as "User Defined Aperture" (uda) in ZEMAX, with the same radius of curvature and an asphericity of the anterior cornea surface (see Table 1). The inlay thickness was assumed as 5 μm, and diagrams of the evaluated DCIs and SACI are shown in Figure 1.

2.3. Metrics. The image quality provided by the corneal inlays in this study was assessed using different merit functions. First, the MTFs were computed for different object vergences in the range from +0.5 D to –3.5 D in steps of 0.1 D. The best focus position of the retina remained the same for all MTF calculations. In each case, the MTFa was calculated as the numerical integral (using the trapezoid rule) for MTFs in a frequency range from 9.5 cpd to 59.9 cpd. These spatial frequencies correspond approximately to the sizes of letters of visual acuity charts between +0.5 logMAR and –0.2 logMAR.

Additionally, simulated images of a visual acuity test chart were obtained from the PSF provided by ZEMAX by means of the numerical convolution using a Matlab (MathWorks, Inc. R2018b) code. The simulations were performed with polychromatic light using 5 wavelengths as previously mentioned.

3. Results and Discussion

Figure 2 shows the MTFs provided by the three corneal inlays at the far and near foci for 3.0 mm and 4.5 mm pupil diameters, simulating the eye response to photopic and mesopic lighting conditions, respectively. In order to enhance the differences, the MTFs in the near focus were represented on a logarithmic scale in the range from 0.03 to 1.

Note that, except for the distance focus and 3.0 mm pupil diameters, the performance of both models of DCI is superior to the SACI, even though the diffractive effects of the SACI (harmful for the image quality, in this case) have not been considered in the simulations. A better MTF curve was achieved by DCI #2 at the far focus for both pupils but with minimum differences. On the other hand, DCI #1 provides a better near focus than DCI #2. These results can also be verified in terms of area under MTF. Figure 3 shows MTFa computed for 3.0 mm and 4.5 mm pupils in the range of frequencies that are important in terms of visual acuity.

For 3.0 mm pupil diameter, bigger differences can be observed between the three designs. DCI #1 has the lower values for the far focus, but the higher values for the near focus. These differences are attenuated for 4.5 mm pupil. In this case, all the three inlays have a comparable performance at the far focus, but both DCIs maintain an effective near focus.

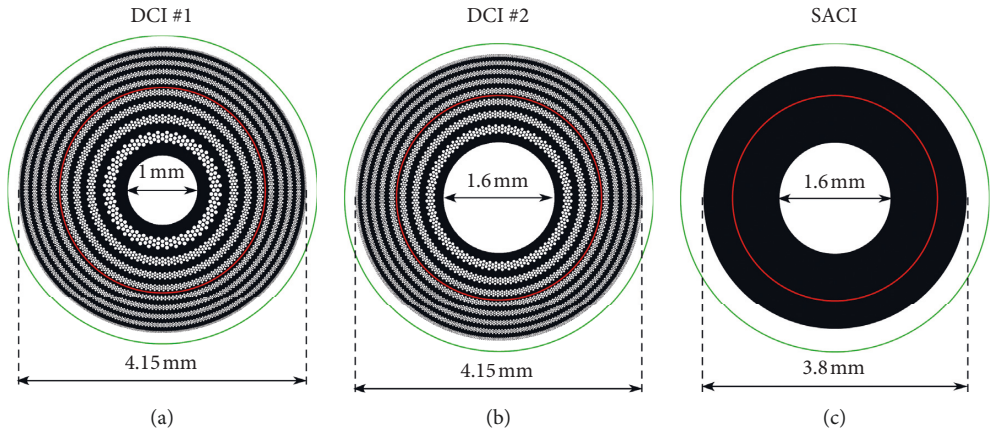

Figure 1: Diagrams of the corneal inlays evaluated in this study. The red and green circles represent 3.0 mm and 4.5 mm pupil diameters, respectively.

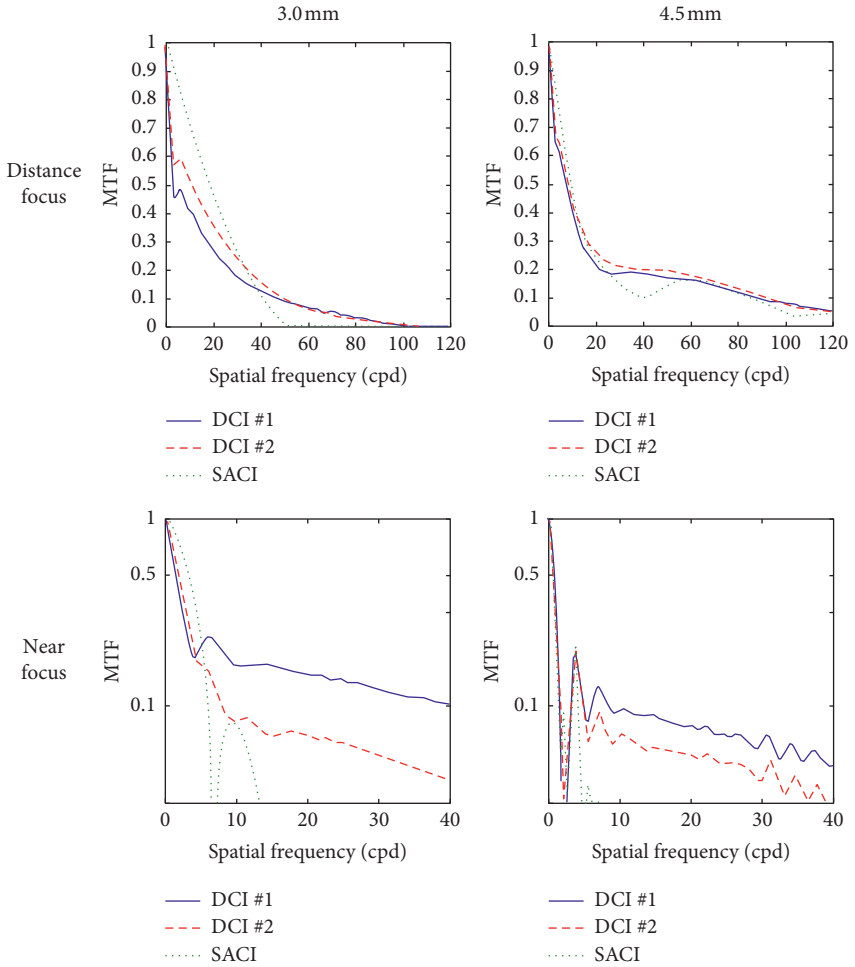

Figure 2: MTFs at the far and near foci provided by the three corneal inlays considered in this study.

Figures 2 and 3 reveal the image quality of the studied corneal inlays; however, the main difference between the DCIs and SACI performance relies in the light throughput, which is more explicit in the comparison between the images obtained from the corresponding PSFs. Figures 4 and 5 show the PFSs provided by the model eye with two pupil diameters, virtually implanted with the different inlays, for point objects at far and near distances. Note that the scales of the PSFs are different, indicating the different intensities achieved with each inlay model. In these figures, the corresponding simulated images of three Snellen "E"s, with sizes corresponding to 0.4, 0.2, and 0 logMAR visual acuities are shown next to the corresponding PSF.

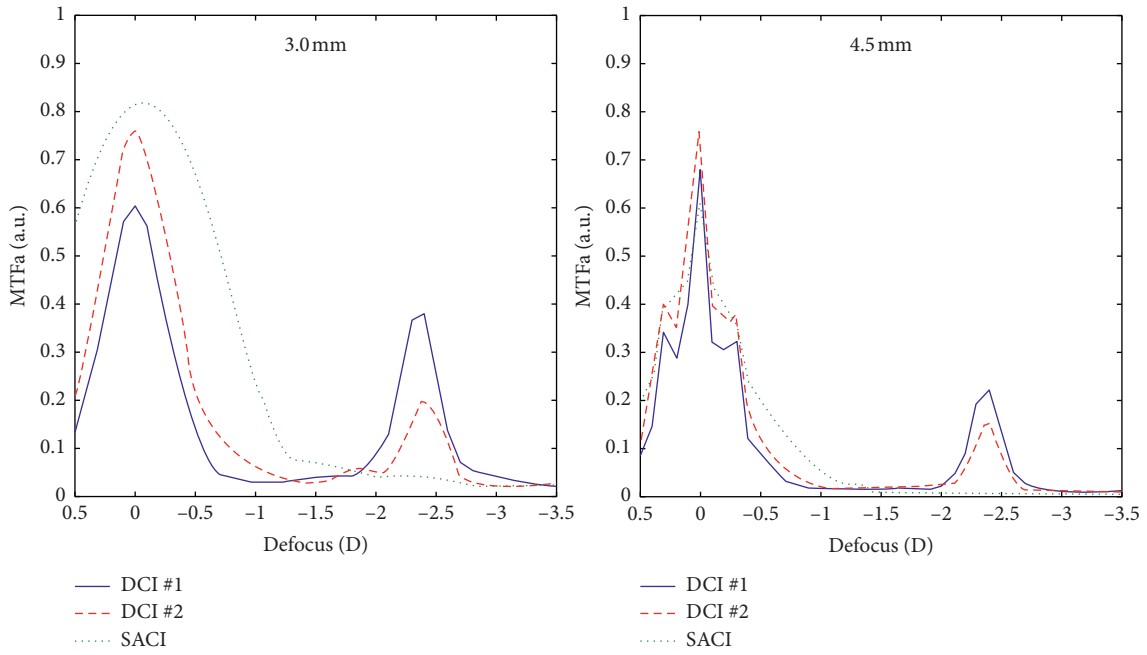

Figure 3: Comparative MTFa, in arbitrary units (a.u.), for 3.0 and 4.5 mm pupil diameters.

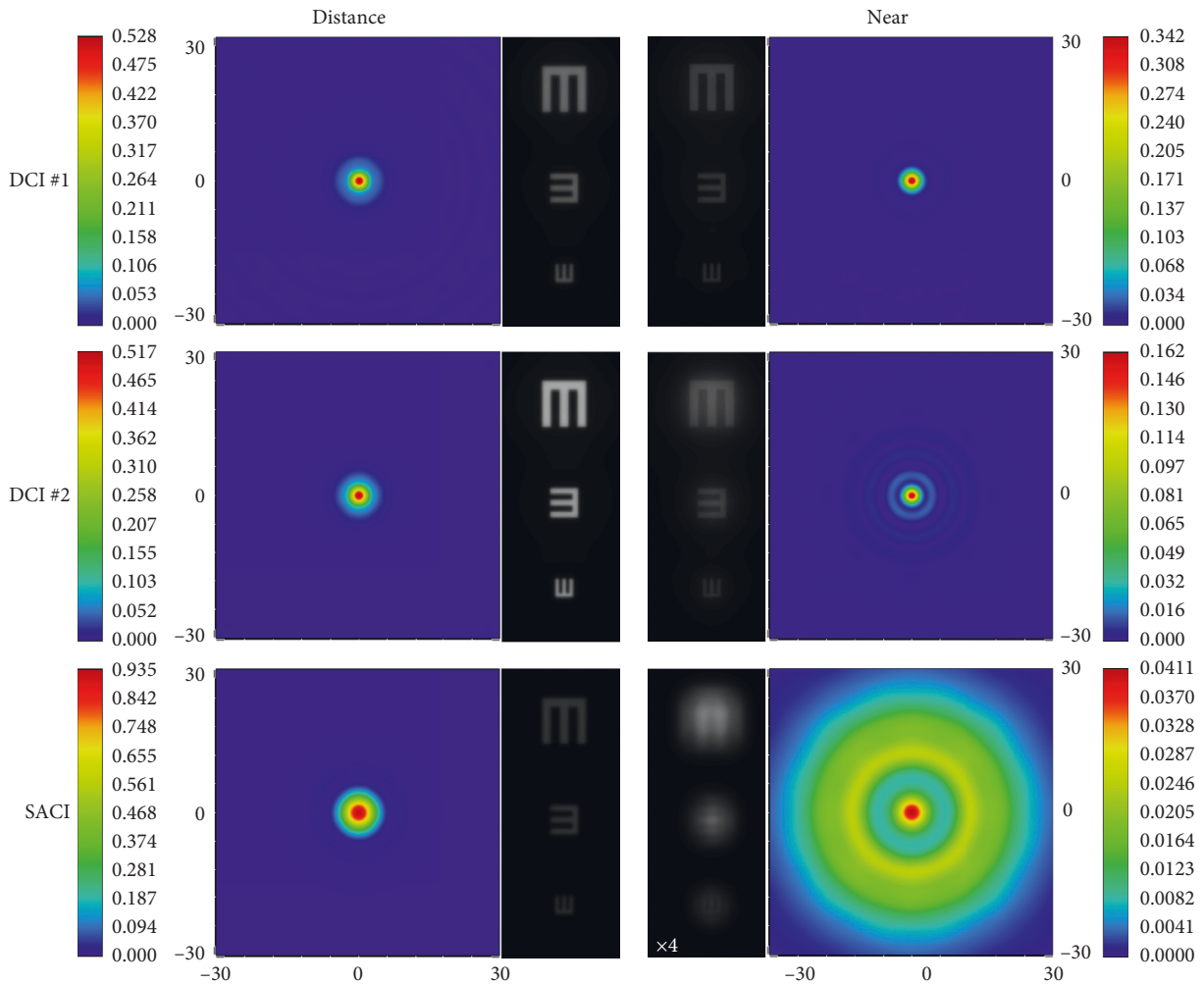

Figure 4: PSFs and the corresponding simulated images of the three inlays for distance and near objects Zemax model eye with a pupil diameter of 3.0 mm.

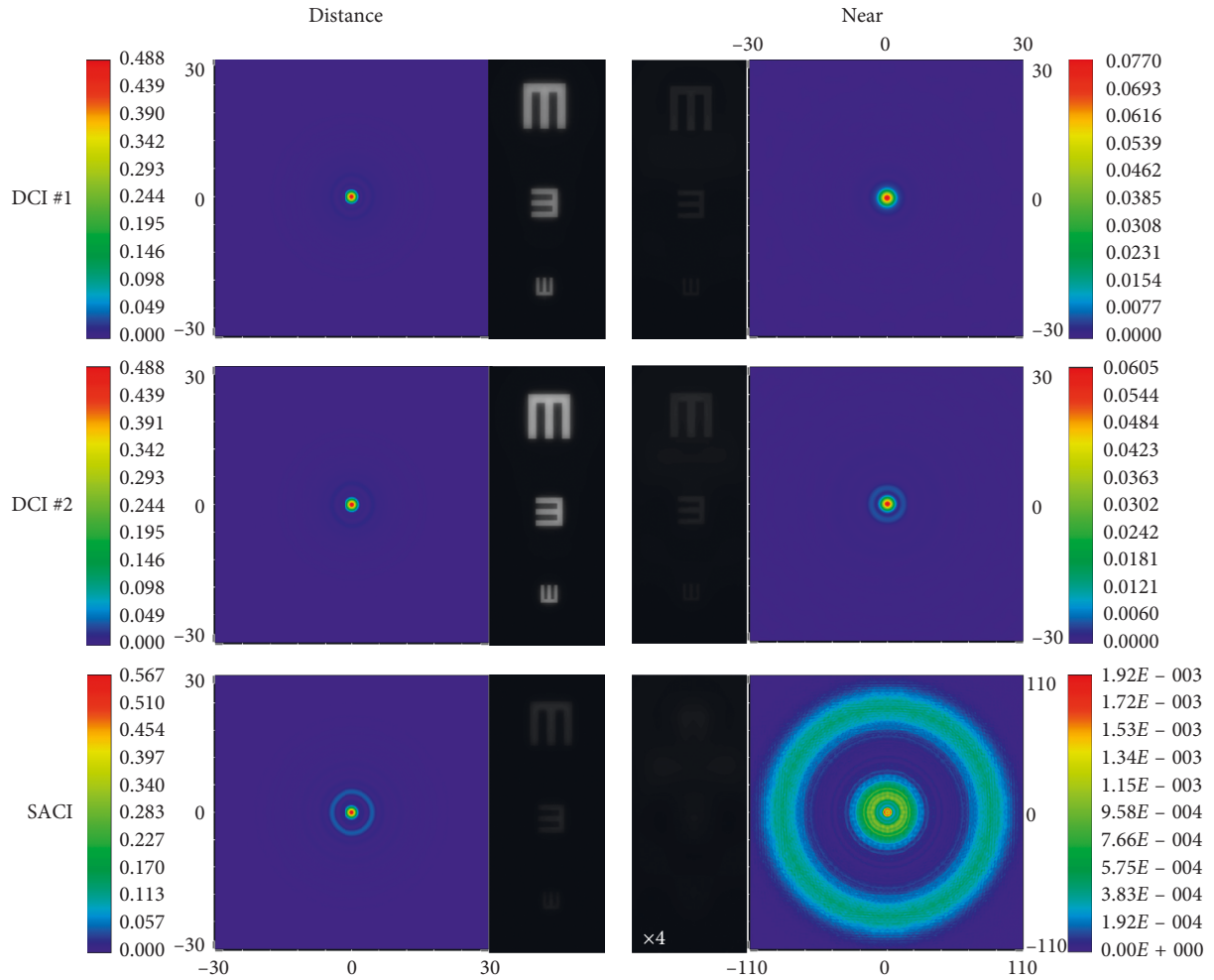

Figure 5: PSFs and the corresponding simulated images of the three inlays for distance and near objects Zemax model eye with a pupil diameter of 4.5 mm.

These images have been obtained as the convolution of the corresponding PSF with the test object. In this way, the relative intensity of the images and the spatial extension of the PSFs can be directly compared, except for the SACI at the near focus; in this case, the image intensity has been multiplied by a factor of 4 because otherwise this image would be almost black. Note that in Figure 5, the area of the PSF window has been extended to cover the spread of the PSF of the SACI at the near focus.

The image quality and the relative image intensity between them can be clearly observed in Figures 4 and 5. As can be seen, the image obtained with SACI is attenuated significantly. This is a very important fact because it was demonstrated that although the *binocular* distance visual acuity with a monocularly implanted SACI induces a *binocular* summation, the visual acuity for near distance seems to be close to the near distance acuity of the eye with SACI [9].

4. Conclusions

In conclusion, we performed an optical simulation on a new customizable treatment option for correcting presbyopia, the DCI. We found that the larger transmission of DCI compared with the SACI makes the proposed inlay highly luminous efficient, and its diffractive structure provides a near focus. Moreover, by using different models of the DCI, we have shown that the intensity ratio between the far and near foci can be controlled by adjusting the diffractive structure, which seems to be clinically relevant taking into account the particular patient's visual needs. In fact, in this study, we studied two different designs and demonstrated that the intensity of the foci of the DCIs depends on the radius of the central zone, being more intense in the near focus for the DCI #1 than for the DCI #2, but the opposite happens for the far focus. The PSFs and the simulated images show the improved performance of the DCI in comparison with the SACI, especially in near vision.

Data Availability

The data supporting the results of the current article are available from the corresponding author upon request.

Conflicts of Interest

The authors declare that there are no conflicts of interest regarding the publication of this paper.

Acknowledgments

D. Montagud–Martinez and V. Ferrando acknowledge the financial support from the Universitat Politècnica de València, Spain (fellowships FPI–2016 and PAID–10–18, respectively). This work was supported in part by the Ministerio de Economía y Competitividad, Spain, (grant DPI2015–71256–R) and by the Generalitat Valenciana (Grant PROMETEO/2019/048), Spain.

References

[1] T. R. Fricke, N. Tahhan, S. Resnikoff et al., "Global prevalence of presbyopia and vision impairment from uncorrected presbyopia," *Ophthalmology*, vol. 125, no. 10, pp. 1492–1499, 2018.

[2] W. N. Charman, "Developments in the correction of presbyopia II: surgical approaches," *Ophthalmic and Physiological Optics*, vol. 34, no. 4, pp. 397–426, 2014.

[3] O. F. Yilmaz, N. Alagoz, G. Pekel et al., "Intracorneal inlay to correct presbyopia: long–term results," *Journal of Cataract & Refractive Surgery*, vol. 37, no. 7, pp. 1275–1281, 2011.

[4] O. Seyeddain, A. Bachernegg, W. Riha et al., "Femtosecond laser–assisted small–aperture corneal inlay implantation for corneal compensation of presbyopia: two–year follow–up," *Journal of Cataract & Refractive Surgery*, vol. 39, no. 2, pp. 234–241, 2013.

[5] J. J. Castro, M. Soler, C. Ortiz, J. R. Jiménez, and R. G. Anera, "Binocular summation and visual function with induced anisocoria and monovision," *Biomedical Optics Express*, vol. 7, no. 10, pp. 4250–4362, 2016.

[6] J. J. Castro, C. Ortiz, J. R. Jiménez, S. Ortiz–Peregrina, and M. Casares–López, "Stereopsis simulating small–aperture corneal inlay and monovision conditions," *Journal of Refractive Surgery*, vol. 34, no. 7, pp. 482–488, 2018.

[7] W. D. Furlan, S. García–Delpech, P. Udaondo, L. Remón, V. Ferrando, and J. A. Monsoriu, "Diffractive corneal inlay for presbyopia," *Journal of Biophotonics*, vol. 10, no. 9, pp. 1110–1114, 2017.

[8] L. Kipp, M. Skibowski, R. L. Johnson et al., "Sharper images by focusing soft X–rays with photon sieves," *Nature*, vol. 414, no. 6860, pp. 184–188, 2001.

[9] J. Tabernero, C. Schwarz, E. J. Fernández, and P. Artal, "Binocular visual simulation of a corneal inlay to increase depth of focus," *Investigative Opthalmology & Visual Science*, vol. 52, no. 8, pp. 5273–5277, 2011.

Hindawi
Journal of Ophthalmology
Volume 2019, Article ID 5815040, 9 pages
https://doi.org/10.1155/2019/5815040

Clinical Study

Comparison of the Clinical Outcomes between Echelette Extended Range of Vision and Diffractive Bifocal Intraocular Lenses

Xin Liu, Xiaohui Song, Wei Wang, Yanan Zhu, Danni Lyu, Xingchao Shentu, Peiqing Chen, Yibo Yu, and Ke Yao

Eye Center, The Second Affiliated Hospital of College of Medicine, Zhejiang University, Hangzhou, Zhejiang 310000, China

Correspondence should be addressed to Ke Yao; xlren@zju.edu.cn

Received 16 April 2019; Accepted 20 August 2019; Published 23 September 2019

Guest Editor: Pablo Pérez-Merino

Purpose. To compare the clinical outcomes of echelette extended range of vision (ERV) and diffractive bifocal intraocular lenses (IOLs). *Methods*. This is a prospective, consecutive, nonrandomized clinical trial. Seventy-three eligible patients (109 eyes) received the implantation of echelette ERV IOL (Tecnis Symfony ZXR00) or diffractive bifocal IOL (Tecnis ZMB00). 1 week, 1 month, and 3 months after surgery, visual acuities at different distances were examined. At 3 months, defocus curves, contrast sensitivities (CSs) with and without glare, optic path difference (OPD) scans, and questionnaires were evaluated. Regression analyses were applied to discover influence factors on postoperative vision. *Results*. ZXR00 showed better distance ($P < 0.05$) and intermediate ($P < 0.001$) visual acuities, while ZMB00 was better at distance-corrected near visual acuity ($P < 0.001$). Multivariate analyses indicated that worse intermediate ($P < 0.001$) and near vision ($P = 0.013$) of ZMB00 might occur in patients with longer axial length. ZXR00 demonstrated smoother defocus curve and higher CSs. Superior modulation transfer function (MTF) and higher Strehl ratio ($P < 0.05$) were shown in ZXR00. In questionnaire evaluation, ZXR00 received better outcomes in self-reported vision, Visual Function-14 (VF-14) questionnaire, Quality of Vision (QoV) questionnaire, satisfaction, and recommendation grades. Spectacle dependence did not differ between ZXR00 and ZMB00 statistically. *Conclusion*. ZXR00 proved to be remarkable in distance and intermediate vision, defocus curve smoothness, CSs, and visual comfort, while ZMB00 achieved better near vision. ZXR00 may attain better near vision if postoperative SE remains slightly negative. Patients with relatively longer axial length might receive less favorable intermediate and near vision after ZMB00 implantation. This trial is registered with ChiCTR-ONC-17011119.

1. Introduction

Intraocular lens (IOL) implantation has become a common practice for the increasingly large population of cataract patients; however, it compromised ocular accommodating ability, leading to postoperative presbyopia and a high spectacle dependence rate up to 80% [1]. Multiple solutions, like the monovision of the 1950s, the bifocal IOLs of the 1980s, and the accommodating IOLs, trifocal IOLs, and extended range of vision (ERV) IOLs of the 21st century, were developed to tackle the problem.

Compared to monofocal IOLs, multifocal intraocular lenses (MIOLs) like bifocal and trifocal ones are able to provide clear images at each focus and alleviate the problem of presbyopia. They are mostly designed on the principles of diffraction and refraction. However, the modification of the light path by MIOLs has created new challenges such as dysphotopsia, decreased contrast sensitivity (CS), and compromised night vision [2].

ERV IOLs, on the other hand, were not approved by the U.S. Food and Drug Administration until 2016. Instead of adding certain focus, ERV IOLs extended the depth of focus. The effects of ERV IOLs were achieved based on the principles of echelette diffractive ring (Tecnis Symfony ZXR00), spherical aberration induction (SIFI MiniWell), or pinhole effect (Acu-Focus IC-8) [3]. Unlike MIOLs, ERV IOLs tend to retain CS to the similar level of monofocal IOLs [4].

Clinical trials have demonstrated the presbyopia-correcting effect in bifocal IOL [5] and ERV IOL [6], respectively, but direct comparison between diffractive echelette ERV IOL and diffractive bifocal IOL, which would be helpful to highlight the design of echelette apart from other confounding factors, remains to be rare. Although Black [7] and de Medeiros et al. [8] reported visual outcomes after blended implantation of diffractive echelette ERV IOL and diffractive bifocal IOL, thorough evaluations including visual acuity, defocus curve, CS, modulation transfer function (MTF), Strehl ratio, and subjective evaluation that stress the difference between these 2 IOLs were necessary to provide optimal IOL-selection strategies.

This study chose Tecnis Symfony ZXR00, the most widely used diffractive echelette ERV IOL, and Tecnis ZMB00, a diffractive bifocal IOL commonly applied in our center as well as an analogous to ZXR00, to analyze their differences on clinical performance.

2. Materials and Methods

2.1. Patient Enrolment. This prospective, consecutive, nonrandomized clinical trial was conducted at the Eye Center, the Second Affiliated Hospital of College of Medicine, Zhejiang University, Hangzhou, Zhejiang, China, from August 2016 to March 2018.

Patients diagnosed with cataract and interested in presbyopia correction were informed about the study. Thorough examinations were performed to select eligible participants. Inclusion criteria were as follows: (a) age from 50 to 80 years old; (b) cataract nuclear density Emery Grade I to III; (c) axial length from 21.0 to 26.0 mm; (d) angle kappa no more than 0.5 mm; (e) corneal astigmatism within 4.0 mm zone no more than 1.5 diopters (D); and (f) corneal endothelial cell count (measured by Noncon ROBO Pachy SP-9000, Konan Medical, Inc., Tokyo, Japan) no less than 1500/mm^2. Patients were excluded if they had any of the following: (a) ocular comorbidities that would influence postoperative visual acuity; (b) previous ocular surgeries; (c) traumatic cataract; (d) unstable posterior capsule or loose zonular fibers; and (e) severe systemic diseases that would disable the cooperation with postoperative examinations. Seventy-three eligible patients were consecutively enrolled. Patients who had definite requirement on intermediate vision (such as TV watching, board games, and household duties) were implanted with ZXR00, while those who required definite near vision (such as reading, writing, and knitting) were implanted with ZMB00. The investigators of postoperation examinations and patients themselves were masked to the type of IOLs implanted.

2.2. Intraocular Lenses. Tecnis Symfony ZXR00 (Johnson & Johnson Vision, Santa Ana, California, USA) is a hydrophobic UV-filtering C-loop IOL. With an overall diameter of 13.0 mm and an optic diameter of 6.0 mm [9], the acrylic acid IOL is a biconvex. Its anterior surface is designed to provide a negative spherical aberration of 0.27 μm. Its posterior surface is composed of an achromatic design and an echelette, a special type of diffraction grating [10], to extend the range of vision. The refractive area within the 9 rings of diffractive zone has a diameter of 1.7 mm. Its light utilization ratio is 92%.

Tecnis ZMB00 (Johnson & Johnson Vision, Santa Ana, California, USA) shared a similar design as ZXR00 except that its posterior surface is composed of 22 concentric diffractive rings, providing a near addition of +4.0 D (+3.0 D on spectacle plane) [11]. The refractive area within the diffractive zone has a diameter of 1.0 mm, and the light efficiency is about 82%, with a 1 : 1 distribution between two foci.

2.3. Surgical Procedure. IOL power was chosen to target within 0.5 D deviation from emmetropia. All surgeries were performed under topical anesthesia by 4 senior surgeons, each with experience of more than 10,000 cases of cataract surgeries. The IOLs were implanted through a 2.0 mm limbal corneal incision. Standard phacoemulsification or femtosecond laser-assisted technique was carried out depending on the preference of the participants. Postoperative topical therapy included dexamethasone-tobramycin for 2 weeks and pranoprofen for 1 month.

2.4. Patient Examinations. Under consistent environmental lighting condition, patients were examined at 5 m, 80 cm, and 40 cm for monocular uncorrected (UCDVA) and corrected (CDVA) distance visual acuities, monocular uncorrected (UCIVA) and corrected (CIVA) intermediate visual acuities, monocular uncorrected (UCNVA) and corrected (CNVA) near visual acuities, as well as monocular distance-corrected intermediate (DCIVA) and near (DCNVA) visual acuities. In addition, monocular defocus curves from +2.5 D to −4.0 D based on best distance-corrected status were also detected. CS with and without glare under mesopic condition was measured by Glare Tester CGT-1000 (Takagi Seiko Co., Ltd., Japan) based on best near-corrected status. 0.5% tropicamide was used for pupil dilation in order to complete optic path difference (OPD) scan (OPD-Scan II, Nidek Co., Ltd., Japan) within 3.0 mm and 5.0 mm pupil. Furthermore, an assessor-directed questionnaire that included Visual Function-14 (VF-14) questionnaire [12], Quality of Vision (QoV) questionnaire [13], day vision score, night vision score, spectacle dependence, satisfaction grade, and recommendation grade was completed at the last visit for every operation. In particular, the final score of VF-14 was calculated as the total scores divided by the number of questions effectively answered (thus excluding "not applicable" responses), multiplied by 25, and then deducted from 100 [14].

2.5. Statistical Analyses. Statistical analyses were performed using SPSS 19.0 for Windows (SPSS, Inc., Chicago, Illinois, USA). The normality of data was evaluated using the Kolmogorov–Smirnov test. Comparisons between 2 groups were made by *t*-tests or Wilcoxon–Mann–Whitney *U*-tests, depending on data normality and homogeneity of variance.

Repeated measures one-way ANOVAs were applied for comparison across time, while post hoc Bonferroni tests were applied when needed. For categorical data, Chi-square tests were applied. STATA 13 (StataCorp LLC, College Station, Texas, USA) was used for multivariate analyses with linear regressions. P values less than 0.05 were considered statistically significant. All tests were analyzed in two-tailed style.

3. Results

A total of 73 patients (109 eyes) attended to at least 1 follow-up visit. Missing data were due to personal inconvenience, refusal to mydriasis for OPD scan, or temporary device failure. A total of 38 patients (56 eyes) were implanted with ZXR00, while 35 patients (53 eyes) were implanted with ZMB00. No significant difference was found between the 2 groups regarding preoperative characteristics (Table 1). No intraoperative complication occurred.

3.1. Visual Acuities. 39 eyes implanted with ZXR00 and 28 eyes implanted with ZMB00 completed all 3 follow-up visits, where repeated measurements of uncorrected visual acuities and spherical equivalent (SE) showed no significant change within either group, except that better UCNVA was gained in ZXR00 after 1 month ($P = 0.008$) (Table 2).

Table 3 shows ZXR00 achieved better outcomes in UCDVA ($P = 0.012$) and UCIVA ($P < 0.001$), as well as in CDVA ($P = 0.008$) and DCIVA ($P < 0.001$), while ZMB00 proved to be excellent in DCNVA ($P = 0.001$); no significant differences were discovered between the 2 groups regarding UCNVA, CIVA, and CNVA. Table 3 also shows that patients implanted with ZXR00 required less spectacle correction of SE to gain the best intermediate vision ($P = 0.036$), but required more to gain the best near vision ($P < 0.001$) than patients implanted with ZMB00. Postoperative SE between the 2 groups differed ($P = 0.025$), with the ZXR00 group being relatively more myopic.

Multivariate analysis (Table 4) after adjustment of age, gender, keratometry, and anterior chamber depth suggested the negative effect of longer axial length on DCIVA in ZMB00 ($P < 0.001$, 95% CI 0.067~0.209). In the analysis of DCIVA in ZXR00, no significant correlation was detected among the observed factors.

The relation between longer axial length and worse vision was also revealed in the DCNVA of ZMB00 ($P = 0.013$, 95% CI 0.030~0.238) (Table 5). In the analysis of DCNVA in ZXR00, only age stood out as potential relative factor in the multivariate model, indicating ZXR00 implanted eyes achieved better DCNVA in older patients ($P = 0.018$, 95% CI −0.015~−0.002).

3.2. Defocus Curve. Defocus curve was tested with every increment of 0.5 D 3 months after surgery (Figure 1). In contrast to ZMB00, ZXR00 advanced in defocus curve from 0 D to −2.0 D but lagged from −2.5 D to −4.0 D. Overall, the curve of ZXR00 was smooth, while ZMB00 peaked at 0 D and −3.0 D.

3.3. Contrast Sensitivity. Either with glare (Figure 2(a)) or without glare (Figure 2(b)), ZXR00 achieved higher CS at nearly all ranges of spatial frequency, especially at medium spatial frequency (target sizes of 2.5 and 1.6 degree).

3.4. Optic Path Difference Scan. 3 months after operation, 34 of the ZXR00 implanted eyes and 26 of the ZMB00 implanted eyes received effective OPD scans. ZXR00 exceeded in modulation transfer function (MTF) values at overall spatial frequency for 3.0 mm (Figure 3(a)) and 5.0 mm (Figure 3(b)) pupil. Strehl ratio was also higher in ZXR00 than in ZMB00 for either 3.0 mm (0.06 ± 0.06 vs. 0.03 ± 0.03, $P = 0.021$) or 5.0 mm (0.02 ± 0.01 vs. 0.01 ± 0.01, $P = 0.005$) pupil.

3.5. Questionnaire Evaluation. A total of 98 eyes completed subjective evaluations 3 months after operation. Table 6 shows better outcomes in the ZXR00 group, including greater VF-14 score, lower QoV score, higher self-reported vision score (day and night), higher satisfaction grade, and higher recommendation grade (all $P < 0.05$). Spectacle dependence showed no statistical difference between the 2 groups ($P = 0.426$). Only 1 female patient, aged 77 years old, who had her right eye implanted with ZMB00, demanded IOL explantation because of severe glare.

4. Discussion

This prospective study compared clinical outcomes of an echelette ERV IOL and a diffractive bifocal IOL with similar structures but different optic principles.

As the overall visual performance stabilized after 1 month, clinical outcomes at 3 months after operation were presented. ZXR00 showed better UCDVA and UCIVA, while the difference in UCNVA was not significant. As the postoperative SE differed between the 2 groups, spectacle-corrected vision performance should be taken into consideration. In this way, ZXR00 still advanced in CDVA and DCIVA, but fell behind in DCNVA (0.38 ± 0.17 logMAR). Consistently, patients in the ZXR00 group required fewer positive diopter additions of spectacle to gain the best intermediate vision, but more to gain the best near vision.

The superiority of UCDVA and CDVA in ZXR00 over ZMB00 could be explained by its achromatic design [15]; a clinical study showed better distance acuity in ZXR00 compared not only to MIOLs, but also to monofocal IOLs [16]. Better UCIVA and DCIVA, on the other hand, reflect the structure of diffractive echelette in ZXR00 to extend the depth of focus. The "extended range" of ZXR00 failed to cover the near range, resulting in a poorer DCNVA. Our result of monocular DCNVA at 40 cm (0.38 ± 0.17 logMAR) in ZXR00 is consistent with the studies of Pedrotti (0.33 ± 0.10 logMAR) [4], Hogarty (0.31 ± 0.10 logMAR) [17], and Pilger (0.33 ± 0.12 logMAR) [18]. Nevertheless, our study found that a little negative postoperative SE could compensate for this disadvantage by improving the UCNVA, a strategy similarly indicated by the study of Cocherner et al. [19, 20], who found that a micro-monovision of −0.5 D

Table 1: Participant characteristics.

Parameter	ZXR00	ZMB00	P value
Patients/eyes (n)	38/56	35/53	
Implantation type			0.840
Monocular (n)	20 (35.7%)	17 (32.1%)	
Binocular (n)	36 (64.3%)	36 (67.9%)	
Age (years), mean ± SD	68.77 ± 8.22	66.87 ± 6.53	0.186
Gender			0.825
Male (n)	13 (23.2%)	14 (26.4%)	
Female (n)	43 (76.8%)	39 (73.6%)	
UCDVA (logMAR), mean ± SD	0.58 ± 0.38	0.70 ± 0.45	0.145
Keratometry (D), mean ± SD	43.78 ± 1.51	43.90 ± 1.43	0.677
Axial length (mm), mean ± SD	23.65 ± 0.70	23.73 ± 0.94	0.627
Anterior chamber depth (mm), mean ± SD	2.81 ± 0.46	2.76 ± 0.45	0.604
IOL power (D), mean ± SD	21.12 ± 1.49	20.83 ± 2.13	0.417
Angle kappa (mm), mean ± SD	0.20 ± 0.11	0.24 ± 0.14	0.176
Corneal astigmatism (D), mean ± SD	0.58 ± 0.22	0.53 ± 0.27	0.314
Corneal endothelial cell count (mm^2), mean ± SD	2532.0 ± 260.4	2596.21 ± 234.9	0.180
Nuclear hardness			0.337
Emery Grade I (n)	20 (35.7%)	21 (39.6%)	
Emery Grade II (n)	30 (53.6%)	22 (41.5%)	
Emery Grade III (n)	6 (10.7%)	10 (18.9%)	
Surgical technique			0.099
Standard (n)	22 (39.3%)	13 (24.5%)	
Femtosecond-assisted (n)	34 (60.7%)	40 (75.5%)	

n number of eyes; UCDVA = uncorrected distance visual acuity; logMAR = logarithm of the minimum angle of resolution; mm = millimeter; D = diopter; IOL = intraocular lens; SD = standard deviation.

Table 2: Repeated measurements of visual acuities after IOL implantation.

Parameter	Postoperative visit			P value
	1 week	1 month	3 months	
UCDVA (logMAR), mean ± SD				
ZXR00 (eyes = 39)	0.10 ± 0.14	0.11 ± 0.15	0.09 ± 0.13	0.606
ZMB00 (eyes = 28)	0.22 ± 0.21	0.19 ± 0.16	0.19 ± 0.17	0.415
UCIVA (logMAR), mean ± SD				
ZXR00 (eyes = 39)	0.19 ± 0.16	0.18 ± 0.17	0.14 ± 0.12	0.161
ZMB00 (eyes = 28)	0.38 ± 0.24	0.35 ± 0.15	0.30 ± 0.15	0.112
UCNVA (logMAR), mean ± SD				
ZXR00 (eyes = 39)	0.44 ± 0.19	0.35 ± 0.20†	0.34 ± 0.20†	0.008
ZMB00 (eyes = 28)	0.32 ± 0.18	0.28 ± 0.19	0.25 ± 0.18	0.126
SE (D), mean ± SD				
ZXR00 (eyes = 39)	−0.19 ± 0.49	−0.21 ± 0.60	−0.19 ± 0.64	0.964
ZMB00 (eyes = 28)	0.23 ± 0.69	0.22 ± 0.71	0.12 ± 0.79	0.088

$^{\dagger}P < 0.05$ compared to the visual acuity of 1 week after operation. UCDVA = uncorrected distance visual acuity; UCIVA = uncorrected intermediate visual acuity; UCNVA = uncorrected near visual acuity; SE = spherical equivalent; D = diopter; SD = standard deviation.

myopia in 1 eye led to better visual outcome for ZXR00 implantation. For ZMB00, it should be cautiously implanted in people with longer axial length, for it is correlated with worse intermediate and near vision based on our analyses.

In consistent with the visual acuities of different distances, the smooth defocus curve of ZXR00 excelled from 0 D to −2.0 D but fell behind ZMB00 from −2.5 D to −4.0 D. As for CS, ZXR00 overwhelmingly exceeded ZMB00. The target size of CS showed spatial frequency range from 6 to 12 cycles per degree (cpd) [21]. Target sizes of 6.3° and 4° represent low spatial frequency related to the magnocellular pathway, which is involved in recognizing moving objects [22]. Target sizes of 1° and 0.7°, on the contrary, represent high spatial frequency related to the parvocellular pathway, which is involved in recognizing object details [22]. Popularization of MIOLs has been challenged by compromised CS, especially under glare conditions [23], which could endanger night drivers. However, previous in vitro [24] and clinical [16] researchers stated that ZXR00 rivaled monofocal IOLs in CS. The consistent advantage of better CS in ZXR00 over ZMB00 here may be attributed to its fewer diffractive rings and achromatic designs [25].

OPD scans showed that ZXR00 implantation resulted in higher MTF values and Strehl ratio, which were consistent with its excellent distance visual acuity and CS.

Table 3: Visual acuities and refractive outcomes 3 months after IOL implantation.

	ZXR00 (eyes = 45)	ZMB00 (eyes = 34)	P value
UCDVA (logMAR), mean ± SD	0.10 ± 0.13	0.19 ± 0.19	0.012
UCIVA (logMAR), mean ± SD	0.15 ± 0.13	0.29 ± 0.17	<0.001
UCNVA (logMAR), mean ± SD	0.35 ± 0.19	0.26 ± 0.21	0.057
CDVA (logMAR), mean ± SD	−0.01 ± 0.07	0.03 ± 0.08	0.008
CIVA (logMAR), mean ± SD	0.03 ± 0.11	0.08 ± 0.15	0.134
CNVA (logMAR), mean ± SD	0.10 ± 0.20	0.10 ± 0.18	0.719
DCIVA (logMAR), mean ± SD	0.12 ± 0.13	0.32 ± 0.19	<0.001
DCNVA (logMAR), mean ± SD	0.38 ± 0.17	0.22 ± 0.24	0.001
Int SE add (D), mean ± SD	0.72 ± 0.52	0.94 ± 0.38	0.036
Near SE add (D), mean ± SD	1.84 ± 0.62	0.45 ± 1.14	<0.001
SE (D), mean ± SD	−0.22 ± 0.61	0.12 ± 0.73	0.025

UCDVA = uncorrected distance visual acuity; UCIVA = uncorrected intermediate visual acuity; UCNVA = uncorrected near visual acuity; CDVA = corrected distance visual acuity; CIVA = corrected intermediate visual acuity; CNVA = corrected near visual acuity; DCIVA = distance-corrected intermediate visual acuity; DCNVA = distance-corrected near visual acuity; SE = spherical equivalent; int SE add = addition of diopters to spectacle from the best corrected distance vision to achieve the best corrected intermediate vision; near SE add = addition of diopters to spectacle from the best corrected distance vision to achieve the best corrected near vision; D = diopter; SD = standard deviation.

Table 4: Multivariate analysis on the DCIVA (logMAR) 3 months after IOL implantation.

IOL	Correlation indicators	Variables				
		Age (year)	Gender†	Keratometry (D)	Axial length (mm)	Anterior chamber depth (mm)
ZXR00 (eyes = 45)	Coefficient	−0.001	0.024	0.018	0.039	−0.012
	P value	0.810	0.730	0.326	0.334	0.811
	LCI	−0.007	−0.115	−0.019	−0.042	−0.116
	UCI	0.005	0.163	0.055	0.120	0.092
ZMB00 (eyes = 34)	Coefficient	0.007	0.147	0.024	0.138	−0.002
	P value	0.154	0.053	0.401	<0.001	0.978
	LCI	−0.003	−0.002	−0.034	0.067	−0.153
	UCI	0.016	0.296	0.082	0.209	0.149

†For gender, 0 indicates male while 1 indicates female. DCIVA = distance-corrected intermediate visual acuity; IOL = intraocular lens; D = diopter; LCI = lower bound of 95% confidence interval; UCI = upper bound of 95% confidence interval.

Table 5: Multivariate analysis on the DCNVA (logMAR) 3 months after IOL implantation.

IOL	Correlation indicators	Variables				
		Age (year)	Gender†	Keratometry (D)	Axial length (mm)	Anterior chamber depth (mm)
ZXR00 (eyes = 45)	Coefficient	−0.008	0.015	0.008	0.003	−0.043
	P value	0.018	0.852	0.705	0.956	0.485
	LCI	−0.015	−0.148	−0.035	−0.092	−0.165
	UCI	−0.002	0.178	0.052	0.098	0.080
ZMB00 (eyes = 34)	Coefficient	0.009	0.116	0.009	0.134	−0.144
	P value	0.187	0.286	0.822	0.013	0.192
	LCI	−0.004	−0.102	−0.075	0.030	−0.364
	UCI	0.022	0.333	0.094	0.238	0.077

†For gender, 0 indicates male while 1 indicates female. DCNVA = distance-corrected near visual acuity; D = diopter; LCI = lower bound of 95% confidence interval; UCI = upper bound of 95% confidence interval.

The questionnaire analyses uncovered that although near vision was compromised in ZXR00, its spectacle dependence was no more than that of ZMB00. Similar results were seen in previous nonrandomized [16] and randomized [26] studies, where, despite the poorer near vision of ZXR00, the spectacle dependency rate did not differ significantly from a +3.0 D bifocal IOL, or from a trifocal IOL that had near addition powers of +2.17 D and +3.25 D. This could be attributed to the smooth defocus curve of ZXR00 allowing patients the convenience of slightly adjusting reading distance for better vision. ZXR00 even reported higher VF-14 score, self-reported vision score, satisfaction grade, and recommendation grade.

One study showed that glare, one of the most commonly seen photic phenomena of presbyopia-correcting IOLs [26–29], appeared at comparable frequency between ZXR00 and apodized diffractive-refractive bifocal IOLs [16]. But our study revealed better visual quality of ZXR00 by achieving lower QoV score than ZMB00, especially in the bothersome subscale.

Limitations existed in our study, though, as it was not a randomized clinical trial with a 100% follow-up rate and

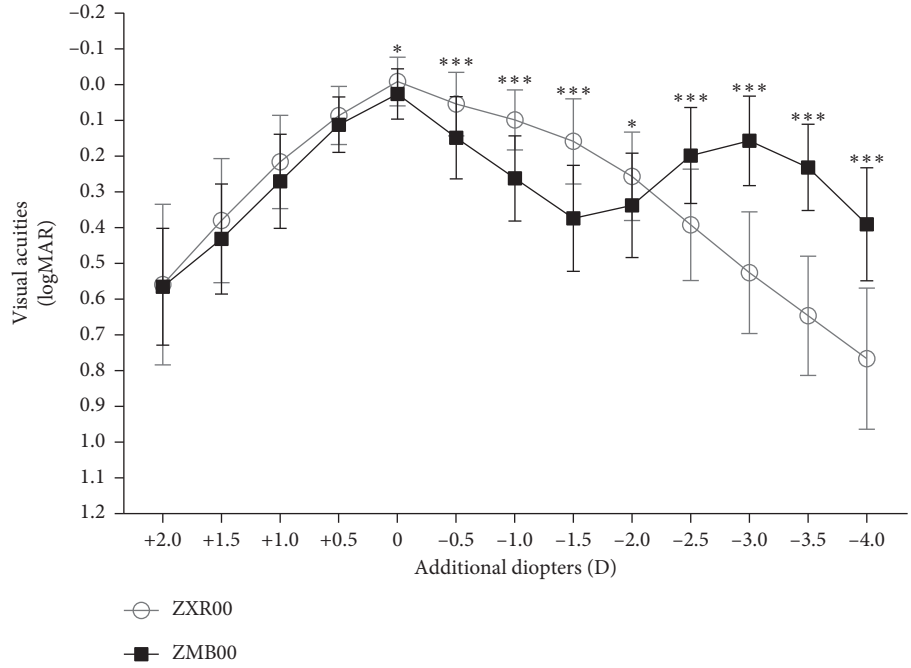

Figure 1: Defocus curves 3 months after IOL implantation (D = diopter; * = $P < 0.05$; ** = $P < 0.01$; *** = $P < 0.001$).

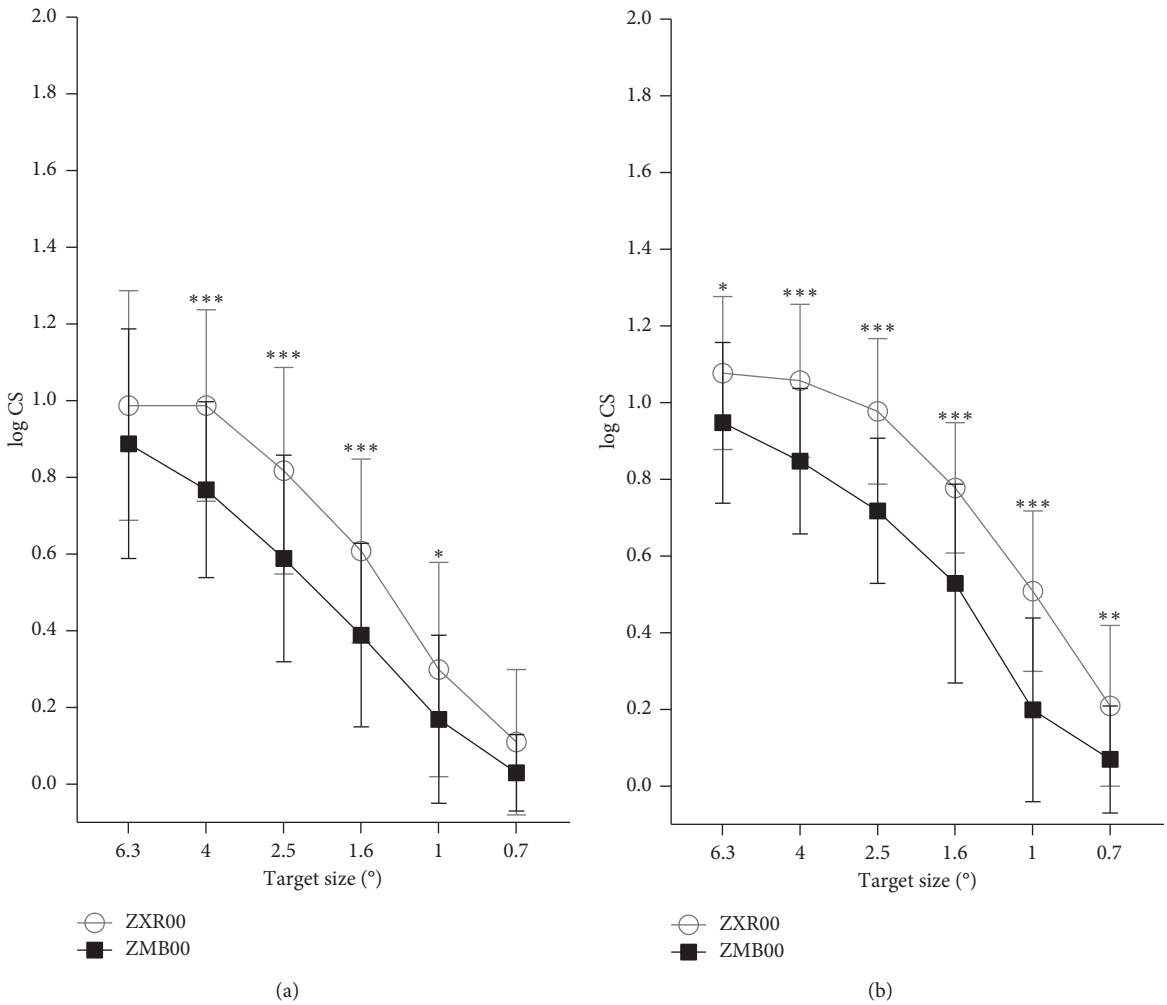

Figure 2: Contrast sensitivities with (a) and without (b) glare under mesopic condition 3 months after IOL implantation (CS = contrast sensitivity; ° = degree of angle; * = $P < 0.05$; ** = $P < 0.01$; *** = $P < 0.001$).

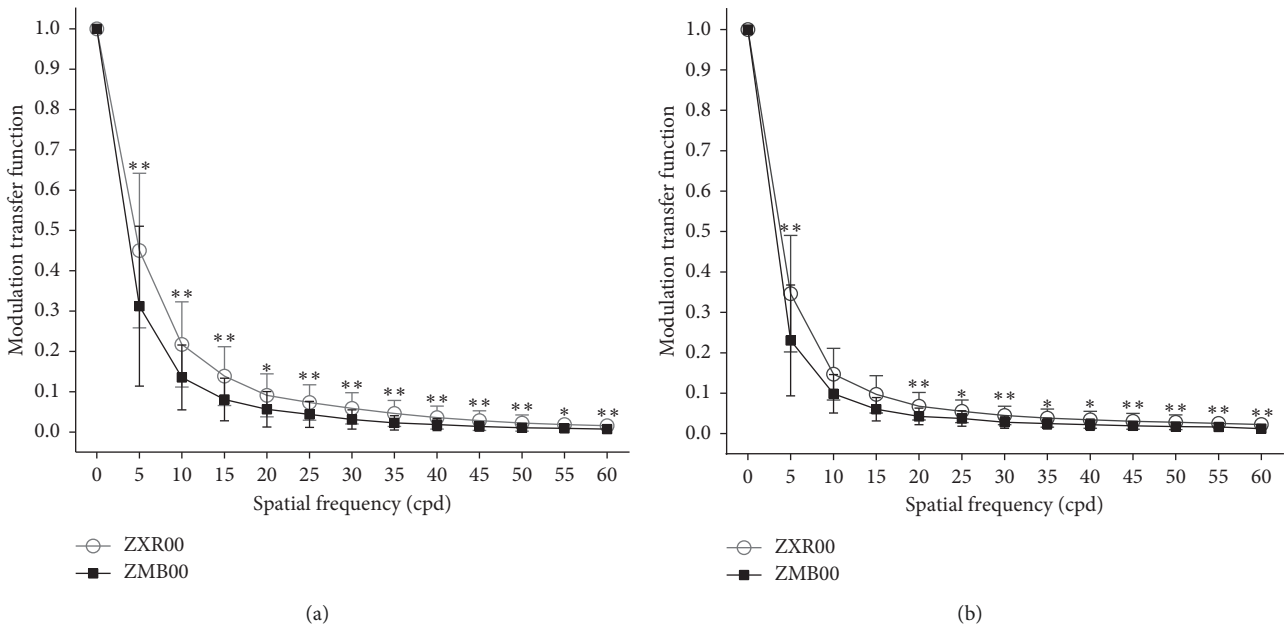

Figure 3: Modulation transfer function for 3.0 mm (a) and 5.0 mm (b) pupil 3 months after IOL implantation (cpd = cycle per degree; * = $P < 0.05$; ** = $P < 0.01$; *** = $P < 0.001$).

Table 6: Subjective evaluation by questionnaire 3 months after IOL implantation.

Questionnaire	ZXR00 (eyes = 54)	ZMB00 (eyes = 44)	P value
VF-14 score, mean ± SD	90.54 ± 12.63	85.54 ± 13.34	0.021
QoV score, mean ± SD	5.06 ± 6.15	8.54 ± 8.35	0.022
Frequency score	2.20 ± 2.43	3.39 ± 2.99	0.042
Severity score	1.65 ± 2.13	2.64 ± 2.69	0.023
Bothersome score	1.20 ± 1.74	2.52 ± 2.82	0.006
Self-reported vision			
Day score, mean ± SD	9.30 ± 1.24	8.39 ± 1.54	0.001
Night score, mean ± SD	8.74 ± 1.46	7.73 ± 1.88	0.004
Spectacle dependence			0.426
Independent (n)	32 (59.3%)	21 (47.7%)	
Occasionally (n)	18 (33.3%)	17 (38.7%)	
Often (n)	4 (7.4%)	6 (13.6%)	
Most of time (n)	0	0	
Always (n)	0	0	
Satisfaction grade			0.045
Very satisfied (n)	26 (48.1%)	11 (25.0%)	
Good (n)	19 (35.2%)	17 (38.6%)	
Partial improvement (n)	9 (16.7%)	12 (27.3%)	
Little improvement (n)	0	2 (4.5%)	
No improvement (n)	0	1 (2.3%)	
Worse (n)	0	1 (2.3%)	
Recommendation grade			0.045
Strong (n)	24 (44.4%)	11 (25.0%)	
Possible (n)	17 (31.5%)	13 (29.6%)	
Probable (n)	13 (24.1%)	18 (40.9%)	
Against (n)	0	2 (4.5%)	
No opinion (n)	0	0	

n number of eyes; VF-14 = Visual Function-14; QoV = Quality of Vision; SD = standard deviation.

unanimous bilateral IOL implantation due to patients' compliance. In addition, the possible correlation between axial length and visual outcomes in ZMB00 needs further exploration.

5. Conclusions

In conclusion, our study provides certain clinical advice in choosing presbyopia-correcting IOLs. ZXR00 is outstanding

in distance and intermediate visual acuities, smooth defocus curve, high CS, and fair visual comfort. ZXR00 may attain better near vision if postoperative SE remains slightly negative. ZMB00 is better in near vision, but patients like night drivers should be cautious because of its lower CS and more visual disturbances. Patients with relatively longer axial length should also be informed about less favorable vision before implanted with ZMB00.

Data Availability

The data used to support the findings of this study are available from the corresponding author upon request.

Conflicts of Interest

The authors declare that there are no conflicts of interest regarding the publication of this paper.

Authors' Contributions

Xin Liu and Xiaohui Song contributed equally to this study.

Acknowledgments

The authors acknowledge Huilan Guo, Department of Public Health, College of Medicine, Zhejiang University, Hangzhou, Zhejiang, China, for statistical advice. This work was supported by the Key Research and Development Program of Zhejiang Province of China (2015C03042) and by the National Natural Science Foundation of China (81570822 and 81600716).

References

[1] D. Calladine, J. R. Evans, S. Shah, and M. Leyland, "Multifocal versus monofocal intraocular lenses after cataract extraction," *Cochrane Database of Systematic Reviews*, vol. 9, 2012.

[2] S. R. de Silva, J. R. Evans, V. Kirthi, M. Ziaei, and M. Leyland, "Multifocal versus monofocal intraocular lenses after cataract extraction," *Cochrane Database of Systematic Reviews*, vol. 12, 2016.

[3] K. M. Rocha, "Extended depth of focus IOLs: the next chapter in refractive technology?," *Journal of Refractive Surgery*, vol. 33, no. 3, pp. 146–149, 2017.

[4] E. Pedrotti, E. Bruni, E. Bonacci, R. Badalamenti, R. Mastropasqua, and G. Marchini, "Comparative analysis of the clinical outcomes with a monofocal and an extended range of vision intraocular lens," *Journal of Refractive Surgery*, vol. 32, no. 7, pp. 436–442, 2016.

[5] F. A. Bartol-Puyal, P. Talavero, G. Gimenez et al., "Reading and quality of life differences between Tecnis ZCB00 monofocal and Tecnis ZMB00 multifocal intraocular lenses," *European Journal of Ophthalmology*, vol. 27, no. 4, pp. 443–453, 2017.

[6] G. Savini, D. Schiano-Lomoriello, N. Balducci, and P. Barboni, "Visual performance of a new extended depth-of-focus intraocular lens compared to a distance-dominant diffractive multifocal intraocular lens," *Journal of Refractive Surgery*, vol. 34, no. 4, pp. 228–235, 2018.

[7] S. Black, "A clinical assessment of visual performance of combining the TECNIS® Symfony Extended Range of Vision IOL (ZXR00) with the +3.25 D TECNIS Multifocal 1-piece IOL (ZLB00) in subjects undergoing bilateral cataract extraction," *Clinical Ophthalmology*, vol. 12, pp. 2129–2136, 2018.

[8] A. L. de Medeiros, A. G. de Araujo Rolim, A. F. P. Motta et al., "Comparison of visual outcomes after bilateral implantation of a diffractive trifocal intraocular lens and blended implantation of an extended depth of focus intraocular lens with a diffractive bifocal intraocular lens," *Clinical Ophthalmology*, vol. 11, pp. 1911–1916, 2017.

[9] J. J. Esteve-Taboada, A. Dominguez-Vicent, A. J. Del Aguila-Carrasco, T. Ferrer-Blasco, and R. Montes-Mico, "Effect of large apertures on the optical quality of three multifocal lenses," *Journal of Refractive Surgery*, vol. 31, no. 10, pp. 666–676, 2015.

[10] A. Dominguez-Vicent, J. J. Esteve-Taboada, A. J. Del Aguila-Carrasco, T. Ferrer-Blasco, and R. Montes-Mico, "In vitro optical quality comparison between the mini WELL ready progressive multifocal and the TECNIS Symfony," *Graefe's Archive for Clinical and Experimental Ophthalmology = Albrecht von Graefes Archiv Fur Klinische und experImentelle Ophthalmologie*, vol. 254, no. 7, pp. 1387–1397, 2016.

[11] D. H. Chang, "Visual acuity and patient satisfaction at varied distances and lighting conditions after implantation of an aspheric diffractive multifocal one-piece intraocular lens," *Clinical Ophthalmology*, vol. 10, pp. 1471–1477, 2016.

[12] J. Khadka, J. Huang, K. Mollazadegan et al., "Translation, cultural adaptation, and Rasch analysis of the visual function (VF-14) questionnaire," *Investigative Ophthalmology & Visual Science*, vol. 55, no. 7, pp. 4413–4420, 2014.

[13] C. McAlinden, K. Pesudovs, and J. E. Moore, "The development of an instrument to measure quality of vision: the quality of vision (QoV) questionnaire," *Investigative Ophthalmology & Visual Science*, vol. 51, no. 11, pp. 5537–5545, 2010.

[14] F. Kishimoto and H. Ohtsuki, "Comparison of VF-14 scores among different ophthalmic surgical interventions," *Acta Medica Okayama*, vol. 66, no. 2, pp. 101–110, 2012.

[15] H. A. Weeber and P. A. Piers, "Theoretical performance of intraocular lenses correcting both spherical and chromatic aberration," *Journal of Refractive Surgery*, vol. 28, no. 1, pp. 48–52, 2012.

[16] E. Pedrotti, F. Carones, F. Aiello et al., "Comparative analysis of visual outcomes with 4 intraocular lenses: monofocal, multifocal, and extended range of vision," *Journal of Cataract and Refractive Surgery*, vol. 44, no. 2, pp. 156–167, 2018.

[17] D. T. Hogarty, D. J. Russell, B. M. Ward, N. Dewhurst, and P. Burt, "Comparing visual acuity, range of vision and spectacle independence in the extended range of vision and monofocal intraocular lens," *Clinical & Experimental Ophthalmology*, vol. 46, no. 8, pp. 854–860, 2018.

[18] D. Pilger, D. Homburg, T. Brockmann, N. Torun, E. Bertelmann, and C. von Sonnleithner, "Clinical outcome and higher order aberrations after bilateral implantation of an extended depth of focus intraocular lens," *European Journal of Ophthalmology*, vol. 28, no. 4, pp. 425–432, 2018.

[19] B. Cochener and G. Concerto Study, "Clinical outcomes of a new extended range of vision intraocular lens: international Multicenter Concerto Study," *Journal of Cataract and Refractive Surgery*, vol. 42, no. 9, pp. 1268–1275, 2016.

[20] B. Cochener, "Influence of the level of monovision on visual outcome with an extended range of vision intraocular lens," *Clinical Ophthalmology*, vol. 12, pp. 2305–2312, 2018.

[21] D. Gatinel and Y. Houbrechts, "Comparison of bifocal and trifocal diffractive and refractive intraocular lenses using an optical bench," *Journal of Cataract and Refractive Surgery*, vol. 39, no. 7, pp. 1093–1099, 2013.

[22] M. A. P. D. Chaves, W. T. Hida, P. F. Tzeliks et al., "Comparative study on optical performance and visual outcomes between two diffractive multifocal lenses: AMO Tecnis® ZMB00 and AcrySof® IQ ReSTOR® Multifocal IOL SN6AD1," *Arquivos Brasileiros de Oftalmologia*, vol. 79, no. 3, pp. 171–176, 2016.

[23] S. Cillino, A. Casuccio, F. Di Pace et al., "One-year outcomes with new-generation multifocal intraocular lenses," *Ophthalmology*, vol. 115, no. 9, pp. 1508–1516, 2008.

[24] D. Gatinel and J. Loicq, "Clinically relevant optical properties of bifocal, trifocal, and extended depth of focus intraocular lenses," *Journal of Refractive Surgery*, vol. 32, no. 4, pp. 273–280, 2016.

[25] M. S. Millan and F. Vega, "Extended depth of focus intraocular lens: chromatic performance," *Biomedical Optics Express*, vol. 8, no. 9, pp. 4294–4309, 2017.

[26] G. Monaco, M. Gari, F. Di Censo, A. Poscia, G. Ruggi, and A. Scialdone, "Visual performance after bilateral implantation of 2 new presbyopia-correcting intraocular lenses: trifocal versus extended range of vision," *Journal of Cataract and Refractive Surgery*, vol. 43, no. 6, pp. 737–747, 2017.

[27] B. Cochener, G. Boutillier, M. Lamard, and C. Auberger-Zagnoli, "A comparative evaluation of a new generation of diffractive trifocal and extended depth of focus intraocular lenses," *Journal of Refractive Surgery*, vol. 34, no. 8, pp. 507–514, 2018.

[28] S. Escandon-Garcia, F. J. Ribeiro, C. McAlinden, A. Queiros, and J. M. Gonzalez-Meijome, "Through-focus vision performance and light disturbances of 3 new intraocular lenses for presbyopia correction," *Journal of Ophthalmology*, vol. 2018, Article ID 6165493, 8 pages, 2018.

[29] A. Hamid and A. Sokwala, "A more natural way of seeing: visual performance of three presbyopia correcting intraocular lenses," *Open Journal of Ophthalmology*, vol. 6, no. 3, pp. 176–183, 2016.

Hindawi
Journal of Ophthalmology
Volume 2019, Article ID 8731626, 7 pages
https://doi.org/10.1155/2019/8731626

Research Article

Assessment of the Association between In Vivo Corneal Morphogeometrical Changes and Keratoconus Eyes with Severe Visual Limitation

J. S. Velázquez,[1] **F. Cavas**,[1] **J. Alió del Barrio**,[2,3] **D. G. Fernández-Pacheco**,[1] **and J. Alió**[2,3]

[1]*Department of Structures, Construction and Graphic Expression, Technical University of Cartagena, 30202 Cartagena, Spain*
[2]*Keratoconus Unit of Vissum Corporation Alicante, 03016 Alicante, Spain*
[3]*Department of Ophthalmology, Miguel Hernández University of Elche, 03202 Alicante, Spain*

Correspondence should be addressed to F. Cavas; francisco.cavas@upct.es

Received 18 June 2019; Revised 6 August 2019; Accepted 23 August 2019; Published 22 September 2019

Academic Editor: Biju B. Thomas

Assessing changes suffered by the cornea as keratoconus progresses has proven to be vital for this disease diagnosis and treatment. This study determines the corneal biometric profile in eyes considered as affected by keratoconus (KC) showing severe visual limitation, by means of in vivo 3D modelling techniques. This observational case series study evaluated new objective indices in 50 healthy and 30 KC corneas, following a validated protocol created by our research group, which has been previously used for diagnosis and characterization of KC in asymptomatic (preclinical) and mild visually impaired eyes. Results show a statistically significant reduction of corneal volume and an increase of total corneal area in the severe KC group, being anterior and posterior corneal surfaces minimum thickness points the best correlated parameters, although with no discrimination between groups. Receiving operator curves were used to determine sensitivity and specificity of selected indices, being anterior and posterior apex deviations the ones which reached the highest area under the curve, both with very high sensitivity (96.7% and 90%, respectively) and specificity (94.0% and 99.9%, respectively). The results suggest that once severe visual loss appears, anterior corneal topography should be considered for a more accurate diagnosis of clinical KC, being anterior apex deviation the key metric discriminant. This study can be a useful tool for KC classification, helping doctors in diagnosing severe cases of the disease, and can help to characterize corneal changes that appear when severe KC is developed and how they relate with vision deterioration.

1. Introduction

Keratoconus (KC) is a bilateral noninflammatory corneal ectasia with a prevalence of 54.5 per 100,000, which is characterized by a stromal thinning that makes the cornea acquire a conical shape, leading to mild to marked visual impairment [1].

The geometric decompensation that causes the conical shape is localized mainly in the temporal lower quadrant of the mean peripheral region [2] due to a loss of tenacity that the corneal structure suffer by a reorientation of its anatomophysiology [3]. In addition, this morphologic decompensation inducts an increase of the high-order optical aberrations [4], showing the patients high values of irregular astigmatism and presenting as their main refractive sign the impossibility of a complete optical compensation of their ametropia by spherocylindrical lenses. Consequently, their corrected visual acuity will be diminished with respect to patients without corneal pathology [5].

There are many classifications in the scientific literature about the degree of severity of keratoconus [6]; however, it is difficult in clinical practice to handle the multiple indices in which these classifications are based, for a proper evaluation

of the disease progression. Also, some of these classifications present some singularities, such as Keratoconus Severity Scores [2], which does not consider pachymetry, or the Amsler–Krumeich classification, which does not take into account that patients, depending on their manifest refraction, may show important refractive fluctuations caused by the corneal multifocality that generates the corneal shape [6]. Besides that, from an optical point of view, patients show a certainly deteriorated spectacle-corrected visual acuity during the disease development, in a way that their visual performance worsens with the progression of the severity degree of keratoconus. Following this criterion, a classification of the stages of the disease has been developed [5, 7], depending on the corrected distance visual acuity (CDVA).

Furthermore, our research group has developed a three-dimensional (3D) virtual model of the cornea by means of computational geometry [8]. These models have been validated for the diagnosis of keratoconus basing on geometric parameters of volume [9], to predict the response to refractive surgeries [10, 11] or the response to the intrastromal ring segment implantation in corneas with keratoconus [12], to analyse nonsurgical corneal modifications, such as applanation tonometry for intraocular pressure measurement [13], or to analyse the behaviour of corneal tissue properties in different scenarios [14]. However, to our knowledge the virtual model has not been used to define the biometric profile in keratoconus eyes with severe visual limitation.

Therefore, developing and validating new methods for the characterization of the changes suffered by the cornea in severe KC cases is important to help attaining a better clinical management of it and avoiding the possibility of irreversible vision losses. Thus, the purpose of this work is to evaluate the potential value of a virtual 3D model for the diagnostic of corneas affected by severe KC, conceiving cornea as a 3D refractive structure. To do so, we have based on the characterization of its biometric profile (Figure 1) by means of morpho-biometric indices that register the optic-geometric decompensation that takes place during this phase of the disease, as well as we have quantified the existence of correlations between these indices.

2. Materials and Methods

2.1. Participants. This observational case series study evaluated 80 corneas of 80 patients (selected at random to avoid interference) structured in two groups: a normal group (healthy corneas), which included 50 subjects presenting no ocular pathology (37.79 ± 14.76 years), and a second group, composed of 30 patients diagnosed with severe KC (31.63 ± 7.39 years). The classification protocol for normal or severe KC cases was run according to reported state of the art clinical and topographic evaluations [15]. Just one eye of each patient was selected at random, according to a software-generated dichotomic random number sequence (0,1), seeking to elude any possible correlation that might exist between both eyes of the same patient [9].

All patients were selected according to the RETICS grading [7]. To be included in the study, patients should have been diagnosed as Grade IV keratoconus (severe visual limitation, $0.2 < \text{CDVA} \leq 0.4$ in decimal scale or $6/30 < \text{CDVA} \leq 6/15$ in Snellen chart), focal central/paracentral steepening and corneal thinning visible in corneal tomography, 3 mm (inferior-superior) I-S mean keratometric difference >1.5 D, and asymmetric bow tie with or without skewed radial axes over 21 degrees. Patients who had undergone any previous ocular surgical procedure, suffering from any irritation of the ocular surface, with signs of significant dry eye, or who wore contact lenses in the precedent four weeks to their first visit were excluded from the study [16].

Vissum Instituto Oftalmologico, Alicante, Spain (Vissum), was the place in which these evaluations took place where the patients were satisfactorily informed about the study and signed freely their will to participate. The study was endorsed by the hospital's Clinical Research Ethics Committee, according to the ethical guidelines dictated in the Declaration of Helsinki (Seventh revision, October 2013, Fortaleza, Brazil).

The data used for this investigation were included in the official database "Iberia" of keratoconus cases created for the purpose of multicentre study of keratoconus in the National Network for Clinical Research in Ophthalmology RETICS-OFTARED.

2.2. Examination Protocol. All subjects selected for this study were examined using Sirius System® (CSO, Florence, Italy), and following a validated protocol previously created by our research group, which has been thoroughly described in preceding studies [8, 9]. This protocol comprises two stages: first, a 3D virtual modelling and then geometric characterization (Figure 2), and it has proved itself successful when used for diagnosis and characterization of KC in asymptomatic (preclinical) and mild visually impaired eyes [17, 18].

The final output of this protocol after its application, is a patient-specific 3D virtual model of the cornea, which is then analysed to find several morpho-biometric indices (Figure 2). These indices studied herein, along with their characteristics, have been previously described in [19] and are summarized in Table 1, but are used for the first time to study KC eyes with severe visual impairment. In this work, the surface finally generated with Rhinoceros software was distorted looking for the minimisation of the nominal distance between the points in the space and the surface itself. This distance was ultimately estimated by the software, showing a mean value for its error of $4.370 \times 10^{-16} \pm 3.67 \times 10^{-16}$ mm (mean ± standard deviation).

2.3. Statistical Analysis. Both Kolmogorov–Smirnov test and Shapiro–Wilk test were run to check data normality. According to these tests and thereafter, a Student's t-test was used for normally distributed samples, while Mann –Whitney–Wilcoxon U test was chosen for not-normally distributed ones. Correlation between parameters was assessed by means of Pearson coefficient (for normally distributed data) or Spearman's coefficient (not normally distributed). A significance level of 0.05 was fixed for p-values in all statistical tests. Receiver operating characteristic (ROC) curves were used to determine which

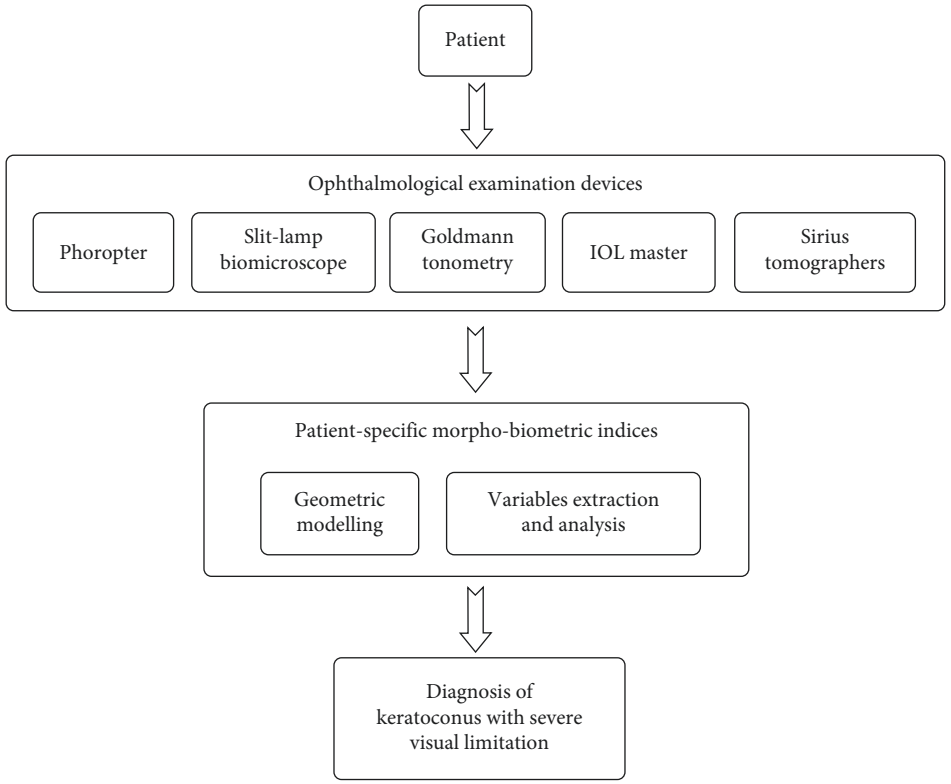

Figure 1: Use of patient-specific morpho-biometric indices for diagnosis of keratoconus with severe visual limitation.

parameters could be useful in terms of characterization of diseased corneas, and optimal cutoffs were established using Youden's J index, basing on sensitivity and specificity values [20, 21]. Graphpad Prism V 6 (GraphPad Software, La Jolla, USA) and IBM SPSS V 23.0 software (SPSS, Chicago, USA) were used to make all the analyses.

3. Results

Most of the modelled morpho-biometric indices showed statistically significant differences when comparing healthy and severe KC corneas, as shown in Table 2 below.

3.1. ROC Analysis. The predictive value of the modelled indices was established by an ROC analysis (Figure 3). Five morpho-biometric indices were identified with an area under the ROC (AUROC) above 0.85 (Table 3).

Table 4 summarizes all significant correlations between the modelled biometric parameters for the severe KC group. Correlation coefficients between parameters for the normal group have not been included, as their mutual relations have already been addressed in a previous study [18].

4. Discussion

From a visual point of view, patients of keratoconus disease show a deteriorated spectacle-corrected visual acuity, in such a way that when the disease progresses towards a higher degree of severity, the visual performance of patients gets worse. Thus, it is of great interest evaluating in a jointly manner both the geometric decompensation that takes place in corneal structure due to its structural weakening and the level of visual limitation that patients show during the disease progression. In this work, we analysed the biometric profile of the cornea conceived as a 3D refractive structure for advanced degrees of keratoconus, whose patients present a severe degree of visual limitation, according to the RETICS classification [7].

The volumetric morpho-biometric indices showed a statistically significant reduced total corneal volume in the severe KC group when compared with the healthy eyes group, which is in line with the corneal thinning described by some authors as the disease progresses [16, 22, 23] due to a loss of tenacity in the corneal structure [13, 24]. These results are consistent with the ones reported by previous studies, which have evaluated the same anatomic index with devices based on Scheimpflug technology [23, 25] and similar to the ones reported in previous studies for advanced degrees of keratoconus [9]. Also, some significant positive correlations between corneal volume and sagittal plane apex area of the posterior surface ($R^2 = 0.919$, $p \leq 0.001$), and with sagittal plane area at minimum thickness point ($R^2 = 0.931$, $p \leq 0.001$) were found, so that when the volume diminishes by the loss of structural resistance that takes place for the progression of the disease, the sagittal areas ($\text{Splarea}_{\text{papex}}/\text{Splarea}_{\text{minthk}}$) also diminish as the corneal curvature increases. This agrees with the findings of significant lower volumes associated with pachymetric reductions in grade II and higher keratoconus eyes [23].

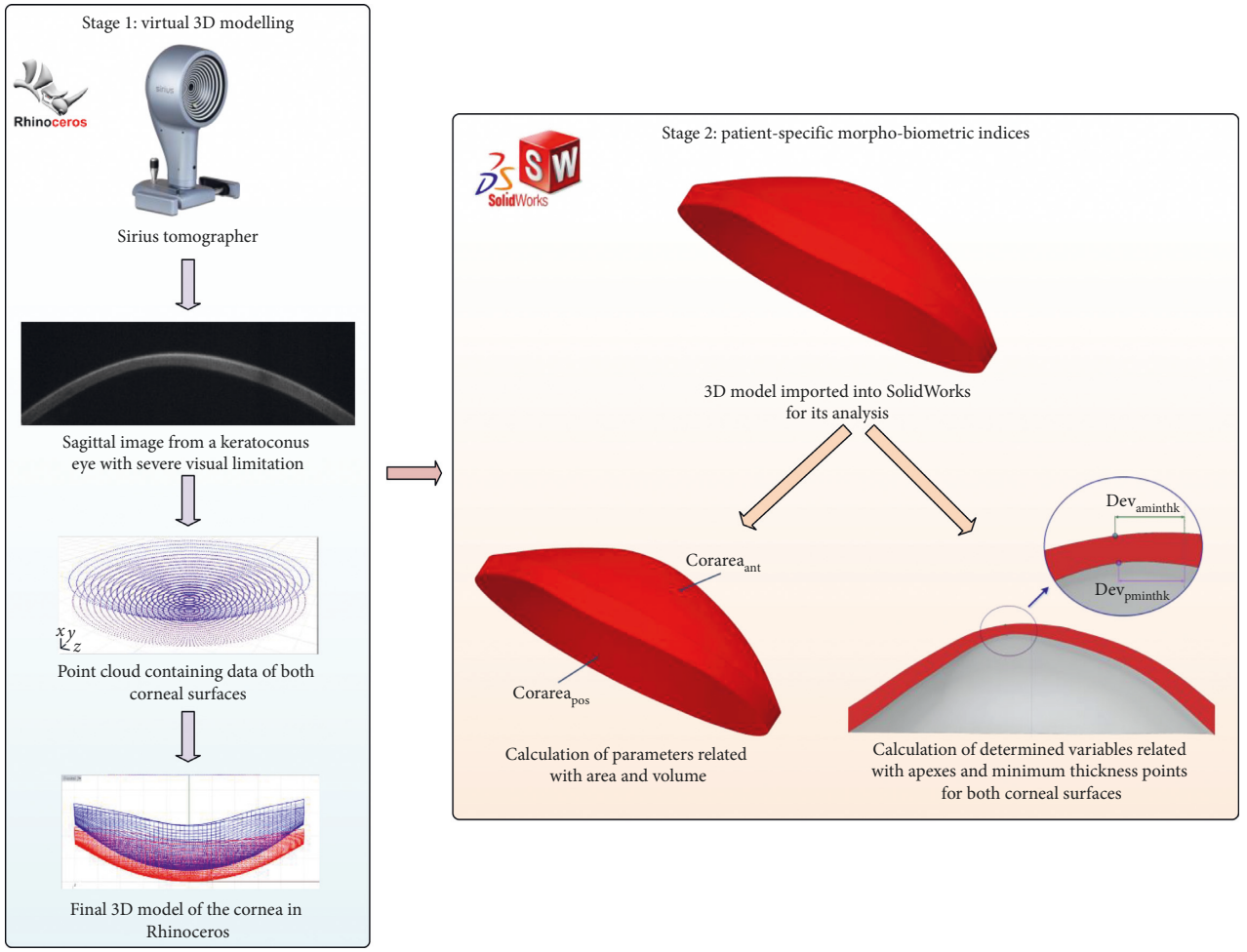

Figure 2: Protocol followed for the creation of the 3D virtual model and its later analysis.

Table 1: Patient-specific morpho-biometric indices analysed in the study [19].

Morpho-biometric parameters	Description
Total corneal volume (Vol_{tot}) (mm^3)	Volume limited by front, back, and peripheral surfaces of the solid model generated
Anterior/posterior corneal surface area ($Corarea_{ant}$/ $Corarea_{pos}$) (mm^2)	Area of the front/exterior and rear/interior surfaces
Total corneal surface area ($Corarea_{tot}$) (mm^2)	Sum of anterior, posterior, and perimeter corneal surface areas of the solid model generated
Sagittal plane apex area ($Splarea_{papex}$) (mm^2)	Area of the cornea within the sagittal plane passing through the optical axis and the highest point (apex) of the posterior corneal surface
Anterior and posterior apex deviation (Dev_{aapex}/Dev_{papex}) (mm)	Average distance from the optical axis to the highest point (apex) of the anterior/posterior corneal surfaces
Sagittal plane area in minimum thickness point ($Splarea_{minthk}$) (mm^2)	Area of the cornea within the sagittal plane passing through the optical axis and the minimum thickness point (maximum curvature) of the posterior corneal surface
Anterior and posterior minimum thickness point deviation ($Dev_{aminthk}$/$Dev_{pminthk}$) (mm)	Average distance in the XY plane from the optical axis to the minimum thickness points (maximum curvature) of the anterior/posterior corneal surfaces
Centre of mass X, Y, Z (COM_X, COM_Y, COM_Z) (mm)	Centre of mass coordinates X, Y, Z of the solid

In addition, regarding the morpho-biometric indices of the anterior and posterior surface areas, these present a statistically significant augmentation, being the greater the area of the posterior surface than the one of the anterior surface, which can be explained by the tendency of the cornea to retain a conical-shaped architecture in the advanced stages of the disease, in which the relation between both surfaces is modified by a higher increase of the

Table 2: Descriptive values and differences in the modelled morpho-biometric indices among the normal and severe KC groups.

Morpho-biometric indices	Normal group ($n = 50$)				Severe KC group ($n = 30$)					
	Mean	SD	Min	Max	Mean	SD	Min	Max	z	p
Vol_{tot} (mm^3)	25.72	1.53	23.23	29.07	23.74	1.85	20.17	28.40	5.18	≤0.01
$Corarea_{ant}$ (mm^2)	43.08	0.14	42.77	43.33	43.80	0.59	42.66	45.11	−6.56	≤0.01
$Corarea_{pos}$ (mm^2)	44.24	0.26	43.53	44.71	45.44	0.95	43.78	47.97	−6.78	≤0.01
$Corarea_{tot}$ (mm^2)	103.89	1.12	100.73	105.66	105.20	2.13	102.35	112.68	−3.14	≤0.01
$Splarea_{papex}$ (mm^2)	4.32	0.26	3.93	4.87	3.86	0.40	2.96	5.02	6.33	≤0.01
$Splarea_{minthk}$ (mm^2)	4.31	0.26	3.92	4.86	3.84	0.40	2.97	5.03	6.41	≤0.01
Dev_{aapex} (mm)	0.00	0.00	0.00	0.00	0.03	0.02	0.00	0.06	−8.26	≤0.01
Dev_{papex} (mm)	0.07	0.02	0.04	0.09	0.26	0.12	0.05	0.59	−6.68	≤0.01
COM_X (mm)	0.04	0.02	0.01	0.09	−0.01	0.06	−0.20	0.12	4.23	≤0.01
COM_Y (mm)	0.03	0.02	0.00	0.08	−0.01	0.09	−0.13	0.33	2.57	0.02
COM_Z (mm)	0.77	0.02	0.71	0.81	0.85	0.08	0.70	1.06	−5.56	≤0.01
$Dev_{aminthk}$ (mm)	0.83	0.21	0.44	1.27	0.91	0.36	0.16	1.68	−1.12	0.27
$Dev_{pminthk}$ (mm)	0.76	0.20	0.38	1.24	0.85	0.34	0.10	1.60	−1.23	0.23

SD: standard deviation; P: statistical test; z: z-score.

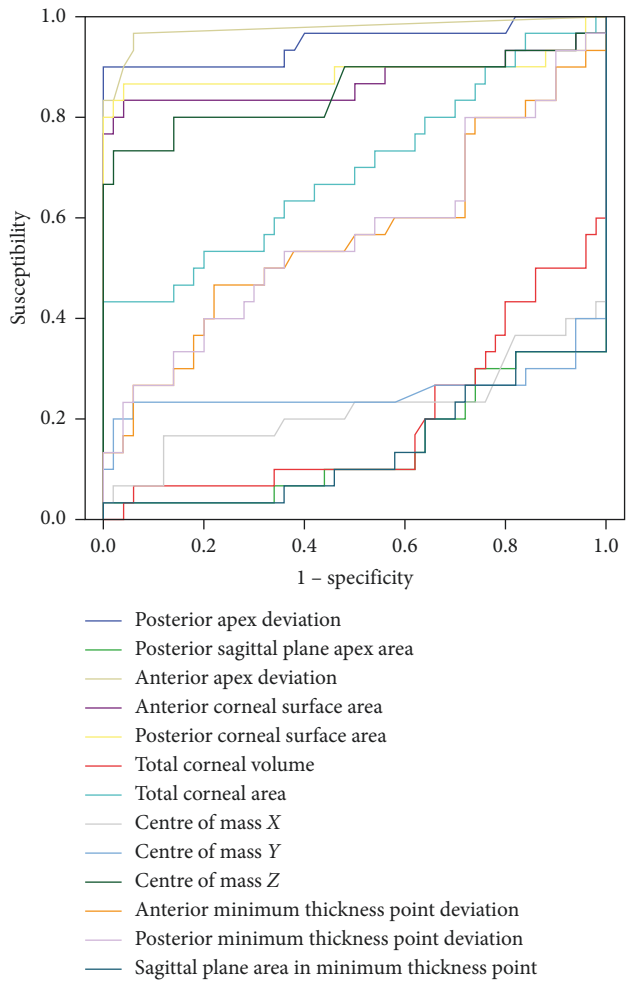

Figure 3: Curves for modelled indices detecting severe KC.

posterior surface curvature than the one in the anterior surface, motivated by the biomechanical weakening that cornea manifests for a reorientation of its anatomophysiology [26]. A tendency in this line of structural weakening has been reported in previous studies [13, 26, 27]. Vega-Estrada et al. [7] observed a significant increase in dioptric power of the posterior corneal surface with respect to the anterior in advanced phases of the disease. According to these findings, corneal multifocality that produces the conical shape that locally acquires corneal surface, drives to a worsening in patient's visual performance. Besides, anterior, posterior, and total corneal surface areas show a strong positive correlation between them, and their values increase in the severe KC group, which can be explained by the fact that structural weakening caused by the presence of fewer collagen fibres in each lamella leads to a severe local protrusion that increases the corneal surface [2] by the effect of the intraocular pressure over a structurally weakened biomechanical architecture. These results are coincident with the ones presented in other studies [16, 22, 28].

The anterior and posterior corneal surface minimum thickness point deviations show the strongest correlation between them ($R^2 = 0.995$, $p \leq 0.001$). However, these are the only parameters that show no statistical difference for group discrimination ($p = 0.271$ and $p = 0.229$, respectively). This addresses the relationship between both corneal surface curvatures for keratoconus eyes, as it has already been made in previous studies for both diseased and normal eyes [16, 28], but also that in the case of severe visual limitation, this deviation varies so greatly among individuals that discrimination is impossible.

Anterior apex deviation and posterior apex deviation increase for the severe KC group. This displacement of the optical axis has been described as one of the signs of the later stages of the disease [1]. This is in concordance with some authors' findings [23] that suggest a strong correlation between apex deviation and pachymetric progression index of the front and back elevations with CDVA of the analysed patients. Also, posterior apex deviation presents an important variability with respect to the anterior apex deviation, this is motivated by the tendency of the aspheric profile to reproduce the cornea's physiologic prolatism in advanced phases of the disease [16, 28]. It can even be observed a paraboloid type geometry in virtual 3D models, a fact that can be relevant to explain the asymmetry that shows the posterior corneal surface in advanced keratoconus. This variability has been reported in previous studies [15, 29, 30],

Table 3: The area under the ROC results.

Morpho-biometric indices	AUROC	Sensitivity	Specificity	Cutoff value
$Corarea_{ant}$	0.874	83.3	96.0	≥43.275 mm^2
$Corarea_{pos}$	0.890	86.7	96.0	≥43.160 mm^2
Dev_{aapex}	0.977	96.7	94.0	≥0.001 mm
Dev_{papex}	0.948	90.0	99.9	≥0.098 mm
COM_Z	0.852	73.3	98.0	≥0.809 mm

Table 4: The significant correlation coefficient values for the modelled variables in the severe KC group.

Measurement correlation	Severe KC group ($n = 30$)	
	Correlation coefficient	p value
$Splarea_{papex}/Vol_{tot}$	0.919	≤0.001
$Corarea_{ant}/Corarea_{pos}$	0.917	≤0.001
$Corarea_{ant}/Corarea_{tot}$	0.835	≤0.001
$Corarea_{pos}/Corarea_{tot}$	0.899	≤0.001
$Vol_{tot}/Corarea_{tot}$	0.439	0.015
$COM_Y/Splarea_{papex}$	0.448	0.013
COM_Z/Dev_{aapex}	0.366	0.046
$COM_Z/Corarea_{ant}$	0.925	≤0.001
$COM_Z/Corarea_{pos}$	0.874	≤0.001
$COM_Z/Corarea_{tot}$	0.873	≤0.001
$Dev_{aminthk}/Dev_{papex}$	0.597	≤0.001
$Dev_{pminthk}/Dev_{papex}$	0.611	≤0.001
$Splarea_{minthk}/Splarea_{papex}$	0.989	≤0.001
$Vol_{tot}/Splarea_{minthk}$	0.931	≤0.001
COM_X/COM_Y	−0.375	0.041
$COM_X/Dev_{aminthk}$	−0.429	0.018
$COM_X/Dev_{pminthk}$	−0.476	0.008
$COM_Y/Splarea_{minthk}$	−0.403	0.027
Dev_{aapex}/Dev_{papex}	0.995	≤0.001

being this one the first in which posterior surface asymmetry is quantified for keratoconus eyes with severe visual limitation. Besides, this geometric tendency is correlated with the increase of optical aberrations in advanced degrees of keratoconus [5, 22, 31].

Results also suggest a strong correlation between centre of mass Z and anterior, posterior, and total corneal surfaces ($R^2 = 0.925$, $p \leq 0.001$; $R^2 = 0.874$, $p \leq 0.001$; $R^2 = 0.873$, $p \leq 0.001$, respectively) as well as a displacement of the centre of mass along the Z-positive axis, which is logical, as the loss of corneal volume that steeps the surfaces, should also force the centre of mass to move towards the protrusion, as a consequence of the corresponding displacement of both apex points in the Z-coordinate. This is in line with the findings of some authors [32, 33], which found that the mean maximum anterior and posterior corneal elevations were higher in eyes with subclinical or clinical keratoconus.

Regarding the ROC analysis, the anterior apex deviation reached the highest area under the curve (AUC, 0.977) with very high sensitivity (96.7%) and specificity (94.0%) due to the fact that the apex is the maximum curvature point of the corneal surface. Moreover, the posterior apex deviation also shows high discrimination capability (AUC, 0.948) with very good sensitivity (90%) and excellent specificity (99.9%). Anterior and posterior corneal surfaces and centre of mass show high AUC, but although their specificity is high, their sensitivity is not as good as the one for the deviation of the apices.

In conclusion, the analysis of corneal biometric parameters using patient-specific 3D modelling has ascertained statistically significant differences between normal and KC eyes with severe visual limitation. This computer-assisted custom approach has determined several indices that successfully characterize the profile of keratoconic eyes affected by severe visual limitation. Therefore, this analysis has proven to be a useful tool for KC classification, helping doctors to achieve reliable diagnoses in severe cases of the disease, as well as it has helped to better characterize corneal changes that take place when severe KC is developed and how they relate with vision deterioration.

Data Availability

The data used to support the findings of this study were supplied by "Iberia" under license and so cannot be made freely available. Requests for access to these data should be made to Dr. Jorge Alió, jlalio@vissum.com, National Network for Clinical Research in Ophthalmology RETICS-OFTARED.

Conflicts of Interest

The authors have no conflicts of interest to declare.

Acknowledgments

This publication has been carried out in the framework of the Thematic Network for Cooperative Research in Health (RETICS) reference number RD16/0008/0012 financed by the Carlos III Health Institute-General Subdirection of Networks and Cooperative Investigation Centers (R&D&I National Plan 2013–2016) and the European Regional Development Fund (FEDER).

References

[1] Y. S. Rabinowitz, "Keratoconus," *Survey of Ophthalmology*, vol. 42, no. 4, pp. 297–319, 1998.

[2] F. Cavas-Martínez, E. De la Cruz Sánchez, J. N. Martínez, F. F. Cañavate, and D. Fernández-Pacheco, "Corneal topography in keratoconus: state of the art," *Eye and Vision*, vol. 3, no. 1, 2016.

[3] J. W. Ruberti, A. Sinha Roy, and C. J. Roberts, "Corneal biomechanics and biomaterials," *Annual Review of Biomedical Engineering*, vol. 13, no. 1, pp. 269–295, 2011.

[4] A. C. Ferdi, V. Nguyen, D. M. Gore, B. D. Allan, J. J. Rozema, and S. L. Watson, "Keratoconus natural progression," *Ophthalmology*, vol. 126, no. 7, pp. 935–945, 2019.

[5] J. L. Alió, D. P. Piñero, A. Alesón et al., "Keratoconus-integrated characterization considering anterior corneal aberrations, internal astigmatism, and corneal biomechanics," *Journal of Cataract & Refractive Surgery*, vol. 37, no. 3, pp. 552–568, 2011.

[6] A. Martínez-Abad and D. P. Piñero, "New perspectives on the detection and progression of keratoconus," *Journal of Cataract & Refractive Surgery*, vol. 43, no. 9, pp. 1213–1227, 2017.

[7] A. Vega-Estrada, J. L. Alio, L. F. Brenner et al., "Outcome analysis of intracorneal ring segments for the treatment of keratoconus based on visual, refractive, and aberrometric impairment," *American Journal of Ophthalmology*, vol. 155, no. 3, pp. 575–584.e1, 2013.

[8] F. Cavas-Martínez, D. G. Fernández-Pacheco, E. De la Cruz-Sánchez et al., "Geometrical custom modeling of human cornea in vivo and its use for the diagnosis of corneal ectasia," *PLoS One*, vol. 9, no. 10, Article ID e110249, 2014.

[9] F. Cavas-Martínez, L. Bataille, D. G. Fernández-Pacheco, F. J. F. Cañavate, and J. L. Alio, "Keratoconus detection based on a new corneal volumetric analysis," *Scientific Reports*, vol. 7, no. 1, 2017.

[10] I. Seven, A. Vahdati, V. S. De Stefano, R. R. Krueger, and W. J. Dupps Jr., "Comparison of patient-specific computational modeling predictions and clinical outcomes of LASIK for myopia," *Investigative Opthalmology & Visual Science*, vol. 57, no. 14, pp. 6287–6297, 2016.

[11] I. Simonini and A. Pandolfi, "Customized finite element modelling of the human cornea," *PLoS One*, vol. 10, no. 6, Article ID e0130426, 2015.

[12] M. A. Lago, M. J. Rupérez, C. Monserrat et al., "Patient-specific simulation of the intrastromal ring segment implantation in corneas with keratoconus," *Journal of the Mechanical Behavior of Biomedical Materials*, vol. 51, pp. 260–268, 2015.

[13] M. Á. Ariza-Gracia, J. Zurita, D. P. Piñero, B. Calvo, and J. F. Rodríguez-Matas, "Automatized patient-specific methodology for numerical determination of biomechanical corneal response," *Annals of Biomedical Engineering*, vol. 44, no. 5, pp. 1753–1772, 2016.

[14] I. Seven, A. S. Roy, and W. J. Dupps Jr., "Patterned corneal collagen crosslinking for astigmatism: computational modeling study," *Journal of Cataract & Refractive Surgery*, vol. 40, no. 6, pp. 943–953, 2014.

[15] S. Huseynli, J. Salgado-Borges, and J. L. Alio, "Comparative evaluation of Scheimpflug tomography parameters between thin non-keratoconic, subclinical keratoconic, and mild keratoconic corneas," *European Journal of Ophthalmology*, vol. 28, no. 5, pp. 521–534, 2018.

[16] R. Montalbán, J. L. Alio, J. Javaloy, and D. P. Piñero, "Comparative analysis of the relationship between anterior and posterior corneal shape analyzed by scheimpflug photography in normal and keratoconus eyes," *Graefe's Archive for Clinical and Experimental Ophthalmology*, vol. 251, no. 6, pp. 1547–1555, 2013.

[17] F. Cavas Martinez, D. Garcia Fernandez-Pacheco, F. J. Fernandez Cañavate et al., "Detección de queratocono temprano mediante modelado 3D personalizado Y análisis de sus parámetros geométricos," *Dyna Ingenieria E Industria*, vol. 94, no. 1, pp. 175–181, 2019.

[18] F. Cavas-Martínez, D. Fernández-Pacheco, F. Cañavate, J. Velázquez-Blázquez, J. Bolarín, and J. Alió, "Study of morpho-geometric variables to improve the diagnosis in keratoconus with mild visual limitation," *Symmetry*, vol. 10, no. 8, p. 306, 2018.

[19] F. Cavas-Martínez, D. G. Fernández-Pacheco, D. Parras, F. J. F. Cañavate, L. Bataille, and J. Alió, "Study and characterization of morphogeometric parameters to assist diagnosis of keratoconus," *BioMedical Engineering Online*, vol. 17, no. S1, 2018.

[20] T. A. Lasko, J. G. Bhagwat, K. H. Zou, and L. Ohno-Machado, "The use of receiver operating characteristic curves in biomedical informatics," *Journal of Biomedical Informatics*, vol. 38, no. 5, pp. 404–415, 2005.

[21] M. S. Pepe, *The Statistical Evaluation of Medical Tests for Classification and Prediction*, OUP, Oxford, UK, 2003.

[22] H. N. Colak, F. A. Kantarci, A. Yildirim et al., "Comparison of corneal topographic measurements and high order aberrations in keratoconus and normal eyes," *Contact Lens and Anterior Eye*, vol. 39, no. 5, pp. 380–384, 2016.

[23] D. P. Piñero, J. L. Alió, A. Alesón, M. E. Vergara, and M. Miranda, "Corneal volume, pachymetry, and correlation of anterior and posterior corneal shape in subclinical and different stages of clinical keratoconus," *Journal of Cataract & Refractive Surgery*, vol. 36, no. 5, pp. 814–825, 2010.

[24] G. Labiris, Z. Gatzioufas, H. Sideroudi, A. Giarmoukakis, V. Kozobolis, and B. Seitz, "Biomechanical diagnosis of keratoconus: evaluation of the keratoconus match index and the keratoconus match probability," *Acta Ophthalmologica*, vol. 91, no. 4, pp. e258–e262, 2013.

[25] S. S. Wahba, M. M. Roshdy, R. S. Elkitkat, and K. M. Naguib, "Rotating scheimpflug imaging indices in different grades of keratoconus," *Journal of Ophthalmology*, vol. 2016, Article ID 6392472, 9 pages, 2016.

[26] C. J. Roberts and W. J. Dupps Jr., "Biomechanics of corneal ectasia and biomechanical treatments," *Journal of Cataract & Refractive Surgery*, vol. 40, no. 6, pp. 991–998, 2014.

[27] R. Ambrósio Jr., B. T. Lopes, F. Faria-Correia et al., "Integration of scheimpflug-based corneal tomography and biomechanical assessments for enhancing ectasia detection," *Journal of Refractive Surgery*, vol. 33, no. 7, pp. 434–443, 2017.

[28] R. Montalbán, J. L. Alio, J. Javaloy, and D. P. Piñero, "Correlation of anterior and posterior corneal shape in keratoconus," *Cornea*, vol. 32, no. 7, pp. 916–921, 2013.

[29] M. Aghazadeh Amiri, H. Hashemi, S. Ramin et al., "Corneal thickness measurements with scheimpflug and slit scanning imaging techniques in keratoconus," *Journal of Current Ophthalmology*, vol. 29, no. 1, pp. 23–27, 2017.

[30] G. H. Bae, J. R. Kim, C. H. Kim, D. H. Lim, E. S. Chung, and T.-Y. Chung, "Corneal topographic and tomographic analysis of fellow eyes in unilateral keratoconus patients using pentacam," *American Journal of Ophthalmology*, vol. 157, no. 1, pp. 103–109.e1, 2014.

[31] F. Aslani, M. Khorrami-Nejad, M. A. Amiri, H. Hashemian, F. Askarizadeh, and B. Khosravi, "Characteristics of posterior corneal astigmatism in different stages of keratoconus," *Journal of Ophthalmic and Vision Research*, vol. 13, no. 1, pp. 3–9, 2018.

[32] U. de Sanctis, C. Loiacono, L. Richiardi, D. Turco, B. Mutani, and F. M. Grignolo, "Sensitivity and specificity of posterior corneal elevation measured by pentacam in discriminating keratoconus/subclinical keratoconus," *Ophthalmology*, vol. 115, no. 9, pp. 1534–1539, 2008.

[33] R. Ishii, K. Kamiya, A. Igarashi, K. Shimizu, Y. Utsumi, and T. Kumanomido, "Correlation of corneal elevation with severity of keratoconus by means of anterior and posterior topographic analysis," *Cornea*, vol. 31, no. 3, pp. 253–258, 2012.

Hindawi
Journal of Ophthalmology
Volume 2019, Article ID 4101256, 7 pages
https://doi.org/10.1155/2019/4101256

Research Article

Correlations of Corneal Spherical Aberration with Astigmatism and Axial Length in Cataract Patients

Min Zhang,[1,2,3] **Dongjin Qian**,[1,2,3] **Qinghe Jing**,[1,2,3] **Jiahui Chen**,[1,2,3] **Michael Deng**,[1,2,3] **and Yongxiang Jiang**[1,2,3]

[1]*Department of Ophthalmology and Vision Science, Eye and ENT Hospital of Fudan University, Shanghai, China*
[2]*NHC Key Laboratory of Myopia (Fudan University), Laboratory of Myopia, Chinese Academy of Medical Sciences, Shanghai, China*
[3]*Key Laboratory of Visual Impairment and Restoration of Shanghai, Shanghai, China*

Correspondence should be addressed to Yongxiang Jiang; yongxiang_jiang@163.com

Received 18 April 2019; Accepted 3 August 2019; Published 10 September 2019

Guest Editor: Pablo Pérez-Merino

Purpose. To clarify the distribution of corneal spherical aberrations (SAs) in cataract patients with different corneal astigmatism and axial length. *Setting*. Department of Ophthalmology and Vision Science of the Eye and ENT Hospital of Fudan University, Shanghai, China. *Design*. Retrospective case series. *Methods*. The axial length, corneal SAs, and other corneal biometrics were collected in cataract patients with Pentacam HR and IOLMaster 500. The statistical analysis of the corneal SAs was based on the stratification of axial length and anterior corneal astigmatism. *Results*. In total, 6747 eyes of 6747 patients were recruited, with 2416 eyes (58.17 ± 16.81 years old) in the astigmatism group (anterior corneal astigmatism ≥1 D) and others (61.82 ± 12.64 years old) in the control group. In patients with astigmatism <2 D, the total and anterior SAs decreased as the axial length increased ($P < 0.001$). The total corneal SAs of patients with astigmatism of 2-3 D stabilized at around 0.29 μm, whereas those of patients with anterior corneal astigmatism ≥3 D tended to be variable. Age and anterior corneal astigmatism had positive and negative effects, respectively, on SA in the regression model. *Conclusions*. Axial length has a negative effect on the anterior and total corneal SAs, which stabled around 0.33 μm and 0.30 μm in patients with axial length of ≥26 mm, respectively. Individualized SA adjustments are essential for patients undergoing aspheric toric IOL implantation with preoperative anterior corneal astigmatism of 1-2 D or ≥3 D. Toric IOLs with a negative SA of −0.20 μm are recommended for patients with anterior corneal astigmatism of 2-3 D if no customized therapy is warranted.

1. Introduction

Intraocular lenses (IOLs) have been designed for and are implanted into aphakic eyes to substitute for natural lenses, partly to rectify the spherical refractive power in the ocular optical system. Further advances have been made to restore the ocular physiological status: multifocal IOLs for both distance and near vision, toric IOLs to compensate for corneal primary astigmatism, and aspheric IOLs for the correction of corneal spherical aberrations (SAs).

Astigmatism of order 2 is a low-order aberration and SA is a high-order aberration. Nowadays other astigmatism belonging to high-order aberrations were beyond the correction of both IOLs and glasses. So only astigmatism of order 2 was studied and is shortened as astigmatism in this article. Postoperative residual ocular astigmatism and SAs lead to halo or other visual complaints and worsen the optical performance, even when the best-corrected visual acuity is good. The overall prevalence of astigmatism ranges from 86.8% to 99% [1]. A considerable proportion of these eyes in patients with cataract require correction of astigmatism (43.9% of patients with corneal astigmatism of ≥1.0 D in Southern China, 46.70% in Northern China, 37.80% in Thailand, and 40.41% in the United Kingdom), which can be effectively accommodated by the cylindrical power of the toric IOLs available, as demonstrated in previous clinical studies [1–10]. The correction of SA is also widely performed and is clinically important [11, 12].

When an aspheric toric IOL is required, the correction of astigmatism is usually considered first [12, 13]. However, because different aspheric modifications can be made with the aspheric toric IOLs currently available on the market from different companies, which have different aspheric values, postoperative ocular aberrations can be rectified and the correct selection of the optical parameters of the IOL is important.

Therefore, in this study, we (1) clarify the differences in the corneal biometrics of patients when the cutoff point for defining preoperative corneal astigmatism is 1 D, (2) present the total and anterior corneal SA states associated with different astigmatism levels and axial length levels, and (3) identify the main factors associated with SAs, especially the statistical correlations between astigmatism and SA. Some recommendations are also made for the proper correction of SAs using toric IOLs with an aspheric design.

2. Methods

In this retrospective case series, we recruited patients scheduled for cataract surgery between September 29, 2016, and August 15, 2018, at the Eye and ENT Hospital of Fudan University, Shanghai, China. The main inclusion criteria and exclusion criteria were described in our previous study [14]. This study was approved by the Human Research Ethics Committee of the Eye and ENT Hospital of Fudan University, and adhered to the tenets of the Declaration of Helsinki. Written informed consent was provided by all the patients.

All ocular data were collected, defined, and presented following the methods of Zhang et al. [14], using the rotating Scheimpflug camera (Pentacam HR; Oculus, Wetzlar, Germany) and the partial coherence interferometry (IOLMaster 500; Carl Zeiss Meditec, Jena, Germany). These data included the anterior corneal astigmatism, central corneal thickness (CCT), anterior corneal eccentricity and the SAs of the total cornea (total SA), anterior corneal surface (anterior SA), posterior corneal surface (posterior SA), index of surface variance (ISV), index of vertical asymmetry (IVA), keratoconus index (KI), center keratoconus index (CKI), index of height asymmetry (IHA), and index of height decentration (IHD). All 6 conic coefficients (ISV, IVA, KI, CKI, IHA, and IHD) were collected with a cornea scan of 8 mm diameter, whereas others were collected with a cornea scan of 6 mm diameter centered at the corneal apex under the automode of Pentacam. Corneal astigmatism was divided into with the rule (WTR), against the rule (ATR), and oblique astigmatism according to the steep corneal meridian [14].

All patients were divided into four levels based on their anterior corneal astigmatism, with cutoffs = 1 D, 2 D, and 3 D. To identify practical and operational parameters for clinical IOL selection, all the patients were also stratified into seven levels according to their axial length: <20 mm, 20–22 mm (20 mm included while 22 mm not, similarly hereinafter), 22–24.5 mm, 24.5–26 mm, 26–28 mm, 28–30 mm, and ≥30 mm. This resulted in a total of 28 individual groups, with two preliminary stratifications (by anterior corneal astigmatism and axial length). In those patients with astigmatism ≥1 D (including the 1-2 D, 2-3 D, and ≥3 D levels), summarized as the "astigmatism group," astigmatism correction was considered when planning their surgery. Patients with astigmatism <1 D were considered as the control group.

3. Statistical Analysis

To avoid any possible contralateral effect, only one eye of each cataract patient was enrolled in this retrospective clinical study.

All continuous data are shown as mean ± standard deviation (SD). The Kolmogorov–Smirnov test was used to assess the normality of the distributions of continuous data. Because the sample of patients with axial length of <20 mm was small ($n = 7$), this group was removed from subsequent analyses, and only 24 cross-groups were analyzed. One-way analysis of variance (ANOVA) was used to compare the continuous variables among the 24 cross-groups and two-way ANOVA was used to compare the four astigmatism levels and six axial length groups twice, once when the data were stratified by axial length and then again when the data were stratified by astigmatism levels. When either the astigmatism level or axial length was taken as the stratification factor, the other was considered to be the explanatory variable. If a significant difference was detected, a further post hoc multiple comparison test with Bonferroni correction was performed to identify the exact level making the difference. Pearson's χ^2 test was used to compare categorical items among the WTR, ATR, and oblique astigmatism groups. Pearson r correlation analyses were used to explore the relationship between corneal biometrics with astigmatism and axial length. A multiple regression analysis was used to explore the exact statistical contributions of the explanatory variables to the corneal SAs adjusted by age as described before [14], in the astigmatism group, the control group, and all the enrolled patients. All data were analyzed with SPSS 23.0 (SPSS, IBM Corp., Armonk, NY, USA). $P < 0.05$ was considered to indicate statistical significance.

4. Results

In total, 6747 eyes of 6747 patients were recruited in this study, among which 2416 eyes had anterior corneal astigmatism of ≥1 D. The numbers of patients in the cross-groups (axial length × astigmatism) are presented in Table 1.

The demographic data, corneal biometric data, and axial length of these patients are shown in Table 2 and Supplementary Material Table 1, with comparisons between the two groups. The average age of the patients in the astigmatism group was lower than that in the control group (58.17 ± 16.81 vs. 61.82 ± 12.64 years, respectively, $P < 0.001$). In addition, several statistically significant correlations of the corneal biometrics were found with the axial length and the anterior corneal astigmatism (Supplementary Material Table 2). The compositions of the astigmatism types varied with the different astigmatism levels and axial length (both $P < 0.001$; Supplementary Material Tables 3 and 4).

The distributions of anterior corneal SA and total corneal SA are presented in Figures 1 and 2, respectively. Gradual step-down trends in the anterior and total corneal SAs were

Table 1: Numbers of patients in seven axial length categories and four astigmatism groups.

Count (percentage in all)		Axial length (mm)							Total
		<20	20–22	22–24.5	24.5–26	26–28	28–30	≥30	
Astigmatism (D)	<1	5 (0.07%)	209 (3.10%)	2690 (39.87)	530 (7.86%)	380 (5.63%)	221 (3.28%)	296 (4.39%)	4331 (64.19%)
	1-2	1 (0.01%)	76 (1.13%)	907 (13.44%)	289 (4.28%)	264 (3.91%)	198 (2.93%)	248 (3.68%)	1983 (29.39%)
	2-3	1 (0.01%)	22 (0.33%)	121 (1.79%)	51 (0.76%)	55 (0.82%)	39 (0.58%)	62 (0.92%)	351 (5.20%)
	≥3	0 (0%)	6 (0.09%)	25 (0.37%)	16 (0.24%)	14 (0.21%)	7 (0.10%)	14 (0.21%)	82 (1.22%)
Total		7 (0.10%)	313 (4.64%)	3743 (55.48%)	886 (13.13%)	713 (10.57%)	465 (6.89%)	620 (9.19%)	6747

Table 2: Demographic data of the astigmatism group and the control group.

Mean ± SD	Astigmatism group	Control group	P value
Eyes	2416	4331	—
Age (years)	58.17 ± 16.81	61.82 ± 12.64	<0.001*
Gender (male/Female)	1024/1392	1834/2497	0.976**
CCT (mm)	538.85 ± 31.56	538.29 ± 31.66	0.486*
Axial length (mm)	25.72 ± 3.18	24.63 ± 2.66	<0.001*

SD = standard deviation; CCT = central corneal thickness. *Independent two-sample t-test; **Pearson's χ^2 test.

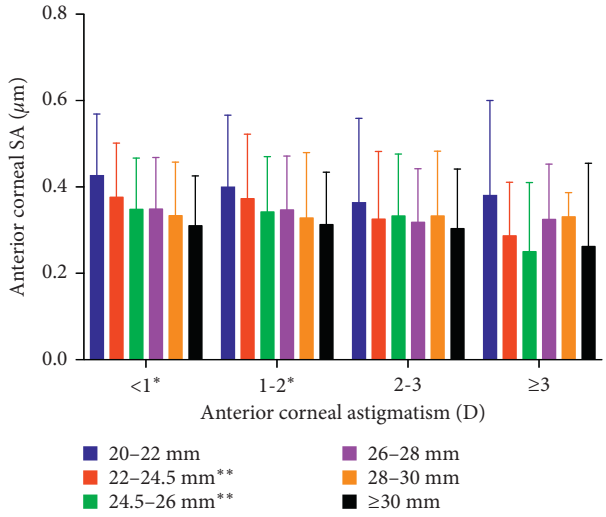

Figure 1: Anterior corneal SA values among cross-groups. Anterior SA = anterior corneal spherical aberration. *$P < 0.001$ among the different axial length levels when the astigmatism levels were taken as the stratification factor. **$P < 0.001$ among the different astigmatism levels when the axial length groups were taken as the stratification factor.

detected as the axial length increased in patients with astigmatism <1 and 1-2 D. Although no statistically significant differences in SA were detected as axial length increased in patients with astigmatism >3 D, as mentioned above, the figures show a very variable pattern in these patients. The mean values for anterior, posterior, and total SAs differed significantly among the 24 cross-groups (all $P < 0.001$). Both the anterior and total SAs differed significantly among different axial lengths in patients with astigmatism <1 D or 1-2 D (all $P < 0.001$). Both the total SAs and anterior SAs showed significantly different astigmatism levels in patients with axial

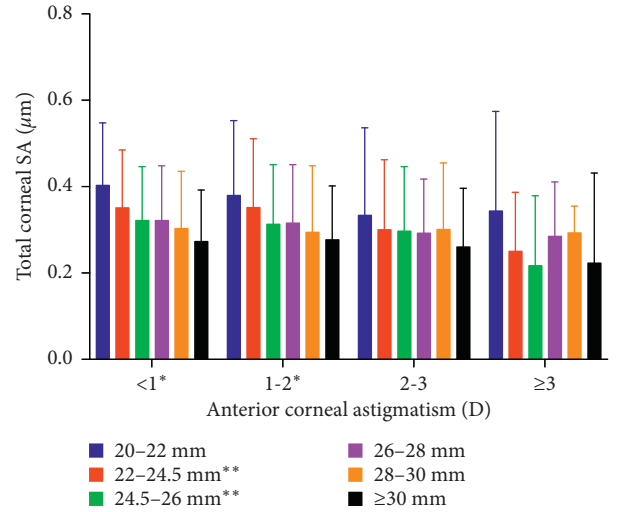

Figure 2: Total corneal SA values among cross-groups. Total SA = total corneal spherical aberration. *$P < 0.001$ among the different axial length levels when the astigmatism levels were taken as the stratification factor. **$P < 0.001$ among the different astigmatism levels when axial length levels were taken as the stratification factor.

length of 22–24.5 mm and 24.5–26 mm. Further analysis showed that the anterior SA differed significantly between patients with axial length of 20–22 mm and those with axial length of 22–24.5 mm ($P < 0.001$) and between those with axial length of 22–24.5 mm and those with axial length of 24.5–26 mm ($P = 0.002$) in the astigmatism <1 D group. The differences in total SA between the following pairs were also statistically significant: axial length of 20–22 mm and 22–24.5 mm in astigmatism <1 D level ($P < 0.001$); axial length of 22–24.5 mm and 24.5–26 mm in astigmatism <1 D level ($P = 0.002$); axial length of 22–24.5 mm and 24.5–26 mm in astigmatism 1–2 D level ($P = 0.035$); and astigmatism of 1-2 D and 2-3 D in the axial length 22–24.5 level ($P = 0.010$). All these data indicate that, in patients with axial lengths ≥26 mm and astigmatism ≥2 D, the total SA and anterior SA varied only slightly. The mean values for total anterior corneal SA could then be calculated, and were 0.29 μm and 0.32 μm in patients with astigmatism of ≥2 D, and 0.30 μm and 0.33 μm in patients with axial length of ≥26 mm, respectively.

In multiple linear regression analyses of the astigmatism group, the control group, and the whole study population, age correlated positively with total SA and posterior SA (all $P < 0.001$; Table 3). When adjusted for age, the axial length

Table 3: Results of multiple linear regressions* of the total corneal spherical aberrations and anterior corneal spherical aberrations in the astigmatism group, the control group, and the total enrolled patients.

		Astigmatism group			Control group			Total		
		Coefficient	Beta	*P* value	Coefficient	Beta	*P* value	Coefficient	Beta	*P* value
Total SA	Age	0.005	0.521	<0.001	0.005	0.444	<0.001	0.005	0.478	<0.001
	AL	−0.007	−0.139	<0.001	−0.008	−0.155	<0.001	−0.007	−0.147	<0.001
	CCT	—	—	—	<0.001	−0.027	0.045	0	−0.027	0.009
Anterior SA	Age	0.004	0.445	<0.001	0.004	0.361	<0.001	0.004	0.4	<0.001
	AL	−0.005	−0.117	<0.001	−0.007	−0.148	<0.001	−0.006	−0.135	<0.001
	CCT	<0.001	−0.056	0.002	<0.001	−0.051	<0.001	<0.001	−0.053	<0.001

*Anterior corneal astigmatism was removed as a factor in all regressions. Beta = standardized coefficient; total SA = total corneal spherical aberration; anterior SA = anterior corneal spherical aberration; AL = axial length; CCT = central corneal thickness.

correlated negatively with the total SA and posterior SA in the regression models (all $P < 0.001$; Table 3). Based on the absolute value of beta, which represents the corresponding variable's relative contribution in the regression model, age was weighted 3-4 times more strongly than axial length.

A shift from ATR to WTR with age was also detected (Supplementary Material Table 5), which is consistent with previous findings [15, 16].

5. Discussion

Phacoemulsification combined with IOL implantation is now much more than a sight-restoring surgery and is indeed a refractive surgery, with the aims of excellent spectacle-independent optical performance and less expensive visual improvement [1, 17].

Postoperative aberrations negatively affect ocular outcomes, which range from halo in both high-contrast and ideal lighting conditions to impaired low-contrast or high-contrast visual acuity when the magnitude of the aberration is large. Among these outcomes, astigmatism and primary SA are the most important low-order and high-order aberrations, respectively, and both are highly prevalent worldwide [18, 19].

The amplitudes of all corneal aberrations, presented as Zernike polynomial coefficients, are affected by the size, shape, and compositional distribution of the cornea [20]. Therefore, corneal astigmatism and corneal SAs must sometimes be revised at the same time. In refractive cataract surgery, toric IOLs are required if patients have an expected postoperative corneal astigmatism of >0.75 D or preoperative corneal astigmatism of >1.00 D. Toric IOLs with SAs of 0, −0.1, −0.18, −0.20, and −0.27 μm are available in clinical practice. When a preoperative corneal SA is identified and individualized correction is possible, the appropriate toric IOL must be selected from among those with different aspheric values.

The careful design of IOLs that considers both a patient's astigmatism and SA is important in achieving the best surgical effect. However, previous studies have only compared the visual outcomes of spherical toric IOL implantation and aspheric toric IOL implantation [12, 13] or aspheric toric IOL implantation and aspheric nontoric IOL implantation [21]. To our knowledge, no research has focused on the role of preoperative examinations in design strategies, so we undertook such an analysis.

Both the anterior corneal surface and the internal optics (the posterior corneal surface and the crystalline lens) contribute to the wavefront aberrations passing through the eye [22]. Crystalline lenses must be removed in cataract surgery and only the corneal properties need be documented preoperatively. Because the effect of posterior corneal astigmatism is much smaller than that of anterior corneal astigmatism, we did not analyze it here. Extreme myopic astigmatism and oblique astigmatism, such as keratoconus [23], are also beyond the scope of this study.

The implantation of toric IOLs is reported not only to compensate for ocular astigmatism but also to reduce any SA [24, 25]. Uncorrected astigmatism reduces the small visual benefit possible by correcting ocular SA with soft contact lenses [26]. However, a postoperative net SA of +0.1 μm is recommended because it allows better contrast sensitivity and an extended depth of focus compared with the aberration-free condition [27–31].

Of the 2416 eyes with astigmatism >1 D (astigmatism group) analyzed in this study, 1983 (82.08%) had astigmatism of 1–2 D, which was the level of most patients in the astigmatism group. At this astigmatism level, the anterior and total SAs were found to vary among the different axial length groups ($P < 0.001$). When the patients were stratified according to axial length, in those with axial length of 22–24.5 and 24.5–26 mm, SA differed according to the level of astigmatism (both $P < 0.001$). The patients in these two axial length groups comprised a large proportion of the cataract population (4629/6747 = 68.60%). This suggests that it is clinically essential to assess the preoperative SA and determine the SA required for correction because these patients constitute such a large proportion of the clinic population.

Although astigmatism of 1-2 D requires individualized SA correction when the astigmatism was ≥2 D, SA tended to be stable (no significant difference in SA was detected in patients with astigmatism of 2–3 D or >3 D; also see Figures 1 and 2). The mean value of the total corneal SA of patients with anterior corneal astigmatism ≥2 D was 0.29 μm. To achieve a postoperative ocular SA of +0.10 μm, toric IOLs with a negative SA of −0.20 μm should be selected. Because of the small group size of ≥3 D astigmatism subgroup (82 eyes) compared with 2–3 D astigmatism subgroup

(351 eyes), the 0.32 μm mean total corneal SA in patients with astigmatism of ≥3 D and the not small standard deviation values of total corneal SA in this group (see the ≥3 D astigmatism subgroup in Figure 2), we suggest the selection of −0.20 μm toric IOLs only for patients with astigmatism of 2-3 D and individualized design for those with astigmatism of ≥3 D.

We used multiple regression analyses to identify the factors associated with corneal SAs. It was no surprise to find that astigmatism did not contribute to either the anterior or total corneal SA in the regression models because Miller et al. reported that they observed no association between elevated astigmatism and SA [32]. The negative coefficients for axial length in the regression were consistent with the decreasing trend in SA values as the axial length increased in patients with astigmatism of 1-2 D (axial length < 20 mm was omitted from the analysis because the population was small).

Age was a factor positively affecting SAs, consistent with previous findings [33, 34]. Other corneal biometrics are also reported to correlate with age [35]. Because the members of the astigmatism group were significantly younger than those in the control group, the differences in the corneal biometrics of the two groups can be partly attributed to age, but age does not fully account for the negative role of axial length in the regression model.

There were some limitations in our study. First, posterior corneal astigmatism was not taken into account because of its small magnitude [36], and total corneal astigmatism was replaced with anterior corneal astigmatism in the statistical analyses. The anterior-posterior astigmatism axis, the magnitude of posterior astigmatism, and keratometric astigmatism all lead to estimation errors [37], and this caused the corneal astigmatism values to be overestimated in this study [38, 39]. Second, only IOLMaster was used to measure axial length. IOLMaster does not have a non-accommodative fixation target and tends to provide inaccurate (usually shorter) axial length in subjects with small pupils. Third, we did not consider dry eye conditions in this analysis (although we excluded patients with dry eye disease). However, the presence of dry eye conditions in individual patients would have affected the accuracy of our topographic results, and therefore the analytical results [40]. Fourth, no vector analysis was performed because no decomposed corneal astigmatism J0 and J45 values were available because of the limitations of our devices [19]. Finally, no white-to-white distance was measured in patients with large and small corneas, which reportedly influence surgically induced astigmatism and postoperative astigmatism [41]. Because of the retrospective design and no postoperative data available, more comprehensive study designs and data collection methods are required in future prospective studies.

6. Conclusions

The axial length had a negative effect on the anterior and total corneal SAs, which stabled around 0.33 μm and 0.30 μm in patients with axial length of ≥26 mm, respectively. The anterior corneal SA of patients with anterior corneal astigmatism <2 D decreased as the axial length increased. The total corneal SA of patients with anterior corneal astigmatism of 2-3 D stabilized at around 0.29 μm, whereas those with anterior corneal astigmatism of ≥3 D tended to be variable. Care should be taken when designing the correction of ocular SAs in patients undergoing aspheric toric IOL implantation. Individualized SA adjustments are essential for patients with anterior corneal astigmatism of 1-2 D or ≥3 D. Toric IOLs with a negative SA of −0.20 μm are recommended for patients with anterior corneal astigmatism of 2-3 D if customized therapy is not warranted.

Data Availability

More information about ocular statistical results is accessible in the supplementary materials. The raw data used to support the findings of this study have not been made available because of privacy policies.

Conflicts of Interest

The authors declare that they have no conflicts of interest.

Acknowledgments

This study was funded by the Ministry of Science and Technology of China (National Key Research and Development Program, no. 2018YFC0116000) and the National Natural Science Foundation of China (grant no. 81770908).

Supplementary Materials

Supplementary Material Table 1 presented the conic coefficients of cataract patients with comparisons between the two groups. Supplementary Material Table 2 presented the correlations of the corneal biometrics with the axial length and the anterior corneal astigmatism. Supplementary Material Tables 3 and 4 indicated the compositions of the astigmatism types with the different astigmatism levels and axial length. Supplementary Material Table 5 showed the differences in the proportions of WTR, ATR, and oblique astigmatism in different age levels, indicating a shift from ATR to WTR with age. (*Supplementary Materials*)

References

[1] D. Anderson, M. Dhariwal, C. Bouchet, and M. S. Keith, "Global prevalence and economic and humanistic burden of astigmatism in cataract patients: a systematic literature review," *Clinical Ophthalmology*, vol. 12, pp. 439–452, 2018.

[2] Z. Guan, F. Yuan, Y.-Z. Yuan, and W.-R. Niu, "Analysis of corneal astigmatism in cataract surgery candidates at a teaching hospital in Shanghai, China," *Journal of Cataract & Refractive Surgery*, vol. 38, no. 11, pp. 1970–1977, 2012.

[3] T. V. Cravy, "Calculation of the change in corneal astigmatism following cataract extraction," *Ophthalmic Surgery*, vol. 10, no. 1, pp. 38–49, 1979.

[4] D. Lin, J. Chen, Z. Liu et al., "Prevalence of corneal astigmatism and anterior segmental biometry characteristics before surgery in Chinese congenital cataract patients," *Scientific Reports*, vol. 6, no. 1, p. 22092, 2016.

[5] P. S. Moulick, D. Kalra, A. Sati, S. Gupta, M. A. Khan, and A. Singh, "Prevalence of corneal astigmatism before cataract surgery in Western Indian population," *Medical Journal Armed Forces India*, vol. 74, no. 1, pp. 18–21, 2018.

[6] T. Ferrer-Blasco, R. Montés-Micó, S. C. Peixoto-de-Matos, J. M. González-Méijome, and A. Cerviño, "Prevalence of corneal astigmatism before cataract surgery," *Journal of Cataract & Refractive Surgery*, vol. 35, no. 1, pp. 70–75, 2009.

[7] X. Yuan, H. Song, G. Peng, X. Hua, and X. Tang, "Prevalence of corneal astigmatism in patients before cataract surgery in Northern China," *Journal of Ophthalmology*, vol. 2014, Article ID 536412, 7 pages, 2014.

[8] M. I. Khan and M. Muhtaseb, "Prevalence of corneal astigmatism in patients having routine cataract surgery at a teaching hospital in the United Kingdom," *Journal of Cataract & Refractive Surgery*, vol. 37, no. 10, pp. 1751–1755, 2011.

[9] K. Lekhanont, W. Wuthisiri, P. Chatchaipun, and A. Vongthongsri, "Prevalence of corneal astigmatism in cataract surgery candidates in Bangkok, Thailand," *Journal of Cataract & Refractive Surgery*, vol. 37, no. 3, pp. 613–615, 2011.

[10] B. Agresta, M. C. Knorz, C. Donatti, and D. Jackson, "Visual acuity improvements after implantation of toric intraocular lenses in cataract patients with astigmatism: a systematic review," *BMC Ophthalmol*, vol. 12, no. 1, p. 41, 2012.

[11] A. Kingston and I. Cox, "Population spherical aberration: associations with ametropia, age, corneal curvature, and image quality," *Clinical Ophthalmology*, vol. 7, pp. 933–938, 2013.

[12] C. Pérez-Vives, T. Ferrer-Blasco, S. García-Lázaro, C. Albarrán-Diego, and R. Montés-Micó, "Optical quality comparison between spherical and aspheric toric intraocular lenses," *European Journal of Ophthalmology*, vol. 24, no. 5, pp. 699–706, 2014.

[13] P. Naripthaphan, P. Pachimkul, and S. Chantra, "Comparison of visual outcomes for aspheric and spherical toric intraocular lens implantation in cataract patients with pre-existing corneal astigmatism: a randomized control trial," *Journal of the Medical Association of Thailand*, vol. 97, no. 11, pp. S102–S110, 2014.

[14] M. Zhang, D. Qian, Q. Jing, J. Chen, and Y. Jiang, "Analysis of corneal spherical aberrations in cataract patients with high myopia," *Scientific Reports*, vol. 9, no. 1, p. 1420, 2019.

[15] A. Mathur, M. Suheimat, and D. A. Atchison, "Pilot study: effect of age on visual acuity with defocus and astigmatism," *Optometry and Vision Science*, vol. 92, no. 3, pp. 267–271, 2015.

[16] O. Collier Wakefield, R. Annoh, and M. A. Nanavaty, "Relationship between age, corneal astigmatism, and ocular dimensions with reference to astigmatism in eyes undergoing routine cataract surgery," *Eye*, vol. 30, no. 4, pp. 562–569, 2016.

[17] D. A. M. Lyall, S. Srinivasan, J. Ng, and E. Kerr, "Changes in corneal astigmatism among patients with visually significant cataract," *Canadian Journal of Ophthalmology*, vol. 49, no. 3, pp. 297–303, 2014.

[18] E.-H. Oh, H. Kim, H. S. Lee, K.-Y. Hwang, and C.-K. Joo, "Analysis of anterior corneal astigmatism before cataract surgery using power vector analysis in eyes of Korean patients," *Journal of Cataract & Refractive Surgery*, vol. 41, no. 6, pp. 1256–1263, 2015.

[19] R. Duman, R. Duman, E. Cetinkaya et al., "Analysis of corneal astigmatism with NIDEK axial length scan in caucasian cataract surgery candidates," *Nigerian Journal of Clinical Practice*, vol. 21, no. 4, pp. 456–461, 2018.

[20] A. Guirao, J. Tejedor, and P. Artal, "Corneal aberrations before and after small-incision cataract surgery," *Investigative Opthalmology & Visual Science*, vol. 45, no. 12, pp. 4312–4319, 2004.

[21] S. Maedel, N. Hirnschall, Y.-A. Chen, and O. Findl, "Rotational performance and corneal astigmatism correction during cataract surgery: aspheric toric intraocular lens versus aspheric nontoric intraocular lens with opposite clear corneal incision," *Journal of Cataract & Refractive Surgery*, vol. 40, no. 8, pp. 1355–1362, 2014.

[22] J. E. Kelly, T. Mihashi, and H. C. Howland, "Compensation of corneal horizontal/vertical astigmatism, lateral coma, and spherical aberration by internal optics of the eye," *Journal of Vision*, vol. 4, no. 4, pp. 262–271, 2004.

[23] Y. W. Goh, S. Misra, D. V. Patel, and C. N. McGhee, "Combining primary and piggyback intraocular lenses to treat extreme myopic astigmatism in stable keratoconus following cataract surgery," *Clinical and Experimental Optometry*, vol. 96, no. 2, pp. 242–244, 2013.

[24] L. Toto, L. Vecchiarino, E. D'Ugo et al., "Astigmatism correction with toric IOL: analysis of visual performance, position, and wavefront error," *Journal of Refractive Surgery*, vol. 29, no. 7, pp. 476–483, 2013.

[25] C. Y. Park and R. S. Chuck, "Residual refractive error and visual outcome after cataract surgery using spherical versus aspheric IOLs," *Ophthalmic Surgery, Lasers, and Imaging*, vol. 42, no. 1, pp. 37–43, 2011.

[26] H. H. Dietze and M. J. Cox, "Correcting ocular spherical aberration with soft contact lenses," *Journal of the Optical Society of America A*, vol. 21, no. 4, pp. 473–485, 2004.

[27] G. H. H. Beiko, W. Haigis, and A. Steinmueller, "Distribution of corneal spherical aberration in a comprehensive ophthalmology practice and whether keratometry can predict aberration values," *Journal of Cataract & Refractive Surgery*, vol. 33, no. 5, pp. 848–858, 2007.

[28] T. Ferrer-Blasco, "Effect of partial and full correction of corneal spherical aberration on visual acuity and contrast sensitivity," *Journal of Cataract & Refractive Surgery*, vol. 35, no. 5, pp. 949–951, 2009.

[29] X. Li, Y. Wang, and R. Dou, "Aberration compensation between anterior and posterior corneal surfaces after Small incision lenticule extraction and femtosecond laser-assisted laserin-situkeratomileusis," *Ophthalmic and Physiological Optics*, vol. 35, no. 5, pp. 540–551, 2015.

[30] F. Yi, D. Robert Iskander, and M. Collins, "Depth of focus and visual acuity with primary and secondary spherical aberration," *Vision Research*, vol. 51, no. 14, pp. 1648–1658, 2011.

[31] E. A. Villegas, E. Alcón, S. Mirabet, I. Yago, J. M. Marín, and P. Artal, "Extended depth of focus with induced spherical aberration in light-adjustable intraocular lenses," *American Journal of Ophthalmology*, vol. 157, no. 1, pp. 142–149, 2014.

[32] J. M. Miller, E. M. Harvey, and J. Schwiegerling, "Higher-order aberrations and best-corrected visual acuity in Native American children with a high prevalence of astigmatism," *Journal of American Association for Pediatric Ophthalmology and Strabismus*, vol. 19, no. 4, pp. 352–357, 2015.

[33] H. Hashemi, M. Khabazkhoob, E. Jafarzadehpur et al., "Higher order aberrations in a normal adult population," *Journal of Current Ophthalmology*, vol. 27, no. 3-4, pp. 115–124, 2015.

[34] M. Zhang, Q. Jing, J. Chen, and Y. Jiang, "Analysis of corneal higher-order aberrations in cataract patients with high

myopia," *Journal of Cataract & Refractive Surgery*, vol. 44, no. 12, pp. 1482–1490, 2018.

[35] P. Artal, E. Berrio, A. Guirao, and P. Piers, "Contribution of the cornea and internal surfaces to the change of ocular aberrations with age," *Journal of the Optical Society of America A*, vol. 19, no. 1, p. 137, 2002.

[36] D. A. Atchison, M. Suheimat, A. Mathur, L. J. Lister, and J. Rozema, "Anterior corneal, posterior corneal, and lenticular contributions to ocular aberrations," *Investigative Opthalmology & Visual Science*, vol. 57, no. 13, pp. 5263–5270, 2016.

[37] T. Zheng, Z. Chen, and Y. Lu, "Influence factors of estimation errors for total corneal astigmatism using keratometric astigmatism in patients before cataract surgery," *Journal of Cataract & Refractive Surgery*, vol. 42, no. 1, pp. 84–94, 2016.

[38] G. Savini and K. Naeser, "An analysis of the factors influencing the residual refractive astigmatism after cataract surgery with toric intraocular lenses," *Investigative Ophthalmology & Visual Science*, vol. 56, no. 2, pp. 827–835, 2015.

[39] T. Kohnen, "Astigmatism measurements for cataract and refractive surgery," *Journal of Cataract & Refractive Surgery*, vol. 38, no. 12, p. 2065, 2012.

[40] M. J. Bradley, J. Coombs, and R. J. Olson, "Analysis of an approach to astigmatism correction during cataract surgery," *Ophthalmologica*, vol. 220, no. 5, pp. 311–316, 2006.

[41] S. Theodoulidou, I. Asproudis, C. Kalogeropoulos, A. Athanasiadis, and M. Aspiotis, "Corneal diameter as a factor influencing corneal astigmatism after cataract surgery," *Cornea*, vol. 35, no. 1, pp. 132–136, 2016.

Hindawi
Journal of Ophthalmology
Volume 2019, Article ID 7929014, 13 pages
https://doi.org/10.1155/2019/7929014

Research Article

Quantitative Multiparameter Evaluation of Vacuoles in Intraocular Lenses Employing a High-Magnification Digital Microscopy Method

Vincent Spiezio,[1] **Bennett N. Walker**,[2] **Don Calogero**,[2] **and Ilko K. Ilev**[1]

[1]*Optical Therapeutics and Medical Nanophotonics Laboratory, Office of Science and Engineering Laboratories, Center for Devices and Radiological Health, U.S. Food and Drug Administration, Silver Spring, Maryland 20993, USA*
[2]*Office of Device Evaluation, Center for Devices and Radiological Health, U.S. Food and Drug Administration, Silver Spring, Maryland 20993, USA*

Correspondence should be addressed to Vincent Spiezio; vincent.spiezio@fda.hhs.gov

Received 6 March 2019; Revised 23 May 2019; Accepted 9 July 2019; Published 4 August 2019

Guest Editor: Damian Siedlecki

As small imperfections with micrometric sizes, fluid-filled vacuoles, also referred to as glistenings, in intraocular lenses (IOLs) have been known to induce significant unwanted light scattering that in several cases presumably cause complaints and sometimes lead to IOL explantation and replacement. This unwanted scatter is of particular concern for patients viewing bright light in reduced-light conditions such as when driving at night, as the scattered light toward the retina can cause temporary blindness. In this study, we have developed and implemented an accurate test methodology based on a high-magnification digital microscopy approach for quantitative multiparameter evaluation and classification of IOL vacuoles depending on their critical optical characteristics including vacuole size, density, shape, and orientation within the IOL material. Using the multiparameter database developed by evaluating vacuole characteristics, we established a classification grading system that can be used to evaluate vacuole effects on light scattering.

1. Introduction

Intraocular lens (IOL) implantation to treat cataracts and aphakia is one of the most commonly performed surgical procedures, with about 3.6 million per year in the United States alone [1, 2]. Since IOLs were first introduced, new IOL designs and materials have been developed and utilized to improve their optical properties and clinical outcomes. However, some newer designs and materials used in IOLs have an increased tendency to form small, micrometer-sized, fluid-filled vacuoles within the bulk of the IOL [3–18]. These vacuoles, also commonly referred to as glistenings, have been shown to reduce contrast sensitivity (CS) and visual acuity (VA) [13, 14, 17, 19–21], in some cases requiring IOL explantation [17, 21].

However, in many cases, vacuoles have been found to have a negligible impact on visual function [5, 7, 10]. A recent study by van den Berg [22] demonstrated a lack of correlation between straylight and VA, indicating rather that small aberrations within the lens are more responsible for loss of VA. Wider angle straylight, on the other hand, most commonly causes a loss of CS, which is not as noticeable or as great a cause for concern. In some cases, however, straylight can also cause disability glare, so further distinctions need to be made between the angular degree of scattered light and clinical effects.

Currently, one of the most commonly employed methods to classify vacuole severity is the use of a grading scale, in which IOLs are classified based on the number of vacuoles counted or observed [6, 7, 13, 14, 23, 24]. This is usually done through slit-lamp imaging, but in one case, Scheimpflug imaging was used [23]. The grading scales generally range from grade 0, having no or trace vacuoles, to the highest grade, usually either 3 or 4, having extremely severe vacuoles. Various test methods have been employed

to measure the clinical and nonclinical effects of vacuoles and light scatter in general, including subjective patient reports and VA tests [7, 10, 11, 13, 14, 16, 17, 19–21], integrating spheres and transmission measurements [16, 21, 24–26], C-Quant straylight meter measurements [18, 20, 27–29], and *in vivo* slit-lamp and Scheimpflug tests and measurements [7, 10, 11, 13–17, 19–21, 23]. In addition, two different methods have been independently developed to physically scan around the back of the IOL to measure forward scattered light [26, 27, 30, 31]. However, these methods and reported studies have only been correlated with vacuoles solely in terms of vacuole size and density.

While vacuoles generally manifest as rounded structures, they also may appear oblong- or rod-like when observed under a microscope. This geometric feature has been studied in a previously published work, illustrating that it results from either flattened ellipsoid or disc-shaped vacuoles oriented at a non-normal angle to the IOL plane [9]. However, it is conventionally assumed in most previously published studies on characterizing individual vacuoles that all vacuoles are round and behave as spheres while not considering the general shape and orientation aspect that causes a significant portion of vacuoles appear either oblong- or rod-like [4, 8, 20, 32]. None of the current grading systems account for specific vacuole shape and orientation, rather looking only at the density and effective diameter. This minimally classified vacuole characteristic may have an additional effect on light-scattering properties of IOLs and merit further investigation.

In the present study, we developed and implemented an accurate test methodology based on a high-magnification digital microscopy approach to quantitatively evaluate and classify IOL vacuoles depending on their critical multiparameter optical characteristics including vacuole size, density, shape, and orientation. This quantitative multiparameter evaluation method was used to establish a new classification grading system that can potentially be employed to evaluate vacuole effects on light scattering.

2. Materials and Methods

To quantitatively evaluate multiparameter optical characteristics of light-scattering vacuoles in IOLs (such as vacuole size, density, shape, and orientation), we developed an experimental test methodology using a high-magnification digital microscopy approach illustrated in Figure 1(a). The test system includes a digital optical microscope (VHX-100, Keyence, Inc.) that provides some advanced features essential for this study such as high magnification in the range of 75x to 5000x, a large objective working distance of 3 mm to 48 mm, and a submicron spatial resolution for precisely measuring IOL vacuole size, density, shape, and orientation.

Before investigation of IOL vacuoles, the accuracy of the microscope measurements was validated. To do this, a 100 μm calibrated microscopic scale with a minimum spatial resolution of 2 μm was measured with a digital microscope at 150x and 2000x magnification, along with the measured field of view (FOV), as illustrated in Figure 1(b). Experimentally assessing the measurement tool on the digital microscope provides an accuracy within 2% and 3% for 150x and 2000x magnification, respectively.

For vacuole characterization, seven monofocal IOL test samples were acquired from the manufacturer with varying degrees of induced vacuoles that had been naturally generated while stored in a balanced salt solution. The material and IOL models were not specified, but these variables have no effect on the methodology or conclusions of this study [24]. Of these lenses, IOLs #1–6 contain fewer than 500 vacuoles, with vacuole diameters generally between 30 and 50 μm, which is atypical of IOL vacuoles. The seventh IOL contains approximately 300,000 vacuoles roughly 5 μm across, which is more typical, and is used to validate the methodology used to characterize vacuoles in IOLs #1–6. IOLs were placed in a saline-filled cuvette simulating *in situ* conditions and then positioned under the digital microscope objective on a precise *x*-*y*-*z* translational stage. The IOL vacuoles in IOLs #1–6 were imaged and evaluated using the digital microscope with a magnification of 75x (Figures 2(a) to 2(f) for IOL test samples #1 to #6, respectively), 100x (Figures 3(a) to 3(f) for IOL test samples #1 to #6, respectively), and 150x (Figures 4(a) to 4(f) for IOL test samples #1 to #6, respectively).

For IOLs #1–6, vacuole evaluation was performed using two different methods. For the first IOL evaluation method, referred to as "Method 1," multiple images were taken at different locations on the IOL at 100x and 150x magnification and later analyzed to determine the vacuole density as well as various geometrical characteristics. For images taken at 150x magnification, because of the reduced depth of field (DOF) relative to 75x and 100x, multiple images had to be taken at different depths throughout the IOL and were combined to create a composite image. Using a precise measurement tool on the digital microscope, each individual vacuole in the 150x composite images was counted, and each vacuole's major and minor axes were measured.

For the images taken at 100x magnification, the vacuoles were only counted, without measuring them, as the vacuoles appear too small to reliably measure but are large enough to identify. In addition, at 100x magnification, the measured FOV is approximately 3.64 mm × 2.65 mm, giving a total area of about 9.4 mm^2. This corresponds to about 1/3 of the total surface area of a 6 mm diameter IOL. At 150x magnification, the FOV is approximately 2.08 mm × 1.56 mm or about 3.2 mm^2, which corresponds to only about 1/9 of the total IOL surface area. This smaller FOV requires taking more images throughout the IOL to accurately infer the density of vacuoles. Therefore, 100x magnification is used predominantly for more precisely determining the overall density measurements for each IOL.

For the second IOL evaluation method, referred to as "Method 2," digital microscope imaging to identify and measure each individual vacuole in each IOL was performed. Because the lowest available magnification of 75x used in the study is not able to image the entire IOL at once, composite images of each IOL were created. Images were taken throughout IOLs #1–6 using 100x magnification, so that a composite image of the entire IOL could be stitched together. Each vacuole was then identified, and its dimensions

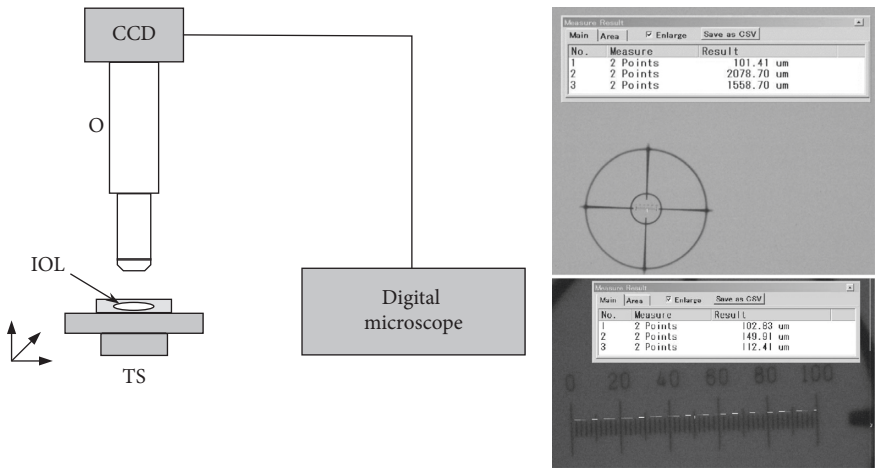

(a) (b)

Figure 1: (a) Schematic diagram of the high-magnification digital microscopy-based approach for quantitative characterization of IOL vacuoles: O, high-magnification (75x to 5000x) microscope objective; CCD, digital camera; IOL, test IOL sample placed at *in situ* simulation conditions; TS, *x*-*y*-*z* translational stage. (b) 100 μm calibration scale with a minimum spatial resolution of 2 μm measured with the digital microscope at 150x (upper picture) and 2000x (lower picture) magnification, along with the measured FOV.

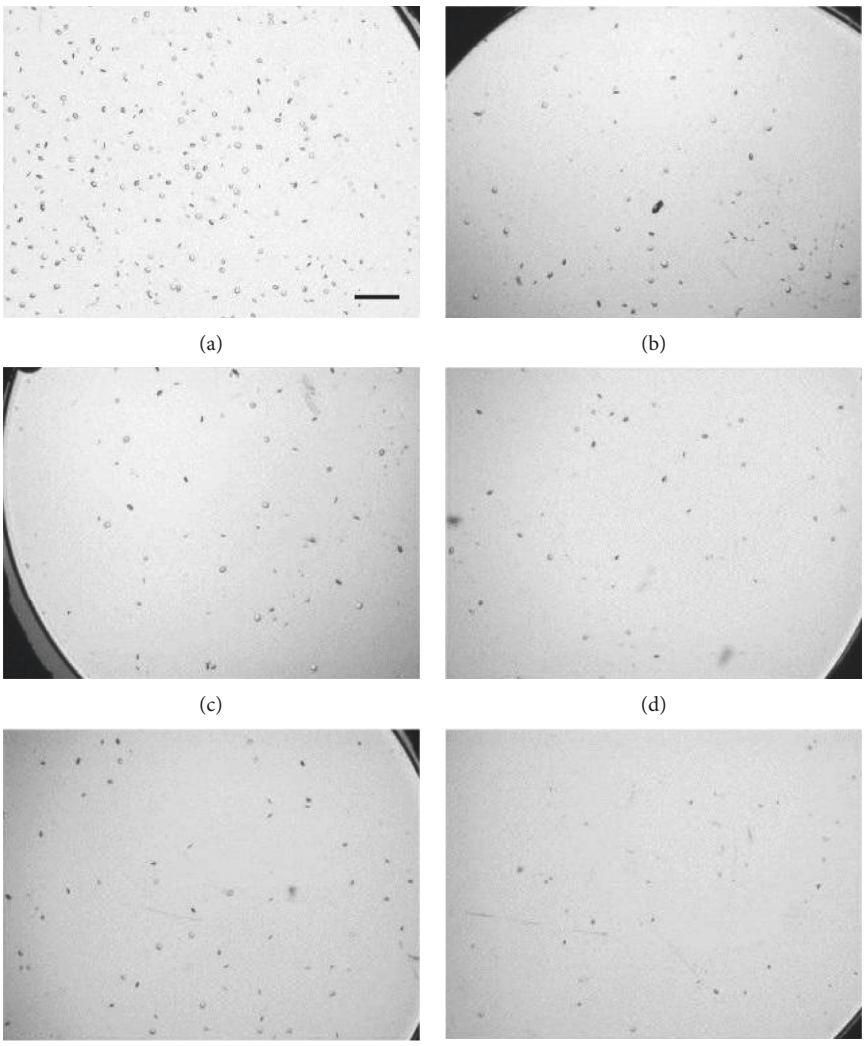

(a) (b)

(c) (d)

(e) (f)

Figure 2: Images of IOL #1 (a), #2 (b), #3 (c), #4 (d), #5 (e), and #6 (f) at 75x magnification. Scale bar, 500 μm.

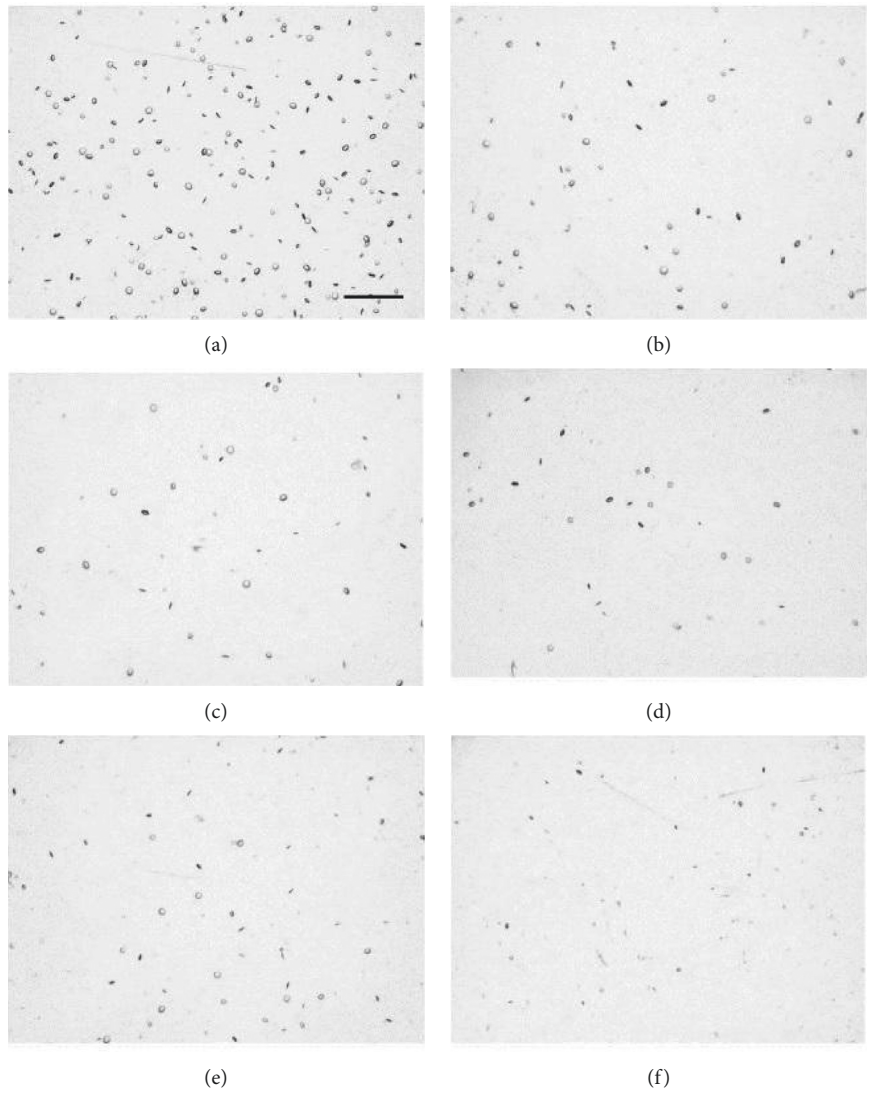

Figure 3: Images of IOL #1 (a), #2 (b), #3 (c), #4 (d), #5 (e), and #6 (f) at 100x magnification. Scale bar, 500 μm.

were measured using ImageJ image processing software. Due to the differences in background brightness and shading throughout the images, as seen in Figure 5, a direct automatic measurement using ImageJ was unfeasible and unreliable, so each vacuole was identified and measured manually. A typical stitched composite image of IOL #1 is shown in Figure 5.

For IOL #7, imaging and analysis was done similarly to IOLs #1–6, but with some key differences. Because vacuoles were much smaller and denser, counting and measuring each individual vacuole as was done in Method 2 is impractical, so a modified version of Method 1 was used exclusively. Three composite images were taken near the center of IOL #7 at 2000x magnification due to the low DOF, and each vacuole was manually measured and characterized using a measurement tool on the digital microscope. One of these images is shown in Figure 6.

As performed for IOLs #1–6, each vacuole in the three images taken of IOL #7 was counted and measured to demonstrate the validity of this method for smaller size vacuoles. The total number of vacuoles present, as well as overall vacuole characteristics, was inferred based on analysis of the three images, assuming consistent distribution throughout the lens.

One previous study demonstrated that vacuoles are in fact either discs or flattened ellipsoids [9]. However, as most published studies gloss over this important vacuole characteristic, we have performed an independent investigation on it. For IOL #1, 7 images are taken at 100x magnification, tilting the IOL from −40° to 20° from normal incidence in 10° angular increments. To examine the effects that the angle of observance has on the apparent shapes of vacuoles, a small section of each image is looked at. Figures 7(a)–7(g) show images of vacuoles present in IOL #1 taken at −40°–+20°, respectively, in 10° increments.

As shown in Figure 7, four different vacuoles are numbered to assist in determining the changes in apparent shape that occur when changing the angle of observation. At −40° (Figure 7(a)), vacuoles labeled 1 and 3 appear elongated. As the angle of observation increases to 20°

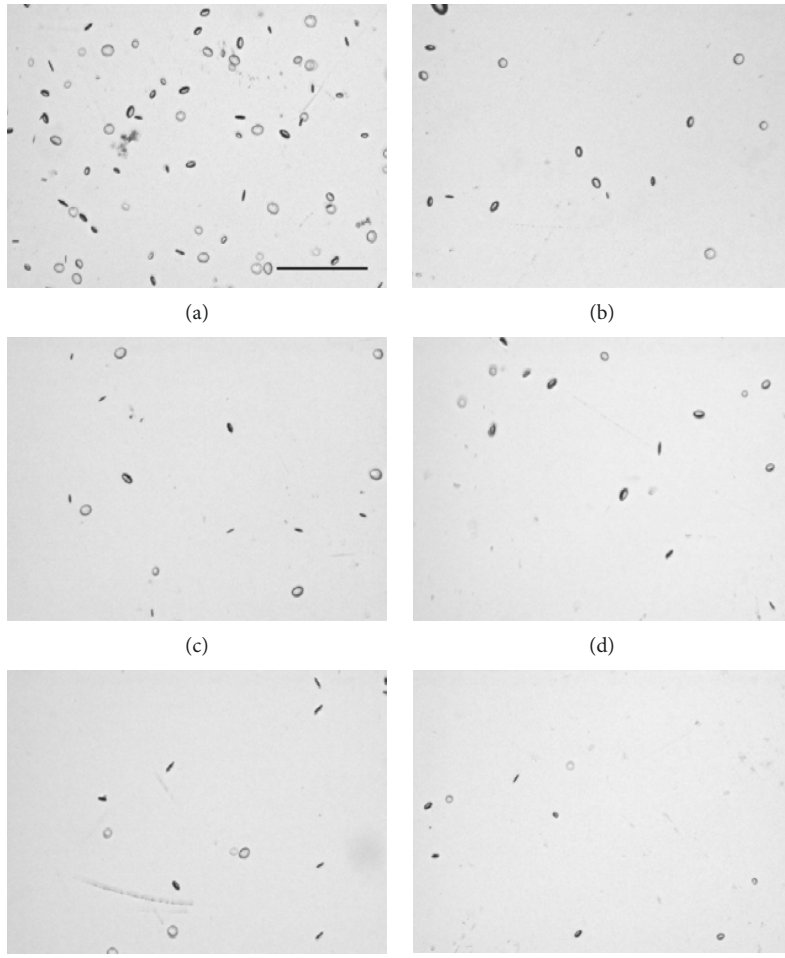

Figure 4: Composite images of IOL #1 (a), #2 (b), #3 (c), #4 (d), #5 (e), and #6 (f) at 150x magnification. Scale bar, 500 μm.

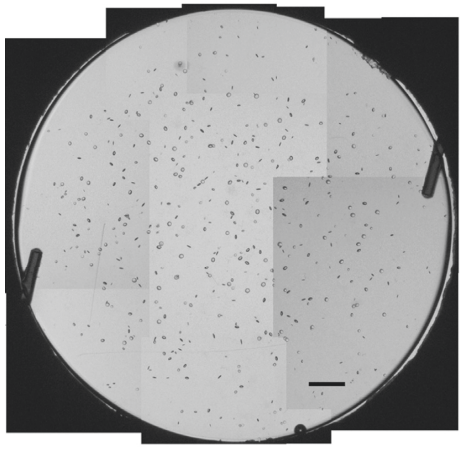

Figure 5: Stitched composite image of IOL #1 at 100x magnification. Scale bar, 500 μm.

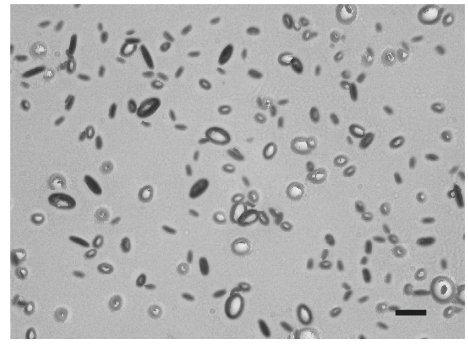

Figure 6: 2000x magnification composite image of IOL #7. Scale bar, 10 μm.

(Figure 7(g)), these vacuoles appear to widen, becoming more rounded. Conversely, the vacuoles labeled 2 and 4 are rounded at −40°, and by 20°, they are further elongated. This helps to confirm that vacuoles manifest as either discs or flattened ellipsoids and that vacuoles that appear elongated are simply being viewed at a steep angle.

Knowing that vacuoles are in fact either discs or flattened ellipsoids, despite their apparent oblong- or rod-like appearance, a method was developed to classify vacuoles based on their rotation angle with respect to the IOL. For each vacuole, a rotation angle compared to the normal incidence angle was estimated, with 0° being in the same plane as the

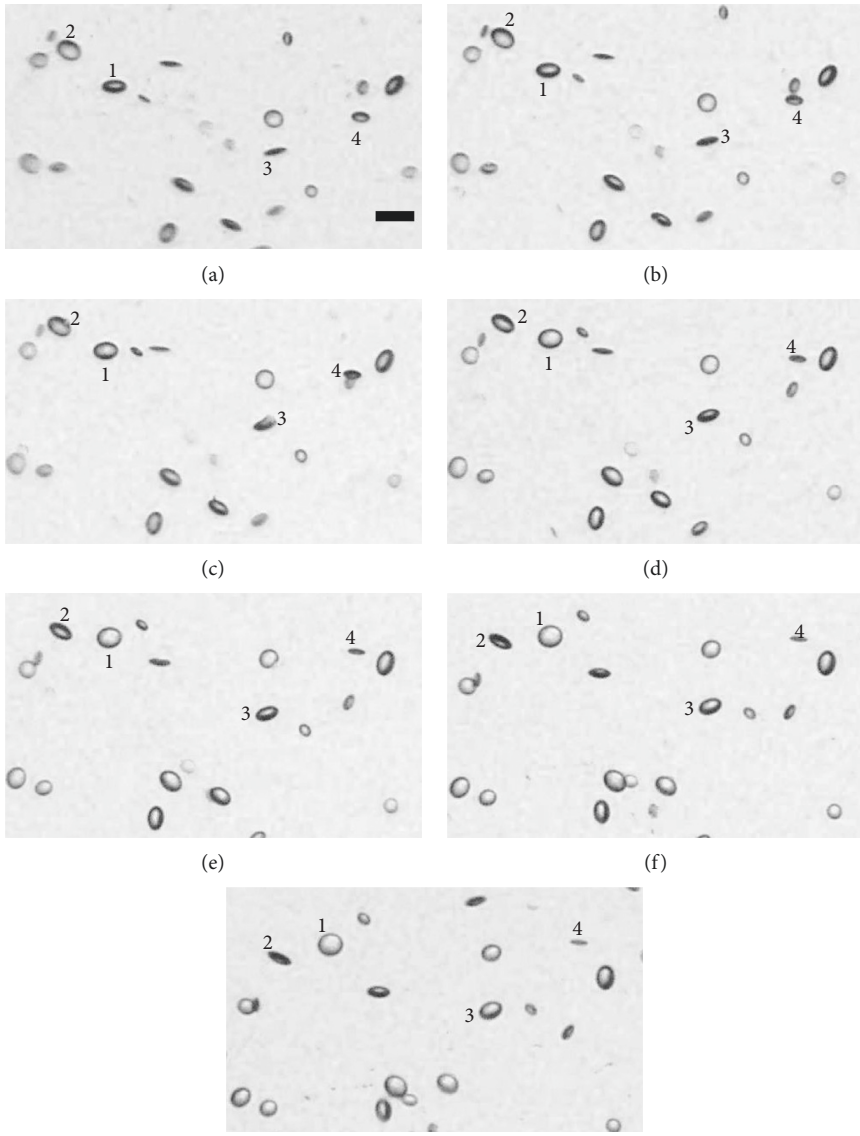

Figure 7: Vacuoles present in IOL #1 taken with the IOL angled −40° (a), −30° (b), −20° (c), −10° (d), 0° (e), 10° (f), and 20° (g) from a normal incidence angle of observance, imaged at 100x magnification. Scale bar, 100 μm.

IOL, appearing to be a perfect circle. The rotation angle was estimated using the following equation:

$$R = \cos^{-1}\frac{Y}{X}, \quad (1)$$

where X is the measured major axis length, Y is the measured minor axis length, and R is the rotation angle. This dependence provides the approximate rotation of each vacuole from normal, knowing what the resulting apparent dimensions of the vacuoles appear to be. This calculated angle assumes that these vacuoles have a negligible thickness, so that when viewed at a steep angle, the primary surface being seen is the vacuole face and not the edge. In addition, it assumes that the vacuole is circular and not elliptical.

Five vacuole orientation groups are defined based on the approximate rotation angle of the individual vacuole. The rotation ranges are chosen based on the microscopic visual appearances of individual vacuoles, with each grouping assigned based on the calculated rotation. These five vacuole groups, defined based on the estimated rotation angle, are shown in Table 1.

To supplement the data gathered at 100x and 150x magnification, several individual vacuoles are imaged and measured at 450x magnification. The acquired data include images of vacuoles from each orientation group described in Table 1, and representative examples from each group are shown in Figure 8 (Figures 8(a) to 8(e) for vacuole group 1 to group 5, respectively). The 450x magnification used here was too high to acquire representative samples of vacuoles present in each IOL, but it was sufficient and necessary to acquire high-resolution images of individual vacuoles.

To validate the accuracy and precision of the measurements taken, four individual vacuoles in IOL #1 were imaged four times at 150x magnification. These vacuoles

Table 1: Defined rotation of each vacuole orientation group.

Vacuole orientation group	Rotation angle
Group 1	0–20°
Group 2	20–45°
Group 3	45–60°
Group 4	60–80°
Group 5	80–90°

were each measured, with the resulting tilt angle and groupings determined. These results were compared to each other to determine the repeatability of the methodology used here. These four representative vacuoles in IOL #1, numbered as 1–4, are shown in Figure 9.

3. Results

The total number of vacuoles in IOLs #1–6, as well as the average vacuole diameter, was measured and calculated for both IOL evaluation methods used. For vacuoles counted using Method 1, the overall number of vacuoles was estimated, assuming a uniform distribution of vacuoles throughout the IOL. This estimation also assumes some standard IOL geometric parameters including an IOL diameter of 6 mm, a center thickness of 0.7 mm, an edge thickness of 0.5 mm, and spherical front and back surfaces, giving an IOL volume of roughly 17 mm^3. Estimation of total vacuole count also assumes a thickness of 0.7 mm for the 100x and 150x images in which vacuoles were counted. The vacuole counts for Method 2 represent the total number of vacuoles counted in the entire stitched composite image. These results are shown in Table 2.

Of the six IOL samples studied, IOL #1 had by far the highest number of vacuoles, with the remaining five IOLs having more similar numbers of vacuoles. This assessment was validated using the vacuole counts at both 100x and 150x magnification. Error was calculated based on the standard deviation of the vacuoles counted in multiple images of the same IOL. As expected, the standard deviation for the vacuoles counted at 100x magnification is significantly lower than that at 150x magnification, as a larger portion of the IOL is imaged at a time. In addition, the estimated vacuole count was more accurate at 100x magnification than at 150x magnification.

For each IOL imaged using Method 2, the diameter of each individual vacuole was measured, and the average vacuole diameter in each lens was calculated. In addition, for vacuoles imaged from individual 150x magnification images, as done in Method 1, the approximate average vacuole diameter including the standard deviation related to the estimated accuracy and precision of the diameter value was calculated. These are shown in Table 3.

For each IOL, the overall number of vacuoles present from each orientation group was determined. For Method 1, the total number of vacuoles in each group was counted in each 150x image, to determine the average number of vacuoles in each group, as well as the standard deviations. This is shown in Figure 10. For Method 2, each individual vacuole in the stitched IOL image was identified, measured, and placed into one of the five groups. The number of vacuoles from each orientation group in each IOL using Method 2 is shown in Figure 11.

As expected, IOL #1 has more vacuoles from each group than the remaining IOLs. While IOLs #2–6 have similar overall densities of vacuoles, the distribution for the groups of vacuoles present vary greatly. As shown in Figures 10 and 11, the only consistent pattern seen is that vacuoles perfectly normal and perfectly perpendicular, represented, respectively, by groups 1 and 5, are relatively less common. For vacuole orientation groups 2, 3, and 4, there is no consistent pattern for which vacuoles are present more often than others.

Likewise, each vacuole present in the three images of IOL #7 was identified, measured, and characterized based on the groupings defined in Table 1. The total number of vacuoles counted throughout the three images and their proportion for each orientation group are shown in Table 4. As with IOLs #1–6, orientation groups 1 and 5 contain the least number of vacuoles, with most vacuoles being in groups 2–4.

Throughout the three images, an average of 195 vacuoles are counted and measured, with a standard deviation of 7 vacuoles between the three images taken. Each image taken at 2000x magnification has a total FOV of approximately $150\,\mu m \times 110\,\mu m$. Assuming a thickness of 0.7 mm, this corresponds to a volume of 1.2×10^{-3} mm^2 or about 0.07% of the total volume of the IOL. Assuming a uniform thickness of 0.7 mm at the imaged location, the total number of vacuoles throughout the lens is estimated to be about 300,000.

As described previously, the repeatability of the study was also validated through replicate measurements of the four vacuoles shown in Figure 9. These vacuole measurements and the standard deviation between them are shown in Table 5. The propagation of this uncertainty to the calculated vacuole tilt angle is shown in Table 6.

As shown in Table 5, the standard deviation between measurements is quite small, never exceeding $5\,\mu m$. However, because the vacuole sizes are also relatively small, this results in a percent standard deviation that generally falls between 5 and 10%. The propagation of this deviation to calculated orientation is shown in Table 6 and results in an uncertainty in orientation of nearly 10 degrees in one case.

4. Discussion

The six IOL samples tested have varying densities of vacuoles and varying distributions of the five orientation groups of vacuoles studied. To further evaluate the effects of vacuole orientation, we determined the theoretical distribution of vacuole orientations and compared these to the actual distributions. If a vacuole has an equal probability of assuming any orientation, the distribution should be directly based on the ranges used to define the five orientation groups defined in Table 1. Thus, the theoretical distribution that could be associated with each vacuole orientation group is illustrated in Table 7, alongside the experimental average distribution measured in IOLs #1–6.

As shown in Table 7, there is a discrepancy between the actual experimental and theoretical vacuole distributions,

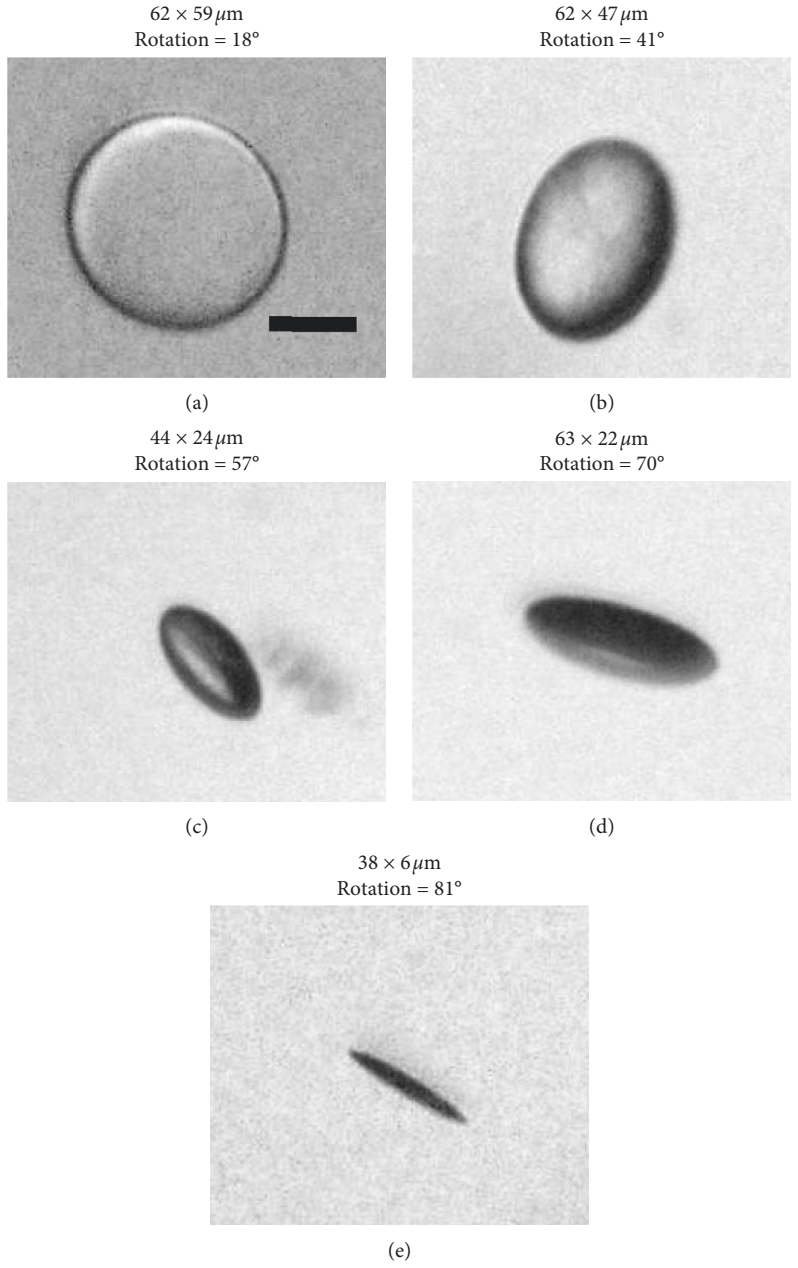

Figure 8: Representative examples of vacuoles in group 1 (a), group 2 (b), group 3 (c), group 4 (d), and group 5 (e) with their measured dimensions and calculated rotations, imaged at 450x magnification. Scale bar, 25 μm.

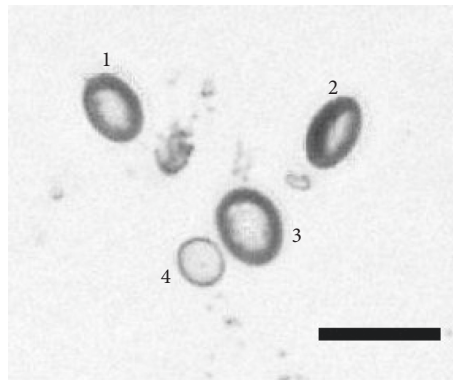

Figure 9: Four vacuoles from IOL #1 imaged at 150x magnification. Scale bar, 100 μm.

Table 2: The number of vacuoles counted in the stitched images of each IOL and the estimated vacuole count from 100x and 150x images.

IOL #	Total number of vacuoles counted	Estimated number of vacuoles from 100x images	Estimated number of vacuoles from 150x images
#1	470	538 ± 35	599 ± 47
#2	106	127 ± 11	142 ± 32
#3	125	127 ± 10	112 ± 17
#4	68	75 ± 7	81 ± 21
#5	109	111 ± 18	130 ± 29
#6	57	55 ± 9	73 ± 23

Table 3: The average vacuole diameter for vacuoles in each IOL and the estimated average vacuole diameter from 150x magnification images.

IOL #	Average vacuole diameter (μm)	Estimated average vacuole diameter from 150x images (μm)
#1	51	51 ± 3
#2	53	54 ± 3
#3	46	55 ± 2
#4	45	52 ± 3
#5	47	54 ± 4
#6	36	38 ± 3

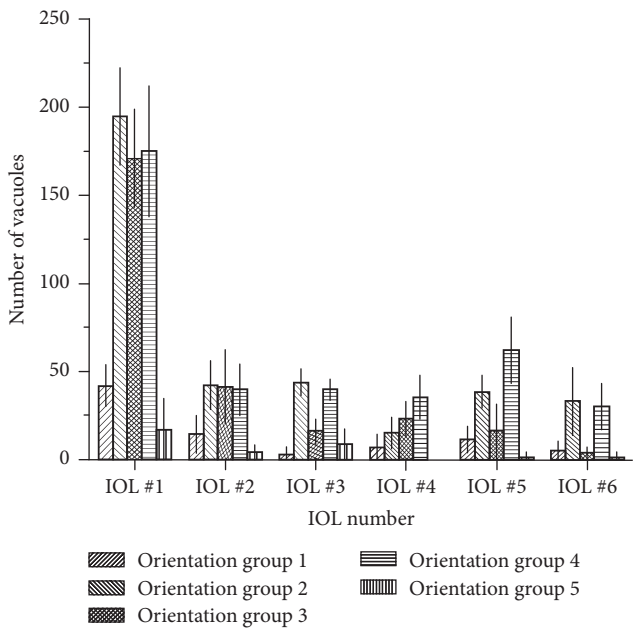

Figure 10: Estimated numbers of each vacuole orientation group in IOLs #1–6. Error bars represent standard deviations in estimated numbers.

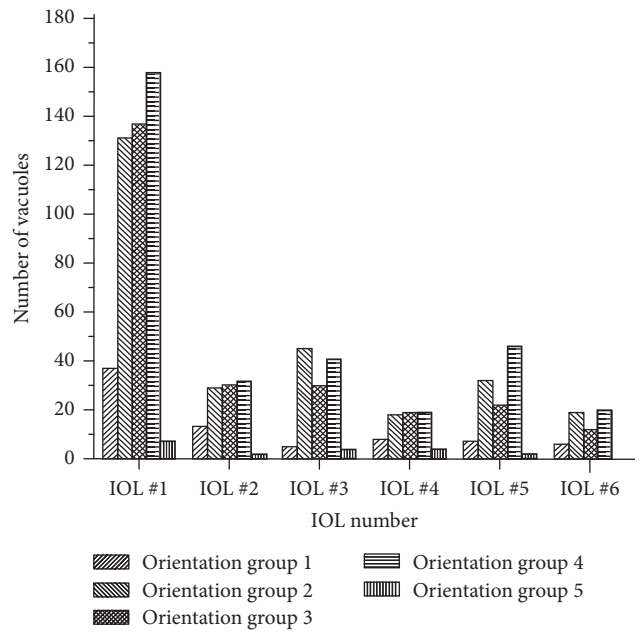

Figure 11: Counted number of each vacuole orientation group from stitched composite images of IOLs #1–6.

particularly in groups containing the smallest and largest rotation angles. This could be related to either a tendency of vacuoles to assume certain orientations within the lens, possibly due to polymer orientation, or from random and systematic error present in the evaluation methods used. As stated earlier, there is little known about vacuole orientation within IOLs, so further research needs to be done regarding whether the vacuole formation could be associated with a specific trend to orient in certain ways.

Another vacuole characteristic that may affect the calculated vacuole rotations is vacuole thickness. While due to some methodology and equipment limitations, objective classification of each vacuole's thickness was not experimentally performed, some specific assessment can be made regarding vacuole thickness. For IOLs #1–6, the vacuole with the smallest apparent minor axis in each IOL is identified, as shown in Table 8.

In calculation of vacuole tilt relative to the IOL plane, the thickness is assumed to be negligible. However, through investigation of the distribution of vacuole "tilts," as well as the minimum measured minor axis, the approximate thickness can be reasonably estimated. In IOLs #1–6, there

Table 4: The total number of vacuoles for each orientation group counted for the three 2000x magnification images of IOL #7, along with the percentage distribution of each group.

Vacuole orientation group	Number counted	Percentage of total (%)
#1	17	3
#2	107	18
#3	227	38
#4	241	41
#5	0	0

Table 5: Average dimensions of vacuoles #1–4, along with calculated standard deviation.

Vacuole number	Average measured dimensions (μm)	Standard deviation (μm)	Percent standard deviation (%)
#1	59.2×43.8	2.6×2.9	4.4×6.6
#2	64.8×38.5	3.7×3.3	5.7×8.6
#3	65.1×48.6	0.7×1.4	1.1×3.0
#4	43.0×34.0	2.3×4.8	5.4×14.1

Table 6: Average calculated orientations of vacuoles #1–4, along with calculated standard deviation.

Vacuole number	Average orientation angle (degrees)	Standard deviation (degrees)	Percent standard deviation (%)
#1	42.1	3.7	9
#2	53.3	5.4	10
#3	41.7	2.5	6
#4	37.2	9.3	28

Table 7: Vacuole orientation group distribution assuming random vacuole orientation.

Vacuole orientation group	Percent distribution (%)	Average measured distribution in IOLs #1–6 (%)
Group 1	22	9 ± 3
Group 2	28	30 ± 4
Group 3	17	25 ± 4
Group 4	22	32 ± 5
Group 5	11	2 ± 2

are 935 total vacuoles identified and measured. From the inferred tilts, assuming negligible thickness, the vacuole oriented closest to perpendicular to the IOL has a calculated tilt of 83.6°. If one assumes that there is an equal probability of a vacuole assuming any orientation, this means that there is a 6.4° range, between 83.6° and 90°, that contains no vacuoles. Assuming that any vacuole tilt or orientation is equally likely, the odds of none of the 935 identified vacuoles being in this range is 1 in 9×10^{29}. It is more likely that some of the vacuoles are in this range, but their thickness slightly alters the inferred tilt. Assuming equal distributions, there should be approximately 10 total vacuoles oriented within 1 degree of 90° with respect to the IOL. We can therefore assume that the vacuoles with the smallest measured minor axes, shown in Table 8, are in fact these theoretical perpendicular vacuoles, and the measured 5-6 μm minor axes is in fact the thickness.

We can further investigate vacuole thickness in IOL #7. Of the 592 identified vacuoles, the highest calculated "tilt" for a vacuole is 75°. The likelihood of none of the vacuoles having a tilt between 75 and 90 degrees is approximately 1 in 7.5×10^{46}. As with IOLs #1–6, this discrepancy indicates that vacuoles have a non-negligible thickness affecting the estimated vacuole tilt and that the vacuoles having estimated tilts in the 70-degree range are likely closer to 90°. The measured minor axis for the identified vacuole with 75° estimated tilt is roughly 2 μm; however, several other vacuoles characterized as being in orientation group 4 have measured minor axes closer to 1 μm. This indicates that, for these smaller vacuoles, the thickness is roughly 1 μm, or perhaps a bit smaller. While vacuole thickness likely contributes to scatter by individual vacuoles, the main impact on vacuole characterization as done in this study is likely the mischaracterization of vacuoles that are in group 4 as being in group 4.

Table 8: The measured major and minor axes for the vacuole with the smallest minor axis length in IOLs #1–6.

IOL #	Major axis length (μm)	Minor axis length (μm)
#1	31	5
#2	45	5
#3	23	6
#4	36	5
#5	36	5
#6	31	6

Between the uncertainty of vacuole thickness and the implicit error in vacuole measurements, it may be more practical to treat vacuole groups 1 and 2 as a single group and treat vacuole groups 4 and 5 as a single group. As investigated earlier, a vacuole thickness of 5 μm, if not accounted for, essentially sets an upper inferred angle limit of 84° for a 50 μm vacuole. For a smaller vacuole with a 5 μm thickness, this limit is even lower. Combined with measurement inaccuracies, this may very well result in some low-tilt group 5 vacuoles being mischaracterized as group 4, blurring the line between group 4 and group 5. Likewise, a 50 μm group 1 vacuole with 0° tilt may be measured with up to 10% inaccuracy, as shown earlier in Table 5. This could result in a calculated tilt of up to 26°, if one axis is incorrectly measured as 45 μm rather than 50 μm. This potential error blurs the line between group 1 and group 2 vacuoles, making consolidation of these vacuole groups an attractive choice. The decision to consolidate the 5 orientation groups into 3 broader groups would weaken the overall strength of the methodology and characterization, but may be necessary, depending on the accuracy and precision of the equipment and methods used.

Additional consideration must be given to the unusual sizes of vacuoles presented in this study. Most observations of vacuoles note sizes between 2–10 μm, with sizes larger than 20 μm being rare [4–8, 15, 20, 26, 28]. The vacuoles studied here are in some cases larger than 50 μm, with vacuoles smaller than 20 μm being rare. However, there are limited cases and situations in which larger vacuoles, on the order of 100 μm across, have been observed. One noteworthy case observed large vacuoles forming shortly after cataract surgery, requiring immediate explantation. The vacuoles' sizes were not directly measured or reported, but examination of the figures reveals vacuoles are roughly 100 μm across, or perhaps a bit larger [17]. In addition, vacuoles' sizes have been found to be directly related to the osmolarity of the surrounding medium, with low salinity media producing vacuoles up to 200 μm across [9]. The exact procedure used for the formation of vacuoles used in this study is not known, so while the sizes seen here may not be the most commonly reported, they are not unheard of. However, the main purpose of this study is to evaluate individual vacuoles' sizes and orientations as well as catalog characteristics for each of these evaluated vacuoles throughout the lens, and this should be minimally affected by the size of the individual vacuole.

While the test methodology introduced in this study can be demonstrated to work for vacuoles of sizes in the micron and submicron range, considerations must be given to potential limitations of this method for characterizing small-sized vacuoles. For vacuoles of the size studied in IOLs #1–6 or larger, we would not expect any additional issues characterizing vacuoles. However, for smaller vacuoles, certain limitations of this study may manifest. First, because this method requires manual measuring of vacuoles, the magnification on the digital microscope must be high enough for this to be possible. Magnifications of 100x and 150x, which were primarily employed in this study, would likely work for vacuoles down to about 10 μm, albeit with some loss of accuracy. For vacuoles approaching 1 μm across, higher magnifications were demonstrated to be necessary. While 2000x magnification was capable of imaging the individual vacuoles, there is a corresponding loss of FOV. This lower FOV corresponds to only about 0.06% of the total IOL surface or 0.07% of the total IOL volume. Because of this, it would be inaccurate to assume that a few sample images of the IOL would be able to represent the entire lens, especially if the small vacuoles are sparse. In addition, if an IOL has both large and small vacuoles, a magnification large enough to image the small vacuole may be too high to contain a large vacuole in the FOV. While this could limit the ability to generalize characteristics of small vacuoles throughout an IOL, the ability to characterize individual vacuoles should be unaffected regardless of vacuole size.

With a strengthened ability to characterize individual vacuoles, the next step to take is quantitative evaluation of vacuole properties that cause scatter and straylight, particularly that which is expected to affect patients' vision. Extensive work has already been done in this field, most recently by Labuz et al., linking vacuole density and area obscured to C-Quant straylight measurements [18, 28]. However, these studies, like most previous studies, primarily focus on vacuole density and average size [4–7, 13, 14, 17, 20, 26, 32]. Vacuole orientations with respect to the incoming light, however, have not yet been correlated with measured scatter. Further work can be done, using these existing methodologies and results, to link vacuole orientations to scatter.

One additional factor to consider is the direction of scatter by individual vacuoles. As described by van den Berg [22], the point spread function (PSF) defining defocused light can be divided into two domains, these being the central domain caused mainly by aberrations and the peripheral domain caused by straylight and wide-angle scatter. Wide-angle peripheral scatter, as described by van den Berg and by Werner et al. [31], is unlikely to lower VA in any meaningful way, as even a large drop in CS will not affect acuity or visual function. However, close-angle scatter, caused by aberrations or microaberrations, will directly impact VA through distortion of the image projected onto the macula. Further evaluation of scatter caused by vacuoles of differing orientations should be performed to clarify this effect, specifically how orientation affects the angle of scattered light.

That being said, moving forward, it may be beneficial to examine the effects that vacuole orientation groupings have on scatter. One can surmise that orientation of vacuoles of groups 1 and 2 will likely cause the least straylight and scatter, as incoming light normal to the IOL will also be normal to the vacuole, transmitting through with minimal scattering. However, what little light is scattered is also more likely to be in the central domain described by van den Berg [22], resulting in a loss of VA. This phenomenon can be observed in the vacuole images presented in Figure 8; the backlit group 1 and group 2 vacuoles allow light to reach the microscope objective, making them appear white, while the group 4 and group 5 vacuoles divert the light from reaching the objective, making them appear

dark. In the same way, the differing scatter potentials of differently oriented vacuoles likely affect light scatter in the eye in different ways, so investigation into the clinical and *in vitro* effects of differently oriented vacuoles should be performed.

5. Conclusion

The effects of vacuoles on IOL clarity and light scatter have been extensively studied but mainly in terms of overall density and average size of the individual vacuoles. The orientation of the vacuoles and the distribution of differently oriented vacuoles have not been studied or considered when correlating the scattered light with vacuoles. The present study is focused on a comprehensive quantitative evaluation of IOL samples with varying densities of vacuoles and compared not only the size and densities of the vacuoles present but also the shape and orientation of the vacuoles. A grading scale was developed to compare vacuoles of similar sizes but differing orientations within the IOL. It was shown that similar IOLs with similar vacuole densities can have differing orientations of vacuoles throughout the lens, which should be considered in future studies evaluating scattering by IOL vacuoles.

The presented classification method can be used in future studies of vacuoles, particularly regarding their scattering potential. In addition, digital microscopy could be further refined and utilized to better image IOLs *in vivo*, without requiring explantation. This would allow accurate, noninvasive assessment of vacuole presence, sizes, and orientations, allowing more informed clinical decisions to be made.

Data Availability

The data used to support the findings of this study are available from the corresponding author upon request.

Disclosure

The mention of commercial products, their sources, or their use in connection with material reported herein is not to be construed as either an actual or implied endorsement of such products by the Department of Health and Human Services.

Conflicts of Interest

The authors declare that there are no conflicts of interest related to this article.

Acknowledgments

This project was supported in part by the Research Participation Program at the Center for Devices and Radiological Health (CDRH), U.S. Food and Drug Administration (FDA), administered by the Oak Ridge Institute for Science and Education (ORISE).

References

[1] The Eye Diseases Prevalence Research Group, "Prevalence of cataract and pseudophakia/aphakia among adults in the United States," *Archives of Ophthalmology*, vol. 122, no. 4, pp. 487–491, 2004.

[2] W. Wang, W. Yan, K. Fotis et al., "Cataract surgical rate and socioeconomics: a global study," *Investigative Opthalmology & Visual Science*, vol. 57, no. 14, pp. 5872–5881, 2016.

[3] K. Kawat, K. Hayakawa, and T. Suzuki, "Simulation of 20-year deterioration of acrylic IOLs using severe accelerated deterioration tests," *Tokai Journal of Experimental and Clinical Medicine*, vol. 37, no. 3, pp. 22–65, 2012.

[4] K. Kato, M. Nishida, H. Yamane, K. Nakamae, Y. Tagami, and K. Tetsumoto, "Glistening formation in an AcrySof lens initiated by spinodal decompositionof the polymer network bytemperature change," *Journal of Cataract & Refractive Surgery*, vol. 27, no. 9, pp. 1493–1498, 2001.

[5] A. Waite, N. Faulkner, and R. J. Olson, "Glistenings in the single-piece, hydrophobic, acrylic intraocular lenses," *American Journal of Ophthalmology*, vol. 144, no. 1, pp. 143-144, 2007.

[6] C. Pérez-Vives, "Biomaterial influence on intraocular lens performance: an overview," *Journal of Ophthalmology*, vol. 2018, Article ID 2687385, 17 pages, 2018.

[7] E. Mönestam and A. Behndig, "Impact on visual function from light scattering and glistenings in intraocular lenses, a long-term study," *Acta Ophthalmologica*, vol. 89, no. 8, pp. 724–728, 2011.

[8] N. Z. Gregori, T. S. Spencer, N. Mamalis, and R. J. Olson, "In vitro comparison of glistening formation among hydrophobic acrylic intraocular lenses," *Journal of Cataract & Refractive Surgery*, vol. 28, no. 7, pp. 1262–1268, 2002.

[9] D. M. Saylor, D. Coleman Richardson, B. J. Dair, and S. K. Pollack, "Osmotic cavitation of elastomeric intraocular lenses," *Acta Biomaterialia*, vol. 6, no. 3, pp. 1090–1098, 2010.

[10] K. Hayashi, A. Hirata, M. Yoshida, K. Yoshimura, and H. Hayashi, "Long-term effect of surface light scattering and glistenings of intraocular lenses on visual function," *American Journal of Ophthalmology*, vol. 154, no. 2, pp. 240.e2–251.e2, 2012.

[11] A. A. Gamidov, A. A. Fedorov, I. A. Novikov, A. A. Kas'yanov, and V. I. Siplivyy, "Analyzing causes for opacification of acrylic IOLs," *Vestnik Oftal'Mologii*, vol. 131, no. 3, pp. 64–70, 2015.

[12] B. E. Thomes and T. A. Callaghan, "Evaluation of in vitro glistening formation in hydrophobic acrylic intraocular lenses," *Clinical Ophthalmology*, vol. 7, pp. 1529–1534, 2013.

[13] L. Xi, Y. Liu, F. Zhao, C. Chen, and B. Cheng, "Analysis of glistenings in hydrophobic acrylic intraocular lenses on visual performance," *International Journal of Ophthalmology*, vol. 7, no. 3, pp. 446–451, 2014.

[14] C. Schweitzer, I. Orignac, D. Praud, O. Chatoux, and J. Colin, "Glistening in glaucomatous eyes: visual performances and risk factors," *Acta Ophthalmologica*, vol. 92, no. 6, pp. 529–534, 2014.

[15] M. Rønbeck, A. Behndig, M. Taube, A. Koivula, and M. Kugelberg, "Comparison of glistenings in intraocular lenses with three different materials: 12-year follow-up," *Acta Ophthalmologica*, vol. 91, no. 1, pp. 66–70, 2013.

[16] S. Yoshida, H. Matsushima, M. Nagata, T. Senoo, I. Ota, and K. Miyake, "Decreased visual function due to high-level light scattering in a hydrophobic acrylic intraocular lens," *Japanese Journal of Ophthalmology*, vol. 55, no. 1, pp. 62–66, 2011.

[17] L. Werner, J. Storsberg, O. Mauger et al., "Unusual pattern of glistening formation on a 3-piece hydrophobic acrylic intraocular lens," *Journal of Cataract & Refractive Surgery*, vol. 34, no. 9, pp. 1604–1609, 2008.

[18] G. Łabuz, D. Knebel, G. U. Auffarth et al., "Glistening formation and light scattering in six hydrophobic-acrylic intraocular lenses," *American Journal of Ophthalmology*, vol. 196, pp. 112–120, 2018.

[19] T. Hiraoka, K. Miyata, T. Hayashidera et al., "Influence of intraocular lens subsurface nanoglistenings on functional visual acuity," *PLoS One*, vol. 12, no. 3, Article ID e0173574, 2017.

[20] B. S. Henriksen, K. Kinard, and R. J. Olson, "Effect of intraocular lens glistening size on visual quality," *Journal of Cataract & Refractive Surgery*, vol. 41, no. 6, pp. 1190–1198, 2015.

[21] H. Matsushima, M. Nagata, Y. Katsuki et al., "Decreased visual acuity resulting from glistening and sub-surface nanoglistening formation in intraocular lenses: a retrospective analysis of 5 cases," *Saudi Journal of Ophthalmology*, vol. 29, no. 4, pp. 259–263, 2015.

[22] T. J. T. P. van den Berg, "The (lack of) relation between straylight and visual acuity. Two domains of the point-spread-function," *Ophthalmic and Physiological Optics*, vol. 37, no. 3, pp. 333–341, 2017.

[23] H. Biwer, E. Schuber, M. Honig, B. Spratte, M. Baumeister, and T. Kohnen, "Objective classification of glistenings in implanted intraocular lenses using Scheimpflug tomography," *Journal of Cataract & Refractive Surgery*, vol. 41, no. 12, pp. 2644–2651, 2015.

[24] D.-H. Kim, R. H. James, R. J. Landry, D. Calogero, J. Anderson, and I. K. Ilev, "Quantification of glistenings in intraocular lenses using a ballistic-photon removing integrating-sphere method," *Applied Optics*, vol. 50, no. 35, pp. 6461–6467, 2011.

[25] L. Werner, C. Morris, E. Liu et al., "Light transmittance of 1-piece hydrophobic acrylic intraocular lenses with surface light scattering removed from cadaver eyes," *Journal of Cataract & Refractive Surgery*, vol. 40, no. 1, pp. 114–120, 2014.

[26] M. van der Mooren, L. Franssen, and P. Piers, "Effects of glistenings in intraocular lenses," *Biomedical Optics Express*, vol. 4, no. 8, pp. 1294–1304, 2013.

[27] K. K. Das, J. C. Stover, J. Schwiegerling, and M. Karakelle, "Technique for measuring forward light scatter in intraocular lenses," *Journal of Cataract & Refractive Surgery*, vol. 39, no. 5, pp. 770–778, 2013.

[28] G. Labuz, N. J. Reus, and T. J. T. P. van den Berg, "Straylight from glistenings in intraocular lenses: in vitro study," *Journal of Cataract & Refractive Surgery*, vol. 43, no. 1, pp. 102–108, 2017.

[29] G. Łabuz, F. Vargas-Martín, T. J. T. P. van den Berg, and N. López-Gil, "Method of in vitro assessment of straylight from intraocular lenses," *Biomedical Optics Express*, vol. 6, no. 11, pp. 4457–4464, 2015.

[30] B. N. Walker, R. H. James, D. Calogero, and I. K. Ilev, "A Novel full-angle scanning light scattering profiler to quantitatively evaluate forward and backward light scattering from intraocular lenses," *Review of Scientific Instruments*, vol. 86, no. 9, article 095004, 2015.

[31] L. Werner, J. C. Stover, J. Schwiegerling, and K. K. Das, "Light scattering, straylight, and optical quality in hydrophobic acrylic intraocular lenses with subsurface nanoglistenings," *Journal of Cataract & Refractive Surgery*, vol. 42, no. 1, pp. 148–156, 2016.

[32] E. DeHoog and A. Doraiswamy, "Evaluation of loss in optical quality of multifocal intraocular lenses with glistenings," *Journal of Cataract & Refractive Surgery*, vol. 42, no. 4, pp. 606–612, 2016.

Hindawi
Journal of Ophthalmology
Volume 2019, Article ID 2593404, 7 pages
https://doi.org/10.1155/2019/2593404

Research Article

Diagnostic Sensitivity of Different Reference Bodies When Using Scheimpflug Tomography in a Myopic Population with Keratoconus

Daniel Garcerant, Ignacio Jiménez-Alfaro, and Nicolás Alejandre

Fundación Jiménez Díaz, Madrid, Spain

Correspondence should be addressed to Daniel Garcerant; danielgarcerant@hotmail.com

Received 25 April 2019; Revised 17 June 2019; Accepted 25 June 2019; Published 18 July 2019

Guest Editor: Laura Remon

Purpose. To establish which reference body offers the greatest sensitivity in keratoconus (KC) diagnosis, obtain normative data for the myopic population with toric ellipsoid reference bodies, and determine the cutoff points for a population with KC. *Methods*. A retrospective, observational study of the entire Scheimpflug tomographer database of the Fundación Jiménez Díaz in Madrid was conducted to identify a normal myopic and a KC myopic population. Three different reference bodies were tested on all patients: best fit sphere (BFS), best fit toric ellipsoid with fixed eccentricity (BFTEFE), and best fit toric ellipsoid (BFTE). Anterior and posterior elevation measurements at the apex and thinnest point were recorded, as well as the root mean square of posterior elevations (RMS-P). Normative data were extracted, and receiver operating characteristic (ROC) curves were generated to obtain cutoff points between the normal and KC population. *Results*. A total of 301 eyes were included, comprising 219 normal myopic and 82 myopic KC eyes. BFS and BFTEFE produced the best results when measuring posterior elevation at the thinnest point. BFTE had better sensitivity with the RMS-P. From all measurements, best sensitivity (100%) was achieved with a cutoff point of 8 μm of posterior elevation at the thinnest point using the BFTEFE. BFTE was found to hide the cone in certain patients. *Conclusions*. Posterior elevation measured at the thinnest point with a BFTEFE is the best-performing parameter and, therefore, is recommended to discriminate between normal and KC patients within a myopic population.

1. Introduction

Keratoconus is a bilateral, asymmetric, and progressively degenerative disease. Due to the gradual thinning and steepening of the cornea caused by this illness, patients experience increasing irregular astigmatism, which decreases visual acuity [1, 2]. The impact that this disease has on the quality of life can be significant, and as lost vision is difficult to regain, early detection is essential for proper follow-up and treatment [3, 4].

This early detection becomes even more important in patients undergoing laser refractive surgery. Laser procedures performed on individuals with subclinical and otherwise stable disease can cause these patients to enter the progressive stage [5–8]. As a result, this population requires the most sensitive screening.

Changes in posterior elevation have been described as one of the first detectable alterations in patients with keratoconus [9–11]. In addition, the root mean square (RMS) of elevation values is believed to be highly effective in discriminating between keratoconic and normal eyes [12]. The best fit sphere (BFS) reference body has traditionally been used in elevation maps; nevertheless, there is growing evidence that a toric ellipsoid would be a more useful reference body [12–15]. Given the different toric ellipsoid options available in Scheimpflug tomography, more studies are needed to determine which is the best between the best fit toric ellipsoid (BFTE) and best fit toric ellipsoid with fixed eccentricity (BFTEFE).

To the best of our knowledge, only one study has performed this same comparison [12]. Other existing research studies in the field have used the BFTE as the reference body

[13–15]. No previous studies assessing the toric ellipsoid reference body have separated their study populations according to refraction, and it has been demonstrated that myopic and hyperopic populations have different normative data as seen on elevation maps [16, 17]. In light of these issues, the present study aims to establish which reference body offers the best sensitivity, obtain normative data for the myopic population using toric ellipsoid reference bodies, and establish cutoff points for the keratoconus population.

2. Materials and Methods

A retrospective, observational study was conducted at the Fundación Jiménez Díaz in Madrid. The study protocols used were in adherence to the tenets of the Declaration of Helsinki. No informed consent was retrieved, as the study was retrospective and participant identities cannot be derived from published data. Local institutional review board approval was obtained prior to data collection. The cornea unit at our institution has a Scheimpflug tomographer (OCULUS Pentacam HD®), and the entire tomographic database was reviewed to obtain the sample of normal and keratoconic myopic eyes.

General inclusion criteria for all eyes (both normal and keratoconus) were as follows: findings on corneal tomography with a quality specification (QS) of "OK" (indicating best possible quality, in which the measurement is correct and reproducible), with corneal coverage of at least 9 mm and no extrapolated data in the central 8 mm. All eyes were required to have simple or compound myopia (mixed astigmatism was excluded). All patients were 18 years of age or older, had not used contact lenses prior to tomography measurements for at least 1 week for soft lenses and 2 weeks for hard lenses. None had a history of corneal surgery or disease that could alter the corneal shape, such as scars, pterygium, and nodules.

Further specific inclusion criteria for normal patients were absence of abnormal findings on biomicroscopy, best-corrected visual acuity of 1.0 on the decimal scale, pachymetry within 475 μm and 650 μm, and no personal or family history of ectasia.

Additional inclusion criteria for keratoconus eyes were the following: abnormal posterior elevation according to the global consensus on keratoconus and ectatic diseases and at least 2 other topographic alterations compatible with keratoconus (corneal thickness spatial profile, percentage thickness increase, inferior/superior index, maximum Ambrosio's relational thickness index, etc.) [18–21]. After selecting keratoconus patients, only those meeting criteria for Stage 1 of the Amsler-Krumeich classification were included.

The patient's age and eyes were recorded. Tomographic data included the root mean square of elevation values for the posterior corneal surface (RMS-P). The elevation of the anterior corneal surface and posterior corneal surface was measured at the following points: anterior elevation at the apex (AA), posterior elevation at the apex (PA), anterior elevation at the thinnest point (AT), and posterior elevation at the thinnest point (PT) using 3 different reference bodies (i.e., BFS, BFTE, and BFTEFE). The elevation map was set in the "float," "optimise shift," and manual mode with fixed 8 mm diameter. All reference bodies included are the standard options available in the "front" and "back" elevation maps display. No enhanced reference bodies such as the Belin/Ambrósio enhanced ectasia display (BAD-D) were used.

For the anterior surface, the BFTEFE uses a fixed eccentricity of +0.47, which is equivalent to an asphericity (Q value) of −0.22. For the posterior surface, it establishes a fixed eccentricity of −0.45, equivalent to an asphericity (Q value) of −0.20. This corresponds to the mean value of the population in the 8 mm zone. The BFTE does not have a fixed eccentricity but rather calculates it each time to best fit the eye studied.

Measuring points are corneal positions chosen to facilitate replication of the measurement. This is why the corneal apex as well as the thinnest point was selected, where pathologic changes are most likely to occur. On the other hand, the RMS is simply a different way to calculate the average of a set of measurements. The reason to use the RMS, and not the more familiar mean, is that when data analyzed have both positive and negative values (like elevation maps have), negative values cancel out positive values when they are added while calculating the mean (e.g., the mean of two elevation values such as +5 μm and −5 μm would give a result of 0 μm, and an average elevation of 0 μm would suggest no elevation, which is not the case). The RMS, instead, calculates the average in a different way. By calculating the square of each value and then the square root of it, all measures end up being positive even if the initial value was of negative sign (overcoming the problem of having positive and negative values). Using the previous example, the square of −5 μm is +25 and the square root of +25 is +5. This way, the RMS of two elevation values like +5 μm and −5 μm would result in 5 μm, meaning that the average elevation value for this cornea is 5 μm away from the reference body. As all values are turned into a positive sign, the result does not indicate whether the value given is above or below the reference body and it only provides information on its distance from the reference body. The RMS can be viewed by right-clicking on the upper part of the elevation maps.

The following information was calculated for all parameters: mean, median, standard deviation, and the percentiles 2.5, 5, 95, and 97.5. The groups were analyzed for normality using the Shapiro–Wilk test. Student's t-test was used to determine the presence of statistically significant differences between the normal and keratoconic population at each point of measurement. Receiver operating characteristic (ROC) curves were obtained, and the best cutoff values were calculated according to the Youden index, searching for maximum potential effectiveness by combining sensitivity and specificity.

3. Results

A search was done of all the entries contained in the tomographic database at the Fundación Jiménez Díaz hospital from January 2009 until March 2016. Charts and

tomographies from a total of 3638 patients were studied. A total of 301 eyes met the inclusion and exclusion criteria, of which 219 were normal myopic eyes and 82 were myopic keratoconic eyes. Table 1 contains the basic demographic data of the patients studied. The most frequent reasons for exclusion were the failure to meet tomographic quality standards, past surgery, use of contact lenses, and other diseases of the cornea.

Anterior and posterior elevation measurements were taken at the apex and thinnest point, and RMS-P was recorded, using the 3 different reference bodies. Mean, median, standard deviation, and percentile data are summarized in Table 2. Although mean and standard deviation were calculated, the groups studied did not show a normal distribution according to the Shapiro–Wilk test, and therefore, median and percentile values are the correct measures of central tendency and dispersion to assess this population. All points measured show statistically significant difference between the normal and keratoconic population, with the exception of the AA and PA when measured with the BFTE. Toric ellipsoid bodies showed a closer fit. Three out of 4 measurements taken of the normal population using the BFTEFE had a median of 0 (AA, AT, and PT). BFTE had 2 out of 4 measurements with a median of 0 (AA and AT), and BFS had none. For the normal population, the 97.5 percentile of the measures of posterior elevation at the thinnest point was 15.6 μm for BFS, 6.55 μm for BFTEFE, and 4 μm for BFTE.

The normal myopic population was compared to the keratoconic myopic population to determine the best cutoff point to discriminate normal from diseased eyes. Table 3 shows the cutoff points obtained according to the maximum potential effectiveness. The sensitivity, specificity, positive predictive value (PPV), and negative predictive value (NPV) results obtained, when these cutoff points were used, are shown in the same table. Values obtained at the corneal apex show the worst performance.

Measurements taken at the thinnest point and RMS-P showed the best results; of these, BFS and BFTEFE had superior outcomes at the thinnest point of the posterior elevation map. Cutoff values at this position were 17.5 μm for BFS, 8 μm for BFTEFE, and 3.5 μm for BFTE. Comparing all measurement points from all reference bodies, the best sensitivity (100%) was achieved with the BFTEFE in the PT. The second most sensitive measurement was the BFS in the PT, with a sensitivity of 97.6%. The BFTE had the best performance with the RMS-P, with a sensitivity of 92.7% at a cutoff point of 5.87 μm.

Though this study did not include a subclinical keratoconus population, data from normal myopic population can be used to identify suspicious cases. As the BFTEFE at the PT was the measurement with the greatest degree of sensitivity, it is interesting to outline the percentile associated with the cutoff point of 5 μm (p95) and 6.55 μm (p97.5). An additional calculation was made at a cutoff point of 6 μm, showing this to be p97.

Elevation data are obtained manually, meaning that the 3 reference bodies had to be individually visualized and changed in each patient. During this process, it was noticed that in some patients, the BFTE completely hid the cone while the BFS and BFTEFE did not. Two examples of this behavior are shown in Figure 1.

Table 1: Demographic data.

Parameter	Group	
	KC myopic ($n = 82$ eyes)	Normal myopic ($n = 219$ eyes)
Age, median	37 (IQR 23–57)	33 (IQR 22–55)
Sex		
Male	64.6%	46.1%
Female	35.4%	53.9%
Eye		
Right	52.4%	45.2%
Left	47.6%	54.8%

KC, keratoconus; IQR, interquartile range.

4. Discussion

The prevalence of keratoconus varies by region and has been reported to be as low as 0.0003% in a Russian population and up to 4% in an Iranian location [22, 23]. In the United States (US), prevalence has been reported around 0.05% [24]. When prevalence is analyzed in the setting of refractive surgery candidates, percentages are consistently above the general population, with reports of 6.4% [25], 8.59% [26], and up to 24% [27]. Furthermore, it is estimated that over 11 million LASIK procedures were performed in the US by 2011 [28]. This becomes relevant as these procedures have demonstrated a high risk of developing a postsurgical ectasia in the keratoconus population [5–8]. It is therefore clear that although the percentage of iatrogenic ectasia may be considered low, the high volume of surgeries performed makes it an unacceptable frequent encounter in corneal clinics [29, 30]. Consequently, screening processes must continuously search for the most sensitive diagnostic tools.

Elevation maps can be used to detect posterior elevation, that is, one of the earliest signs of keratoconus [9–11]. These maps compare a patient's cornea to a reference body, performing the calculation of the reference body at each individual exam to best fit the studied cornea, outlining the differences in both [31]. Historically, most ophthalmologists are most familiar with the BFS, as it is the one with the most available data, and several tools have been developed based on this reference surface [10, 32, 33]. Doubt has been cast over the toric ellipsoid reference body due to the risk of masking the cone [33]. Nevertheless, recent studies have revisited this option, finding advantages in terms of sensitivity [12–15]. The ideal reference body should be one that most closely resembles the studied cornea to be able to detect early variations from normality while avoiding an almost perfect fit in the cone of pathologic corneas; as such a close fit would mask the cone. The results of our study show that the reference body that best fits this description is the toric ellipsoid with fixed eccentricity.

Corneas are not perfect spheres but rather are prolate and toric [34]. This is why toric ellipsoid reference bodies couple better with the studied cornea than the sphere

Table 2: Mean, median, standard deviation, and percentiles for each measurement point in the normal and keratoconic population.

Parameter	Group	Mean	SD	Median	Percentiles				P
					2.5%	5%	95%	97.5%	
BFS RMS-P	KC myopic	29.0	8.34	27.1	15.3	17.5	42.0	44.5	<0.001
	Normal myopic	15.1	6.97	13.7	5.33	5.91	28.2	31.5	
BFS AA	KC myopic	5.02	4.68	4.00	−2.00	0.00	14.9	18.0	<0.001
	Normal myopic	1.80	1.11	2.00	0.00	0.00	4.00	4.00	
BFS PA	KC myopic	13.3	12.8	12.0	−10.9	−3.00	32.0	35.9	<0.001
	Normal myopic	1.96	3.06	2.00	−4.00	−3.00	8.0	8.0	
BFS AT	KC myopic	13.0	5.80	12.0	5.00	6.00	23.0	27.0	<0.001
	Normal myopic	2.21	1.71	2.00	−0.55	0.00	5.00	5.55	
BFS PT	KC myopic	34.7	12.7	32.0	18.0	19.0	53.0	70.8	<0.001
	Normal myopic	4.81	4.31	4.00	−2.55	−1.00	13.0	15.6	
BFTEFE RMS-P	KC myopic	13.6	4.73	12.4	6.40	8.14	22.2	25.0	<0.001
	Normal myopic	4.20	1.35	4.07	2.36	2.50	6.84	7.60	
BFTEFE AA	KC myopic	3.51	4.63	3.00	−2.98	−2.00	13.0	16.9	<0.001
	Normal myopic	−0.27	1.07	0.00	−2.00	−2.00	1.00	2.00	
BFTEFE PA	KC myopic	10.3	12.6	9.50	−12.9	−6.00	29.9	33.9	<0.001
	Normal myopic	−1.90	3.18	−2.00	−8.00	−7.00	4.00	4.55	
BFTEFE AT	KC myopic	7.96	5.48	6.00	1.02	2.00	20.0	21.0	<0.001
	Normal myopic	−0.21	0.93	0.00	−2.00	−2.00	1.00	1.00	
BFTEFE PT	KC myopic	24.4	12.0	22.5	9.00	10.0	45.8	57.8	<0.001
	Normal myopic	0.07	2.80	0.00	−5.00	−4.10	5.00	6.55	
BFTE RMS-P	KC myopic	10.2	3.79	9.45	4.27	4.92	17.1	18.1	<0.001
	Normal myopic	3.84	1.09	3.73	2.20	2.34	6.03	6.33	
BFTE AA	KC myopic	−0.79	2.23	−1.00	−4.97	−4.00	3.00	4.97	0.469
	Normal myopic	−0.35	0.67	0.00	−1.00	−1.00	1.00	1.00	
BFTE PA	KC myopic	−1.61	5.16	−1.00	−11.0	−9.00	5.95	6.00	0.068
	Normal myopic	−3.11	1.44	−3.00	−6.00	−6.00	−1.00	0.00	
BFTE AT	KC myopic	3.15	3.10	3.00	−1.98	0.00	8.90	11.0	<0.001
	Normal myopic	−0.29	0.69	0.00	−2.00	−1.00	1.00	1.00	
BFTE PT	KC myopic	10.5	7.41	9.00	−1.00	−0.95	21.0	24.0	<0.001
	Normal myopic	−1.05	2.40	−1.00	−5.00	−5.00	3.00	4.00	

AA, anterior elevation at the apex; AT, anterior elevation at the thinnest point; BFS, best fit sphere; BFTE, best fit toric ellipsoid; BFTEFE, best fit toric ellipsoid with fixed eccentricity; KC, keratoconus; RMS-P, root mean square of posterior elevations; SD, standard deviation; PA, posterior elevation at the apex; PT, posterior elevation at the thinnest point.

Table 3: Cutoff values between normal and keratoconus population at each measuring point with the statistical measures obtained at these cutoff values.

Parameter	Cutoff	Sensitivity	Specificity	PPV	NPV	AUC (95% CI)
BFS RMS-P	18.7	0.939	0.763	0.597	0.971	0.900 (0.870, 0.940)
BFS AA	3.50	0.585	0.941	0.787	0.858	0.760 (0.680, 0.840)
BFS PA	7.50	0.744	0.945	0.836	0.908	0.840 (0.770, 0.910)
BFS AT	5.50	0.951	0.973	0.929	0.982	0.990 (0.990, 1.000)
BFS PT	17.5	0.976	0.991	0.976	0.991	1.000 (1.000, 1.000)
BFTEFE RMS-P	7.99	0.951	0.982	0.951	0.982	0.990 (0.990, 1.000)
BFTEFE AA	1.50	0.659	0.968	0.885	0.883	0.800 (0.730, 0.870)
BFTEFE PA	4.50	0.732	0.973	0.909	0.906	0.860 (0.790, 0.920)
BFTEFE AT	1.50	0.963	0.977	0.940	0.986	0.980 (0.950, 1.000)
BFTEFE PT	8.00	1.000	0.995	0.988	1.000	1.000 (1.000, 1.000)
BFTE RMS-P	5.87	0.927	0.945	0.864	0.972	0.980 (0.960, 1.000)
BFTE AA	−1.50	0.402	0.977	0.868	0.814	0.590 (0.510, 0.680)
BFTE PA	−1.50	0.512	0.900	0.656	0.831	0.620 (0.520, 0.710)
BFTE AT	0.50	0.841	0.932	0.821	0.940	0.910 (0.860, 0.960)
BFTE PT	3.50	0.866	0.968	0.910	0.951	0.950 (0.920, 0.990)

AA, anterior elevation at the apex; AT, anterior elevation at the thinnest point; AUC, area under the curve; BFS, best fit sphere; BFTE, best fit toric ellipsoid; BFTEFE, best fit toric ellipsoid with fixed eccentricity; CI, confidence interval; NPV, negative predictive value; RMS-P, root mean square of posterior elevations; PA, posterior elevation at the apex; PPV, positive predictive value; PT, posterior elevation at the thinnest point.

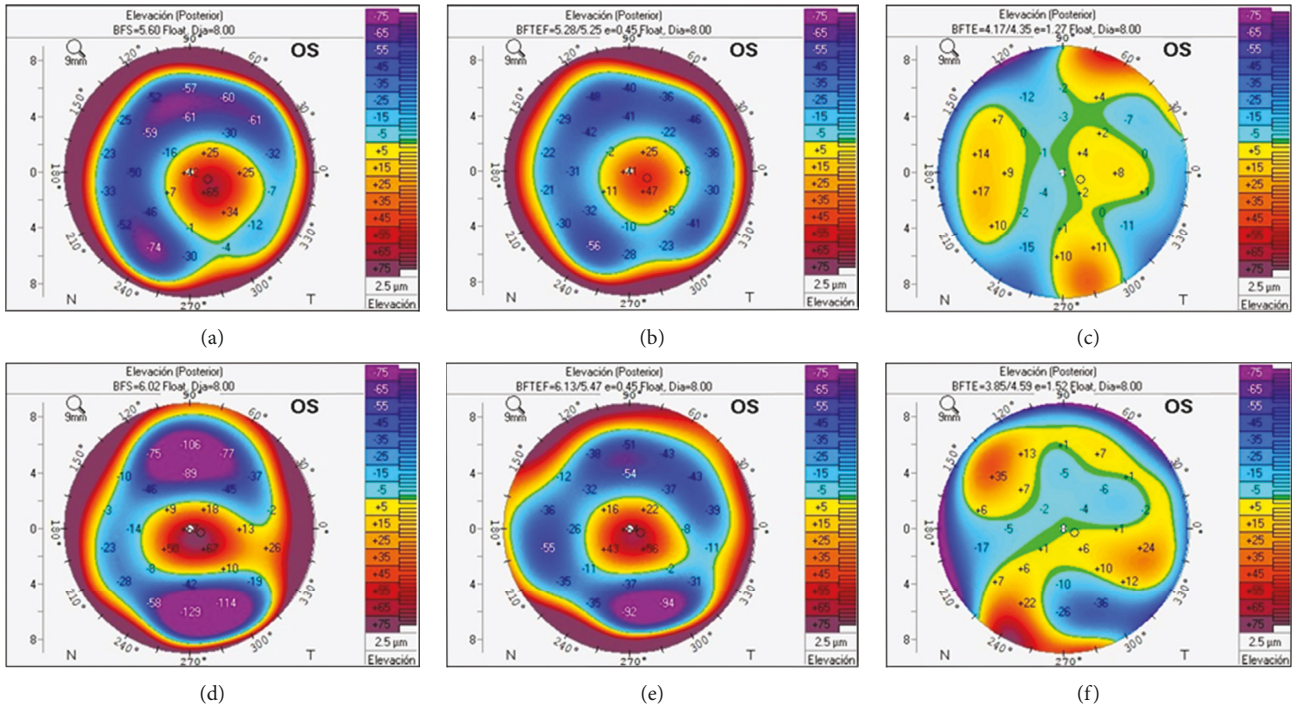

(a) (b) (c)

(d) (e) (f)

Figure 1: (a–c) The posterior elevation of a patient measured with the BFS (a), BFTEFE (b), and BFTE (c). It is quite evident how, in certain occasions, the BFTE can hide the cone. (d–f) The same problem in a different patient.

does. This is evidenced by looking at the measures of central tendency of the BFTEFE and BFTE, which are closer to 0 than those obtained by the BFS. Also, dispersion measurements of the BFS show a wider range compared to both toric ellipsoid bodies, meaning a bigger difference between the reference body and the cornea. Among the toric ellipsoid bodies, the tomographer offers 2 options: toric ellipsoid and toric ellipsoid with fixed eccentricity. To understand the difference between both, it is important to understand what eccentricity means. Eccentricity is a measurement that shows how much an ellipse differs from a circle. Ellipses must have an eccentricity value above 0 (0 is a circle) and less than 1 (1 is a parabola). Fixed eccentricity is the key factor, as it prevents this reference body from creating a nearly exact match, which would mask the cone, while providing a comparative surface that best resembles a normal corneal shape, enabling the early detection of differences. When the option with no fixed eccentricity was used (BFTE), we found several cases in which the reference body masked the cone (Figure 1). This might partly explain the lower sensitivity of the BFTE, and we do not recommend this option. The BFS does not mask the cone and behaves well but, as explained before, the cornea is not a sphere, which is why the sensitivity is not as good as the one obtained with a BFTEFE. Of all the parameters measured, the best results were achieved when measuring posterior elevation at the thinnest point with the BFTEFE, obtaining a sensitivity of 100% when a cutoff point of 8 was used. It is also important to note that this sensitivity is not obtained by sacrificing specificity, as it is near 100% (0.995) as well. BFTEFE consistently showed better performance for all parameters, including PPV and NPV. It is nonetheless important to point out that for KC diagnosis, clinicians should not rely on one single parameter but rather a combination of them. It also must be borne in mind that this study did not include a usual elevation measurement other studies have used such as maximum elevation. This measurement poses a special problem: in cases of high astigmatism, normal patients would show a high elevation value, falsely indicating disease [35]. This does not happen when the measurement is taken at the thinnest point.

These results confirm those obtained by Sideroudi et al. [12], the only difference being that their cutoff point was 7 μm rather than 8 μm as in our study. Though the difference was slight, our groups were not exactly the same, as our research was carried out in a myopic population, and their study did not discriminate according to refraction. Though being a parameter with very good performance, RMS-P does not offer better sensitivity than posterior elevation at the thinnest point. To the best of our knowledge, ours is the first study to assess the cutoff values in a normal and keratoconic myopic population for toric ellipsoid reference bodies.

To arrive at a cutoff point for suspicious cases (a population not included in the study), normative data from the normal population can be used. It should be taken into account that only 5% of the normal population would have 5 μm or more of posterior elevation measured at the PT with the BFTEFE. Using a cutoff point of 6 μm, it would be 3% of the normal population. Depending on the intentions of screening and whether more or less sensitivity is desired, either of these two values would be useful.

Actual color scales for elevation maps in the Pentacam® are designed to highlight pathologic elevation using "hot colors" based on the BFS range. When using a BFTEFE, these same color scales become less intuitive as the range of values with this reference body is lower and, as a result, "hot colors" would only start to appear in more advanced cases. A suggestion would therefore be to include another option in the color scale to change the step width every 1.5 μm (the actual minimal increase is 2.5 μm). By creating this new option, ophthalmologists would be able to view a similarly intuitive image to what they are used to.

As this is a retrospective study, certain sources of bias are expected. First, a lack of data impeded many patients from being included. Second, factors that alter corneal tomography (contact-lens use, scars) may not have been recorded in the charts ending up with the inclusion of patients that should have been excluded. Nevertheless, since all reference bodies were tested in all subjects, we expect this bias to affect the population equally. Third, the most significant difficulty and probable source of bias is the lack of definition for keratoconus within the scientific community. Difficulties in establishing universally accepted diagnostic criteria became evident in the global consensus on keratoconus and ectatic disease [18]. Studies involving this population use different inclusion criteria. Including patients based on tomographic parameters in a study testing some of these same parameters was the biggest challenge as not to bias the sample in favor of one of the reference bodies tested, specially the BFS, as it is the reference body historically used in our cornea service and therefore the one that the investigators are familiar with. Using clinical signs was not an option, as they are not necessarily present in the earliest phases of the disease, which was our targeted population. The strategy to overcome this was not to assume a specific value for pathologic posterior elevation while screening but to allow values surrounding previously suggested abnormal measures in combination with other clear pathologic tomographic alterations that did not rely on posterior elevation.

This study assessed the role of different reference bodies in the diagnosis of keratoconus. Detecting progression is another field in which much has been done but there is still no consensus. Maximum keratometry (Kmax) is probably the most widely used parameter but is not yet the ideal one. The usual cutoff has been set in a 1-diopter increase in 1 year. However, variations of up to 1.34 diopters can be obtained in the same patient on exams taken on the same day, especially in advanced keratoconus [36]. Given the more accurate fit of the BFTEFE, it could be hypothesized that it would be a good tool to detect progression. Studies will be needed to prove this.

On a similar matter, novel techniques have been introduced in the search for the most sensitive tool. Ambrosio developed an index integrating corneal biomechanics and tomographic data, showing promising results [37]. Studies undertaken in this area have most often used and compared biomechanics to sphere-based reference bodies, especially the BAD-D [38–42]. It would be of interest to know how the BFTEFE behaves against these parameters and whether its integration would enhance detection.

5. Conclusions

BFTEFE outperformed the BFS and BFTE in diagnosing KC. Of the different measuring points studied, the greatest sensitivity when differentiating between the normal and KC population was achieved by posterior elevation measured at the thinnest point with the BFTEFE, using a cutoff point of 8 μm. The BFTE was found to hide the cone in certain patients and, therefore, should be considered unreliable for KC screening.

Data Availability

The data used to support the findings of this study are included within the article.

Conflicts of Interest

The authors declare that they have no conflicts of interest.

Acknowledgments

Thanks are due to Ignacio Mahillo for support with statistical analysis and Julio Prieto and Pablo Landa for technical support. The Fundación Jiménez Díaz (the hospital where the study took place) provided support through the statistician.

References

[1] L. J. Davis, K. B. Schechtman, B. S. Wilson et al., "Longitudinal changes in visual acuity in keratoconus," *Investigative Opthalmology & Visual Science*, vol. 47, no. 2, pp. 489–500, 2006.

[2] M. Suzuki, S. Amano, N. Honda, T. Usui, S. Yamagami, and T. Oshika, "Longitudinal changes in corneal irregular astigmatism and visual acuity in eyes with keratoconus," *Japanese Journal of Ophthalmology*, vol. 51, no. 4, pp. 265–269, 2007.

[3] S. M. Kymes, J. J. Walline, K. Zadnik, J. Sterling, and M. O. Gordon, "Changes in the quality-of-life of people with keratoconus," *American Journal of Ophthalmology*, vol. 145, no. 4, pp. 611–617, 2008.

[4] J. C. K. Tan, V. Nguyen, E. Fenwick, A. Ferdi, A. Dinh, and S. L. Watson, "Vision-related quality of life in keratoconus," *Cornea*, vol. 38, no. 5, pp. 600–604, 2019.

[5] C. F. Schmitt-Bernard, C. Lesage, and B. Arnaud, "Keratectasia induced by laser in situ keratomileusis in keratoconus," *Journal of Refractive Surgery*, vol. 16, no. 3, pp. 368–370, 2000.

[6] T. Seiler and A. W. Quurke, "Iatrogenic keratectasia after LASIK in a case of forme fruste keratoconus," *Journal of Cataract & Refractive Surgery*, vol. 24, no. 7, pp. 1007–1009, 1998.

[7] R. K. Chiang, A. J. Park, C. J. Rapuano, and E. J. Cohen, "Bilateral keratoconus after LASIK in a keratoconus patient," *Eye & Contact Lens: Science & Clinical Practice*, vol. 29, no. 2, pp. 90–92, 2003.

[8] J. B. Randleman, M. Woodward, M. J. Lynn, and R. D. Stulting, "Risk assessment for ectasia after corneal refractive surgery," *Ophthalmology*, vol. 115, no. 1, pp. 37–50, 2008.

[9] S. Huseynli, J. Salgado-Borges, and J. L. Alio, "Comparative evaluation of Scheimpflug tomography parameters between thin non-keratoconic, subclinical keratoconic, and mild keratoconic corneas," *European Journal of Ophthalmology*, vol. 28, no. 5, pp. 521–534, 2018.

[10] K. Miháltz, I. Kovács, Á. Takács, and Z. Z. Nagy, "Evaluation of keratometric, pachymetric, and elevation parameters of keratoconic corneas with pentacam," *Cornea*, vol. 28, no. 9, pp. 976–980, 2009.

[11] Z. Schlegel, T. Hoang-Xuan, and D. Gatinel, "Comparison of and correlation between anterior and posterior corneal elevation maps in normal eyes and keratoconus-suspect eyes," *Journal of Cataract & Refractive Surgery*, vol. 34, no. 5, pp. 789–795, 2008.

[12] H. Sideroudi, G. Labiris, A. Giarmoukakis, N. Bougatsou, and V. Kozobolis, "Contribution of reference bodies in diagnosis of keratoconus," *Optometry and Vision Science*, vol. 91, no. 6, pp. 676–681, 2014.

[13] I. Kovács, K. Miháltz, M. Ecsedy, J. Németh, and Z. Z. Nagy, "The role of reference body selection in calculating posterior corneal elevation and prediction of keratoconus using rotating Scheimpflug camera," *Acta Ophthalmologica*, vol. 89, no. 3, pp. e251–e256, 2011.

[14] D. Smadja, M. R. Santhiago, G. R. Mello, R. R. Krueger, J. Colin, and D. Touboul, "Influence of the reference surface shape for discriminating between normal corneas, subclinical keratoconus, and keratoconus," *Journal of Refractive Surgery*, vol. 29, no. 4, pp. 274–281, 2013.

[15] E. M. Mostafa, "Comparison between corneal elevation maps using different reference surfaces with Scheimpflug-Placido topographer," *International Ophthalmology*, vol. 37, no. 3, pp. 553–558, 2017.

[16] F. Gilani, M. Cortese, R. R. Ambrósio Jr. et al., "Comprehensive anterior segment normal values generated by rotating Scheimpflug tomography," *Journal of Cataract & Refractive Surgery*, vol. 39, no. 11, pp. 1707–1712, 2013.

[17] J. T. Kim, M. Cortese, M. W. Belin, R. Ambrosio Jr., and S. S. Khachikian, "Tomographic normal values for corneal elevation and pachymetry in a hyperopic population," *Journal of Clinical & Experimental Ophthalmology*, vol. 2, no. 2, p. 130, 2011.

[18] J. A. P. Gomes, D. Tan, C. J. Rapuano et al., "Global consensus on keratoconus and ectatic diseases," *Cornea*, vol. 34, no. 4, pp. 359–369, 2015.

[19] R. Ambrósio Jr., R. S. Alonso, A. Luz, and L. G. C. Velarde, "Corneal-thickness spatial profile and corneal-volume distribution: tomographic indices to detect keratoconus," *Journal of Cataract & Refractive Surgery*, vol. 32, no. 11, pp. 1851–1859, 2006.

[20] R. Ambrósio Jr., A. L. C. Caiado, F. P. Guerra et al., "Novel pachymetric parameters based on corneal tomography for diagnosing keratoconus," *Journal of Refractive Surgery*, vol. 27, no. 10, pp. 753–758, 2011.

[21] Y. S. Rabinowitz and P. J. McDonnell, "Computer-assisted corneal topography in keratoconus," *Journal of Refractive Surgery*, vol. 5, no. 6, pp. 400–408, 1989.

[22] H. Hashemi, S. Heydarian, A. Yekta et al., "High prevalence and familial aggregation of keratoconus in an Iranian rural population: a population-based study," *Ophthalmic and Physiological Optics*, vol. 38, no. 4, pp. 447–455, 2018.

[23] E. N. Gorskova and E. N. Sevost'ianov, "Epidemiology of keratoconus in the Urals," *Vestnik Oftalmologii*, vol. 114, no. 4, pp. 38–40, 1998.

[24] R. H. Kennedy, W. M. Bourne, and J. A. Dyer, "A 48-year clinical and epidemiologic study of keratoconus," *American Journal of Ophthalmology*, vol. 101, no. 3, pp. 267–273, 1986.

[25] Y. Hori-Komai, I. Toda, N. Asano-Kato, and K. Tsubota, "Reasons for not performing refractive surgery," *Journal of Cataract & Refractive Surgery*, vol. 28, no. 5, pp. 795–797, 2002.

[26] T. A. Althomali, I. M. Al-Qurashi, S. M. Al-Thagafi, A. Mohammed, and M. Almalki, "Prevalence of keratoconus among patients seeking laser vision correction in Taif area of Saudi Arabia," *Saudi Journal of Ophthalmology*, vol. 32, no. 2, pp. 114–118, 2018.

[27] A. M. Al-Amri, "Prevalence of keratoconus in a refractive surgery population," *Journal of Ophthalmology*, vol. 2018, Article ID 5983530, 5 pages, 2018.

[28] K. J. Corcoran, "Macroeconomic landscape of refractive surgery in the United States," *Current Opinion in Ophthalmology*, vol. 26, no. 4, pp. 249–254, 2015.

[29] A. S. Rad, M. Jabbarvand, and N. Saifi, "Progressive keratectasia after laser in situ keratomileusis," *Journal of Refractive Surgery*, vol. 20, no. 5, pp. S718–S722, 2004.

[30] I. G. Pallikaris, G. D. Kymionis, and N. I. Astyrakakis, "Corneal ectasia induced by laser in situ keratomileusis," *Journal of Cataract & Refractive Surgery*, vol. 27, no. 11, pp. 1796–1802, 2001.

[31] M. W. Belin, D. Litoff, S. J. Strods, S. S. Winn, and R. S. Smith, "The PAR technology corneal topography system," *Refractive & Corneal Surgery*, vol. 8, no. 1, pp. 88–96, 1992.

[32] K. Kamiya, R. Ishii, K. Shimizu, and A. Igarashi, "Evaluation of corneal elevation, pachymetry and keratometry in keratoconic eyes with respect to the stage of Amsler-Krumeich classification," *British Journal of Ophthalmology*, vol. 98, no. 4, pp. 459–463, 2014.

[33] W. B. Michael, S. K. Stephe, and R. Ambrosio Jr., *Elevation Based Corneal Tomography*, Jaypee Highlights, Panama City, Panama, 2012.

[34] P. Benes, S. Synek, and S. Petrova, "Corneal shape and eccentricity in population," *Collegium Antropologicum*, vol. 37, no. 1, pp. 117–120, 2013.

[35] S. S. Khachikian and M. W. Belin, "Posterior elevation in keratoconus," *Ophthalmology*, vol. 116, no. 4, p. 816.e1, 2009.

[36] P. Kosekahya, M. Koc, M. Caglayan, H. Kiziltoprak, C. U. Atilgan, and P. Yilmazbas, "Repeatability and reliability of ectasia display and topometric indices with the Scheimpflug system in normal and keratoconic eyes," *Journal of Cataract & Refractive Surgery*, vol. 44, no. 1, pp. 63–70, 2018.

[37] R. Ambrósio Jr., B. T. Lopes, F. Faria-Correia et al., "Integration of Scheimpflug-based corneal tomography and biomechanical assessments for enhancing ectasia detection," *Journal of Refractive Surgery*, vol. 33, no. 7, pp. 434–443, 2017.

[38] J. Steinberg, M. Siebert, T. Katz et al., "Tomographic and biomechanical Scheimpflug imaging for keratoconus characterization: a validation of current indices," *Journal of Refractive Surgery*, vol. 34, no. 12, pp. 840–847, 2018.

[39] M.-R. Sedaghat, H. Momeni-Moghaddam, R. Ambrósio Jr. et al., "Diagnostic ability of corneal shape and biomechanical parameters for detecting frank keratoconus," *Cornea*, vol. 37, no. 8, pp. 1025–1034, 2018.

[40] T. C. Y. Chan, Y. M. Wang, M. Yu, and V. Jhanji, "Comparison of corneal tomography and a new combined tomographic biomechanical index in subclinical keratoconus," *Journal of Refractive Surgery*, vol. 34, no. 9, pp. 616–621, 2018.

[41] Y. M. Wang, T. C. Y. Chan, M. Yu, and V. Jhanji, "Comparison of corneal dynamic and tomographic analysis in normal, forme fruste keratoconic, and keratoconic eyes," *Journal of Refractive Surgery*, vol. 33, no. 9, pp. 632–638, 2017.

[42] T. C. Chan, Y. M. Wang, M. Yu, and V. Jhanji, "Comparison of corneal dynamic parameters and tomographic measurements using Scheimpflug imaging in keratoconus," *British Journal of Ophthalmology*, vol. 102, no. 1, pp. 42–47, 2018.

Hindawi
Journal of Ophthalmology
Volume 2019, Article ID 2796126, 9 pages
https://doi.org/10.1155/2019/2796126

Research Article

New Approach for the Calculation of the Intraocular Lens Power Based on the Fictitious Corneal Refractive Index Estimation

Joaquín Fernández,[1,2] Manuel Rodríguez-Vallejo,[1] Javier Martínez,[1] Ana Tauste,[1] and David P. Piñero[3,4]

[1]*Department of Ophthalmology (Qvision), Vithas Virgen Del Mar Hospital, 04120 Almería, Spain*
[2]*Department of Ophthalmology, Torrecardenas Hospital Complex, 04009 Almería, Spain*
[3]*Department of Optics, Pharmacology and Anatomy, University of Alicante, Alicante, Spain*
[4]*Department of Ophthalmology, Vithas Medimar International Hospital, Alicante, Spain*

Correspondence should be addressed to David P. Piñero; david.pinyero@ua.es

Received 8 February 2019; Revised 4 April 2019; Accepted 28 April 2019; Published 14 May 2019

Guest Editor: Damian Siedlecki

Purpose. To identify the sources of error in predictability beyond the effective lens position and to develop two new thick lens equations. *Methods*. Retrospective observational case series with 43 eyes. Information related to the actual lens position, corneal radii measured with specular reflection and Scheimpflug-based technologies, and the characteristics of the implanted lenses (radii and thickness) were used for obtaining the fictitious indexes that better predicted the postoperative spherical equivalent (SE) when the real effective lens position (ELP) was known. These fictitious indexes were used to develop two thick lens equations that were compared with the predictability of SRK/T and Barrett Universal II. *Results*. The SE relative to the intended target was correlated to the difference between real ELP and the value estimated by SRK/T (ΔELP) ($r = -0.47$, $p = 0.002$), but this only predicted 22% of variability in a linear regression model. The fictitious index for the specular reflection (n_k) and Scheimpflug-based devices (n_c) were significantly correlated with axial length. Including both indexes fitted to axial length in the prediction model with the ΔELP increased the *r*-square of the model up to 83% and 39%, respectively. Equations derived from these fictitious indexes reduced the mean SE in comparison to SRK/T and Barrett Universal II. *Conclusions*. The predictability with the trifocal IOL evaluated is not explained by an error in the ELP. An adjustment fitting the fictitious index with the axial length improves the predictability without false estimations of the ELP.

1. Introduction

Intraocular lens (IOL) power calculation formulas have evolved since the publication of the Fyodorov formula in 1967 [1, 2]. Nowadays, there are several methods for calculating the IOL power that can be classified in one of the following groups: (1) historical/refraction based, (2) regression, (3) vergence, (4) artificial intelligence, and (5) ray tracing [3]. The first two approaches are considered out of date, the artificial intelligence is growing in popularity but not in predictability [4], and the ray tracing [5, 6] is the promising option that has not still replaced the most used methods based on the vergence formula. An important reason for the absence of a clear evidence of differences between these previous three approaches is the inclusion of some regression components in all of them, including ray tracing [3]. In fact, the main difference between vergence formulas is the number of variables used for estimating the effective-thin lens position (ELP_o), [7] ranging from two in SRK/T, Hoffer Q, and Holladay I formulas to five or seven in the Barrett Universal II or Holladay II formulas, respectively [3].

There are several studies that report the predictability of vergence formulas for eyes with different axial lengths, but high discrepancies are found in the percentage of eyes within ±0.50 D between studies [4, 8–13]. For instance,

Shrivastava et al. [14] reported no differences between SRK/T and the newer formulas in short eyes, but a meta-analysis reported superiority of the Haigis formula [15]. The reality is that there are no clinically relevant differences in the statistics of centrality for the postoperative spherical equivalent (SE) between equations, and special attention should be taken in dispersion [10]. This dispersion of the data has been reported to be lower for the Barrett Universal II, which results in a higher percentage of eyes within ±0.50 D in medium to long eyes [4, 8–13]. The Barrett Universal II was born from the theoretical universal formula which considers the thick lens formula [16] and after an estimation of the lens factor, which is the distance from the iris to the second principal plane of the IOL [17]. Therefore, the thin lens formula can be used considering the ELP_o as the anterior chamber depth (ACD) plus the lens factor which can be derived from the A-constant [17]. Other authors have used the terms surgeon factor [18] or offset [19] instead of lens factor but the aim of these constants was the same: to estimate the location of the second principle plane of the IOL optic from a relatively fixed anatomical reference plane and to compute the ELP_o by means of this factor [16].

If the intended preoperative spherical equivalent (SE) and the postoperative SE are not equal, the constants implemented by different formulas can be optimized for improving refractive results in eyes with different axial lengths [20, 21], but this may contribute to an error in the ELP_o if the lens position is not measured during the postoperative follow-up. The aim of this study was to evaluate if the postoperative SE after implantation of a trifocal IOL was due to an error in the ELP_o estimated with the SRK/T formula and, if this was not the reason, to identify the possible sources of error. For this purpose, the actual lens position (ALP) of each eye was measured after surgery, and the thick lens formula [22] was used to avoid the optical approximations required by the vergence formula [2].

2. Materials and Methods

2.1. Subjects and Procedures. The study was approved by the local Ethics Committee and was performed in adherence to the tenets of the Declaration of Helsinki. Data from 43 subjects measured at the 3-month follow-up visit were retrospectively retrieved from our historical database, including only one eye randomly in the analysis. The tomography obtained at this visit with the Pentacam HR (Oculus, Wetzlar, Germany) was used for collecting data including anterior (r_{1c}) and posterior corneal radii (r_{2c}), corneal thickness (e_c), and ALP measured from corneal vertex (anterior corneal surface) to the anterior IOL surface. The axial length (AXL), the preoperative ACD, and the anterior corneal radius (r_k) were retrieved from the measurements obtained with the IOLMaster 500 system (Carl Zeiss Meditec AG, Germany). The postoperative best spectacle refraction was also obtained for each eye computing the SE. The pupil diameter for the conditions for which the refraction was performed (around 90 lux) was estimated as the mean between photopic and mesopic pupils measured with the Keratograph 5M system (Oculus, Wetzlar, Germany).

2.2. Surgery Procedure. All surgeries were conducted by the same surgeon (X) by means of phacoemulsification or femtosecond laser-assisted cataract surgery (Victus, Bausch & Lomb Inc, Dornach, Germany) through clear corneal incisions of 2.2 mm for manual incisions or 2.5 mm for laser incisions, both at temporal location. The implanted IOL at capsular bag was the Liberty Trifocal (Medicontur Medical Engineering Ltd. Inc., Zsámbék, Hungary) based on the elevated phase shift (EPS) technology, which is an aspheric hydrophilic IOL with +3.50 D of addition for near and +1.75 D for intermediate at the IOL plane. The preoperative calculation of the IOL power was conducted with the SRK/T [19] formula considering the manufacturer recommended constant of 118.9.

2.3. Thick Lens Formula. All the calculations were conducted by means of paraxial optics and coupling the measured optical structures with the thick lens formula [22]. Some approaches were conducted depending on the system used to measure the cornea. For the anterior corneal radius (r_k) obtained with IOLMaster, the corneal power in equation (1) (P_k) should be estimated with a fictitious index (n_k), and the cornea was considered as a single dioptric surface; therefore, corneal principal planes were approximated to the anterior corneal surface (Figure 1(a)). For the measurement of both corneal radii (r_{1c} and r_{2c}) and corneal thickness (e_c) with the Pentacam (Figure 1(b)), the total corneal power was computed with equation (2), and corneal principal planes were calculated since the cornea was considered as a thick lens (Figure 1(b)) [22]:

$$P_k = \frac{n_k - 1}{r_k}, \tag{1}$$

$$P_c = \frac{n_c - 1}{r_{1c}} + \frac{1.3374 - n_c}{r_{2c}} - \left(\frac{e_c}{n_c}\right)\left(\frac{n_c - 1}{r_{1c}}\right)\left(\frac{1.3374 - n_c}{r_{2c}}\right). \tag{2}$$

The characteristics of the IOL implanted in each patient were provided by the manufacturer, including thickness and anterior and posterior radii (these are not detailed in the results as they were required to be kept as confidential by the manufacturer). Therefore, the principal planes were also calculated for the IOLs (Figure 1). Finally, to calculate the equivalent lens for the coupling of the cornea and the IOL, it was required to define the distances between both optical structures (ELP) taking the principal planes as the reference if possible (Figure 1(b)) or the anterior cornea location when the cornea was considered as a thin lens (Figure 1(a)). Different approximations for the real effective lens position depending on the principal planes location were considered: from corneal vertex to second IOL principal plane (equation (3); Figure 1(a)), from second corneal principal plane to first IOL principal plane (equation (4); Figure 1(b)), and from

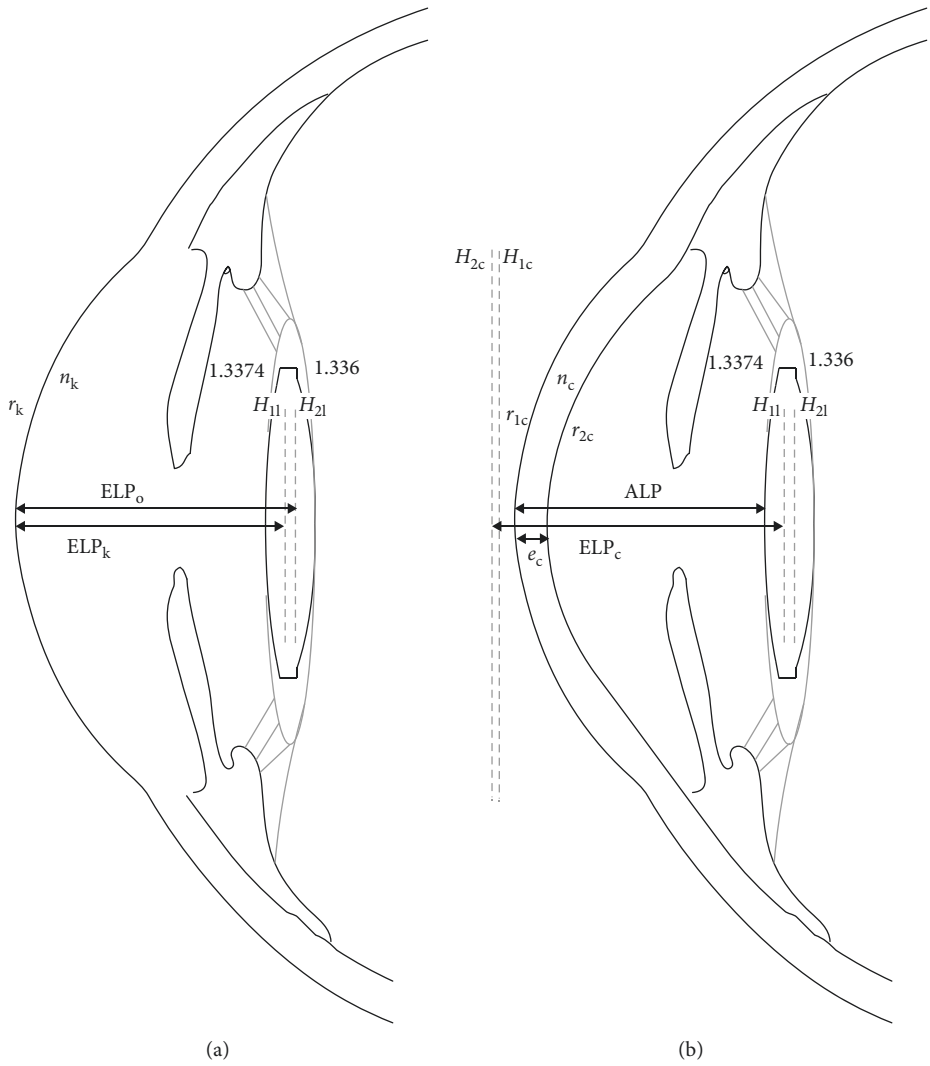

Figure 1: (a) Model for the calculation of the corneal power derived from anterior corneal radius (r_k) and fictitious index (n_k). The effective lens positions for vergence thin lens formula (ELP_o) and for thick lens formula (ELP_k) are shown. 1.3374 and 1.336 are the refractive indexes for the aqueous and vitreous, respectively. (b) Schema for computing the IOL power based on the thick lens formula, both anterior (r_{1c}) and posterior (r_{2c}) corneal radii were measured, and total corneal power was obtained estimating refractive index of the cornea (n_c). Actual lens position (ALP) and effective lens position (ELP_c) from principal planes are represented. H_{1c}, H_{2c}, H_{1l}, and H_{2l} are the first and second principal planes for the cornea and the IOL.

corneal vertex to first IOL principal plane (equation (5); Figure 1(a)):

$$ELP_o = ALP + H_{2l}, \quad (3)$$

$$ELP_c = ALP - H_{2c} + H_{1l}, \quad (4)$$

$$ELP_k = ALP + H_{1l}. \quad (5)$$

While equation (3) was the real ELP_o that should be predicted for the vergence formula [2], the other two were used in the thick lens formula depending if both corneal surfaces radii (ELP_c) (equation (4)) or only anterior corneal radius (ELP_k) (equation (5)) were used.

The SRK/T is a vergence formula; therefore, it predicts what would be the ELP_o (equation (3)), considering the biometric eye parameters and an A-constant associated to the IOL. As we measured the postoperative ALP and calculated the principal planes of the IOL, we can calculate the difference between the ELP_o estimated preoperatively by the SRK/T formula (hereinafter abbreviated as $ELP_{SRK/T}$) [19] and the real ELP_o calculated postoperatively (equation (3)) ($\Delta ELP = ELP_{SRK/T} - ELP_o$). The correlation between ΔELP and the postoperative SE was computed in order to assess the amount of postoperative SE explained by an error in the ELP_o estimation by the SRK/T formula.

The predictability obtained with SRK/T and the predictability that would have expected if Barrett Universal II (white to white and lens thickness not considered) [23] had been used were compared with those achievable with the two thick lens equations, for which the corneal power was derived from the measures of the anterior corneal radius measured with the IOLMaster (equation (1); Figure 1(a)) or both corneal surfaces measured with the Pentacam

(equation (2); Figure 1(b)). For this purpose, the postoperative SE refraction was adjusted to the intended target refraction computed by each formula for the implanted IOL power [24, 25].

2.4. Fictitious Indexes. The fictitious indexes were defined as the refractive indexes used for computing the corneal power that better predicts the postoperative SE after surgery when the real ELP is known. Considering that the corneal radii, ELP, AXL, and the IOL characteristics (radii and thickness) were known after surgery, the only variable for predicting the postoperative SE with the thick lens formula was the fictitious index. Therefore, an iterative process was conducted for obtaining these indexes considering two possibilities: (1) the corneal power was derived from a fictitious index (n_c) considering anterior and posterior corneal radii and corneal thickness (Figure 1(a)) and (2) the corneal power was derived from a fictitious index (n_k) and the anterior corneal radius (Figure 1(b)). This kind of iterative processes has been used for finding the best constant that predicts best the difference between the intended and the actual SE [20]. However, it should be considered that the purpose of refining constants is to correct wrong estimations of ELP_o. In our study, as the real ELP_o was known, other unknown sources of error were investigated and adjusted by modifying the corneal power through the fictitious refractive indexes.

2.5. Statistical Analysis. The normality of data distributions for the variables evaluated was tested with the Shapiro–Wilk test, and parametric statistics were selected for testing hypothesis only if the assumptions were met. Correlations were evaluated with the Pearson r test, and the paired t-test was used for testing differences between real ELP_o and $ELP_{SRK/T}$. The thick lens equation [22] and all the functions required to estimate the fictitious indexes by means of iteration processes were implemented in MATLAB (Mathworks, Inc., Natick, MA). The statistical analyses were performed using the IBM SPSS 24.0 software for Windows (SPSS, Chicago, IL). Mean ± standard deviation [median (interquartile range)] is used in Section 3 for reporting central tendency and data dispersion.

3. Results

Mean age of the sample was 68 ± 8 [70 (7)] years old. The ΔELP was significantly correlated with the postoperative SE relative to the intended target ($r = -0.47$, $p = 0.002$) (Figure 2(a)). A linear regression model predicted that the 22% of the variability in the postoperative SE was explained by an error estimation of the ELP_o [$F(1, 41) = 11.308$, $p = 0.002$, $R^2 = 0.22$]. No significant correlations of ΔELP were found with AXL ($r = 0.23$, $p = 0.15$) and preoperative ACD ($r = -0.23$, $p = 0.14$). The real ELP_o was 5.05 ± 0.29 [5.02 (0.32)] mm, and the $ELP_{SRK/T}$ was 5.36 ± 0.31 [5.39 (0.34)] mm ($t = 7.336$, $p < 0.0005$). The anterior corneal radius measured by specular reflection (r_k) overestimated the value measured by the Scheimpflug-based devices in 0.03 ± 0.05 [0.03 (0.05)] mm ($t = 3.49$, $p = 0.001$), and the difference was correlated with the average of both measures ($r = -0.36$, $p = 0.02$) (Figure 2(b)).

Mean fictitious refractive indexes for n_k and n_c were 1.336 ± 0.003 [1.336 (0.004)] and 1.339 ± 0.017 [1.336 (0.021)], respectively. These indexes were correlated with the axial length of the eye, for both n_c ($r = 0.49$, $p = 0.001$) (Figure 3(a)) and n_k ($r = -0.33$, $p = 0.03$) (Figure 3(b)). A multiple linear regression model for predicting postoperative SE relative to the intended target was conducted including ΔELP and n_k or n_c. The r-square increased from 0.22 to 0.83 after including n_k [$F(2, 40) = 99.425$, $p < 0.0005$, $R^2 = 0.83$], and from 0.22 to 0.39 after including n_c [$F(2, 40) = 12.78$, $p < 0.0005$, $R^2 = 0.39$] in the regression in combination with ΔELP (Table 1).

Two thick equations were developed considering different fictitious indexes depending on axial length. For the thick lens equation considering anterior corneal radius (n_k equation), $n_k = 1.339$ was used for eyes ≤ 22 mm, $n_k = 1.336$ for eyes from 22 to 24.5 mm, and $n_k = 1.333$ for eyes ≥ 24.5 mm. For the thick lens equation considering anterior and posterior corneal radii, $n_c = 1.328$ was used for eyes ≤22 mm, $n_c = 1.339$ for eyes from 22 to 24.5 mm, and $n_c = 1.350$ for eyes ≥24.5 mm. A multiple linear regression was conducted for predicting ALP considering preoperative ACD and AXL, obtaining the following equation for $ALP = 0.527 \cdot ACD + 0.102 \cdot AXL + 0.41$ [$F(2, 40) = 57.20$, $p < 0.0005$, $R^2 = 0.74$]. The predicted ALP instead of the real measured ALP was used for computing the predictability with both thick lens equations since the ALP should be estimated before surgery.

Postoperative SE relative to the intended target was −0.12 ± 0.38 [−0.11 (0.50)] D for the SRK/T (Figure 4(a)), −0.20 ± 0.33 [−0.24 (0.54)] D for Barrett Universal II (Figure 4(b)), −0.01 ± 0.41 [−0.05 (0.62)] D for n_k equation (Figure 4(c)), and −0.02 ± 0.40 [0.01 (0.57)] D for n_c equation (Figure 4(d)). The predictability was significantly correlated with pupil diameter for n_c equation ($r = -0.50$, $p = 0.001$) (Figure 4(e)) and for n_k equation ($r = -0.51$, $p < 0.0005$) (Figure 4(f)). A similar correlation but of less strength was found for Barrett Universal II ($r = -0.31$, $p = 0.04$), but not for SRK/T ($r = -0.04$, $p = 0.79$).

4. Discussion

Optical biometers use the keratometric index (1.3375) for computing the corneal power from anterior corneal radius. However, it is well known that this keratometric index is far from being the one which better predicts the postoperative SE, and current formulas use a fictitious refractive index from 1.3315 to 1.336, close to the tear film refractive index which results in better postoperative SE predictions [7]. The formula used for calculating the IOL power in this study (SRK/T) uses a fictitious index of 1.333, which is within this range. It is well known that SRK/T formula, as any other formulas, reduces the predictability in more or less degree depending on the axial length of the eye, corneal power, and other variables [10]. In our study, we found that an estimated error in the ELP_o with the

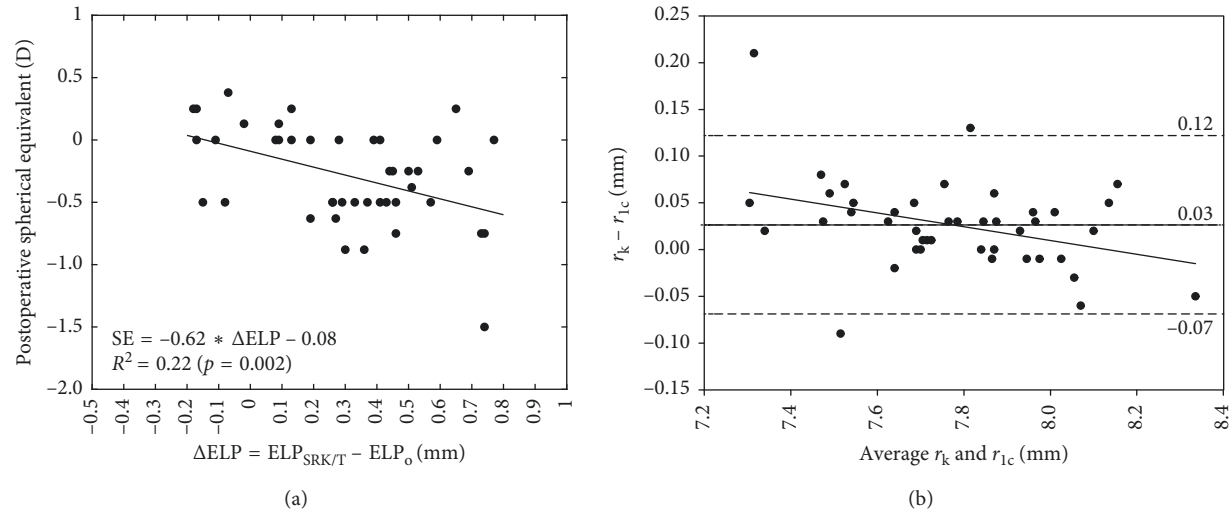

Figure 2: (a) Postoperative spherical equivalent relative to the intended target for the SRK/T versus the difference between the effective lens position estimated by the SRK/T formula ($ELP_{SRK/T}$) and the real obtained from the measurement of the actual lens position and the location of the second principal plane of the IOL (ELP_o). (b) Agreement between anterior corneal radius measured with IOLMaster (r_k) and Pentacam HR (r_{1c}).

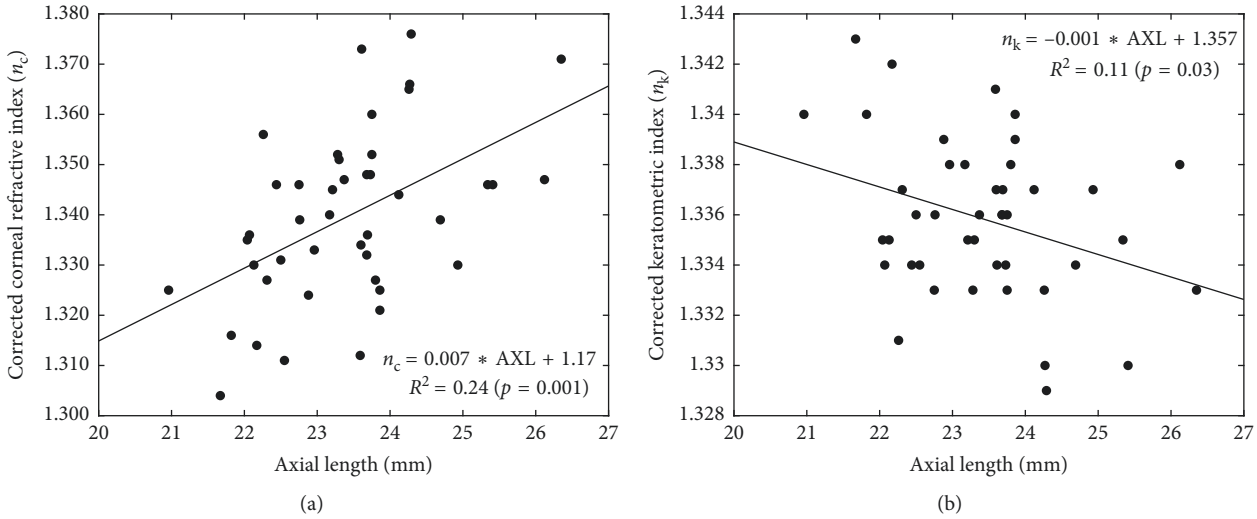

Figure 3: Correlations between the fictitious index (n_c) that minimize the postoperative SE for a known effective lens position considering both corneal radii and thickness (a), and the fictitious index (n_k) derived from the anterior corneal radius (b).

Table 1: Multiple regression linear models for prediction of postoperative SE relative to the intended target.

Variable	B	SEB	β	t	p
Intercept	154.55	12.73		12.14	<0.0005
ΔELP (mm)	−1.44	0.11	−1.07	−13.10	<0.0005
n_k	−115.45	9.52	−0.99	−12.13	<0.0005
Intercept	−14.10	4.20			0.002
ΔELP (mm)	−0.98	0.20	−0.73	−4.99	<0.0005
n_c	10.67	3.16	0.50	3.38	0.002

SRK/T formula explained 22% of the variability in the postoperative SE, but a higher percentage of error remained unknown. It is important to note that in the regression of Figure 2(a), we maintained an outlier in the analysis corresponding to the highest postoperative spherical equivalent of −1.50 D. This value can affect the r-square value due to the small sample. For this reason, we recomputed the regression equation omitting the outlier, and the r-square value decreased to 15% (p = 0.01). This means that the variability explained by a wrong estimation of the ELP_o might be even lower.

Interestingly, we found that when real ELP_o is known, the fictitious index can be fitted in order to reduce the predictability error that was not attributed to the ELP_o. Our mean refractive index for computing corneal power and deriving from anterior corneal surface was $n_k = 1.336$ that has been historically reported by Holladay to be close to the tear film [7, 26]. By contrast, $n_c = 1.339$ was found when anterior and posterior corneal radii were considered. The

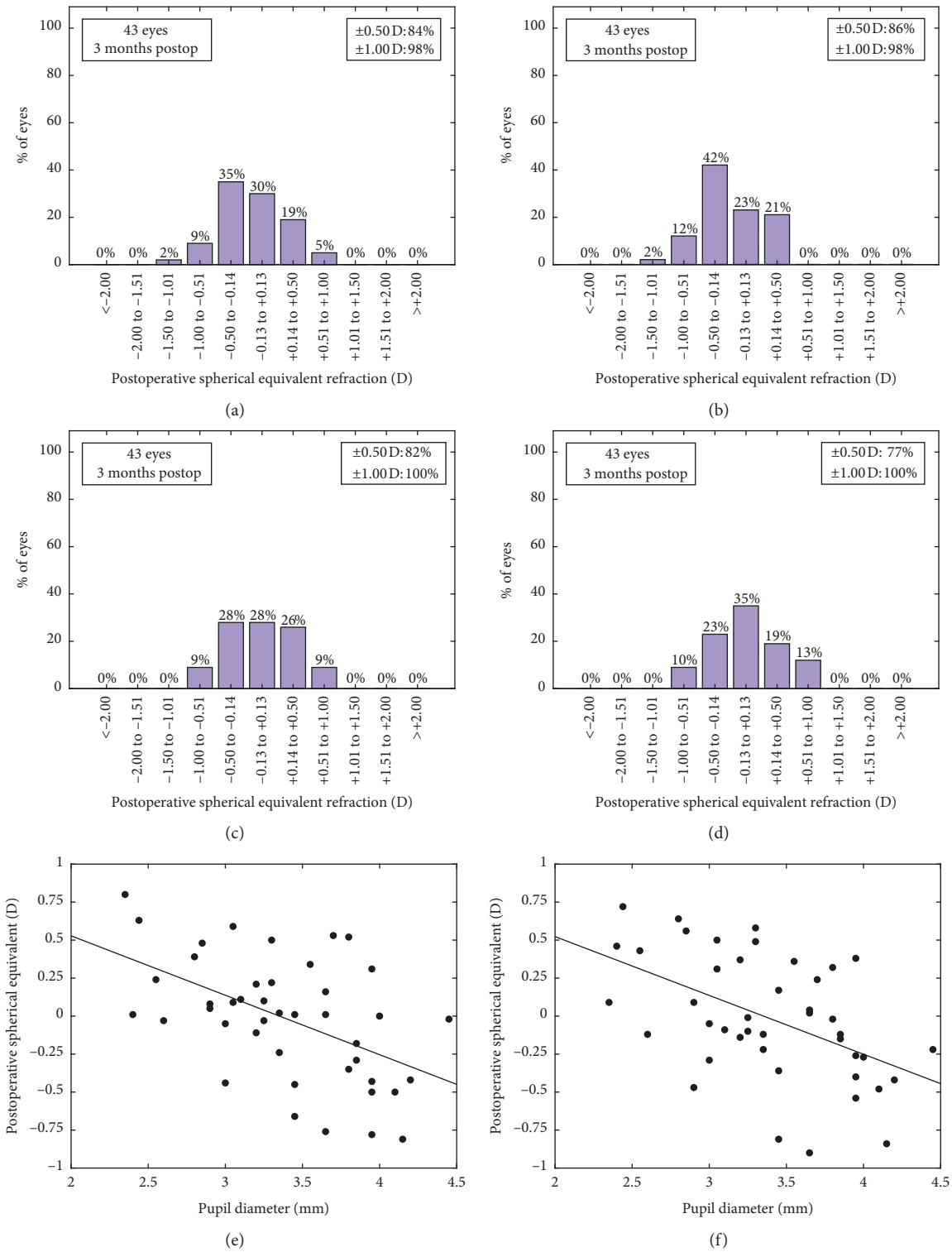

Figure 4: Postoperative spherical equivalent relative to the intended target for (a) SRK/T, (b) Barrett Universal II, (c) n_k equation, and (d) n_c equation (D). Correlations between the postoperative spherical equivalent relative to the intended target and the pupil diameter for (e) n_c equation and (f) n_k equation.

latter finding is also quite important because ray tracing and total corneal refractive power have not demonstrated, as theoretically expected, to provide better predictability than current formulas [27–30]. From our results, it can be concluded that a fictitious index is required for computing corneal power derived from anterior corneal radius, whereas a different fictitious index is required for total corneal power calculation.

Fictitious indexes were correlated with AXL, suggesting that fitting these refractive indexes depending on the axial length, the predictability can be increased without overestimating or underestimating the ELP from its real value. The inclusion of n_k with ΔELP in the model of prediction of postoperative SE relative to the intended target explained 83% of the variability instead of 22%. By contrast, the inclusion of n_c with ΔELP in the model of prediction of postoperative SE after target correction explained 39% of variability. This means that, even though improving the prediction of the real ELP, there would be some error in the postoperative SE that can be corrected by means of modifying de fictitious index and then the corneal power. Furthermore, even though both approaches can improve the predictability, the corneal power derived from specular reflection devices would lead to better results [31]. Possibly, specular reflection devices compute the radius over the tear film whereas with Scheimpflug devices, tear film is ignored. In fact, we found that the difference in the anterior corneal radius measured with Pentacam HR and IOLMaster systems was correlated with the average from both measures, suggesting that some caution should be considered when using equations derived from measurements of different devices.

A very important consideration is to evaluate the mode of change of these fictitious indexes between different approaches to compute the corneal power. Whereas n_k decreased with the increase of axial length and n_c increased in the opposite direction, but with an overestimation of the corneal power with the increase of AXL in both cases. This overestimation can be corrected by means of decreasing n_k or increasing n_c with the increment of AXL. Our results are consistent with those reported by Preussner et al. [32] who found an hyperopic outcome in very long eyes (>28 mm), and this was attributed to an overestimation of the corneal power that can be compensated in normal eyes with a systematically overestimated ELP, but not being possible in very long eyes. In fact, even though our sample does not include very long eyes, applying our linear regression for an eye of 30 mm, we obtained the fictitious refractive index ($n_k = 1.327$) proposed by Preussner et al. [32] for very long eyes.

The mean postoperative SE relative to the intended target with the thick lens formulas derived from the study was reduced in comparison to SRK/T or Barrett Universal II, both showing a myopic shift that can be explained by the overestimation of ELP_o with SRK/T. The higher was the ELP_o, the lower was the eye power, and consequently, an overestimation of ELP_o led to an underestimation of eye power, leading to an overestimating of the required IOL power and resulting in a myopic shift. While the percentage of eyes within ±0.50 D was higher for SRK/T and Barrett Universal II, the percentage of eyes within ±1.00 D was 100% for both thick formulas, with better predictability with n_k equation in comparison to n_c equation. The most interesting finding is that the percentage of cases with an error higher than ±0.50 D corresponded to eyes with the highest and lowest pupil diameters, suggesting that a hyperopic shift can be estimated by the formula as a consequence of the presence of small pupils focusing the image in front of the retina, with the opposite trend for large pupils. This suggests that, using these formulas with the trifocal IOL evaluated in our series, a trend to plus target should be used in patients with smaller pupils and to a minus target in eyes with larger pupils as choosing a negative target in small pupils can lead to higher myopic residuals than those predicted by the formula and vice versa. This reasoning can be also valid for Barrett Universal II after constant fitting, but not for SRK/T for which the correlation with pupil diameter was not significantly manifested.

This study is a first approach for the development of new thick lens equations that can be used when measuring the corneal geometry with specular reflection or Scheimpflug-based devices, but it has some limitations that should be considered. First, the small sample for a particular surgeon supposes that the ALP prediction formula might not be transferable to other surgeons. Higher samples with results obtained from different surgeons are required for a general estimation of the ALP. Second, the sample included eyes with AXL ranging from 20.96 to 26.35 mm and therefore with low number of short and long eyes in comparison to medium or medium-long eyes. Although the tendency of n_k and n_c is clear with axial length, an improvement in the estimation of the fictitious indexes would be obtained by increasing the number of eyes, especially for short, long, and very long eyes. Finally, the predictability of these new formulas has been computed in the same sample for which they were developed. The performance of new studies with these formulas in a different sample for confirming the results of predictability is needed. In fact, in our opinion, future crossover studies are required assigning different formulas to uniform groups instead of predicting what would have happened if different formulas had been used as the current comparative studies of formulas are doing.

In conclusion, in this study, we have demonstrated that the postoperative SE with some of the current vergence formulas can be due to the result of an underestimation or overestimation of the real ELP. However, even if the real ELP was perfectly predicted before surgery, some postoperative SE can appear depending on axial length. This could be corrected by means of fitting the constant of the formula leading to a false ELP prediction or by means of optimizing the fictitious indexes for different axial lengths. We have also demonstrated that the second option reduces the mean postoperative SE, either for specular reflection devices or Scheimpflug-based devices. However, it is important to consider that the slopes of correlation between both approaches are of opposite sign. Another very interesting finding is that higher errors of predictability can be due to pupil diameter changes during refraction with the used multifocal intraocular lens. We suggest to include the pupil diameter in predictability studies for exploring this finding with other multifocal or monofocal IOLs.

Data Availability

The data supporting the results of the current article are available from the corresponding author upon request.

Disclosure

Dr. Fernández is a consultant from Medicontur Medical Engineering Ltd. Inc., Zsámbék, Hungary. Remaining authors declare nothing to disclose.

Conflicts of Interest

The authors declare that they have no conflicts of interest.

Acknowledgments

The authors thank Medicontur Medical Engineering Ltd. Inc., Zsámbék, Hungary, for provide the information required about the Liberty Trifocal in order to conduct this study.

References

[1] S. N. Fyodorov and A. Kolinko, "Estimation of optical power of the intraocular lens," *Vestnik Oftalmologii*, vol. 80, pp. 27–31, 1967.

[2] S. N. Fyodorov, M. A. Galin, and A. Linksz, "Calculation of the optical power of intraocular lenses," *Investigative Ophthalmology*, vol. 14, pp. 625–628, 1975.

[3] D. D. Koch, W. Hill, A. Abulafia, and L. Wang, "Pursuing perfection in intraocular lens calculations: I. Logical approach for classifying IOL calculation formulas," *Journal of Cataract & Refractive Surgery*, vol. 43, no. 6, pp. 717-718, 2017.

[4] J. X. Kane, A. Van Heerden, A. Atik, and C. Petsoglou, "Accuracy of 3 new methods for intraocular lens power selection," *Journal of Cataract & Refractive Surgery*, vol. 43, no. 3, pp. 333–339, 2017.

[5] P.-R. Preussner, J. Wahl, H. Lahdo, B. Dick, and O. Findl, "Ray tracing for intraocular lens calculation," *Journal of Cataract & Refractive Surgery*, vol. 28, no. 8, pp. 1412–1419, 2002.

[6] H. Jin, T. Rabsilber, A. Ehmer et al., "Comparison of ray-tracing method and thin-lens formula in intraocular lens power calculations," *Journal of Cataract & Refractive Surgery*, vol. 35, no. 4, pp. 650–662, 2009.

[7] J. T. Holladay, "Standardizing constants for ultrasonic biometry, keratometry, and intraocular lens power calculations," *Journal of Cataract & Refractive Surgery*, vol. 23, no. 9, pp. 1356–1370, 1997.

[8] S. E. Gökce, I. Montes De Oca, D. L. Cooke, L. Wang, D. D. Koch, and Z. Al-Mohtaseb, "Accuracy of 8 intraocular lens calculation formulas in relation to anterior chamber depth in patients with normal axial lengths," *Journal of Cataract & Refractive Surgery*, vol. 44, no. 3, pp. 362–368, 2018.

[9] T. V. Roberts, C. Hodge, G. Sutton, and M. Lawless, "Comparison of hill-radial basis function, Barrett Universal and current third generation formulas for the calculation of intraocular lens power during cataract surgery," *Clinical & Experimental Ophthalmology*, vol. 46, no. 3, pp. 240–246, 2018.

[10] R. B. Melles, J. T. Holladay, and W. J. Chang, "Accuracy of intraocular lens calculation formulas," *Ophthalmology*, vol. 125, no. 2, pp. 288–294, 2018.

[11] Q. Wang, W. Jiang, T. Lin et al., "Accuracy of intraocular lens power calculation formulas in long eyes: a systematic review and meta-analysis," *Clinical & Experimental Ophthalmology*, vol. 46, no. 7, pp. 738–749, 2018.

[12] J. X. Kane, A. Van Heerden, A. Atik, and C. Petsoglou, "Intraocular lens power formula accuracy: comparison of 7 formulas," *Journal of Cataract & Refractive Surgery*, vol. 42, no. 10, pp. 1490–1500, 2016.

[13] D. L. Cooke and T. L. Cooke, "Comparison of 9 intraocular lens power calculation formulas," *Journal of Cataract & Refractive Surgery*, vol. 42, no. 8, pp. 1157–1164, 2016.

[14] A. K. Shrivastava, P. Behera, B. Kumar, and S. Nanda, "Precision of intraocular lens power prediction in eyes shorter than 22 mm: an analysis of 6 formulas," *Journal of Cataract & Refractive Surgery*, vol. 44, no. 11, pp. 1–4, 2018.

[15] Q. Wang, W. Jiang, T. Lin, X. Wu, H. Lin, and W. Chen, "Meta-analysis of accuracy of intraocular lens power calculation formulas in short eyes," *Clinical & Experimental Ophthalmology*, vol. 46, no. 4, pp. 356–363, 2018.

[16] G. D. Barrett, "Intraocular lens calculation formulas for new intraocular lens implants," *Journal of Cataract & Refractive Surgery*, vol. 13, no. 4, pp. 389–396, 1987.

[17] G. D. Barrett, "An improved universal theoretical formula for intraocular lens power prediction," *Journal of Cataract & Refractive Surgery*, vol. 19, no. 6, pp. 713–720, 1993.

[18] J. T. Holladay, K. H. Musgrove, T. C. Prager, J. W. Lewis, T. Y. Chandler, and R. S. Ruiz, "A three-part system for refining intraocular lens power calculations," *Journal of Cataract & Refractive Surgery*, vol. 14, no. 1, pp. 17–24, 1988.

[19] J. A. Retzlaff, D. R. Sanders, and M. C. Kraff, "Development of the SRK/T intraocular lens implant power calculation formula," *Journal of Cataract & Refractive Surgery*, vol. 16, no. 3, pp. 333–340, 1990.

[20] P. Aristodemou, N. E. Knox Cartwright, J. M. Sparrow, and R. L. Johnston, "Intraocular lens formula constant optimization and partial coherence interferometry biometry: refractive outcomes in 8108 eyes after cataract surgery," *Journal of Cataract & Refractive Surgery*, vol. 37, no. 1, pp. 50–62, 2011.

[21] J. C. Merriam, E. Nong, L. Zheng, and M. Stohl, "Optimization of the A constant for the SRK/T formula," *Open Journal of Ophthalmology*, vol. 5, no. 3, pp. 108–114, 2015.

[22] S. Schwartz, "Thick lenses," in *Geometrical and Visual Optics, Chapter 6*, pp. 77–88, McGraw Hill Medical (ed), New York, NY, USA, 2002.

[23] "APACRS calculator Barrett Universal II formula v1," December 2018, https://www.apacrs.org/barrett_universal2/.

[24] D. Z. Reinstein, T. J. Archer, S. Srinivasan et al., "Standard for reporting refractive outcomes of intraocular lens-based refractive surgery," *Journal of Cataract & Refractive Surgery*, vol. 43, no. 4, pp. 435–439, 2017.

[25] D. Z. Reinstein, T. J. Archer, S. Srinivasan et al., "Standard for reporting refractive outcomes of intraocular lens-based refractive surgery," *Journal of Refractive Surgery*, vol. 33, no. 4, pp. 218–222, 2017.

[26] J. T. Holladay and K. J. Maverick, "Relationship of the actual thick intraocular lens optic to the thin lens equivalent," *American Journal of Ophthalmology*, vol. 126, no. 3, pp. 339–347, 1998.

[27] G. Savini, K. Negishi, K. J. Hoffer, and D. Schiano Lomoriello, "Refractive outcomes of intraocular lens power calculation using different corneal power measurements with a new optical biometer," *Journal of Cataract & Refractive Surgery*, vol. 44, no. 6, pp. 701–708, 2018.

[28] G. Savini, K. J. Hoffer, D. Schiano Lomoriello, and P. Ducoli, "Simulated keratometry versus total corneal power by ray tracing," *Cornea*, vol. 36, no. 11, pp. 1368–1372, 2017.

[29] O. Reitblat, A. Levy, G. Kleinmann, A. Abulafia, and E. I. Assia, "Effect of posterior corneal astigmatism on power calculation and alignment of toric intraocular lenses: comparison of methodologies," *Journal of Cataract & Refractive Surgery*, vol. 42, no. 2, pp. 217–225, 2016.

[30] T. B. Ferreira, P. Ribeiro, F. J. Ribeiro, and J. G. O'Neill, "Comparison of methodologies using estimated or measured values of total corneal astigmatism for toric intraocular lens power calculation," *Journal of Refractive Surgery*, vol. 33, no. 12, pp. 794–800, 2017.

[31] Y. Mejía-Barbosa and D. Malacara-Hernández, "A review of methods for measuring corneal topography," *Optometry and Vision Science*, vol. 78, no. 4, pp. 240–253, 2001.

[32] P. Preussner, P. Hoffmann, and J. Wahl, "Intraocular lens (IOL) calculation in very long eyes," in *Proceedings of the 36th Congress of the ESCRS*, Wien, Austria, September 2018.